# Uncovering the mechanisms of secondary plasmodesmata formation and virus mediated changes in intercellular trafficking

**A Dissertation Presented for the**

**Doctor of Philosophy**

**Degree**

**The University of Tennessee, Knoxville**

**Brandon Chase Reagan**

**May 2021**

Copyright © 2021 by Brandon C. Reagan

All rights reserved.

# DEDICATION

I would like to dedicate this dissertation to my Pop,

Percy Denton Shierling III.

# ACKNOWLEDGEMENTS

I would first like to thank my parents, Kristin and Robert Hill and Tim and Pam Reagan for their constant love and support. Thank you for everything, I would not be where I am today without everything you have done for me.

I would also like to thank my amazing grandparents, Percy (Pop) and Norma (Nana) Shierling for their constant love and support. Thank you for always supporting my scientific curiosity. The time spent at your house working on my experiments and inventions or playing in the pond will always be my favorite memories. Thank you for giving me my very first microscope. Who would have thought that I would one day grow up to be an actual microscopist. I love you so much and I could never thank you enough for all you have done for me.

I would like to thank my sister Samantha (Sami) Hitechew. You are one of my favorite people on Earth. You will always be one of my best friends. I love you and of course Shane and Dean so much. I am so proud of you and I am so thankful that I have you for a sister.

I would like to thank the amazing Dr. Tessa Burch-Smith for her constant guidance and support throughout my time here at the University of Tennessee-Knoxville. She has constantly pushed me to be the best scientist possible and she has opened the door for so many wonderful opportunities for me along the way. I cannot imagine starting my academic career in anyone else's lab.

I would also like to thank the all former and current members of the Burch-Smith lab for creating a welcoming and collaborative environment. I cannot say

thank you enough for all of the help that you all have given me throughout this journey.

I would specifically like to thank Dr. Jessica Fernandez from the Burch-Smith lab for being an outstanding colleague, constant ear for venting and an amazing friend. Thank you for putting up with my sometimes difficult personality. Our friendship may have been tense at first, but you have definitely become one of my best friends.

I would like to thank Dr. Amy Wiles from Mercer University for jumpstarting my academic career. I am so thankful that I had the opportunity to work in your lab during my time at Mercer. Had you not introduced me to the possibility of pursuing research as a career, I definitely would not be where I am today.

I would also like to thank two very special teachers from my childhood. Mrs. Lynn Harbor and Mrs. Jan McGuire. Thank you for encouraging my scientific interests. You may not know it, but I still think of the many times that each of you helped me grow into the scientist I am today. The small comments and words of encouragement instilled a lasting love for science and a desire to learn.

## ABSTRACT

Intercellular communication is critical for all life on earth. From quorum sensing in bacteria to the electrical signals controlling our every move, the ability to share and exchange information with our neighbors is critical for growth and development. In plants, this communication can be achieved through two major pathways, apoplastic signaling or symplastic signaling through membrane lined pores in the cell wall called plasmodesmata. These pores form cytoplasmic bridges between neighboring cells and are used to traffic nutrients and signaling molecules throughout the plant. They also form direct routes for plant pathogens to rapidly spread throughout the plant. Plant viruses are particularly well adapted to take advantage of these intercellular connections. During virus infection, trafficking through plasmodesmata increases in a phenomenon known as gating. The long standing interpretation of this increase in trafficking has been that it allows for rapid spread of the virus into neighboring, uninfected tissues. While the plasmodesmata-virus relationship has been studied extensively and has provided many insights into the functioning and regulation of these small pores, the changes that occur during infection to increase the trafficking remain unknown. The results presented in this dissertation demonstrate that the observed increase intercellular trafficking is the result virus-induced formation of new plasmodesmata. Using this system, details of the mechanisms behind the cell biology of plasmodesmata formation are revealed. Using the data presented

here, new models for gating during virus infection and secondary plasmodesmata formation are proposed.

# TABLE OF CONTENTS


CHAPTER 1 ..... 1
INTRODUCTION TO INTERCELLULAR COMMUNICATION AND VIRUSES ..... 1
I. RNA ON THE MOVE: THE PLASMODESMATA PERSPECTIVE ..... 2
Plasmodesmal structure and composition: how is movement facilitated ..... 3
*Membranes and spaces: Routes for intercellular trafficking* ..... 4
II. VIRUSES REVEAL THE SECRETS OF PLASMODESMAL CELL BIOLOGY 10
MECHANISMS FOR VIRAL MOVEMENT ..... 16
*Mobile ribonucleoprotein complexes* ..... 17
*Tubule forming viruses* ..... 19
*Mobile Vesicular Replication Complexes* ..... 20
*Phloem-limited viruses* ..... 21
HOST PROTEINS AND PLASMODESMATA ..... 22
*Proteins involved in cell wall metabolism and modification* ..... 23
*Proteins with roles in callose metabolism* ..... 24
*Other PD-associated proteins* ..... 27
*Proteins with roles in lipid and membrane metabolism* ..... 29
CYTOSKELETON: GETTING TO OR THROUGH PD ..... 37
*Getting to the plasmodesmata* ..... 38
*Getting through Plasmodesmata* ..... 40
PD DURING VIRUS INFECTION ..... 41
MECHANISMS OF GATING ..... 44
*Callose degradation and gating* ..... 44
*Gating through modification of macromolecule composition* ..... 45
*Gating PD by tubule formation* ..... 46
*Plasmodesmata formation as a mechanism for gating* ..... 47
III. AIMS OF THE DISSERTATION ..... 49
CHAPTER 2 Spatial distribution of organelles in leaf cells and soybean root nodules revealed by focused ion beam- scanning electron microscopy. ..... 50
Abstract ..... 51
Introduction ..... 52
Results ..... 57
HPF/qFS-prepared samples are amenable to FIB/SEM ..... 57
HPF/qFS with 4% $OsO_4$ ..... 63
Chemical Fixation of Root Nodule ..... 65
Discussion ..... 71
Materials and Methods ..... 77
Plant growth and tissue collection ..... 77
High pressure freezing and freeze substitution ..... 77
Chemical fixation of root nodules ..... 78
Sample preparation before FIB/SEM ..... 78
Sample preparation during FIB/SEM ..... 79
Image acquisition using Slice-and-View ..... 79

Image analysis and tomogram construction ..... 79
Tomography mapping ..... 80
Appendix ..... 81
Focused Ion Beam-Scanning Electron Microscopy for investigating plasmodesmal densities ..... 81
INTRODUCTION ..... 81
MATERIALS ..... 85
Resin-embedded sample preparation: ..... 85
Mounting of samples for FIB-SEM: ..... 85
Microscopy: ..... 85
Image processing ..... 85
METHODS ..... 87
Biological sample preparation: ..... 87
Mounting of samples for FIB-SEM: ..... 88
Microscopy: ..... 89
Image processing ..... 94
NOTES ..... 99
CHAPTER 3 Chloroplast-to-nucleus retrograde signaling controls intercellular trafficking via plasmodesmata formation. ..... 102
Abstract ..... 104
Introduction ..... 105
Results ..... 108
Silencing genes for chloroplast gene expression produces varying degrees of chlorosis ..... 108
Intercellular trafficking changes in plants with defective chloroplast RNA processing ..... 109
PD density is altered in plants with defective chloroplast gene expression 113
Discussion ..... 117
Conclusions ..... 121
Materials and Methods ..... 122
Plant material and growth conditions ..... 122
RNA extraction and cDNA synthesis ..... 122
Gene cloning and generation of recombinant VIGS vectors ..... 123
Carotenoid and chlorophyll determination ..... 123
Measuring intercellular trafficking by movement assay ..... 124
Measuring PD density ..... 124
CHAPTER 4 Viruses induce secondary plasmodesmata formation ..... 127
Abstract ..... 128
Introduction ..... 128
Results ..... 134
Tobacco mosaic virus infection results in increased numbers of pitfields .. 134
The TMV movement protein induces PD formation ..... 137
Diverse families of viruses induce secondary PD formation during infection ..... 140

NbREM1 is a negative regulator of PD formation ..... 143
Overexpression of NbREM1.1 blocks virus induced PD formation ..... 147
Discussion ..... 150
Materials and Methods ..... 158
Plant growth ..... 158
RNA extraction and cDNA synthesis ..... 158
Cloning of NbREM1 fragment for VIGS ..... 159
Cloning of NbREM1.1 ..... 159
Cloning TMV MP30-GFP and MP30-V4A-GFP ..... 160
Viruses and virus infection ..... 160
Intercellular Movement Assays ..... 161
Pitfield distribution assays and confocal microscopy ..... 161
PD distribution in upper leaves before systemic virus movement ..... 162
Sample fixation and Transmission electron microscopy ..... 163
Quantification of plasmodesmata frequency by TEM ..... 164
CHAPTER 5 The mechanism of secondary plasmodesmata formation ..... 165
Abstract ..... 166
Introduction ..... 166
Results ..... 172
Secondary PD formation is initiated by single cells ..... 172
GPI-anchored proteins are required for secondary PD formation ..... 174
GPI-anchored β-glucanases are involved in secondary PD formation ..... 177
Callose deposition is required for secondary plasmodesmata formation ..... 180
Loss of Remorin results in decreased accumulation of PDCB1-mCherry in PD pitfields ..... 183
ER-Plasma membrane contact sites are important for secondary PD formation ..... 188
Loss of two Reticulon-like proteins does not affect PD formation ..... 191
Identification of cellular machinery involved in PD formation ..... 195
Endocytosis and not exocytosis is important for PD formation ..... 195
Disruption of the actin cytoskeleton alters intercellular trafficking ..... 199
Disruption of microtubule dynamics results in altered intercellular trafficking ..... 202
Disruption of ER to Golgi trafficking results in decreased intercellular trafficking ..... 203
Discussion ..... 203
Materials and Methods ..... 207
Plant growth ..... 207
Cloning and transient expression ..... 207
Dual axis TEM Tomography ..... 208
Cloning fragments for VIGS ..... 208
Virus induced gene silencing ..... 209
Pitfield distribution assays and confocal microscopy ..... 209
Intercellular Movement Assays ..... 209

Quantification of PDCB1-mCherry enrichment at PD ..... 210
Appendix ..... 212
CHAPTER 6 A new model for plasmodesmata formation and virus-induced gating ..... 226
PD density is correlated with intercellular trafficking ..... 227
Are these new PD different than regular PD? ..... 234
Learning from viruses: details of PD formation uncovered by studying viruses ..... 236
A new role for callose metabolism at PD ..... 238
ER-PM contact sites allow for the formation of the desmotubule ..... 241
Salicylic acid as a regulator of PD formation ..... 242
Concluding Statements ..... 245
References ..... 246
VITA ..... 294

# LIST OF TABLES

Table 1 Primers used for cloning .....212

# LIST OF FIGURES

Figure 1 Plasmodesmal Structure....5
Figure 2 Mechanisms for virus intra- and intercellular movement and modifications made to plasmodesmata (PD) during infection. ....12
Figure 3 Tomographic images of young leaf tissue prepared with 1.0% OsO4 and 0.1% uranyl acetate. ....59
Figure 4 Dividing chloroplast from leaf tissue prepared in 1.0% OsO4 and 0.1% uranyl acetate. ....60
Figure 5 Pitfields of plasmodesmata in leaf tissue prepared in 1.0% OsO4 and 0.1% uranyl acetate. ....61
Figure 6 Tomographic images of leaf tissue fixed in 4% OsO4 ....64
Figure 7 Organelles in close proximity in leaf cells. ....66
Figure 8 Tomographic images of chemically fixed soybean root nodules. ....68
Figure 9 3D analysis of root nodules reveals complex structural features of the symbiosome membrane. ....69
Figure 10 Representative images of mounted blocks, milled trenches, and the exposed block faces. ....92
Figure 11 3D reconstruction of FIB-SEM data and quantification of PD density in a representative FIB-SEM dataset. ....96
Figure 12 Phenotypes of silenced plants and their photosynthetic pigment content. ....110
Figure 13 Measurement of PD-mediated intercellular trafficking in silenced plants. ....111
Figure 14 Quantification of PD density in silenced plants. PD in pitfields were labelled with the general PD marker PDLP1-GFP. ....115
Figure 15 Tobacco mosaic virus induces secondary plasmodesmata formation. ....135
Figure 16 The movement protein of TMV induces PD formation. ....138
Figure 17 PD localization of MP30 is required to increase trafficking and induce PD formation. ....141
Figure 18 Diverse viruses induce PD formation as part of their infection ....144
Figure 19 *NbREM1* is a negative regulator of PD formation. ....145
Figure 20 Overexpression of *NbREM1* decreases trafficking, PD ....148
Figure 21 Overexpression of *NbREM1* block MP30-induced gating of PD ....151
Figure 22 Intermediates in secondary PD formation captured by dual axis TEM tomography. ....173
Figure 23 GPI-anchored proteins are important for PD formation. ....175
Figure 24 Intercellular trafficking is decreased in specific β-glucanase-silenced plants ....178
Figure 25 GPI-anchored β-glucanases are involved in secondary PD formation. ....181
Figure 26 GPI-anchored β-glucanases are involved in virus induced secondary PD formation. ....182

Figure 27 Silencing of specific callose synthases in results in decreased intercellular trafficking. ..... 184
Figure 28 Callose deposition is important for plasmodesmata formation ..... 185
Figure 29 Callose deposition is required for MP30-induced secondary PD formation. ..... 186
Figure 30 Silencing *NbREM1* decreases GPI-anchored protein accumulation at PD. ..... 187
Figure 31 Disruption of ER-PM contact sites results in decreased intercellular trafficking. ..... 189
Figure 32 Membrane contacts are important for plasmodesmata formation. .... 190
Figure 33 ER-PM tethers are required for MP30-induced secondary PD formation. ..... 192
Figure 34 Reticulon-like proteins are important for regulating intercellular trafficking. ..... 193
Figure 35 Reticulon-like B proteins may restrict PD formation ..... 194
Figure 36 Reticulon-like B proteins are not required for MP30-induced PD formation. ..... 196
Figure 37 Endocytosis is important for PD formation and virus induced PD formation ..... 197
Figure 38 Disruption of the cytoskeleton and membrane trafficking pathways alters intercellular trafficking. ..... 200
Figure 39 Intercellular trafficking and pitfield density are positively correlated. . 229
Figure 40 A mechanistic model of secondary PD formation. ..... 230
Figure 41 A new model for virus induced gating of PD through PD formation. 232

# CHAPTER 1

# INTRODUCTION TO INTERCELLULAR COMMUNICATION AND VIRUSES

# I. RNA ON THE MOVE: THE PLASMODESMATA PERSPECTIVE

Disclosure: A version of this portion of my thesis was previously published in the Journal Plant Science by Brandon C. Reagan, Elena E. Ganusova, Jessica C. Fernandez, Tyra N. McCray, and Tessa M. Burch-Smith

Reagan, B. C., Ganusova, E. E., Fernandez, J. C., McCray, T. N., & Burch-Smith, T. M. (2018). RNA on the move: The plasmodesmata perspective. Plant Science, 275, 1-10.

This review article was co-written by Brandon C. Reagan, Jessica Fernandez, Elena Ganusova, Tyra McCray, and Dr. Tessa M. Burch-Smith. *R*eagan, Fernandez, and Ganusova share first-authorship of the paper and were responsible for compiling the literature and preparation of the manuscript.

## Plasmodesmal structure and composition: how is movement facilitated

Communication between neighboring cells is a fundamental requirement for all organisms. From single-celled prokaryotes to multicellular eukaryotes, all organisms relay information between adjacent cells to coordinate growth, development, and responses to the environment [1],[2],[3],[4]. For multicellular organisms, proper coordination of intercellular communication is essential for growth and differentiation of cells into specific tissues. For plants, this communication is facilitated through two primary pathways [5]. Small signaling molecules such as hormones can be secreted out into the extracellular environment, or apoplast, and move to neighboring cells [6, 7]. This form of communication has been suggested to be limited to molecules with Stokes radii less than 4.6nm by the cell wall that surrounds each cell and provides the plant with support and protection from the environment [8]. The cell wall also prevents communication via direct plasma membrane-membrane contact between cells, which is a primary mechanism for intercellular communication in other multicellular organisms [9, 10]. Plants have instead evolved a specialized communication network that connects the cytoplasms of almost every cell in the plant, called the symplast, through cell wall-spanning pores called plasmodesmata (PD) [3],[4]. Symplastic trafficking through PD serves as a route for cells to exchange small molecules such as sucrose with neighboring cells, but also allows for the intercellular movement of proteins and RNA molecules that act

as informational or regulatory factors, and therefore allowing the coordination of responses to external stimuli and intrinsic developmental processes. The formation and function of these PD during development and in response to extrinsic stimuli represented by viruses is the focus of this thesis.

***Membranes and spaces: Routes for intercellular trafficking***

A single PD aperture is usually 30-50 nm in diameter, falling below the limits of resolution of light microscopy. This small size belies the complexity of the structure and composition of the pores. A depiction of the complexity of PD structure, based on models developed by Ding [11] and Overall and Blackmann [12], is presented in Figure 1. The outer boundaries of PD are delimited by the plasma membrane, rendering this membrane continuous between connected cells. Transmission electron microscopy (TEM) studies of PD have suggested the presence of a central protein-rich membranous structure at the center of the pore, referred to as the desmotubule (e.g. [11]). *T*he desmotubule is derived from the endoplasmic reticulum (ER) of the connected cells, and it likely contains numerous proteins to help maintain its high membrane curvature [13]. The space between the desmotubule and plasma membrane is called the cytoplasmic sleeve or annulus. TEM has also identified spoke-like structures that likely tether the PD plasma membrane to the desmotubule [11]. The cytoplasmic sleeve is believed to be the main conduit for intercellular trafficking through PD but trafficking can also occur by diffusion along the ER membrane of the desmotubule [14],[15]. The spoke proteins likely span the cytoplasmic sleeve,

**Figure 1 Plasmodesmal Structure**

(A) In this model, the desmotubule (grey) passes through the center of the pore and is encircled by two full turns of an actin filament (red). Plasma membrane-associated myosins (orange) bridge the cytoplasmic annulus (white space within pore) and form contacts with the actin filament. PD-localized proteins line the desmotubule and the plasma membrane (green ovals). GFP (yellow) is small enough to pass through the cytoplasmic annulus. Dimensions were obtained from previous studies. Drawn to scale. (B) - (D) Transmission electron micrographs of plasmodesmata in *N. benthamiana* leaves. (B) A simple plasmodesma consists of a single pore, (C) twinned PD are two pores within 100 nm of each other, and (D) shows a branched plasmodesma with a central cavity.

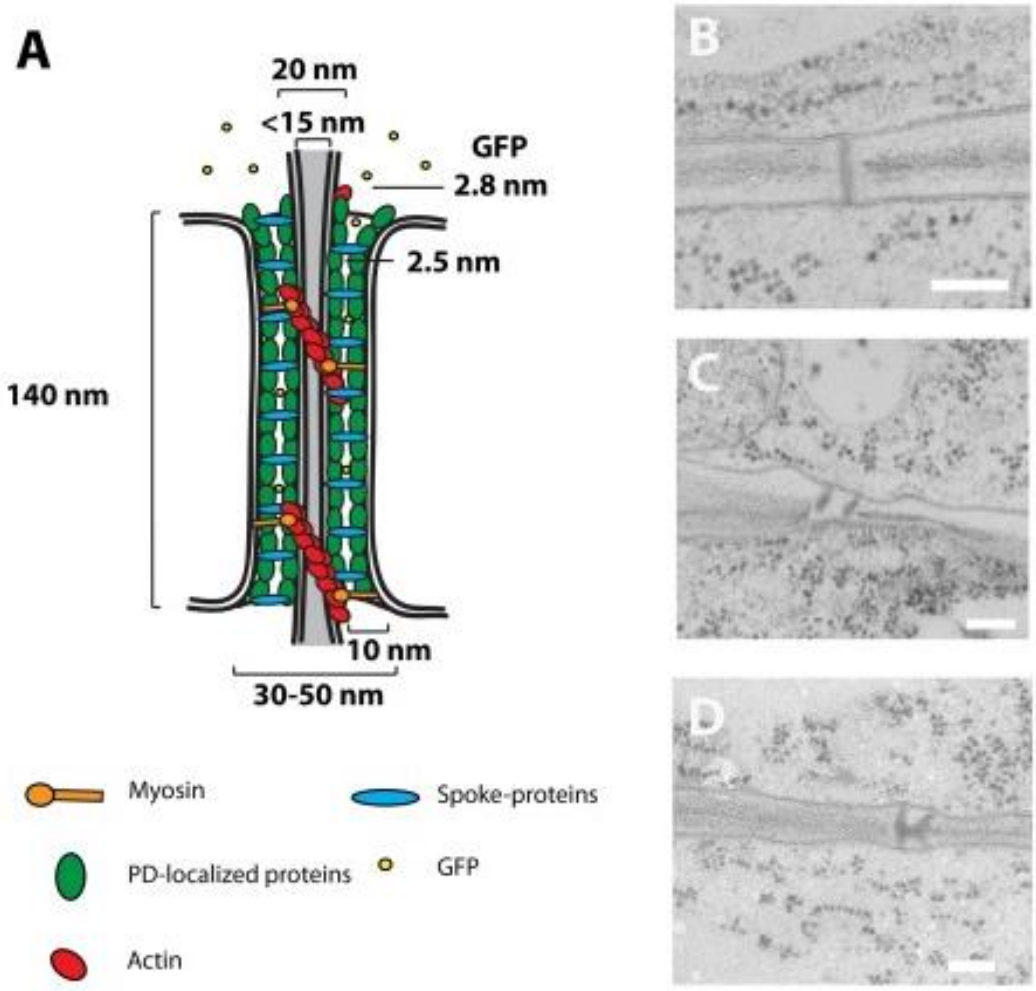
A
20 nm
<15 nm
GFP
2.8 nm
2.5 nm
140 nm
10 nm
30-50 nm
Myosin
Spoke-proteins
PD-localized proteins
GFP
Actin
B
C
D

restricting the area through which movement can occur [11]. One caution in interpreting these models is that they have been generated from a relatively small number of samples, and it cannot be ruled out that the micrographs on which these models are based may in fact represent closed PD or PD that are no longer functional. More studies of more PD in a variety of tissues and at a variety of developmental stages will allow better understanding of PD ultrastructure.

PD often form during cell division when strands of ER become trapped in the cell plate. *T*hese PD are designated as primary PD. In addition, PD may also form when cells are not dividing or across cell walls that are not the product of recent cell divisions, e.g. between root cell files, such PD are called secondary PD. The mechanisms behind secondary PD formation remain poorly understood. Current models of secondary PD formation suggest that occurs at or near existing PD [16]. In this model, known as the multiple twinning model, suggests that the components needed for the insertion of new PD reside at the existing PD. Additionally, the cell wall around existing PD are believed to be primed for the insertion of new PD. The addition of new PD near existing pores is consistent with the generation of highly dense clusters of PD in regions of the cell wall referred to as pitfields. It remains an open question whether primary and secondary PD are functionally distinct [17]. Besides simple pores (Figure 1A and B), PD can also take on more elaborate structures. *T*winned PD, defined as two PD within 100 nm of each other [17], are believed to be intermediates in the *de novo* formation of secondary PD (Figure1C) [18]. *B*ranched PD (Figure1D)

typically consist of multiple openings in each cell wall connected by a space called the central cavity [11]. *G*iven the small dimensions of PD, high-resolution microscopy is necessary for interrogating their structure and function; TEM and super-resolution microscopy are therefore typically used to study PD structure [11],[19],[20],[21].

It is likely that PD exist as a heterogeneous mixture with a variety of macromolecular and structural compositions that help specify the function of a given pore. Strong support for this idea comes from viral MPs that show specificity for different types of PD. *O*ne of the best examples of this is the MP of Potato leafroll virus (PLRV), MP17, which localizes exclusively to branched PD [22]. This finding suggests that there are differences between PD that allow the viral protein to localize to only a subset of the pores. PLRV is phloem-limited, meaning that the viral lifecycle is restricted to the phloem [23]. During co-infection with PLRV and some unrelated, non-phloem-limited viruses, PLRV was able to exit the phloem and enter other plant tissues [24]. This suggests that PLRV alone is incapable of modifying the PD that connect the companion cells to neighboring cells but once the PD are modified, PLRV can spread.

Additionally, structural features of PD are expected to be heterogeneous within the same cell wall. An exciting recent TEM-tomographic study of root PD suggests that PD can adopt multiple structures during development, with considerable changes to the size of the cytoplasmic sleeve as the distance between the desmotubule and plasma membrane varies [25]. *H*owever, the

relationship between PD structure and function has not been elucidated, although it has been suggested that branched PD exert more control over the size of molecules that they can traffic [26], and that PD with no apparent cytoplasmic sleeve can still traffic cargo [25]. It is also possible that only a subset of the PD in a given wall contains the desmotubule, and those that do not therefore have a considerably larger cytoplasmic sleeve volume for molecular trafficking between cells. Understanding how these differences affect trafficking through individual PD will be critical for understanding how PD function is related to pore structure.

# II. VIRUSES REVEAL THE SECRETS OF PLASMODESMAL CELL BIOLOGY

A version of this chapter was previously published in a special issue of the Journal Molecular Plant-Microbe Interactions by Brandon C. Reagan and Tessa M. Burch-Smith.

Reagan, B. C., & Burch-Smith, T. M. (2020). Viruses reveal the secrets of plasmodesmal cell biology. Molecular Plant-Microbe Interactions, 33(1), 26-39.

This review article was co-written by Brandon C. Reagan and Dr. Tessa M. Burch-Smith. I have also spoken about this paper as a special segment of the Webinar “What is New in MPMI.”

Plasmodesmata (PD) are membrane–lined nanopores that connect the contents of neighboring cells to each other. *T*hey allow the passage of small molecules like sugars, amino acids and small fluorescent dyes from one cell to another. They are also used for the intercellular movement of larger molecules like messenger RNAs, protein transcription factors, reporter proteins like green fluorescent protein (GFP) and viruses as ribonucleoprotein complexes or intact virions [27],[28],[29],[30]. Plant viruses have evolved to take advantage of this connectivity for their local cell to cell movement during infection. As such, understanding PD structure and function provides valuable insights into viral life cycles and mechanisms for infectivity. Conversely, viruses have proved invaluable sources of proteins used to probe PD structure and function. The relationship between viruses and PD is inextricably linked to the viral lifestyle and the success of any infection.

The plasma membranes (PM) of the cells connected by PD are continuous through the pore. In addition, strands of endoplasmic reticulum (ER) also traverse the pore in a structure referred to as the desmotubule. Trafficking through the pore occurs mainly via the cytoplasmic sleeve or annulus that lies between the desmotubule and PM of the pore (Figure 2A). The membranes of the desmotubule also comprise a route of cell-to-cell trafficking, exemplified by tobacco mosaic virus [TMV, [15]]. Besides these membranes and spaces, immunohistochemistry has identified numerous components of the cytoskeleton

**Figure 2 Mechanisms for virus intra- and intercellular movement and modifications made to plasmodesmata (PD) during infection.**

A, In current models of PD structure (modeled after Reagan et al. [2018]), unmodified PD has many components and the length of the pore is lined with callose (black jagged lines). A variety of host proteins (green and light blue ovals) line the pore and tether the endoplasmic reticulum (ER)-derived desmotubule to the plasma membranes. Actin filaments (chains of red circles) and myosins (orange) line the pore and may regulate PD function. Many viruses target the chloroplasts of infected cells and trigger changes in structure and function of the chloroplasts. Stromules extend out of chloroplasts along microtubules (MTs) and may deliver signaling molecules such as hydrogen peroxide (black dots) to one or both the nucleus and PD. Additionally many viral proteins (light blue ovals) have been shown to interact with chloroplast proteins (brown squares) and are likely involved in disrupting chloroplast function or in the plant response to the virus. B, During infection with tobacco mosaic virus (TMV) (depicted in the area labeled I), MP30 (light blue circles) accumulates in simple and branched PD and in ER-derived replication complexes. Callose is removed from the wall around the PD, presumably by extracellular or PD-localized β-1,3-glucanases, thereby dilating the pore to accommodate virus movement. MP30 and the TMV replicase (light pink circles) bind to the viral genome and target it to modified PD by moving along the actin cytoskeleton and desmotubule. MP30 also accumulates on MTs at the cell periphery. C, Movement proteins (MPs) like the MP of the phloem limited potato leafroll virus (MP17, dark blue circles) accumulates exclusively in

branched PD. During turnip mosaic virus (TuMV) infection (depicted in area II), the 6K2 protein (yellow circles) promotes the formation of ER-derived vesicular replication complexes (VRCs) that contain 6K2, the replicase (orange squares), and the viral genome. The VRCs are mobile and are targeted to and through PD via the actin cytoskeleton. It is currently unknown how the PD are modified in order to accommodate the large VRC and whether distinct PD are targeted by TuMV, but other potyviruses utilize a suite of other viral proteins to form PD-associated cylindrical inclusions to promote movement (not shown). D, During potato virus X infection (depicted in area III), the triple gene block proteins (TGB1, TGB2, and TGB3) and the capsid protein (CP) facilitate coreplicational insertion into modified PD. TGB2 (dark pink circles) and TGB3 (bright green circles) promote major remodeling of the ER into PD-associated caps. TGB1 (maroon circles) gates PD and facilitates the insertion of the CP (bright green squares) and viral genome into the PD. TGB1 is also involved in the formation of the X-body for virus replication (not shown). E, During grapevine fanleaf virus infection (depicted in area IV), the 2B MP (red circles) is targeted to calreticulin-positive foci (blue rectangle) at the cell periphery, through the ER-Golgi secretory pathway, and, along actin filaments or MTs, form proteinaceous tubules that span PD. The tubule displaces the desmotubule and interacts with host proteins. Fully formed virions (gray hexagons) move through the tubule.

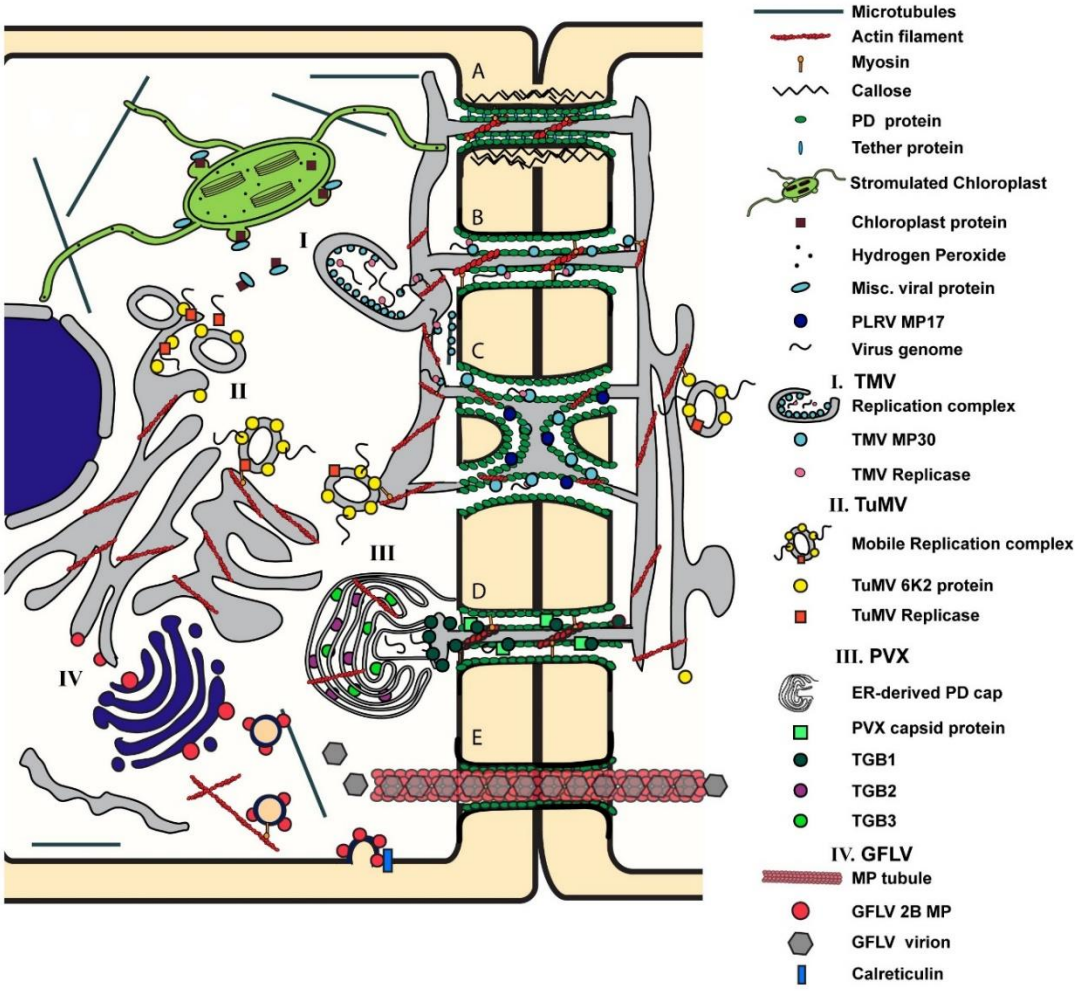
A
B
C
D
E
I
II
III
IV
Microtubules
Actin filament
Myosin
Callose
PD protein
Tether protein
Stromulated Chloroplast
Chloroplast protein
Hydrogen Peroxide
Misc. viral protein
PLRV MP17
Virus genome
I. TMV
Replication complex
TMV MP30
TMV Replicase
II. TuMV
Mobile Replication complex
TuMV 6K2 protein
TuMV Replicase
III. PVX
ER-derived PD cap
PVX capsid protein
TGB1
TGB2
TGB3
IV. GFLV
MP tubule
GFLV 2B MP
GFLV virion
Calreticulin

as being associated with PD. Actin and actin-related proteins, myosin, tropomyosin and centrin have all been localized to PD [31], although their contributions to intercellular trafficking remain unclear (discussed below). *R*ecent proteomic approaches have identified suites of proteins that likely associate with PD including integral membrane proteins that are receptors, membrane-localized kinases, and proteins involved in cell wall carbohydrate metabolism [32],[33]; [34] [35],[36]. This protein repertoire suggests that PD are not simply passive pores through which cargo is trafficked, but rather have the capacity to sense cues and initiate signaling to coordinate appropriate responses.

The lipid composition of PD has also been the focus of recent investigation. Careful isolation and subsequent mass spectrometric analysis of membrane fractions of Arabidopsis PD revealed enrichment in sterols and sphingolipids bearing very long-chain saturated fatty acids [37]. The sterol composition of the membranes was revealed to be important for the protein composition of PD, as drug treatments that inhibited sterol biosynthesis led to changes in the deposition of callose at PD that was in turn associated with the mislocalization of two PD proteins involved in callose metabolism, PLASMODESMATA CALLOSE BINDING1 (PDCB1) and PLASMODESMAL-LOCALIZED β-1,3-GLUCANASE 2 (PdBG2). Both of these proteins carry glycosylphosphatidylinositol (GPI) tails that are important for their localization to membranes and PD [38],[36]. *I*ndeed, GPI anchors are primary signals for PD localization of membrane proteins [39]. Concordant with these recent findings,

PD-associated proteins and PD-localized proteins with roles in lipid trafficking and metabolism have been found to be crucial players in facilitating viral cell-to-cell movement, as will be seen in the following discussion.

Beyond allowing the movement of viruses themselves, PD are also essential for the plant responses to virus infection. *A* critical component of these defense responses is mediated by small RNA molecules. siRNAs move ahead of viruses to initiate defense signals [40], [41]. These siRNAs move cell-to-cell via PD [42]. *L*ittle is known about how these small RNAs affect PD, and so they will not be discussed in this review. Instead, here we discuss what is known about how viruses and viral proteins interact with cell components to manipulate PD for their movement between cells. The literature covering this topic is extensive and we may have inadvertently excluded interesting work from some of our colleagues and we apologize in advance for this oversight.

## MECHANISMS FOR VIRAL MOVEMENT

The primary goal of most plant viruses during infection is to reach the vasculature and spread systemically throughout the plant. The mechanisms of cell-to-cell movement viruses have evolved to achieve this goal are diverse [reviewed in [43]]. The majority of plant viruses encode proteins known as movement proteins (MPs) that are responsible for facilitating the trafficking of the virus to and through the PD. MPs are structurally diverse proteins that perform the same functions: 1) interact with viral genome, 2) target to PD, 3) modify PD function by increasing the trafficking capacity of PD to allow egress from infected

cells and entry into neighboring cells, a process referred to as gating. The major strategies for movement are described below.

***Mobile ribonucleoprotein complexes***

Many viruses have evolved to spread cell-to-cell as ribonucleoprotein complexes (RNP). The best-studied example of this group is TMV, which encodes a 30kDa movement protein (MP30) that binds to RNA in a sequence-independent manner and facilitates the movement of the viral genome to and through PD [Figure 2B and C, [44], [45], [46], [47]]. MP30 localizes to PD and is sufficient to gate PD in the absence of the virus [44], [48], [49]. MP30 also localizes to the ER of infected cells [50], [51] and is involved in the formation of viral replication centers (VRCs) [52], [51]. Early work investigating the structure of MP30 proposed that it was an integral membrane protein that is inserted into the ER membrane [53]. This study revealed that MP30 consists of two hydrophobic alpha helical domains that likely exist as transmembrane domains. More recently, it has been shown that MP30 associates with membranes but is not a transmembrane protein and mutations that enhanced the membrane association inhibited movement [54]. This finding suggests that MP30 acts as a peripheral ER-membrane protein that promotes movement to and through PD. *M*ovement of the TMV RNP was shown to occur via diffusion along the ER membrane with the assistance of various cytoskeletal elements, which will be discussed in greater detail later [55], [15]. In addition to MP30, the TMV replicase has also been implicated in intercellular movement [15], [56]. MP30 and the replicase

collectively associate with the RNP that moves along the desmotubule to traverse the PD (Figure 2B and C). Additionally, a PD-targeting sequence within the N-terminus of MP30 was recently identified [57]. They showed that this 50 amino acid motif was responsible for targeting the RNP to PD, but not for insertion into the PD [57].

Some viruses have evolved to make use of multiple MPs. This is typified by the triple gene block (TGB) viruses (Figure 2D). These viruses encode three separate movement proteins in overlapping ORFs that are involved in different steps of virus replication and movement. Tilsner et al. proposed a new model for potato virus X (PVX) replication and intercellular movement whereby the TGB proteins promote co-replicational insertion into the PD [58]. In this model, TGB2 and 3 are recruited to the openings of PD to promote the formation of ER-derived replication complexes that are associated with the PD [58]. PVX also requires the CP for intercellular movement [59]. The CP of PVX localizes to PD but does not gate the pore [59]. Instead, TGB1 gates PD and is required for the insertion of the CP into the pore [58]. Thus, all three TGB proteins as well as the CP are required for intercellular movement of PVX.

In addition to the MPs, some plant viruses require other viral proteins for efficient cell-to-cell and long-distance spread [60], [61], [62], [63], [64]. This model is best exemplified by the potyviruses, which do not encode a true movement protein, but rely on a group of viral proteins for intercellular movement [65]. The capsid protein of tobacco etch virus (TEV) is required for cell-to-cell and

long distance movement of the virus [60]. Mutations to the C-terminus of the capsid protein resulted in accumulation of encapsidated virions in infected protoplasts, but the virus failed to spread cell-to-cell or long distances [60]. Movement was rescued by expressing wildtype (WT) capsid proteins in the infected plants. The Cylindrical inclusion (CI) protein has also been implicated in potyvirus movement [66], [62]. This protein forms cylindrical structures at the PD to promote spread of the virus. Additionally, the P3N-PIPO protein has also been implicated in the establishment of these PD-associated cylindrical inclusions [64]. Disruption of either protein blocked proper localization of CI to the PD. Localization of this complex to PD has been proposed to occur through an interaction between P3N-PIPO and a PM-associated cation-binding protein, PCaP1 [67].

***Tubule forming viruses***

Some viruses move cell-to-cell as virions [43]. The MPs and sometimes coat proteins of these viruses oligomerize to form specialized structures called tubules that displace normal PD contents for the transport of intact viral particles or virions [Figure 2E, [68]]. When expressed in protoplasts, the movement proteins of these viruses oligomerize and project from the surface of the PM forming tubule-like structures, indicating that tubule formation occurs independently of PD, [69], [70], [71]. While transmission electron microscopy (TEM) has allowed the observation of these tubules, the details about how they form and displace PD content in intact leaves remain elusive. A study of cell-to-cell movement of

broad bean wilt virus 2 used TEM combined with tomography and immunohistochemistry to examine tubule formation by the MP VP37 [72]. During broad bean wilt virus 2 infection, tubules formed predominantly at PD connecting mesophyll cells, with simple PD more likely to be used for tubule formation than branched PD. Other changes caused by VP37 tubules include changes in the callose and cellulose content of the cell wall and an increase in the diameter of the PD containing VP37 tubules versus those without tubules. The adoption of advanced electron microscopy and other super-resolution imaging modalities will be indispensable for elucidating how viral MPs modify PD for tubule formation.

***Mobile Vesicular Replication Complexes***

Many animal viruses are known to utilize host membranes or membrane-derived vesicles for budding from an infected cell and entry into healthy cells [73], [74], but this mechanism is largely absent in plant virus infection. One exception is the potyvirus, turnip mosaic virus (TuMV). TuMV has been proposed to move cell-to-cell as a vesicular replication complex [Figure 2, [65]]. In this model, TuMV utilizes the host endomembrane system to develop membranous complexes that are mobile between cells. The TuMV 6K2 protein induces vesicle formation during infection and these vesicles are mobile within and between cells [75], [65]. In addition, these vesicles contain both the viral RNA and the RNA polymerase [65]. To date, TuMV is the only plant virus proposed to utilize vesicles for intercellular movement. This movement likely occurs through PD, but it is

currently unclear what changes would be needed in order for PD to accommodate the movement of this complex.

***Phloem-limited viruses***

While many plant viruses move systemically throughout their plant hosts, some viruses remain exclusively within the vasculature. These viruses are referred to as phloem limited, and they can move from the companion cells into the sieve tube, but are incapable of being unloaded from the phloem into sink tissues. Potato leaf roll virus (PLRV) is a well-studied phloem-limited virus. Early studies proposed that the PLRV genome did not encode a MP (Harrison et al., 1990) but later work identified a MP of 17 kDa (MP17) that localizes exclusively to branched PD in source tissues, but fails to move cell-to-cell efficiently [Figure 2C, [76], [77]]. When expressed in sink tissues where branched PD are relatively scarce, MP17 is targeted for degradation through the proteasome [17], [77]. The reason why these viruses are unable to unload from the phloem is unclear, but it has been proposed that the MPs of these viruses are incapable of gating PD at the interfaces of the vasculature and surrounding tissues. This model is supported by experiments showing that co-infection by PLRV and non-phloem-limited viruses triggered increased spread of the PLRV into the surrounding parenchymal tissue [78]. Interestingly, when MP17 was constitutively expressed in tobacco and potato plants, defects in sugar allocation were observed [79]. *T*hese plants also had decreased photosynthetic efficiency in source leaves possibly due to accumulation of soluble sugars rather than their export to sink

tissues [79]. The PD in source tissues expressing MP17 were indistinguishable from those in WT plants, but the PD in the phloem appeared enlarged in the presence of MP17 [79]. The reasons for sugar accumulation in source tissues remains to be determined, but further supports the hypothesis that MP17 is incapable of gating PD outside of the phloem. Recent work on citrus tristeza virus has implicated the accumulation of reactive oxygen species (ROS) in the phloem restriction of the virus [80]. Viral p33 was identified as important for initiating the ROS burst observed during infection. Deletion of p33 resulted in decreased ROS accumulation and the mutant viruses invaded the xylem and altered vascular development [80].

## HOST PROTEINS AND PLASMODESMATA

As obligate intracellular parasites viruses rely on their hosts to provide the majority of the cellular machinery they need to complete their infection processes. This has been well documented for replication and the assembly of viral replication factories (reviewed in, [81], [82], [83]. This is also true for cell-to-cell movement via PD. *N*umerous host proteins that are recruited by viruses to facilitate their movement have been identified. These can be divided into broad categories of proteins with roles in cell wall metabolism and modification, those associated with the plasma membrane and the endomembrane systems, cytoskeletal proteins, and proteins from other compartments.

***Proteins involved in cell wall metabolism and modification***

PD are integral components of the cell wall. *I*t should therefore not be surprising that proteins that modify the plant cell wall would be involved in changing the properties of PD, including as it relates to viral intercellular trafficking. *E*xpansins are a class of proteins involved in inducing cell wall creep and extension but whose enzymatic function remains elusive [84]. The α-expansins are responsible for acid-induced extension of cell walls but do not weaken them [84]. An α-expansin, NbEXPA1, was identified among PD-enriched proteins whose levels were specifically altered during TuMV infection of *N. benthamiana* [35]. *N*bEXPA1 localized to PD and VRCs, and its accumulation was decreased in TuMV-infected tissues. Concordantly, overexpression of NtEXPA1 increased replication and cell-to-cell movement of TuMV and another potyvirus plum pox virus while silencing NbEXPA1 reduced replication and systemic spread of TuMV. *N*bEXPA1 is likely a host factor for potyviral replication and cell-to-cell spread. This finding suggests that NbEXPA1 has an important role in cell wall modifications that are involved in establishing PD and their functions.

Besides expansins, reversibly glycosylated polypeptides (RGPs) have been implicated in both cell wall metabolism and virus infection. RGPs are Golgi-localized proteins that are involved in cell wall biosynthesis through their actions as mutases, converting different forms of arabinose into arabinofuranose for inclusion in the cell wall [85]. *A* PD-localized class 1 RGP (SE-WAP41) was first

identified in maize seedlings, and the Arabidopsis homologs were found to localize to both Golgi and PD, suggesting Golgi-to-PD trafficking as a specific route for PD targeting of proteins [86]. Constitutive expression of AtRGP2 fused to GFP resulted in plants with increased callose deposition at PD, stunting and carbohydrate accumulation in leaves along with chlorosis and reduced viral cell-to-cell movement [87]. Conversely, silencing RGPs in *N. benthamiana* resulted in increased rates of systemic spread of TMV-GFP [88]. *A*nother cell wall metabolism enzyme implicated in regulating intercellular communication via PD includes the putative glycosyltransferase KOBITO1 [KOB1, [89]], but no role in viral infection has yet been described for this protein. KOB1 has instead been implicated in regulating intercellular communication during stomatal development.

***Proteins with roles in callose metabolism***

Callose, a β-1, 3-glucan, plays important roles in influencing intercellular trafficking via PD. The accumulation of callose in the cell wall surrounding PD is associated with decreased trafficking through PD, while its removal is often correlated with increased PD flux (reviewed by [90], [91], [92]). These observations have been interpreted as callose accumulation leading to a physical constriction of PD pores, occluding the cytoplasmic annulus that serves as the principal route for intercellular trafficking [27], [30]. *R*ecently, innovative experiments addressing the biophysical parameters of callose-cellulose interactions have raised intriguing questions about this simple interpretation of

callose accumulation at PD. *I*n vitro mixtures of callose and cellulose displayed non-ideal behavior, and further analyses revealed that callose increases the elasticity of crystalline cellulose [93]. These findings should prompt a re-examination of the function of callose in the cell wall and the mechanism by which it acts to regulate PD.

Callose synthesis is carried out by callose synthase (CalS) enzymes, also called glucan synthases (GLSs) while its degradation is mediated by β-1, 3-glucanases (BGs) [90], [94], [92]. *C*alSs/GSLs and BGs are important in mediating the outcomes of plant-pathogen interactions, especially in plant-virus interactions. *T*ransgenic tobacco plants in which expression of the class I BG was silenced by antisense technology had increased deposition of callose resulting in decreased cell-to-cell movement of TMV [95], [96] and PVX [96] as well as that of the 3a MP of cucumber mosaic virus (CMV) [96]. Refining the role of these enzymes in regulating PD, several of them have been localized to PD. At_BG_ppap was identified from purified Arabidopsis cell wall fractions enriched for PD [38]. While At_BG_ppap was found to be essential to controlling turnip vein clearing virus (TVCV) infection, it was constitutively expressed [97]. Curiously, infection by TVCV induced expression of other BGs, *AtBG2* and *AtBG3* that had no apparent role in viral infections.

The PVX TGB protein, TGB12K, required for cell-to-cell movement along with the viral CP and other TGB proteins, increases PD trafficking independent of virus infection [98]. TGB12K-interacting proteins 1, 2 and 3 (TIP1-3) that were

identified as interacting with the movement protein of PVX also interacted with a BG [99]. TIP1 is a cytoplasmic ankyrin repeat protein. *T*he ankyrin protein, ANK1 from tobacco, promotes cell-to-cell movement of the TMV MP and the virus, with increased rates of systemic spread in plants with increased ANK1 levels [100]. Like Tip1, ANK1 is a cytoplasmic protein, but it was recruited to PD where it interacted with TMV MP and acted with TMV MP to reduce callose accumulation at PD. Thus, plant viruses subvert the function of host BGs to facilitate their cell-to-cell movement.

Other PD-localized proteins with roles in callose synthesis or removal are also important for determining the outcome of viral infections. *T*he PLASMODESMATA-LOCATED PROTEIN (PDLP) proteins were identified as PD constituents in a proteomic analysis of a PD-enriched cell wall fraction from Arabidopsis cultured cells [33]. *T*ubule-forming viruses recruit PDLPs for tubule formation for their cell-to-cell movement [101]. The 2B MP of grapevine fanleaf virus (GFLV) was found to interact with PDLP1 at PD. *I*n the pldlp1/2/3 triple mutant cell-to-cell movement of GFLV was reduced, and systemic movement of GFLV and the unrelated cauliflower mosaic virus were significantly delayed. *F*urther analyses of the GFLV-PDLP interaction revealed a role for myosins XI-K and XI-2 in delivery of PDLPs to PD, uncovering a previously unknown route of intracellular targeting [13]. *B*esides tubule forming viruses, PDLP5 may also be important for interactions with other viruses. *T*here was increased cell-to-cell movement of TMV MP30 in pdlp5-1 mutants [102], suggesting that this protein is

important for many viruses although this has not yet been experimentally verified. In addition to being receptors for viruses, PDLPs are now known to be essential components of plant defense responses. PDLP5 is induced by bacterial infection and was originally identified by its induction in response to the Pseudomonas syringae effector as HOPW-1-1 INDUCED GENE 1 [HWI1, [103]]. PDLP5 is required for salicylic acid (SA)-induced accumulation of callose at PD [104]. *P*DLPs are also important for systemic movement of defense molecules required for systemic acquired resistance [SAR, [105], [106]]. *O*verexpression of PDLP5 led to reduced PD trafficking of azelaic acid (AzA) and glycerol-3-phosphate (G3P) and impaired SAR [106]. *S*imilarly, the systemic movement of the essential SAR protein DEFECTIVE IN INDUCED RESISTANCE1 (DIR1) was lost in plants overexpressing PDLP1 or 5, leading to compromised SAR [105]. *A*n interesting additional observation was that trafficking of AzA and G3P was not impaired in Arabidopsis pdlp mutants, but SAR was lost [106]. This result suggests that beyond their roles in regulating PD trafficking by callose, PDLPs may also be components of signaling pathways. This is further supported by the observation that PDLP5 interacts with AZI1 at PD [106]. *T*he role of PDLPs in SAR to viruses has not yet been explicitly addressed.

***Other PD-associated proteins***

Plasmodesmal associated protein kinase (PAPK), a casein kinase purified from PD enriched cell wall fractions, phosphorylated some non-cell autonomous proteins, including TMV MP30 [107]. *T*MV MP30 was phosphorylated at its C-

terminus [108], and this post-translational modification was found to regulate the protein's cell-to-cell movement in at least some hosts [109]. When the phosphorylated sites on the C-terminus (Ser258, Thr261 and Ser265) were replaced with aspartate residues to copy the effect of phosphorylation and this mutant was subsequently transferred to TMV, the phospho-mimic TMV failed to move cell-to-cell or systemically in N. tabacum plants but retained this ability in *N. benthamiana* , N. clevelandii and N. glutinosa [110], [109]. Further studies with mutant MP30s carrying different phospho-mimic patterns revealed that phosphorylation directed the intracellular targeting of MP30, and mutants with strong associations with PD were more likely to move intercellularly, but those localized to ER, microtubules (MT) or ER+MT were less likely to move [110]. Thus, phosphorylation is an important strategy for controlling viral subcellular localization and cell-to-cell spread. Other proteomic analyses have subsequently identified three potential PD-associated kinases, but these were receptor like kinases and their roles in viral infection have not yet been explored [33]. Calreticulin is a conserved ER protein that functions to sequester calcium (Ca2+), the ubiquitous second messenger. *I*mmunolocalization studies revealed that calreticulin associated with PD in maize roots [111]. It was speculated that the association of calreticulin with PD is due to the ER strand, the desmotubule, which is found in most PD [112]. Calreticulin binds to TMV MP30 and, consistent with this observation, increased intracellular Ca2+ levels prevented targeting of MP30 to PD and reduced viral cell-to-cell movement [113].

Pectin methylesterases (PMEs) are cell-wall-associated enzymes that are expressed ubiquitously in plants and are crucial for the remodeling of plant primary cell walls. A tobacco PME was found to interact with TMV MP30 and to also have RNA binding activity [114], [115]. PME also interacted with the MPs of TVCV and cauliflower mosaic virus [114]. Importantly, loss of the TMV MP30 that bound to PME abrogated viral cell-to-cell movement [114]. *F*urther, silencing of PME in the vasculature of tobacco plants inhibited viral movement from the vasculature into neighboring tissues [116]. Together, these results suggest that PME is co-opted to act as a receptor for viral movement, similar to the case of PDLP1.

***Proteins with roles in lipid and membrane metabolism***

***REMORIN***

Perhaps the best understood host membrane protein with a role in virus infection is Remorin (REM), a plant-specific lipid raft and PD protein [117]. First discovered in potato, REM is a small hydrophilic protein that is anchored to the cytosolic face of the plasma membrane and is a component of detergent-insoluble membrane (DIM) fractions from many systems [117], [118]. *P*otato REM, StREM1.3, clusters in microdomains of the plasma membrane and is also found along the length of PD [117]. *W*hile overexpression or silencing of StREM1.3 produced no obvious phenotype in transgenic tomato plants, changes in StREM1.3 expression greatly influenced the outcome of viral infection. Plants with increased StREM1.3 levels had smaller infection foci and severely reduced

systemic movement of PVX, with the inverse observed in plants with reduced REM levels. *C*onsistent with a putative role for REM in cell-to-cell movement of PVX, StREM1.3 interacted with the PVX TGB1 protein [117]. *W*hen transiently expressed, StREM1.3 inhibited the PD-gating abilities of not only PVX TGB1 but also those of TMV MP30 and potato virus Y Hc-Pro [119]. These results support earlier work that identified phosphorylation and binding polyanions as important similarities between REM and TMV MP, suggesting a role for REM intercellular trafficking [120]. *I*ndeed, phosphorylation of StREM1.3 by the calcium-dependent kinase CPK3 modulates REM1.3 localization and association with PD [121].

S-acylation (palmitoylation) of cysteines for plasma membrane targeting has been demonstrated for soybean REM, SYMREM1 [122], and rice GSD1 involved in partitioning photoassimilates [123]. The Arabidopsis homolog of StREM1.3 is also S-acylated [124]. *NbREM1* is a negative factor in RSV infection where it acts to limit viral cell-to-cell movement [94]. S-acylation of *NbREM1*, was downregulated by rice stripe virus (RSV) and *NbREM1* was turned over by autophagy during RSV infection as the virus tried to overcome *REM*-mediated resistance.

Unlike StREM1.3, tobacco REM (Nt(sNN)REM1.2) is usually uniformly distributed in the plasma membrane, possibly due to a weaker association with lipid rafts [125]. Expression of the tomato mosaic virus (ToMV) MP, replicase or virus itself led to Nt(sNN)REM1.2 aggregation at sites close to the ER and VRCs [125]. Nt(sNN)REM1.2 likely interacts directly with ToMV MP in the vicinity of PD,

although no clear association with PD has been reported. *T*he study authors suggest that Nt(sNN)REM1.2 may help direct MP to move to PD from the plasma membrane. Transient expression of Nt(sNN)REM1.2 promoted viral cell-to-cell movement, suggest that unlike the case with StREM1.3, Nt(sNN)REM1.2 may have a positive role in viral infection. *T*he group 4 remorins are less studied than the group 3 remorins. Arabidopsis group 4 remorins, AtREM4.1 and 4.2, are important for geminivirus infection [126]. *T*he atrem4.1 atrem4.2 double mutants were less susceptible to infection by beet curly top virus and beet severe curly top virus suggesting that the AtREM4s are positive regulators of susceptibility. *I*n this system, AtREM4s were found to interact with the immune regulator SnRK, leading to phosphorylation of AtREM4.1. Additionally, AtREM4.1 was found to be a substrate for degradation by the 26S proteasome [126]. Thus, REMs have multiple, diverse roles in modulating the outcome of viral infections, again revealing the complexity of PD-virus interactions.

***SYNAPTOTAGMIN A***

Another plasma membrane protein involved in viral cell-to-cell movement and infectivity is SYNAPTOTAGMIN A (*SYTA*). *SYTA* interacts with the MPs of TMV and the unrelated cabbage leaf curl virus (CaLCuV) [127]. *W*hen *SYTA* expression is repressed, cell-to-cell movement of both MPs is decreased and systemic infection by CaLCuV is delayed, suggesting that *SYTA* facilitates viral cell-to-cell movement. Similar results were observed for the distinct proteins involved in movement of TuMV (P3N-PIPO) and the TVCV MP, suggesting that

SYTA is a general, key factor for MPs [128]. SYTA localizes to ER-PM contact sites and regulates endocytosis. These contact sites are recruited to PD to allow viral cell-to-cell movement, as revealed by studies with the TVCV MP [129]. Consistent with this model, SYTA interacted with the PD localization signal (PLS) of TMV [57]. *T*MV PLS is a 50-amino acid sequence located in the N-terminus of TMV MP that is necessary and sufficient for MP targeting to PD, that does not mediate the movement of the MP through PD [130]. In *SYTA* knockdown plants, TMV PLS failed to target the MP to PD [57].

***Chloroplast-related proteins***

Chloroplasts are hubs for mediating the outcomes of a plethora of plant-microbe interactions [131], [132] and viruses are no exception [133]. Many plant defense responses to pathogens, including viruses, are initiated by chloroplasts and encompass defense hormones whose synthesis is initiated in chloroplasts or are largely the products of chloroplasts. In addition chloroplasts are also sources of numerous signaling molecules like ROS, retrograde signals that transit to the nucleus to control nuclear gene expression, and molecules that act systemically to initiate distal defense responses [131]. It is perhaps not surprising then that chloroplasts are the targets of pathogens as they attempt to disrupt chloroplast-mediated defense. Viruses have long been known to disrupt chloroplasts, and this has been viewed as a critical first step in a successful infection [134]. Not only do viruses directly damage chloroplasts but they also manipulate expression of nuclear genes involved in chloroplast development. One example of this

comes from turnip yellow mosaic virus whose P69 protein interacts with and suppresses the activity of the GOLDEN LIKE (GLK) transcription factors that are critical for chloroplast development [135].

With modern molecular tools, we are now able to test for direct interactions between viral proteins and host proteins. Numerous interactions have been documented [for reviews see, [134], [133]]. Several of these interactions are necessary for the cell-to-cell spread of viruses. Rubisco activase (RCA) and ATP-synthase γ-subunit (AtpC) were isolated in a mass-spectrometry based screen for proteins interacting with the replicase and VRCs of TMV [136]. Expression of both Rca and AtpC genes was suppressed by up to 50% in TMV or TVCV-infected tissue, while infection with CMV or PVX did not change their expression. Virus-induced gene silencing of Rca or AtpC increased the intercellular movement and/or accumulation of TMV and silencing of AtpC enhanced cell-to-cell movement of TVCV. Thus, RCA and AtpC seem to be required specifically for determining the outcome of tobamovirus infections, and they are likely involved in mediating antiviral defense [136]. *H*owever, chloroplasts may have more direct relationships with PD function during infection. This is illustrated by possible physical connections between chloroplasts and PD, and signaling between chloroplasts and PD via the nucleus.

***Chloroplast tubules: Stromules***

Stromules are narrow tubular extensions of chloroplasts, consisting of stroma surrounded by the chloroplast envelope [137]. *T*hey are proposed to

carry out numerous functions in plant cells that allow intracellular communication and distribution of metabolites and signaling molecules, particularly during stress [137]. The MP of abutilon mosaic begomovirus (AbMV) interacts with chloroplast localized HSC70 (cpHSC-1) and induces stromules that extended from the chloroplast body to the cell periphery [138]. cpHSC-1 formed homoligomers that localized to both the chloroplast stroma and stromules. Similarly, the AbMV MP also oligomerized in the chloroplast. Silencing of cpHSC-1 using VIGS led to patches of chlorotic tissue that were correlated with reduced viral DNA, suggesting that AbMV may use cpHSC70 as a chaperone for cell-to-cell movement. Curiously, the localization of PDCB1:mCherry to PD, visible as punctae, was abrogated in AbMV-infected tissue and instead PDCB1:mCherry labeled the apoplast [139]. These results suggest a complex relationship between the geminivirus and chloroplasts for intercellular movement via PD. *K*renz and co-workers proposed a model in which AbMV infection induces the formation of a network of chloroplast stromules that connect with the nucleus and cell periphery, presumably at PD, for intra- and eventual intercellular viral movement. The clustering of chloroplasts around nuclei has been observed during numerous infections including DNA viruses beet curly top virus, tomato yellow leaf curl virus and the RNA virus tobacco rattle virus [140]. However, the formation of stromules was not examined in this study and so the role of stromules in intracellular and intercellular movement was not addressed.

### *Chloroplast proteins controlling PD*

Apart from direct roles in defense responses, chloroplasts may also affect the outcome of plant-virus interactions through their role in modulating PD formation and function. Studies with the chloroplast DEVH RNA helicase *ISE2* have revealed that changes in chloroplast gene expression can have significant effects on PD [141], [142], [143], [144]. This may be mediated by retrograde signals from the chloroplast acting to modulate expression of nuclear genes important for PD formation and function, referred to as Organelle-Nucleus-PD signaling (ONPS) [145], [142]. In *N. benthamiana* plants where *ISE2* was silenced by VIGS, there was increased intercellular trafficking between the epidermis and mesophyll of not only the 2XGFP probe but also of the TMV MP30 [143]. Consistent with this, systemic spread of TMV-GFP and TuMV-GFP was increased in those plants [146]. *T*his increased movement may be due to the increased numbers of twinned and branched PD connecting the epidermis and mesophyll in those silenced plants [143]. Curiously, stable transgenic plants with increased *ISE2* expression, while showing reduced intercellular trafficking of the 2XGFP probe, also had increased rates of viral systemic spread [146]. With the exception of jasmonic acid-mediated responses, no other differences between defense responses in wild type and *ISE2*-overexpressing plants were observed. These results suggest that the interplay between chloroplasts and PD is complex, warranting further exploration. Further, the link between chloroplasts and PD is supported by studies with bacteria and the PDLP proteins, which

reveal a critical role for chloroplast-generated ROS and salicylic acid in mediating callose deposition at PD in response to infection [102], [104], [147].

***Chaperones***

The chaperones HSP70 and HSP90 are crucial players in viral replication and cell-to-cell movement [148]. The HSP70 homolog encoded by the beet yellows virus is involved in viral replication and, as the viral MP, is targeted to PD by the class VIII myosins [149], [150]. Two heat shock cognate 70 (HSc70) proteins from Cucurbita max PD-enriched cell wall fractions were also found in the phloem [151]. When these proteins were purified and microinjected into leaves, they were able to move cell-to-cell through PD, but a third isoform that was not originally identified in the phloem failed to do so. Subsequent analysis identified a C-terminal motif, the SVR motif, on the two non-cell-autonomous Hsc70s that was likely responsible for trafficking. Support for the capacity of this motif to potentiate PD trafficking came from experiments in which the addition of this motif to a human Hsc70 conferred the ability to move from cell to cell, albeit with function limited to chaperones [151].

An HSP-90 cochaperone SGT1 (suppressor of G-two allele of SKP1) is well known for its role in immune receptor-mediated defense responses, where it acts a chaperone to confer stability on immune receptor (Resistance or R) proteins [152]. However, SGT1 interacted with the NSm protein of tomato spotted wilt virus (required for viral cell-to-cell and systemic movement) and in contrast to other systems, silencing SGT1 expression restricted local and systemic spread of

the virus [153]. Recently, SGT1 was also found to interact directly with the TMV 126-kDa-replicase in proximity-dependent biotin identification assays, although this interaction was weak and/or transient [154]. *S*ilencing SGT1 increased susceptibility to TMV, as previously reported [154], [155]. It will be interesting to determine what role SGT1 has in mediating viral intercellular movement, whether it is required for protein stability or acts more directly at PD, as has been described for the chaperonin, CCT8. A screen for factors required for the cell-to-cell movement of the developmentally important KNOTTED1 transcription factors identified a mutant allele of chaperonin CCT8, part of the type II chaperonin complex that assists in protein folding [156]. CCT8 was required for protein folding associated with the traversing of PD, suggesting that host proteins that transit PD are unfolded as they passed through the PD pore. cct8 mutant plants had decreased susceptibility to oilseed rape mosaic virus infection, leading to the notion that viral MPs may also be unfolded during PD transit and require CCT8 for refolding on entering newly infected cells [157].

## CYTOSKELETON: GETTING TO OR THROUGH PD

As with most processes that require targeted intracellular movement, movement of many plant viruses occurs in association with the cytoskeleton [reviewed in [158], [159]]. Different viruses rely on different components of the cytoskeleton for their targeting to the cell periphery and PD [158]. Additionally, cytoskeletal elements have been implicated in PD function and therefore may be essential for viruses to traverse the pore [160], [31].

***Getting to the plasmodesmata***

Several studies have illuminated the importance of the cytoskeleton for the transport of viral proteins and replication complexes to the PD. Myosins VIII and XI-2 are involved in the delivery of proteins, including certain viral movement proteins, to the PD [65], [149]. The role of different components of the cytoskeleton in TMV infection has been debated for many years [161], [162], [163]. *S*pread of TMV was shown to be dependent on Myosin XI-2 [164]. *F*urther, disruption of actin and the ER network disrupted TMV MP30 localization to PD [163]. Disruption of microtubules did not appear to affect intercellular movement of TMV [165], [163]. In contrast, additional studies with temperature-sensitive mutants of TMV indicated a possible role for microtubules in the early stages of infection [50], [161]. MP30 accumulated along the lengths of microtubules at the permissive temperature [161]. This accumulation was proposed to inhibit microtubule-dependent intracellular targeting, specifically through kinesin-dependent transport [166]. In addition, mutant plants with reduced microtubule dynamics are more resistant to TMV infection [167]. Considering these contradictory findings, it is clear that the role of cytoskeletal elements in infection by TMV warrants further investigation.

Disruption of actin microfilaments was also found to inhibit TuMV infection by preventing the movement of 6K2 derived vesicles to the cell periphery [168]. Because virus replication occurs at host membranes, it is not surprising that many plant viruses have evolved to utilize the ER and actin networks for

trafficking. As described above, the TGB proteins promote remodeling of the ER into PD associated caps to promote their intercellular movement [58]. Disruption of actin is required for intercellular movement of PVX [158], [169]. Further, TGB2 of PVX localizes to the ER and associates with actin filaments [158] while PVX TGB1 rearranged the endomembrane system and actin cytoskeleton to the X-Body during infection [170].

While some viruses utilize the cytoskeleton for transport, inhibitors of actin, microtubules and the secretory system had no effect on movement of the tubule-forming Cowpea mosaic virus [CPMV, [171]]. Initially, it was proposed that CPMV may localize to the plasma membrane and PD via diffusion, but mutagenesis studies revealed that specific mutations at the C-terminus of the 48K MP of CPMV prevented proper localization and movement [172], [173]). This suggests that an alternative mechanism is employed by this virus in order to target to PD and that these differences may be related to tubule formation. A study on GFLV revealed that a functional secretory pathway and not the cytoskeleton is required for tubule formation but either microtubules or actin filaments are required for the proper targeting of the MP to PD [Figure 2E, [174]].

The PLRV MP17 was shown to interact with different components of the cytoskeleton at different stages of infection [77]. MP17 is delivered to PD in an actin and ER-Golgi-dependent manner, similar to TMV and other mobile viruses [77]. As mentioned above, MP17 is targeted for degradation in sink tissues, and this targeting is dependent on microtubules [77].

In contrast, the mechanisms of delivery of host non-cell-autonomous proteins to PD remain poorly understood. The major exception to this is for the cell-to-cell movement of the transcription factor SHORTROOT. The mechanisms controlling SHORTROOT movement in developing roots, both intra- and intercellularly have been extensively investigated [175], [176], [177], [178], [179]. SHORTROOT is targeted to the PD for transport and that this targeting utilizes a combination of the ER, endosome system and microtubules for transport [177], [178], [179]. Interestingly, cytoplasmic and nuclear localization are both required for intercellular movement of SHORTROOT, as is the GRAS domain of SHR, indicating that there are multiple layers of regulation for SHR movement [175]. Findings from virus research will be crucial to illuminating this fundamental aspect of plant cell biology that remains obscure.

***Getting through Plasmodesmata***

The role of the cytoskeleton in the regulation of PD function has been debated for many years [180], [181], [31]. While it is clear that some molecules, such as fluorescent dyes and GFP, move passively without the assistance of the cytoskeleton, some proteins have been shown to be targeted to PD and be dependent upon the cytoskeleton. Early studies using immunogold labeling revealed that both actin and myosin localize to PD along the full length of the pore [160], [182]. This finding gave rise to the model of PD structure that includes an actin filament that encompasses the desmotubule, [183], [12], [29]. In an early study fluorescent dyes mixed with actin inhibitors were microinjected into

mesophyll cells, and disruption of actin resulted in increased trafficking while stabilization of the actin filaments inhibited trafficking [184]. Interestingly, additional work with actin and myosin inhibitors found that inhibition of myosin but not actin resulted in defects in general intercellular trafficking [185]. A later study revealed that the CMV MP gates PD through the severing of actin filaments and that actin stabilization could block CMV-mediated gating [186]. Because the cytoskeleton targets many proteins to the PD, it is possible that disturbing the cytoskeleton disrupts delivery of PD-resident proteins that are essential for regulating trafficking, complicating the interpretation of observations of treatments that disrupt cytoskeletal function.

## PD DURING VIRUS INFECTION

Heterogeneity in PD is an emerging theme in PD cell biology. Primary and secondary PD have long been recognized [17]. *A*lso, simple and branched PD have distinct trafficking properties in leaves, with simple PD trafficking higher molecular weight dyes than branched PD in leaves [26]. Plant viruses reinforce the idea that PD are not homogeneous but have specialized functions. *T*MV MP30 was found to localize preferentially to branched PD [11]. MP17 from the phloem-restricted PLRV localizes to branched PD when ectopically expressed in leaves [22]. However, when expressed in roots of Arabidopsis TMV MP30-GFP localized to PD, the majority of which were likely primary and simple, while PLRV MP17-GFP was associated with ER, suggesting that it was unable to interact with the simple primary PD of Arabidopsis roots [17]. Other evidence for

developmentally related changes in PD came from studies with MP17 stably expressed in transgenic potato [187]. During senescence leaves revert to a sink-like state and PD in those leaves are no longer targeted by PLRV MP17, suggesting that PD also revert to a state that no longer allows the interaction.

This seeming preference of viruses for one type of PD raises the question of specialization of PD structure. Recent data suggest that PD have different substructures that may dictate their functions. *U*sing TEM and tomography to generate three-dimensional models of PD in the columella cells in Arabidopsis root tips Nicolas and coworkers reported differences in structures of PD. *T*hey described PD with no apparent cytoplasmic sleeve between the central ER rod of the desmotubule and the PM, PD they called Type 1 [25]. Other PD with a more conventional structure with a cytoplasmic space between the desmotubule and PM and the membranes linked by proteinaceous tethers were dubbed Type 2. Type 2 PD were proposed to arise from Type 1 PD as a part of a developmental progression. *C*uriously, in their intercellular trafficking assays, Type 1 PD with no apparent cytoplasmic sleeve had a higher trafficking capacity for small fluorescent dyes and GFP than did Type 2 PD with an obvious cytoplasmic sleeve [25]. Sphingolipid biosynthesis is important for modulating PD function [188]. Loss of PHLOEM UNLOADING MODULATOR (PLM), a protein involved in sphingolipid biosynthesis, resulted in major changes to PD structure and function [188]. Interestingly, *plm* mutants had increased levels of phloem unloading independent of PD number and callose accumulation [188]. Further, PD in *plm*

mutants lacked detectable cytoplasmic annuluses [188]. Together with the description of Type 1 PD, this finding raises major questions about how PD function is regulated. Another example of PD with a novel structure and function comes from studies on phloem unloading in the Arabidopsis root tip. Using serial block face-SEM (SBF-SEM), PD connecting the protophloem sieve elements to the phloem-pole pericycle cells were found to have specialized funnel shapes [189]. Mathematical modeling revealed that these unique PD were necessary for allowing phloem unloading.

Together, these findings about previously unknown structural features of PD highlight the shortfalls in our understanding of basic PD ultrastructure and its relationship to function. However, they also highlight the importance of powerful imaging modalities like three-dimensional imaging and new live-cell imaging approaches in illuminating the details of PD ultrastructure. A few mutants with altered formation of PD have been identified are potentially powerful tools for unraveling the complex relationship between structure and function. Plants with reduced *ISE2* expression have increased numbers of secondary PD connecting the epidermis and mesophyll of *N. benthamiana* leaves [143]. A genetic screen to identify plant proteins with important roles in PD formation and development identified choline transporter-like 1 (CHER1) as essential for accumulation of PLRV MP17 at PD [190]. CHER1 is required for secondary PD formation since in *cher1*-4 mutants formation of epidermal-mesophyll secondary PD in Arabidopsis leaves was severely reduced. While *ISE2*-silenced plants were more susceptible

to TMV or TuMV [146] the effect of *cher1* mutation on viral infection has not yet been reported.

## MECHANISMS OF GATING

During infection, plant viruses increase intercellular trafficking of fluorescent dyes and small diffusible proteins [191], [192], [193], [49]. This phenomenon is referred to as gating and likely promotes the spread of the virus. Despite being the focus of numerous studies, very little is known about how viruses gate PD. Most of what is known about gating comes from work on TMV. The 30K movement protein of TMV (MP30) has been shown to be responsible for gating PD during infection [191], [49]. Gating is limited to the infection front suggesting that the modifications to PD function are reversible [193]. Other movement proteins from different viruses have also been found to gate PD, but others seem to be unable to gate PD. It is currently not clear what the movement proteins of these viruses are doing to gate the PD. Over the years, several models for how viruses gate PD have been proposed and are discussed below.

### *Callose degradation and gating*

Currently, the leading model for virus-mediated regulation of PD proposes that viruses gate PD by altering the pore structure. It has been proposed that this occurs through the localized degradation of callose along the length of the PD [55]. As discussed earlier, this degradation has been attributed to BGs. In this model, the breakdown of callose around the PD allows the pore to dilate, thereby increasing the size of the cytoplasmic sleeve for intercellular movement of the

virus. Alternatively, it has been suggested that the observed decrease in callose during infection results from the suppression of callose synthases [92]. Recently, it has been shown that RNAs derived from the Potato spindle tuber viroid silence the expression of CALS genes in tomato plants [194]. While inhibiting callose deposition at PD may serve as a mechanism to promote viroid cell-to-cell movement, it remains unclear whether viruses utilize this mechanism. As described above, new models of PD have begun to question the importance of the cytoplasmic sleeve in transport [25], [188]. This finding, coupled with the limited electron microscopy evidence for dilation of PD during virus infection, suggests that alternative models for gating may warrant further investigation.

***Gating through modification of macromolecule composition***

One model for PD gating proposes that viruses may gate PD by interacting with or recruiting specific proteins to PD. The role of PDLPs in tubule formation was discussed earlier in this review. It has been proposed that the PDLPs may serve as anchors to the plasma membrane because previous reports show that viral movement protein tubules do not directly interact with the plasma membrane of PD [69]. Earlier work from this same group and others has emphasized the importance of membranes on PD function [195], [37], [25], [196]. Their work has also identified putative tethers that connect the desmotubule to the PM and may be important for regulating PD function [25]. Because of their reliance on host membranes, it will be interesting to see how virus infection affects PD lipid compositions and how changes in the composition impacts virus

spread. Considering the *plm* mutant with altered sphingolipid biosynthesis and PD structure and function [188], it will be interesting to determine the impact of viral MP on the modified PD and how the mutant supports viral infection.

***Gating PD by tubule formation***

While the majority of plant viruses move intercellularly as mobile viral ribonucleoprotein complexes, a subset of viruses move cell to cell as intact virions with the assistance of proteinaceous tubules, [197], [198], [199], [71]. During tubule formation, the majority of the internal structure of the PD is lost and replaced by a tubule composed of the viral movement and coat proteins [72].

Very little is known about how these modifications affect intercellular transport. Poirson et al. showed that transgenic plants expressing the Alfalfa mosaic virus MP exhibited a minor increase in the size exclusion limit of PD compared to control plants [200]. They found that in the presence of the MP, transport of 3kDa and 4.4kDa dextrans increased compared to the control plants, but they noted that this increase was not large enough to accommodate the movement of the virus. Notably, this paper referred to the previously accepted size limit of 1kDa for PD transport. It is now widely accepted that the size exclusion limit of PD far exceeds this previously accepted limit and therefore investigations into the true impact of tubule formation on PD transport are needed.

Conversely, studies on Carrot mottle umbravirus described extension-like structures that were associated with PD that resemble the tubule structures

described for other viruses [201]. These studies also found that plants infected with carrot mottle virus exhibited decreased symplastic movement of fluorescent dyes indicating that the structural changes made to the PD may inhibit trafficking through the PD [202].

***Plasmodesmata formation as a mechanism for gating***

One mechanism for increasing intercellular trafficking that has historically been less discussed is through the formation of new plasmodesmata, or secondary PD formation. The number of plasmodesmata in a tissue has long been correlated with the trafficking capacity of tissues, with tissues with many PD having increased trafficking capacities and tissues with fewer PD exhibiting lower trafficking capacities. As described above, Burch-Smith et al. first demonstrated that disruption of chloroplast RNA processing could result in changes in PD formation [143]. Loss of the chloroplast localized RNA helicase, *INCREASED SIZE EXCLUSION LIMIT 2* (*ISE2*), resulted in increased intercellular trafficking and an increase in the number of twinned and branched PD, indicating elevated levels of secondary PD formation. Overexpression of *ISE2* results in decreased intercellular trafficking via PD, presumably through a decrease in PD formation, but this correlation has not been definitively shown. Because viruses are known to target the chloroplast, it is plausible that viruses could induce PD formation by disrupting chloroplast function. Interestingly, silencing or overexpression of *ISE2* in *N. benthamiana* resulted in increased susceptibility to TMV and TuMV,

indicating that proper control of chloroplast function is somehow important for virus intercellular spread [146].

# III. AIMS OF THE DISSERTATION

The research presented in this dissertation addresses three primary questions regarding plasmodesmata and their regulation.

**1. How does plasmodesmata density relate to intercellular trafficking capacity?**

**2. How do viruses increase intercellular trafficking through plasmodesmata?**

**3. What is the mechanism of secondary plasmodesmata formation?**

Chapters 2 and 3 focus on the results from two primary research articles and a methods paper that describe new tools for quantifying plasmodesmata densities and how these tools have provided novel insights into the regulation of plasmodesmata formation. Chapter four focuses on how viruses increase intercellular trafficking by inducing secondary PD formation. The results from this chapter are being prepared for submission to *Cell Host & Microbe*. Chapter five describes the results of work focusing on the mechanism of secondary PD formation, specifically addressing the cell biology of pore formation. Chapter six is a discussion section that places my results into the broader context of the plasmodesmata literature.

# CHAPTER 2

# SPATIAL DISTRIBUTION OF ORGANELLES IN LEAF CELLS AND SOYBEAN ROOT NODULES REVEALED BY FOCUSED ION BEAM- SCANNING ELECTRON MICROSCOPY.

Disclosure: This portion of my thesis was previously published in the journal Functional Plant Biology by Brandon C. Reagan, Paul J.-Y. Kim, Preston D. Perry, John R. Dunlap, and Tessa M. Burch-Smith.

Reagan, B. C., Kim, P. J. Y., Perry, P. D., Dunlap, J. R., & Burch-Smith, T. M. (2018). Spatial distribution of organelles in leaf cells and soybean root nodules revealed by focused ion beam-scanning electron microscopy. Functional Plant Biology, 45(2), 180-191.

As the first author of the manuscript, I was responsible for sample preparation, image acquisition, image segmentation, and writing the manuscript.

## Abstract

Analysis of cellular ultrastructure has been dominated by transmission electron microscopy (TEM) and images collected by this technique have shaped our current understanding of cellular structure. More recently, three-dimensional analysis of organelle structures has typically been conducted using TEM tomography. However, TEM tomography application is limited by sample thickness. Focused ion beam/scanning electron microscopy (FIB/SEM) uses a dual beam system to perform serial sectioning and imaging of a sample. Thus FIB/SEM is an excellent alternative to TEM tomography and serial section TEM tomography. *A*nimal tissue samples have been investigated much more often than have plant tissues by this technique. Here, we show that FIB/SEM can be

used to study the 3D ultrastructure of plant tissues in samples previously prepared for TEM via commonly used fixation and embedding protocols. Reconstruction of FIB/SEM sections revealed ultra-structural details of the plant tissues examined. We observed that organelles packed tightly together in *Nicotiana benthamiana* leaf cells may form membrane contacts. 3D models of soybean nodule cells suggested that the bacteroids in infected cells are contained within one large membrane-bound structure and not the many individual symbiosomes that TEM thin-sections suggest. We consider the implications of these organelle arrangements for intercellular signalling.

## Introduction

Over the past few decades, the field of cellular biology has been revolutionized by advancements in microscopy. With the development of fluorescent marker proteins, cellular localization studies with confocal microscopy have allowed us to visualize protein movement in vivo. These studies have provided cellular biologists valuable information with regards to where and when proteins perform their various functions in signaling. Ultrastructural analysis of cells and subcellular structures requires a level of resolution that exceeds the diffraction limit in light microscopy. Electron microscopy provides the necessary level of resolution and therefore has been the predominant method for studying subcellular structures. Understanding the spatial relationships between cellular components is a crucial facet to unravelling how these interact with each other

for signal transduction during growth and development, and in response to environmental signals.

The two primary types of electron microscopy used for these studies are transmission electron microscopy (TEM) and scanning electron microscopy (SEM). The TEM uses a beam of electrons to penetrate a sample and can be used to image the interior structures of materials that have been fixed and stained with electron opaque materials such as osmium and other heavy metals. Thus TEM has been the primary method used for studying cellular ultrastructure, and TEM imaging has provided valuable information about cellular structures in two dimensions. Cell ultra-structural analysis can be taken into the third dimension with TEM tomography. This approach uses a series of TEM images of a sample, taken at a range of angles, to construct a 3D projection of the sample called a tomogram. TEM tomography has proven to be very powerful for studying the three dimensional structure of plant cellular components (e.g. [203], [204], [205]. The primary limitation of the application of TEM tomography is sample thickness, typically restricted to about 150-200 nm for a typical TEM operating below 300 kV [206]. One method to circumvent this size limit is to use serial sectioning coupled with TEM tomography of each section [207]. This is a technically difficult and time-consuming technique, and may result in artefacts appearing as a result of imperfections in the microtome blade or other defects in the sections as well as missing sections of the tissue if sectioning is not executed precisely. Cryo-TEM at very low temperatures has taken TEM tomography to the

level of analysing macromolecules, and it has been used to determine the structure of various proteins at near atomic resolution [208], [209]. While this technique has the potential for elucidating the structure of proteins and organelles in a near-native state, there are several limitations to studying larger structures.

In contrast to the TEM, the SEM sweeps a beam of electrons across a sample to generate an image of the surface. The SEM has historically not been used to study internal cell structure, but several methods have been developed that allow researchers to overcome this limitation. Serial block face scanning electron microscopy (SBF-SEM) has recently been implemented to study cellular ultrastructure of various tissues including plant tissues [210], [211]. This technique uses a microtome mounted inside the chamber of the SEM to make serial sections of a sample. The sample is imaged after each slice and the images are then reconstructed into a 3D projection of the sample. This technique, like serial sectioning for TEM, has limitations. Although sectioning is performed within the microscope, imperfections in the blade could result in damage to the sample that could in turn lead to artefacts in the reconstruction.

Focused ion beam scanning electron microscopy (FIB/SEM) has also been utilized in 3D structural analysis of different samples. With this system, a focused beam of gallium ions is used to mill away a layer of the sample and subsequently a beam of electrons is used to capture an image of the newly exposed surface. Using this technique, sequential layers of the sample can be

imaged and removed. The resulting slices can then be reconstructed into 3D projections of the sample. With the gallium ion beam samples can be milled in steps as small as 5 nm, compared to sections of 15-20 nm generated by SBF-SEM. FIB/SEM could therefore produce images with greater resolution in the z axis compared to the SBF-SEM [211]. In theory, the thickness of a sample that can be imaged by FIB/SEM is determined only by the length of time over which samples are collected, overcoming the sample size limitation of traditional 3D TEM studies. Although FIB/SEM has been used in material science research for several decades, its application in the biological sciences is more recent. The first successful use of this technique in the biological sciences occurred in 1993 when Young and co-workers applied FIB/SEM to the study of arthropod internal morphology [212]. Since then, this technique has been used to study ultrastructural features of arthropods and other animal tissues (e.g. [213], [214], [215]). FIB/SEM has also been used in the study of neuronal connectivity in the brain [216], allowing neurobiologists to study the detailed 3D organization of large brain tissue samples, facilitating the study of the elaborate connections formed in the brain of humans and other organisms. It has also been used to study plaque formation in neurodegenerative diseases such as Alzheimer's and Huntington's disease in Drosophila models [217].

While FIB/SEM has been applied extensively to study animal tissues, it has not been widely deployed in EM studies of plant tissues. There have been a few studies examining algal dictyosome ultrastructure [218], [219]. *F*our studies

have reported the use of this technique to examine higher plant tissues. One study looked at regulation of starch granule number and formation [220], two others examined pollen cells [221], [222] and the fourth looked more broadly at large tissue fields and structural differences between different plant tissues [223]. The studies on leaf tissues both used long chemical fixation protocols in the preparation of their samples [220], [223]. These studies demonstrated that FIB/SEM was suitable for use in investigation of higher plant tissues. *H*owever, it is now well established that the long fixation times and harsh aldehydes used during traditional chemical fixation can introduce structural artefacts in plant EM specimens [224]. These artefacts could potentially disrupt features of the sample and therefore alternative fixation protocols are considered more ideal for plant sample preparation. Currently, the gold standard for plant tissue fixation is high pressure freezing coupled with freeze substitution (HPF/FS, [225], [226]. HPF/FS reduces the number of artefacts in plant EM samples and is therefore the preferred method of fixation for plant specimens for ultrastructural studies. HPF/FS has been successfully used to prepare various animal tissue samples for FIB/SEM [227], [228], [229]). After chemical fixation Bhawana and colleagues treated their samples with other stains including tannic acid in an effort to improve contrast in the samples when imaged by the SEM [223]. Here, we show that both HPF/FS and chemical fixation protocols used for TEM sample preparation can be used to prepare samples of various plant tissues for FIB/SEM without additional steps to improve contrast. In this way detailed 3D models of

plant tissues can be generated from samples also used for thin-section TEM to reveal ultrastructural features that are important for plant signalling.

## Results

### *HPF/qFS-prepared samples are amenable to FIB/SEM*

Previous studies have revealed that chloroplasts may generate signals that contribute to the formation and function of plasmodesmata [142], [145]. We were therefore interested in examining the spatial relationship between chloroplasts and plasmodesmata in leaves. *G*iven the large sizes of the chloroplasts and the cell volumes involved, we determined that FIB/SEM would be an appropriate technique for undertaking these studies. Previous work had suggested that plant samples to be examined by FIB/SEM required special handling [223]. However, given that we have used TEM to examine plasmodesmata structure and distribution in leaves [143], we tested whether samples that were prepared by standard protocols for imaging by TEM could also be used to generate samples for FIB/SEM. *W*e therefore prepared *Nicotiana benthamiana* leaf samples using a protocol combining high pressure freezing and quick freeze substitution [230], [231]. *O*ne group of samples was treated with 1% OsO4 and 0.1% uranyl acetate in acetone as the freeze substitution medium, while another was fixed in 4% OsO4. The samples were then embedded in Eponate 12 resin according to the manufacturer's protocol. These samples produced sufficient contrast in SEM images such that several cells and

organelles could be identified including vacuoles, chloroplasts and nuclei (Figure 3(a)). Figure 3(b) shows a series of images from a tomographic reconstruction and in these images details of organelle structure, like the chloroplast thylakoids and nuclear peri- and interchromatin regions are visible. Large vacuoles fill most of the volume of cells two and three. Cell one appears to have several small vacuoles, but it is likely that these represent protrusions from the large central vacuole. *E*very tenth slice of the first fifty slices in the tomogram is shown. Figure 4 shows a series of tomographic images of a dividing chloroplast. They clearly show the chloroplast approaching division with a constriction forming between the two daughter chloroplasts. Individual plasmodesma and pit fields of plasmodesmata are also visible in these images (Figure 5). Progressing through the full stack reveals that these pit fields are fairly expansive in the Z-plane of the cell wall. Even though plasmodesmata are extremely small, with average diameters of 30-50 nm, details of the pores can be imaged with this technique with a low level of detail and plasmodesmata can be counted with ease. *H*owever, detailed analysis of the ultrastructure of these small channels including the desmotubule and associated membranes would likely require use of other electron microscopy techniques such as TEM tomography. More importantly, our results indicate that FIB/SEM could be used for quantitativestudies of the chloroplast-plasmodesmata spatial relationship.

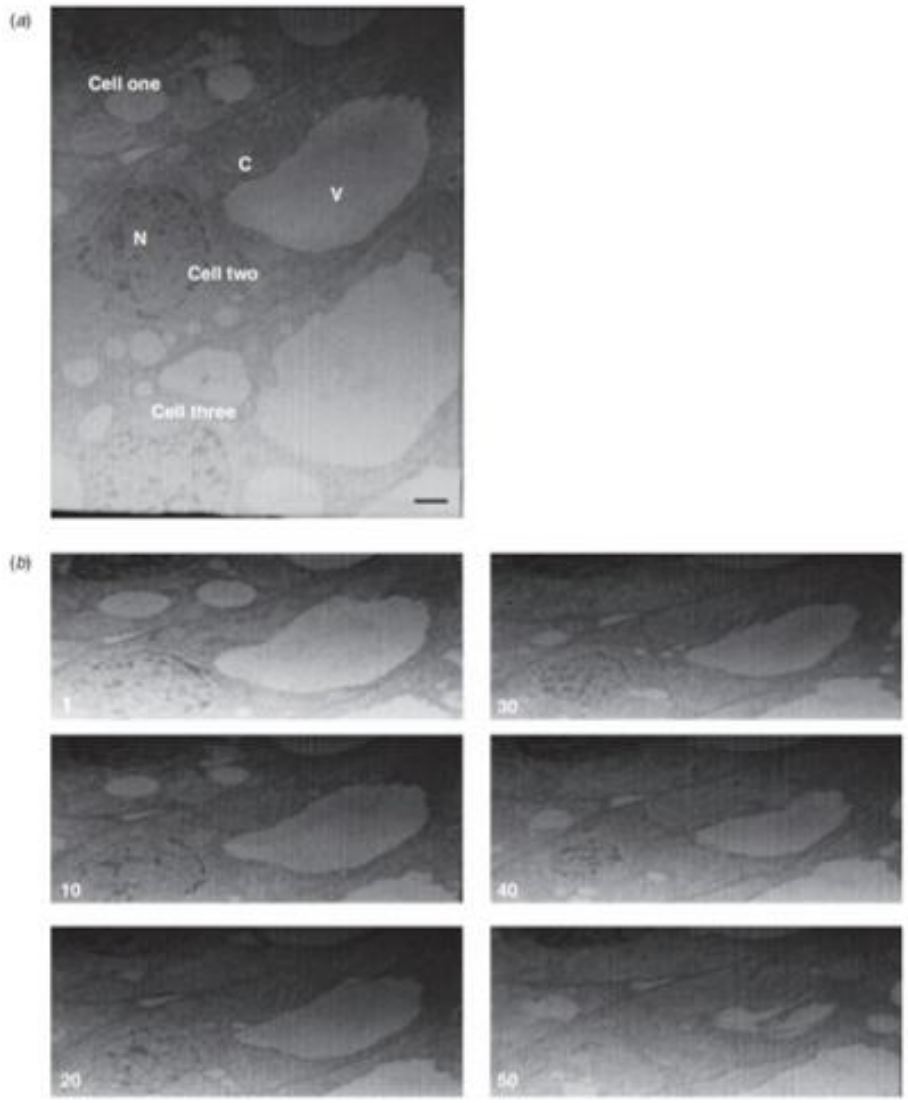


**Figure 3 Tomographic images of young leaf tissue prepared with 1.0% OsO4 and 0.1% uranyl acetate.**

(a) SEM image shows details of three adjacent cells in young leaf tissue. (b) Every 10th image from the first 50 images of the tomogram is shown. Organelles observed include vacuoles (V), nuclei (N), and chloroplasts (C). Images were taken every 20 nm at 10.93k X magnification. Scale bars = 1 μm. Lens vignetting was removed in Photoshop by curves adjusting to generate the figure.

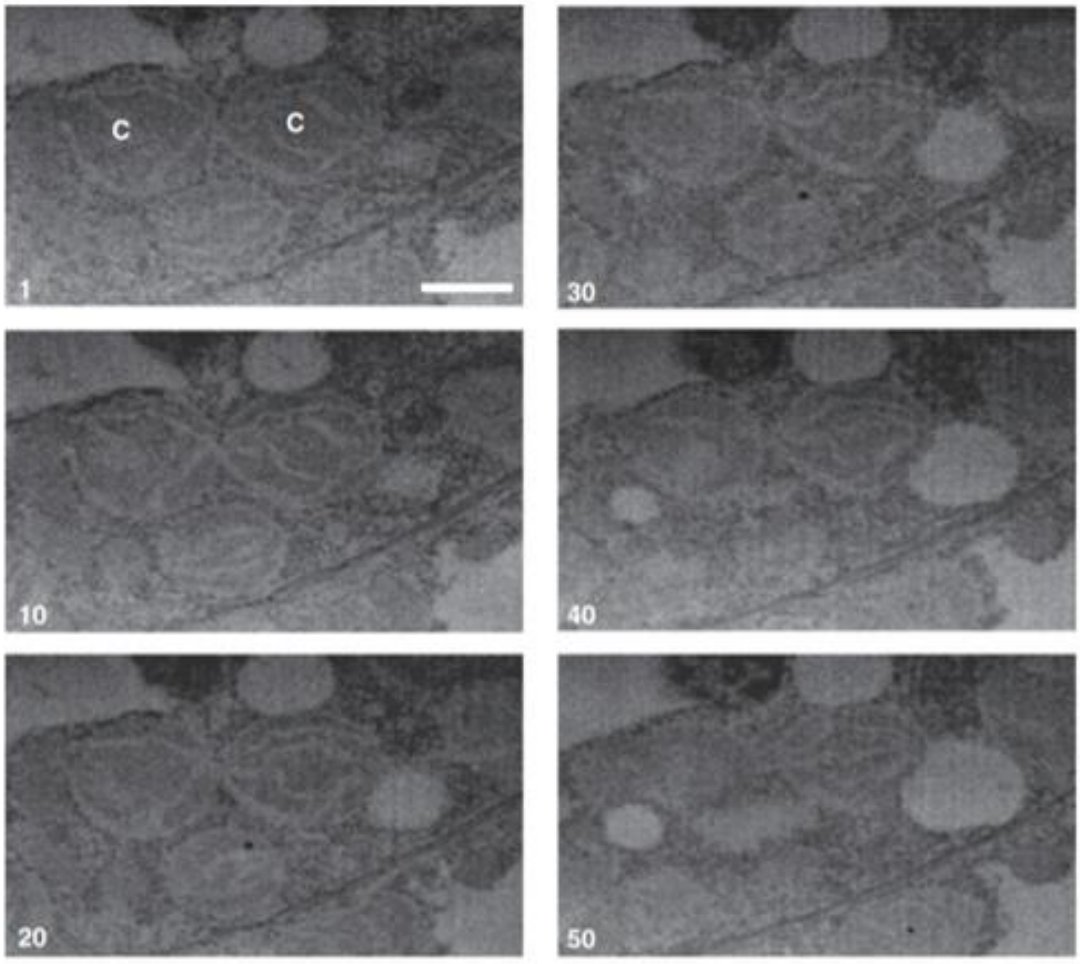


**Figure 4 Dividing chloroplast from leaf tissue prepared in 1.0% OsO4 and 0.1% uranyl acetate.**

Tomographic images of a dividing chloroplast (C). Images were taken every 20 nm. Every 10th image is shown from the first 50 images of the complete stack. Images were collected at 13.04k X magnification. Scale bars = 1 μm. To generate the figure lens vignetting was removed in Photoshop by curves adjusting.

**Figure 5 Pitfields of plasmodesmata in leaf tissue prepared in 1.0% OsO4 and 0.1% uranyl acetate.**

(a) An SEM image reveals the presence of chloroplasts (C) and plasmodesmata (PD). The asterisk denotes a single plasmodesma whose location is indicated in (c) and (d). (b) An overlay of a 3D model on a tomographic image showing cell wall (yellow) and chloroplasts (green). Images were collected at 13.04k X magnification. Scale bar = 1 μm. (c) Pit fields of plasmodesmata are visible in the cell wall between neighbouring cells. The 3D model in (a) was rotated 90° to allow visualization of plasmodesmal openings. (d) Close up view of boxed region in (b).

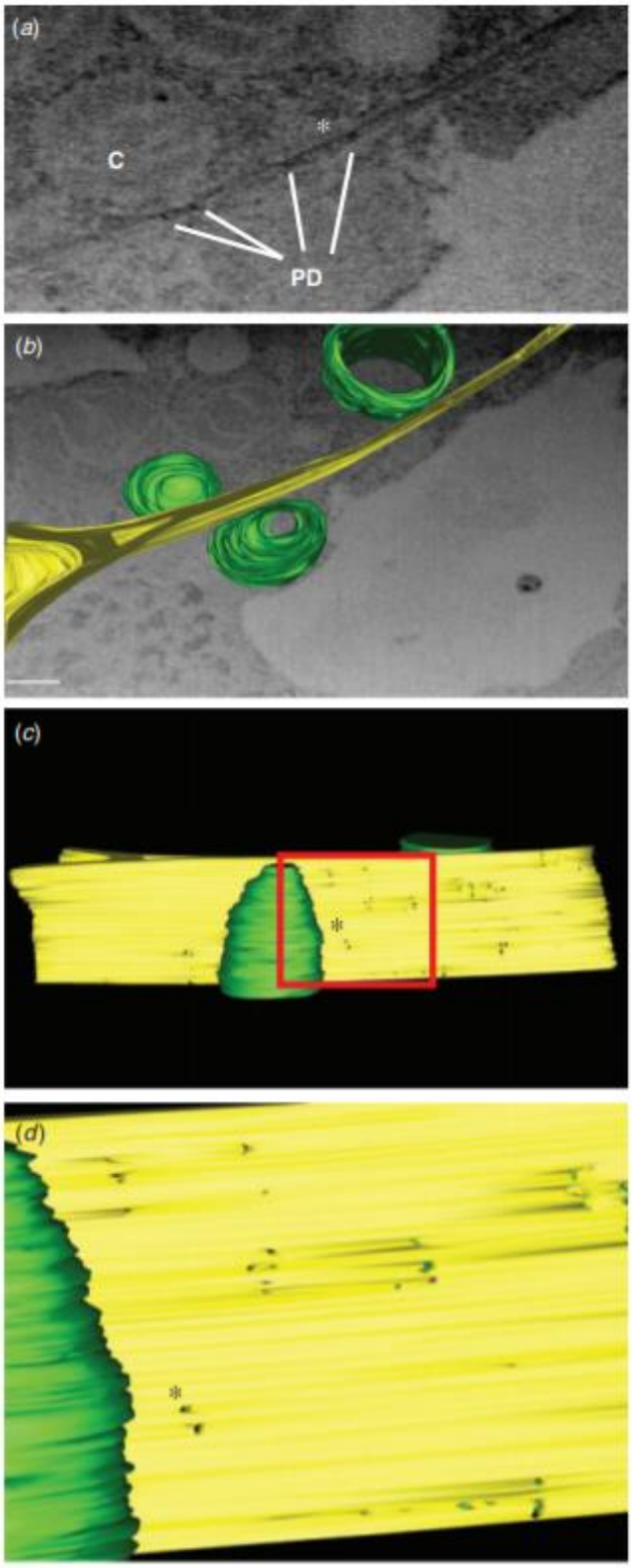
(a)
C
*
PD
(b)
(c)
*
(d)
*

***HPF/qFS with 4% $OsO_4$***

Certain cellular membranes including the ER were not well stained in samples fixed in 1% $OsO_4$ and 0.1% uranyl acetate in acetone, so we used 4% OsO4 in acetone as the freeze substitution medium for other samples. Other fixatives such as low concentrations of tannic acid/ferric chloride could also be used in an attempt to better stain the ER membranes (e.g. [232], [11]. Tomographic images of leaf tissue prepared under these conditions showed even better contrast than those obtained with 1% OsO4 and 0.1% uranyl acetate in acetone FS medium, and improved visualization of ER membranes and other membrane-derived features of the tissue (Figure 6). Tomographic images were collected every 20 nm and every tenth image over the span of the first fifty images of the tomogram is shown (Figure 6). Curtaining effects, or the vertical lines seen in the samples, were more severe in these 4% OsO4 samples than in 1% $OsO_4$ and 0.1% uranyl acetate samples. Curtaining effects are usually caused by defects in the sputter coating or milling face of the sample [233]. Further comparison of samples prepared with 1% OsO4 and 0.1% uranyl acetate compared to 4% OsO4 could address the extent to which the curtaining effect is due to sample preparation. Mitochondria, chloroplasts, and the ER are clearly visible, with chloroplasts showing increased detail in structure compared to the previous samples (Figs. 3 and 4). Large starch granules can also be seen in the chloroplasts and details of the thylakoids are also discernible. *T*he vacuolar contents present as

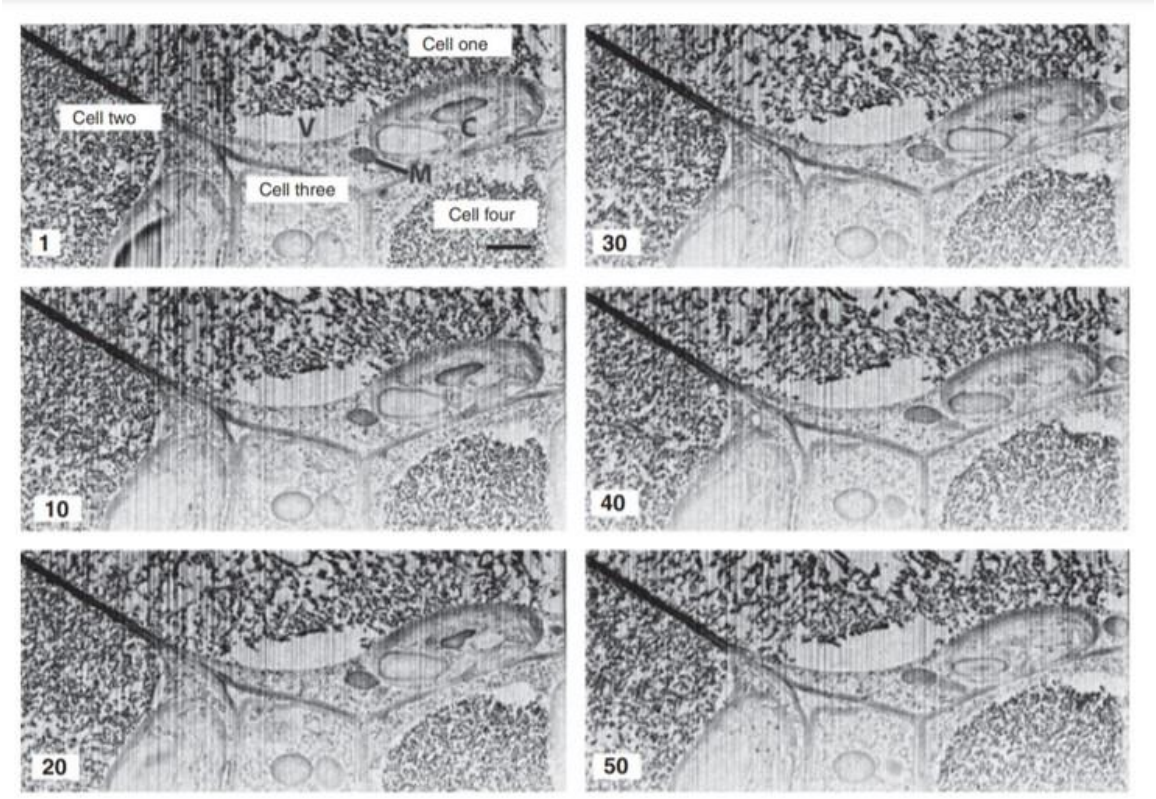


**Figure 6 Tomographic images of leaf tissue fixed in 4% OsO4**

Tomographic images reveal structural details of portions of 4 adjacent cells in young leaf tissue. Every 10th image of the series in shown for the first 50 images. Structural features of various organelles are visible including: large vacuoles (V), mitochondria (M), endoplasmic reticulum (ER), and chloroplast (C). Sequential images were taken ever 20 nm at 22.47k X magnification. Scale bar = 1 μm.

darkly stained reticulate networks (Figure 6), and it is not clear if this is a unique feature of the vacuoles of this sample due to their particular contents or if this is a consequence of the sample preparation protocol.

Close packing of a chloroplast, mitochondrion, Golgi stack, and plasmodesma was observed in this sample (Figure 7A). These close associations may be a consequence of the limited cytosolic space available due to the presence of the large vacuole. In the 3D reconstruction of one of these samples, it appears that there is contact between the mitochondrion, chloroplast, and Golgi (Figure7(b)). From the images and the 3D reconstructions, it appears that these organelles could form membrane contacts or even continuities with each other (Figure 7). Indeed there were places where the membranes of one organelle could not be discerned from that of another, resulting in missing details or holes in our 3D reconstruction. Such membrane continuities have been described extensively [234], [235], but their existence has remained controversial. Nonetheless, the close juxtaposition of these organelles could provide routes for the rapid and efficient movement of metabolites and signaling molecules between organelles.

***Chemical Fixation of Root Nodule***

To extend our studies to a different plant tissue and different fixation protocol, we examined soybean (*Glycine max*) root nodules that had been fixed by conventional chemical protocols. *T*he images have very good contrast and

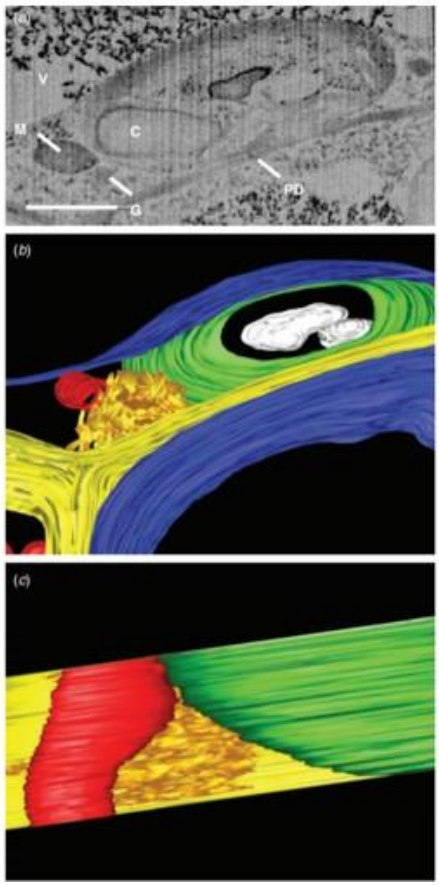


**Figure 7 Organelles in close proximity in leaf cells.**

*(a)* Individual SEM image showing close association between chloroplast (C), mitochondria (M), and Golgi stack (G). The scale bar represents 1 μm. *(b)* 3D reconstruction shows close proximity of mitochondrion (red), Golgi stack (orange) and chloroplast (green). Chloroplast starch granules are shown in white and the vaucolar membrane is shown in blue. The Golgi (orange) appears to touch or form connections to both organelles at multiple sites. The model was rotated 90$^{o}$ relative to image in *(a)* and the vacuole membrane was removed to show organelles' proximity to each other. The model was generated from images shown in Fig. 4 and in *(a)*.

very little curtaining, making tomographic reconstruction relatively straightforward (Figure 8). Tomographic images of this tissue reveal large numbers of bacteroids tightly packed into the cytosol of infected cells (One and Two) but contained within the symbiosome (Figure 8). These tomographic images also contain many of the characteristic features of root nodules including a large intercellular air space (AS) and an adjacent, uninfected cell (Figure 9A). Structural features of the nodule can be identified including the host-derived symbiosome (peribacteroid) membrane (SM). Consistent with earlier studies, infected cells appear to be largely devoid of large vacuoles while the uninfected cell at the bottom of the field of view has a large vacuole. (Figs. 8 and 9(a)). Discontinuous stretches of ER are seen scattered throughout the infected cells (Figure 9). These images also revealed diverse shapes of the individual bacteroids (Figure 9(b)). Further analysis of the 3D structure of these bacteroid clusters revealed elaborate interconnectedness of the symbiosomes, and the bacteroids seem to be located inside one continuous SM forming an elaborate megastructure (Figure 9(c) -(e)). Additionally, mitochondria can be seen in close proximity to one another in one of the infected cells (Two) and in close proximity to the cell wall near the air space (Figure 9(a) and (e)). These mitochondria, though tightly packed in the crowded cytosol, appear to be disconnected from each other, and it is clear that while their outer membranes contact each other, they do not appear to overlap or fuse (Figure 9(e)). While the mitochondria localize to the periphery of the air space, the majority of the bacteroids localize

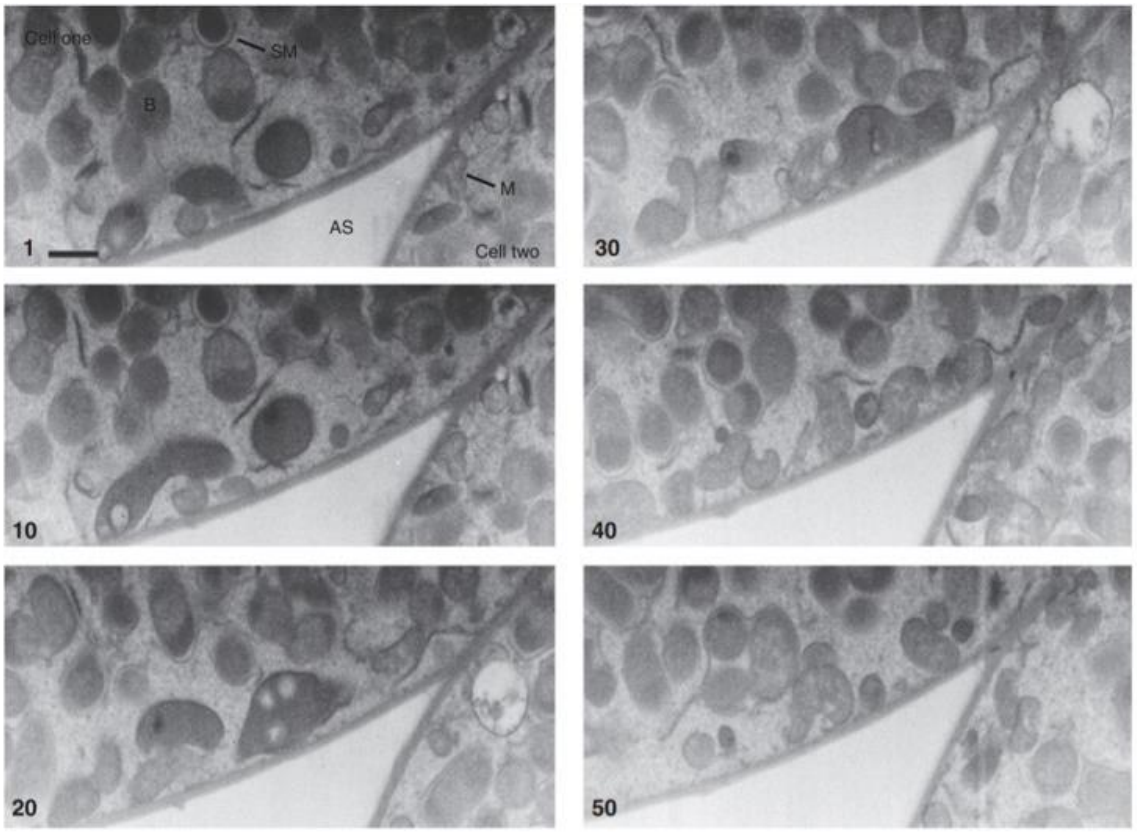


**Figure 8 Tomographic images of chemically fixed soybean root nodules.** Soybean root nodules contain densely packed bacteroids in two infected root cells. Every 10th image is shown for the first 50 images of the tomogram. Structural features of the root nodules are visible including tightly packed bacteroids (B), symbiosome membrane (SM), central air space (AS), and mitochondria (M). Sequential images were taken every 100 nm. Scale bar = 1 μm.

**Figure 9 3D analysis of root nodules reveals complex structural features of the symbiosome membrane.**

(a) Single SEM image shows the complex structure of root nodules. Two infected cells (Cell one and two) are seen adjacent to an uninfected cell (Cell three). Abutting these three cells is an air space (AS). A large vacuole (V) can be seen in the uninfected cell. Clusters of mitochondria (M) localize close to the air pocket. Scale bar = 1 μm. (b) 3D reconstruction of the features characteristic of root nodules. Cell wall (yellow), vacuole (light blue), mitochondria (white), bacteroids (dark blue), symbiosome membrane (transparent red), and ER (green). The ER appears fragmented in the infected cells. (c) Bacteroids are discontinuous within the membrane. (d) The SM appears to be a single continuous structure. (e) SM with the bacteroids showing connectivity of the membrane around the individual bacteroids. The overlay of the symbiosome membrane (transparent red) on the bacteroids (dark blue) makes the structure appear purple. (f) 3D reconstruction showing three closely associated mitochondria in an infected cell near the cell wall next to the air space. The model was generated from images shown in Fig. 6 and in (a).

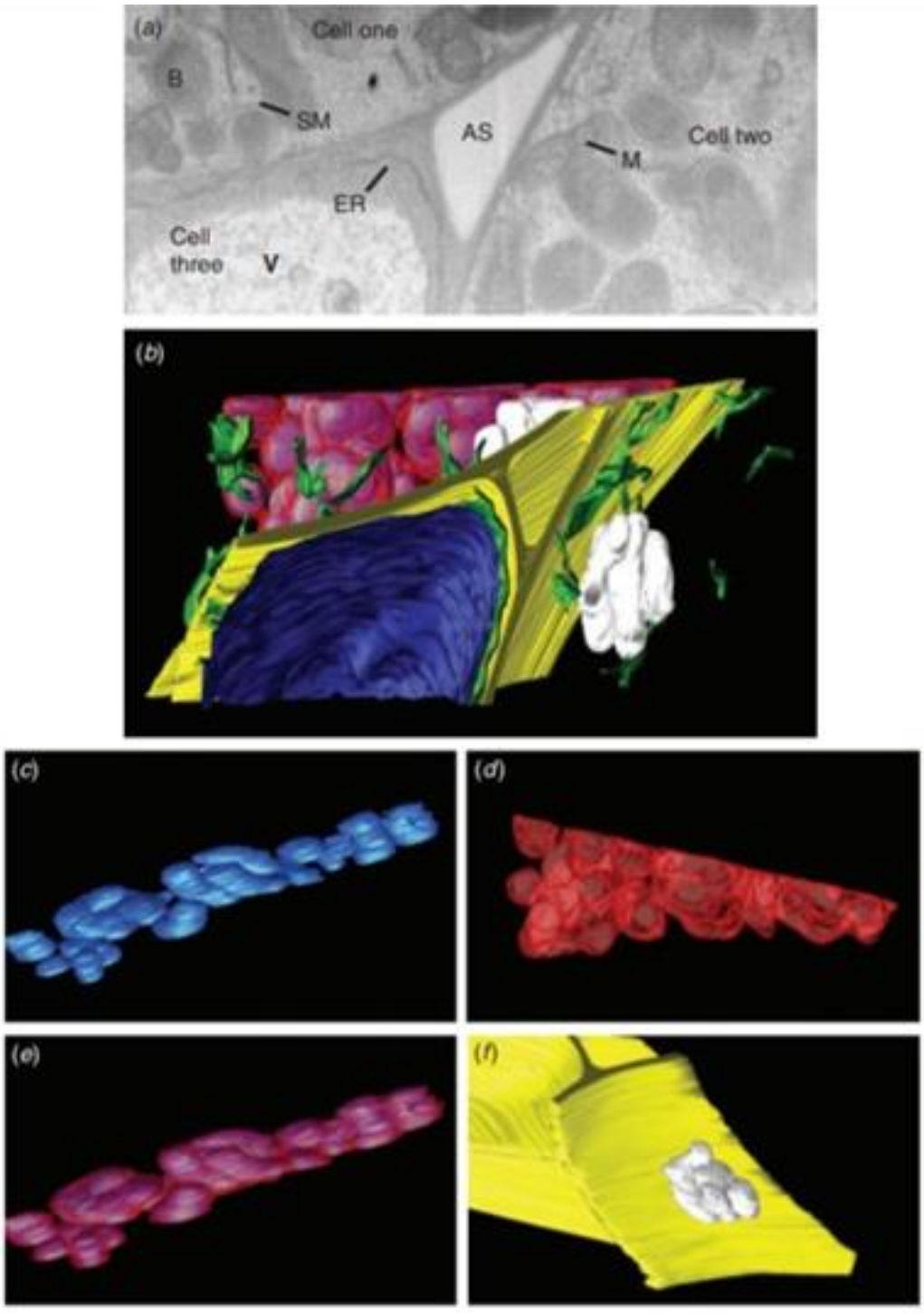
(a)
Cell one
B
SM
AS
Cell two
M
ER
Cell
three
V
(b)
(c)
(d)
(e)
(f)

on the other side of the mitochondria, away from the air space, and appear to take up the majority of the cytoplasm.

## Discussion

FIB/SEM is a little-used tool for studying biological samples. This stems largely from concern about introducing artefacts to the sample through the milling process, such as major charging of the sample, severe damage from the gallium beam, and many other potential causes of uncertainty. This technique is also considered to be impractical and fairly difficult due to the extensive chemical fixation techniques that to date have been used for sample preparation. Here we show that FIB/SEM is not only a powerful technique for studying plant tissue ultrastructure but also that plant tissue samples prepared using standard chemical fixation protocols or HPF/FS are suitable for the technique without additional preparative steps to generate contrast. The use of TEM-ready samples for FIB/SEM, provides an alternative to the much more demanding techniques used for 3D analysis including serial TEM tomography. Further, FIB/SEM overcomes the size limitations of TEM tomography while yielding structural details of organelles at near-TEM resolution. Thus the spatial relationships between organelles and cells in plant tissues could be analysed through this technique. With our various samples, we showed that different TEM sample preparation techniques could be deployed to determine structural features of plant tissues by FIB/SEM. Moreover, FIB/SEM can be used to study many processes including chloroplast differentiation and development (Figure 4),

organellar and tissue development (Figures 5 and 6), and host-microbe interactions (Figure 9). A recent study described a technique to perform immuno-gold labelling prior to embedding of the sample in resin [236]. This technique has been used previously to determine protein localization in plant tissues [237], [182], [238]. It would be interesting to see if FIB/SEM could be employed alongside pre-embedding immunolocalization to study protein distribution in 3-dimensions. This application could potentially allow for detailed analysis of protein localization throughout the cell at a resolution much greater than what can be seen with light microscopy techniques currently used for such 3D analyses.

Our analyses have also revealed intriguing examples of potential membrane interactions (Figure 7). *T*hese apparent membrane contacts would likely be missed when observing individual thin sections of a sample by TEM. Several early studies reported potential membrane connections and contact sites between various organelles in plants [235], [234], [239]. These studies remain controversial because many of these contacts and continuities have been attributed to artefacts of chemical fixation. Our tomograms from samples prepared by HPF/FS confirm that organelles can be very close to each other in a cell, but at this level of resolution we cannot state conclusively that membrane contacts lead to continuities between chloroplast and other organelles in plant cells. *I*t is generally accepted that samples prepared by HPF/FS are free of the membrane disruptions that are known to occur with chemical fixatives. However,

these connections could potentially provide additional routes in a plant cell for signal transmission and metabolite transport between organelles.

From a signaling standpoint, close associations between chloroplasts, ER, mitochondria, and plasmodesmata are particularly interesting. These organelles are known to communicate with each other during metabolism, e.g. photorespiration and fatty acid synthesis. Their close proximity in the plant cell could potentially result in direct membrane contacts facilitating rapid inter-organellar communication. *O*ne model that has recently garnered attention is the hemi-fusion model for chloroplast-ER membrane contacts [240]. This model, based largely on genetic complementation experiments [241], proposes that the membranes of these organelles can form transient fusions, thus allowing bidirectional exchange of intermediates and enzymes in fatty acid synthesis. Similarly, intercellular trafficking via plasmodesmata is likely regulated by chloroplasts and other organelles, including mitochondria [142]. With these potential chloroplast-ER membrane contacts, signals from the chloroplast could be rapidly transmitted to the plasmodesmata via the ER, and could explain how chloroplast localized proteins such as the RNA helicase *ISE2* could play a role in regulating intercellular trafficking [242]. Further experiments including more detailed imaging analysis are required to investigate these possible routes for communication and signalling.

We also used FIB/SEM to investigate the structure of a complex biological structure, the root nodules formed during legume-rhizobium symbioses. For this,

we examined roots of soybean that had been colonized and nodulated by Bradyrhizobium japonicum. Typically, the bacteroids (differentiated rhizobia) within the host symbiotic cells are contained within a host-derived membrane symbiosome membrane (SM). *T*his membrane is then the interface across which nutrients and signals are exchanged between the host and endosymbiont (reviewed in [243]. *T*hese structures have long been studied by thin-section TEM. In thin sections of nodules of tropical legumes including soybean, clusters of bacteroids are frequently seen within the same SM, but these clusters are thought to usually be limited to 1-4 bacteroids. Our data suggest that there are elaborate membrane continuities of the SM (Figs. 6 and 7), strengthening the concept that these symbiosomes are remarkable, structurally complex entities. Overall, the 3D structure of these SM networks appears to have been largely underestimated, with the majority of studies only looking at single sections of the nodule. Instead, by FIB/SEM we find that the bacteroids in an infected root cell are likely all contained within one continuous SM. The elaborate megastructure of the symbiosomes shown here has not been reported previously, even in studies using HPF/FS [244]. *T*he possibility exists that the observed membrane continuities of the SM were a consequence of the chemical fixation of our sample. *H*owever, the rest of our sample suggests that we have good preservation of nodule structure.

From an evolutionary standpoint, it makes sense that the bacteroids would benefit from being surrounded by one continuous host-derived membrane. First,

the bacteroids would not need to synthesize large quantities of membrane components. Second, cohabitation within the SM would facilitate rapid communication between the numerous bacteroids in an infected cell, allowing signaling between bacteroids to occur rapidly without dependence on, or interference from, the host's signaling machinery. It would also allow the rapid diffusion of ammonia away from the bacteroids. Third, the SM likely provides protection from the host's immune responses by shielding the bacteroids in a host-derived membrane system that goes largely unnoticed by the host [245], [246]. These findings about the nature of the SM pose many intriguing questions about symbiosis and could potentially provide new insights into host-microbe interactions. Further, they confirm the versatility and benefit of using FIB/SEM to conduct 3D studies on plant tissues.

Besides the complex SM, our FIB/SEM analysis of the soybean nodules also confirmed several previously reported features. While the intercellular gaps, or air pockets, are frequently found in leaf tissue, they are less common in root tissue and are strategically placed throughout nodules to regulate oxygen concentrations in the tissue. In the nodule, nitrogenase activity is tightly regulated by oxygen concentrations in nodules [247]. Close associations between the mitochondria and the cell wall immediately adjacent to the air pocket were observed in our tomograms (Figure 9). The presence of multiple infected cells in close proximity to an uninfected cell is frequently observed in soybean nodules, with the majority of infected cells being directly connected to one or more

uninfected cell [248]. Previous studies have suggested that the later stages of nitrogen fixation, i.e., synthesis of amides and ureides, occur in the uninfected cells [249], [250]. *T*he association of infected cells with uninfected ones is supported by our FIB/SEM analysis (Figure 9). Additionally, several structural features of the membrane systems of the root cells appear to be severely altered in the rhizobia-colonized cells. Most notably, the large vacuole that typically takes up the majority of the cell volume in uninfected plant cells is absent from the infected cells (Figure 9), as has been reported previously [243], and references therein). Another endomembrane system that appears to be disrupted during infection is the continuity of the ER (Figure 9). In plant cells, the ER typically forms long tubular structures in the cytosol, but interestingly, the ER appears to be largely discontinuous in the infected cell. This discontinuity would be consistent with compromised metabolic function. This would suggest that these infected cells are more dependent on the neighbouring healthy cells for survival. Interestingly, it has been noted that these root nodules have increased numbers of plasmodesmata between infected cells and uninfected cells while the number of plasmodesmata is significantly decreased between neighbouring infected cells [248]. This would suggest an increased demand for intercellular trafficking as the infected cells import nutrients from the neighbouring uninfected cells. Thus, FIB/SEM and the resulting 3D models can be used to interrogate a variety of plant tissues. Here, we have demonstrated a simplified approach to the preparation of plant samples for analysis by this technique, and shown that the

results of FIB/SEM can help illuminate various signaling routes in plant tissues and cells.

## Materials and Methods

### *Plant growth and tissue collection*

*Nicotiana benthamiana* plants used in this study were grown on light carts under continuous light. Young leaves less than 1 cm long on 5-6 week-old plants were collected and leaf discs were removed with a 0.2 mm punch. Soybean (*Glycine max*) seeds were surface sterilized and germinated for 2 days in the dark. Seedlings were transferred to plastic growth pouches and grown in a growth chamber with a cycle of 16 h light at 26°C and 8h dark at 20°C. After 2 days plant roots were inoculated with *Bradyrhizobium japonicum* wild-type strain USDA110 at a concentration of $1X10^9$ cells per plant. Plants were returned to the growth chamber and nodules, 14 days post-inoculation, were excised from lateral roots on the upper 1/3 of the root mass.

### *High pressure freezing and freeze substitution*

Leaf tissues were prepared for electron microscopy by a previously described tandem high pressure freezing and quick freeze substitution protocol [231]. Samples were flash frozen using a Wohlwend Compact 02 high-pressure freezer (Techno Trade International) and the water in the sample was replaced with acetone during quick freeze substitution. The FS solution contained 1% OsO4 + 0.1% uranyl acetate or 4% OsO4 for fixation. After fixation, the samples

were infiltrated and embedded in epoxy resin (Eponate 12, Ted Pella Inc., Redding, CA). *E*mbedding was carried out over five days according to the following protocol: 10% (v/v) resin/acetone (16h), and 25%, 50%, 75% and 100% (24h each). Resin was polymerized at 60°C.

***Chemical fixation of root nodules***

Root nodules were harvested from lateral roots of *Glycine max* and dissected in fixative (sodium phosphate buffered 3% glutaraldehyde). Typically, 1mm thick slices from the centre of the nodule were then transferred to fresh fixative and fixed for 90 minutes. The tissue was then washed 3X for 90 minutes' total in buffer before post fixation in buffered osmium tetroxide (2%) for 90 minutes. Samples were then rinsed in water 3x for 90 minutes' total, dehydrated in a graded ethanol series and finally embedded in low viscosity Spurr epoxy.

***Sample preparation before FIB/SEM***

Blocks were trimmed with a Leica EM UFC7 ultra-microtome (Leica, Buffalo Grove, IL) to expose the plant tissue and to provide a smooth surface for imaging. Semi-thin sections of the sample were visualized using a light microscope and used to identify a region of interest for the slice and view imaging. Next, the tip of the block containing the tissue was carefully removed using a handsaw and glued to an SEM sample mount. The sides of the block were then coated with colloidal graphite paint and sputter coated with a thin layer of gold to ensure conductivity in the SEM.

***Sample preparation during FIB/SEM***

Imaging was performed using a Zeiss Auriga dual beam SEM (Zeiss Microscopy, Thornwood, NY). Once the sample was loaded into the microscope and the region of interest identified and ready for imaging, a thin layer of platinum was deposited on the face of the sample to reduce charging and damage to the surface of the sample. The platinum covered the entire area that was milled over the duration of the run. Next, the block was coarse milled with a high current FIB (30kV 2nA) beam in order to produce a series of trapezoidal trenches about 15 µm deep in the region of interest. *N*ext, a lower beam current (typically 30kV 50-100pA) was used to polish the newly exposed surface.

***Image acquisition using Slice-and-View***

Sequential sectioning and imaging was performed using the Slice and View program (Zeiss Microscopy). For experiments with *N. benthamiana* leaves images were collected every 20 nm and for the soybean nodules they were collected every 100 nm. The total number of images collected was set by the time of the run. The SEM was run at 3kV and images were collected using the in-lens detector (Zeiss Microscopy).

***Image analysis and tomogram construction***

Raw image files were opened in ImageJ [251] and converted into a stack. Images were aligned using the StackReg and TurboReg plugins. Once the images were aligned, images were cropped and image intensities were inverted

to make comparison to the TEM images easier. Brightness and contrast levels were adjusted for optimal visualization of membranes and the stack was saved as a TIFF file.

***Tomography mapping***

The TIFF files were opened in IMOD (University of Colorado, Boulder) and segmentation was performed semi-automatically using the Interpolator function in IMOD. Each organelle was assigned its own object. Contours were drawn and smoothed using the Smooth Contour option in IMOD.

# Appendix

## Focused Ion Beam-Scanning Electron Microscopy for investigating plasmodesmal densities

## INTRODUCTION

Intercellular communication is critical for the development of multicellular organisms. Plasmodesmata (PD) are membrane-lined pores that perforate plant cell walls and form direct cytoplasmic connections between the neighboring cells, facilitating the movement of metabolites and signaling molecules between cells. PD are delimited by the plasma membranes of the connected cells and they contain a second membranous continuity called the desmotubule, a highly derived tightly furled tubule of endoplasmic reticulum (ER) that connects the ER networks of adjacent cells. The current view is that most, if not all, PD in higher plants contain a desmotubule, and some macromolecules use its surface for intercellular spread [15];[55]. These two membranes surround the cells' cytoplasmic continuum, the cytoplasmic sleeve, through which the bulk of diffusive trafficking occurs [252];[253];[254];[25].

The typical textbook image or illustration of a plasmodesma presents a single cylindrical pore with a diameter between 20 and 50 nm. These representations of PD structure come from years of imaging PD by TEM [19]. This stereotypical structure is called a simple plasmodesma, and while such PD are indeed common in many plant tissues, PD can also occur in more elaborate

structures. Twinned PD are two pores found within 100 nm of each other and they are likely sites of *de novo* PD formation [16]. PD can also adopt branched structures with multiple pores that converge at the middle lamella of the cell wall, often forming a dilated region called the central cavity [11]. These different structural classes of PD likely have distinct trafficking capacities [26];[255]. In some instances, simple PD have higher trafficking capacity than do branched PD [26] but an association between twinned and branched PD and increased intercellular trafficking has also been reported [143].

PD can be randomly distributed in a cell wall but often cluster together into groups called pitfields [16];[256],[257]. In recent years, it has become apparent that the number of PD in a cell wall (PD density) and PD trafficking capacity are inherently linked [258];[259];[260]. Several studies have investigated the distribution of PD in different tissues and across plant development [261];[262];[263];[264]. These studies have used transmission electron microscopy (TEM) to image thin sections and often serial thin sections, because PD, with their 20-50 nm diameters, are too small to visualize with light microscopy. While this is a powerful method for quantifying PD densities, it is technically difficult to undertake and requires extensive training or expertise as well as significant hours of data collection and analysis. Recently, alternative methods for quantifying PD densities have been introduced that are less time consuming and that can image larger samples. This flexibility in sample size

allows for the collection of longer lengths of cell wall with higher z-resolution than other approaches.

While individual PD are too small to image with light microscopy, pitfields can be imaged with confocal microscopy using fluorescently labeled PD marker proteins like the PLASMODESMATA LOCATED PROTEINS (PDLPs) or viral movement proteins [260];[265]. Fitzgibbon et al. first demonstrated this approach for studying pitfield densities by developing a high throughout quantification method in transgenic Arabidopsis plants [265]. More recently, we developed a transient expression assay to measure pitfield distributions in *Nicotiana benthamiana* leaves [260]. Combining our assay with the reverse genetics approach of virus induced gene silencing, we generated some of the strongest evidence to date supporting a positive correlation between PD density and intercellular trafficking. While fluorescence microscopy-based techniques allow for the evaluation of pitfield distributions in living tissues, they cannot reveal details of the structures of the individual PD in the pitfields.

Two forms of serial scanning electron microscopy (SEM) have recently emerged as powerful tools for measuring PD densities at EM resolutions [189];[266];[188]. Both methods use SEM to image the newly exposed surface of a sample that has been prepared for TEM. The first method, serial block face scanning electron microscopy (SBF-SEM), uses a specialized setup with a built-in microtome to do serial sectioning within the microscope [267];[268];[269];[210];[211]. This approach has been used in a few studies to

quantify PD distributions in Arabidopsis roots [189];[188]. Additionally, a recent paper outlines a toolkit for the analysis of PD densities with SBF-SEM [188]. The second method, focused ion beam-scanning electron microscopy (FIB-SEM) uses a narrow beam of metal ions to cut away, or mill, the surface of the sample to expose a new surface for SEM imaging [266]. In the FIB-SEM instrument, the electron beam is oriented at 54 degrees to the ion beam and secondary or backscattered electrons produced by the electron beam-sample interactions are used to generate an image of the newly exposed surface of the sample [270]. By repeating the milling and imaging process over a few hours, image data representing microns of sample thickness can be collected from a single FIB-SEM run [271].

Here, we describe a method for measuring PD densities with FIB-SEM. This technique has several advantages over traditional serial-TEM approaches. It can image relatively large samples, in the range of square microns. It also allows for fine control of the step size between images with the theoretical limit of 5 nm, resulting in increased resolution in the z-axis and limiting the number of PD that are missed during image collection using larger step sizes or thicker sections. Using these images, 3D reconstructions of the cellular ultrastructure can be generated with segmentation software such as IMOD (University of Colorado). PD densities can be then be determined from the 3D models of the cell walls under investigation.

# MATERIALS

***Resin-embedded sample preparation:***

1. Samples fixed for TEM and embedded in epoxy resin.
2. Razor blades
3. Ultramicrotome
4. Glass knives
5. Compound microscope
6. Glass slides
7. Toluidine blue stain

***Mounting of samples for FIB-SEM:***

1. Jeweler's Saw
2. SEM Pin Stub Mounts
3. Super glue
4. Carbon paint
5. Plasma Sputtering coater for gold deposition.

***Microscopy:***

1. A Scanning electron microscope with a dual (FIB) beam system. We use a Zeiss Auriga Crossbeam FIB-SEM

***Image processing***

1. ImageJ (http://rsbweb.nih.gov/ij/)

2. IMOD (University of Colorado)

3. A Computer with enough processing power to handle 3D reconstructions in IMOD

The recommended configuration for running IMOD can be found at https://bio3d.colorado.edu/imod/

Briefly, the computer used for segmentation should meet the following standards:

1. Processor: Any up-to-date Intel or AMD Processor, but we recommend a computer with at least four processors for speedy segmentation and model reconstruction.
2. Video Cards: Any modern Nvidia-based card, however 256 MB or higher cards are highly recommended. AMD cards will work for Windows or Mac systems.
3. A minimum of 2GB of memory are required for Linux or Mac systems and 4GB for Windows systems. Computers with more memory are highly recommended.
4. Operating system:
    a. Linux: Red hat Workstation 6 or higher (equivalent levels for Fedora, Ubuntu or Suse will also work).
    b. Windows: Windows 7, 8, or 10 are recommended, however Vista or XP will also run IMOD.
    **c.** Mac: OS X 10.8 or higher is recommended.

5. For Windows: Cygwin (a Unix package) or several Python packages must be installed on the computer. Links for these downloads and the different versions of IMOD can be found at https://bio3d.colorado.edu/imod/download.html

## METHODS

***Biological sample preparation:***

1. We fix our samples by high pressure freezing and freeze substitution (HPF/FS) following the protocol used for TEM sample preparation [266];Drobne 2013}. HPF/FS reduces the frequency of fixation artifacts that can distort the interpretation of imaging data [231]. However, samples prepared by traditional chemical fixation following standard protocols can also be used.
2. Resin embedding: Biological samples used for FIB-SEM tend to be soft and can be easily damaged by the ion beam so they are typically embedded in resin in order to provide a solid surface for milling. Embed sample in hard resin following the same protocol used for sample preparation for TEM. Additional steps for protecting the sample from damage can be taken and will be described below [271].

***Mounting of samples for FIB-SEM:***

1. Block trimming: Blocks should be trimmed as for standard ultrathin sectioning using a glass knife and an ultramicrotome. Using a razorblade, trim away excess resin around the sample. Shape the tip of the block into a trapezoid to help with orientation within the microscope. Load the block into the ultramicrotome chuck and begin coarse trimming with a glass knife. Set the microtome to cut 1-micron sections and trim away excess resin on the tip of the block. Periodically, collect a few 1-micron sections and mount on a glass slide. Stain the sections with Toluidine blue and image with a compound microscope (*see* Note 1). Images of these sections should be collected to identify regions of interest for later electron microscopy. Once the 1-micron sections contain the tissue or structures of interest, begin fine trimming and ultrathin sectioning with a diamond knife. Carefully cut a few 70-100nm sections with the diamond knife and collect sections and mount on a TEM grid. Image with TEM to determine sample quality (*see* Note 2).
2. Block tip removal: Immobilize the trimmed block using a chuck from the ultramicrotome. Using the Jeweler's saw, carefully saw through the block, a few millimeters below the sample. Be sure to make a clean, straight cut through the block to prevent the base of the block from being slanted (*see* Note 3).

3. Mounting of block tip on SEM stub: Once the block tip has been removed, apply a small drop of super glue to a pin stub for SEM and place the block tip on the glue. Make sure that the base of the block is flush with the surface of the stub. Let the glue dry for about 15-30 minutes.
4. Carbon painting: Once the block is securely attached to the stub, apply a thin layer of carbon paint to the base of the block. The carbon is conductive and will prevent charging of the sample. The carbon paint should cover the entire base of the block tip, but should not cover the cleaned and sectioned surface. Spreading the paint can be accelerated using a wooden applicator (*see* Note 4).
5. Sputter coating samples: Once the carbon paint is completely dry (usually after an hour), place the stub in the sputter coater. The goal is to apply a thin layer of gold to the sample surface in order to further limit charging of the sample. The time required for coating may vary between the models of sputter coaters, but we typically coat for about 45 seconds.

***Microscopy:***

1. Sample loading and positioning: Load the sample into the microscope as per the user manual for your system. Position the sample so that the block face is positioned perpendicular to the ion beam and at a 54-degree angle to the electron beam (Figure10b).
2. Identification of regions of interest: Once the sample is loaded into the microscope and positioned for imaging, locate the cleaned block face

while imaging in SEM mode. Increase the magnification to view the block face. The outlines of cell walls are typically visible at this stage. You will want to identify a region where you think there is a lot of cell wall to maximize the length of wall collected in the final image stack. At this stage, you can also attempt to identify specific cell-cell interfaces such as epidermis-epidermis, epidermis-mesophyll or vascular cell contacts for specialized imaging (*see* Note 5).

3. Deposition of platinum coat: Insert the deposition nozzle to apply a thin layer of platinum to the block surface at the region of interest. This will provide an extra layer of protection for your sample and provide a smooth surface for the ion beam to impact. Imperfections in the surface can result in curtaining of the surface during milling (Figure 10e) (*see* Note 7).
4. Trenching: Once a region of interest has been identified, select a large FIB probe to do the course milling, or trenching. Using a large probe (e.g. 30 kV 2 nA) and the “mill for depth” feature, mill a trapezoid into the block face (Figure 10d). The small side of the trapezoid should be positioned just below the region of interest and should be at least 10 µm across. The height of the trapezoid should be no less than 20 µm, and a depth of 15-20 µm. Please note that the length of the short side of the trapezoid will determine how much tissue will be imaged in each section.
5. More trenching: Next, repeat the last step to mill two more trapezoids on either side of the initial trapezoid. These trapezoids should be

perpendicular to the initial trapezoid and line up with the sides of the deposited platinum (Figure 10d). The addition of these trapezoids clears the line of sight between the image surface and the electron detector. These trapezoids can have shorter heights, but the length of the short side should extend further than you intend to mill and image.

6. Cleaning of the block face: Once the course milling is complete, select a smaller FIB probe (30 kV 50–100 pA) to clean up the milled block face.

**Figure 10 Representative images of mounted blocks, milled trenches, and the exposed block faces.**

(a) Resin block tip mounted on an SEM stub, coated with carbon paint and sputter coated with plasmolyzed gold. (b) Cartoon schematic (left) and image (right) of the FIB-SEM configuration. The stage and sample are positioned in the microscope so that the ion beam is oriented at 90 degrees to the block face and the electron beam is positioned at 45 degrees to the block face. (c) Low magnification SEM image of the prepared block face (Scale bar = 500 microns). (d) SEM image of milled trenches in the block face with recommended dimensions for length (L), width (W), and height (H). The light grey portion of the block face (width) corresponds to the layer of platinum deposited prior to milling. (e) Representative image of an uncleaned block face image highlighting examples of curtaining (asterisks), a surface artifact that can occur during FIB milling.

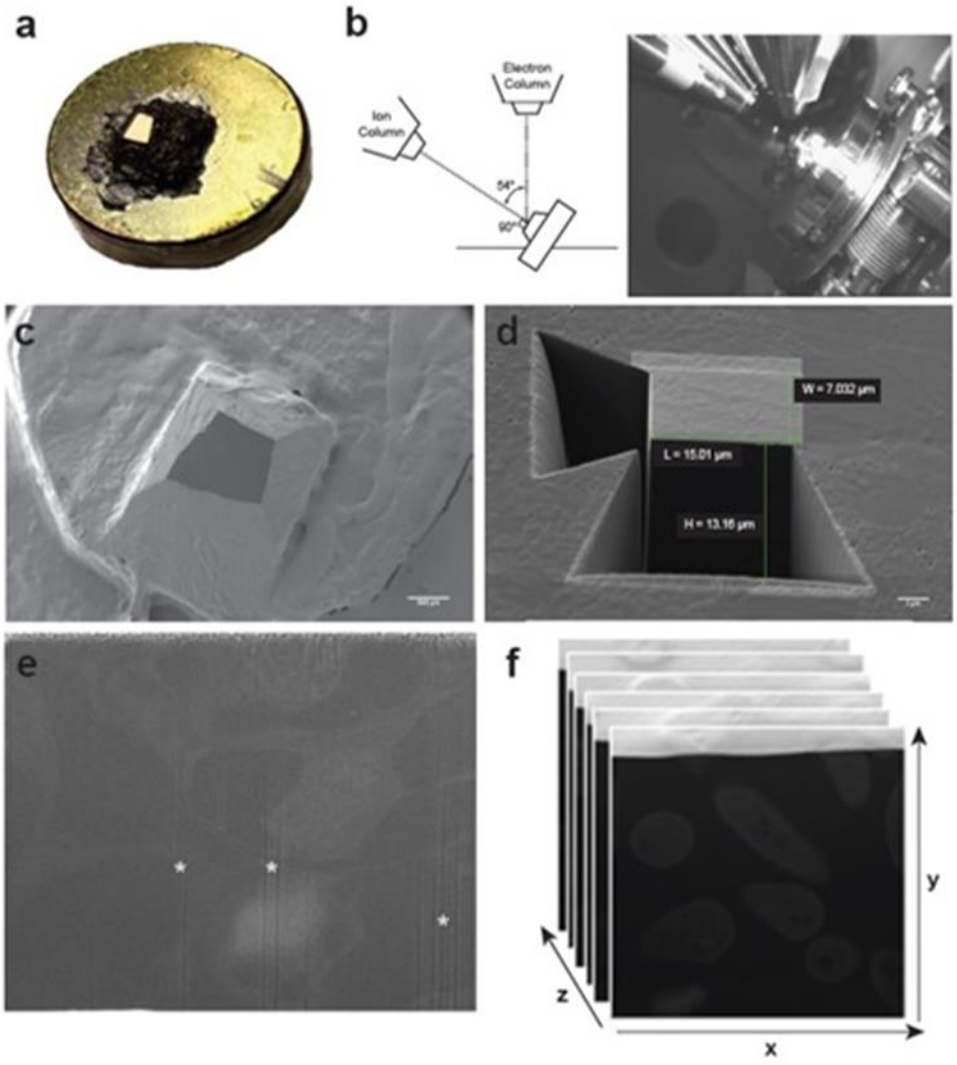
a
b
Electron Column
Ion Column
54°
90°
c
d
W = 7.032 µm
L = 15.01 µm
H = 13.16 µm
e
f
y
z
x

7. Using the selected probe, mill another trapezoid into the sample. This trapezoid should overlap with the top of the first trapezoid. The height of this trapezoid should be substantially smaller (~5 microns) because the milling will take much longer with the smaller probe (*see* Note 8).
8. Milling and image acquisition: Select a FIB probe of the desired size. The step size for a FIB probe is equal to half the radius of the probe. A step size of 25-50nm should be used to minimize PD loss during image acquisition and maximize the amount of tissue collected over the course of several hours but this can be adjusted to suit the user's experimental goals. Imaging should be performed in SEM mode with the SEM operating at 3kV. An SEM image should be collected after each step. The individual images are saved as Tagged Image File Format (TIFF) during acquisition. Serial imaging can be achieved using the "Slice and View" program from Zeiss Microscopy (*see* Note 8).

***Image processing***

1. Generation of image stacks: Once the images have been collected, the raw images need to be converted a stack of the images (Figure 10f). Import the image sequence into ImageJ (http://rsbweb.nih.gov/ij/). Set the scale using the scale bar from the first image collected (*see* Note 8). Once the scale is set, scroll through the image stack. Samples tend to drift during image acquisition and therefore the images need to be aligned. Run the TurboReg plugin for ImageJ and select the Rigid Body option in

the menu (http://bigwww.epfl.ch/thevenaz/turboreg/) to align the images. Once the images in the stack are aligned, the stack needs to be cropped to include only the block face or region of interest. Using the rectangle tool in ImageJ, draw a rectangle that will capture as much of the region of interest as possible. Once the optimized region has been identified, make a copy of this region of the stack by using the duplicate function (Image>Duplicate). Make sure to duplicate the entire stack by selecting the “Duplicate stack” option. This will be the tomogram that you will use for segmentation and counting PD.

2. Image processing: Because the images were collected with the secondary electron detector, the images will look like a negative of a TEM image. Invert the image in order to generate images that have dark stained membranes and lightly stained cytoplasm that look more like standard TEM images (Figure 11a). Save the stack as a stack of TIFFs for further analysis with IMOD).
3. Adjusting for step size: In order for the 3D renderings to accurately depict the cellular ultrastructure, the Z-scale for the tomogram needs to be set in 3Dmod. The Z-scale is equal to the ratio of the section thickness to the pixel size. The section thickness is determined during image acquisition when the probe used for milling is selected. The pixel size is dependent on the image quality and the detector used for image acquisition. The pixel size can be calculated by setting the scale for the tomogram in ImageJ.

**Figure 11 3D reconstruction of FIB-SEM data and quantification of PD density in a representative FIB-SEM dataset.**

(a) Representative SEM image of cells of a *N. benthamiana* leaf collected with FIB-SEM. Portions of four cells are visible in the image. Cell wall (CW), plasmodesmata (PD), chloroplasts (Chl), vacuole (V), and nuclei are visible. The structural class of PD can be determined. The labeled PD are simple (left) and one branched (right). (b) 3D reconstruction of the FIB-SEM dataset in A. The cell wall (grey), chloroplast (green), vacuole (yellow), and nuclei (blue) are shown. (c) Close up view of the 3D model showing a cluster of PD. (d) Image of 3D rendering of the cell wall showing the distribution of PD in the wall. (e) Quantification of total numbers of PD in the data set. (f) Quantification of the PD density (PD/μm2 cell wall).

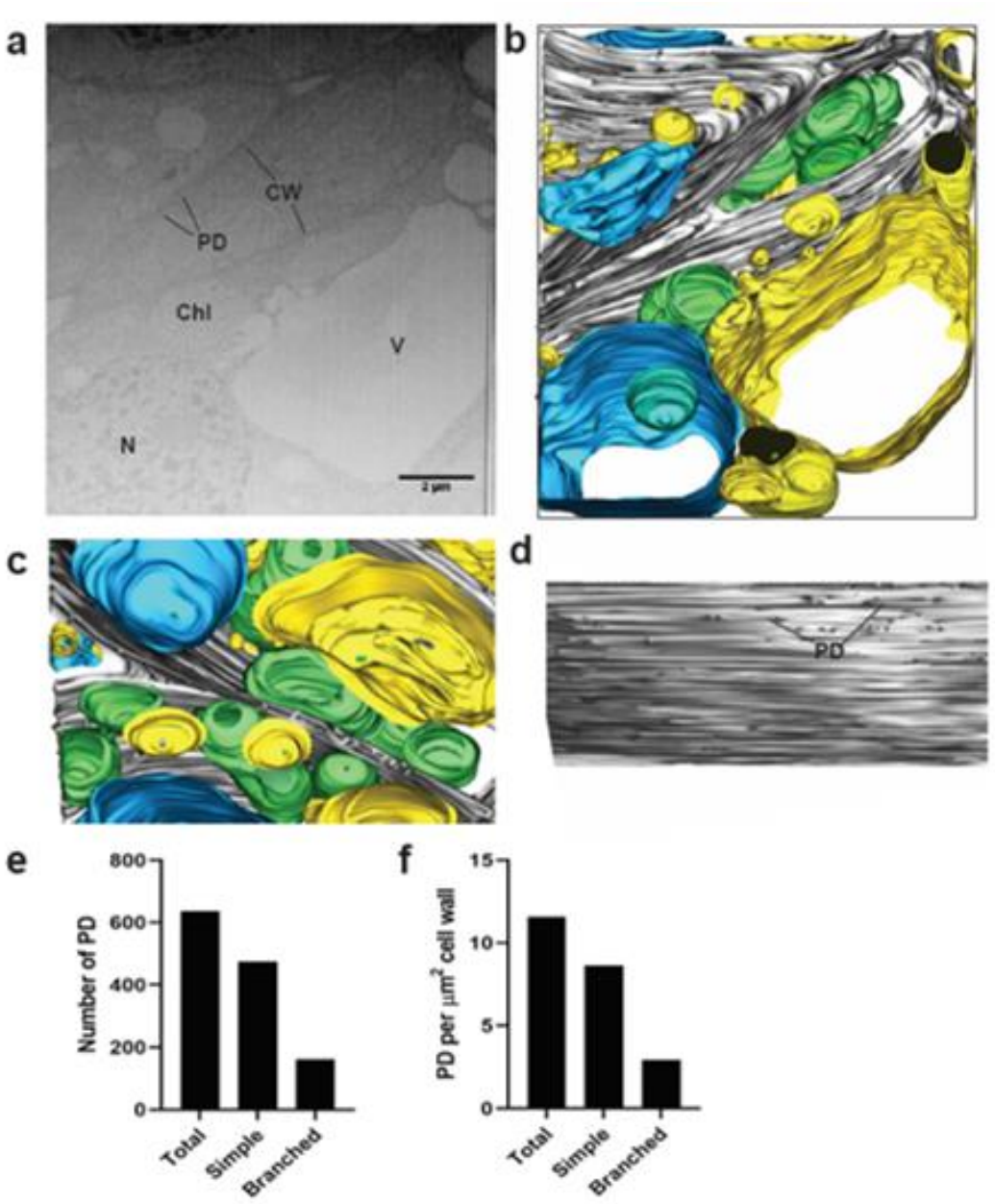
a
CW
PD
Chl
V
N
b
c
d
PD
e
Number of PD
800
600
400
200
0
Total
Simple
Branched
f
PD per µm² cell wall
15
10
5
0
Total
Simple
Branched

4. Image Segmentation: Open the tomogram with IMOD (*see* Note 9). This will open the tomogram in the ZAP window. Using the drawing tools (Special>Drawing Tools), trace the structures of interest in the ZAP window. The progress of contouring can be monitored with the Model View window. Semi-automated segmentation can be achieved using the interpolator function (Special>Interpolator) in IMOD. The interpolator function will use information from a few contours spaced throughout the tomogram (approximately one contour every 20 images) to predict the position of each contour on each section between the reference contours. These predictions work pretty well for simple objects that have high contrast, but do not work as well when then the contrast is low. Each interpolated contour must be manually adjusted using the drawing tools. Once an interpolated contour has been adjusted, the predicted contour (dashed line) can be converted into a true contour by pressing ENTER on the keyboard. This will re-run the interpolation and adjust the remaining predicted contours based on the modified position of the adjusted contour. Once all contours have been adjusted and the segmentation of the desired object is complete, apply a skin to the model by applying a mesh to the model (Image>Model View>Edit>Object>Meshing). Parameters for meshing can be adjusted prior to applying the mesh. Additional objects can be created to include additional components to the 3D model (Figure 11b and c).

5. Quantification of PD densities: PD density can be quantified as the number of plasmodesmata per square micron of cell wall (Figure 11d). The cell wall area is calculated by measuring the length of cell wall in each image. This can be achieved by drawing a line along the length of the cell wall and using the Measure function in ImageJ after the scale has been set. After measuring the cell wall in every image, multiply the sum of these measurements by the step-size used during milling and image acquisition. Next, count the number of PD present in each image. High quality FIB-SEM images allow for the distinction between simple and branched PD. Divide the total number of PD by the cell wall area to calculate the PD density. Ratios of simple to branched PD can also be calculated by quantifying distinct population densities (Figure 11e and f).

## NOTES

**Note 1**: The semi-thin 1-micron section stained with Toluidine blue is very useful as a low-resolution map of the sample that can be used to help in orientation after the sample is viewed in the microscope (*see* Note 5).

**Note 2**: Surface imperfections such as knife marks may make it difficult to identify regions of interest in your sample and will result in an uneven surface that can cause curtaining of your sample during milling (*see* Note 7). Additionally, we recommend that the block should be thin sectioned and imaged with TEM to assess the fixation quality of the sample, but this step will not be discussed in this method instead we refer the reader to these articles [272];[231];[273].

**Note 3**: It is very important to cut straight through the block. If the block containing the sample is mounted at an angle, the electron and ion beam angles will be off in the microscope and may negatively influence the milling and image acquisition.

**Note 4**: The carbon paint dries rapidly so you will want to work very quickly but carefully. Alternately, a carbon marker can be used to cover the base of the block with a thin layer of carbon.

**Note 5**: At this stage it is very helpful to have a map of your block face such as the light microscopy image of a semi-thin section stained with Toluidine blue (*see* Note 1).

**Note 6**: Curtaining is an artifact that occurs during FIB milling when imperfections in the block face interfere with milling and results in an unsmooth surface. It typically presents as numerous lines running top-to-bottom of the sample surface.

**Note 7**: The milling area should start in front of the block face, just ahead of the actual exposed surface. This will ensure that the milling area does not start behind the surface of the sample. If the beam starts milling slightly behind the surface this will result in a barrier between the newly exposed surface and the electron beam, and will generate multiple images of the initial surface and not the underlying material.

**Note 8**: An image captured before milling begins can be used to set the scale. We typically run our samples for 6 hours (measured in seconds). With the 25nm

step size and collecting an image after every step, we can typically expect to collect around 9-10 microns of images in 6 hours.

**Note 9**: A very useful tutorial for 3D segmentation using IMOD can be found at (https://bio3d.colorado.edu/imod/doc/3dmodguide.html). Careful review of this tutorial should be completed prior to segmentation to ensure that all parameters are set properly during segmentation.

# CHAPTER 3
# CHLOROPLAST-TO-NUCLEUS RETROGRADE SIGNALING CONTROLS INTERCELLULAR TRAFFICKING VIA PLASMODESMATA FORMATION.

Disclosure: A version of this chapter was previously published in the journal Philosophical Transactions of the Royal Society B by Elena E. Ganusova, Brandon C. Reagan, Jessica C. Fernandez, Mohammad F. Azim, Amie F. Sankoh, Kyle M. Freeman, Tyra N. McCray, Kelsey Patterson, Chinkee Kim and Tessa M. Burch-Smith.

Ganusova, E. E., Reagan, B. C., Fernandez, J. C., Azim, M. F., Sankoh, A. F., Freeman, K. M., ... & Burch-Smith, T. M. (2020). Chloroplast-to-nucleus retrograde signalling controls intercellular trafficking via plasmodesmata formation. Philosophical Transactions of the Royal Society B, 375(1801), 20190408.

Elena Ganusova and Brandon Reagan share first authorship for this manuscript. I contributed all of the microscopy and image analysis performed in the manuscript. I also developed the assay used to quantify PD densities. This chapter will highlight my contributions to the manuscript.

## Abstract

The signaling pathways that regulate intercellular trafficking via plasmodesmata (PD) remain largely unknown. Analyses of mutants with defects in intercellular trafficking led to the hypothesis that chloroplasts are important for controlling PD, likely by retrograde signaling to the nucleus to regulate expression of genes that influence PD formation and function, an idea encapsulated in the organelle-nucleus-PD signaling (ONPS) hypothesis. ONPS is supported by findings that point to chloroplast redox state as also modulating PD. Here we have attempted to further elucidate details of ONPS. Through reverse genetics, expression of select nucleus-encoded genes with known or predicted roles in chloroplast gene expression was knocked down, and the effects on intercellular trafficking were then assessed. Silencing most genes resulted in chlorosis, and the expression of several photosynthesis and tetrapyrrole biosynthesis associated nuclear genes was repressed in all silenced plants. PD-mediated intercellular trafficking was changed in the silenced plants, consistent with predictions of the ONPS hypothesis. One striking observation, best exemplified by silencing the PNPase homologs, was that the degree of chlorosis of silenced leaves was not correlated with the capacity for intercellular trafficking. *F*inally, we measured the distribution of PD in silenced leaves and found that intercellular trafficking was positively correlated with the numbers of PD. *T*ogether, these results not only provide further support for ONPS but also point to a genetic mechanism for PD formation, clarifying a longstanding question about PD and intercellular trafficking.

## Introduction

Cell-to-cell communication in plants occurs via microscopic but complex pores known as plasmodesmata (PD). PD are membrane-lined cytoplasmic passages that allow movement of metabolites and signaling molecules between neighboring plant cells. They are therefore essential for plant growth, development and defense [274]. They are also conduits for the trafficking of carbon fixed by photosynthesis (in the form of sugars) to the vasculature in source tissues and from the vasculature into sink tissues, thereby facilitating energy distribution throughout the plant [275],[26]. The relatively small number of reported PD mutants underscores the importance of PD to plant growth and development. Plants have evolved a number of mechanisms to control PD function including the regulated deposition and removal of callose in the cell wall surrounding PD [94],[90],[91],[92]. PD function also changes in response to plant hormones upon abiotic and biotic signals from the environment and to developmental programs [30],[142]. Besides callose metabolism and hormones, there is increasing evidence supporting the postulate that chloroplasts exert control over the development and function of PD.

Nuclear genes encode approximately 95% of chloroplast proteins, with the remainder encoded by the chloroplast genome. Disrupting chloroplast function leads to changes in expression of specific nuclear genes. This chloroplast-to-nucleus signaling is referred to as chloroplast retrograde signaling (CRS), [276]. Several CRS pathways and the molecules that initiate them have been identified,

and the mechanistic details are under intensive investigation [277],[278],[279],[280],[281]. *G*ene expression analyses have identified a core suite of 39 genes that respond to all chloroplast-generated signals [282]. This suite includes genes that affect cell wall synthesis and/or modification, sugar transport, stress responses, and ROS responses. This indicates that chloroplast functional status can regulate the expression of nuclear genes including, but not limited to, photosynthesis-associated nuclear genes [283]. *S*everal CRS pathways have been identified, and among the best characterized are those involving the *genomes uncoupled* (*gun*) mutants [15,18]. The *gun2, 3, 4, 5* and *6* mutations affect proteins that participate in the tetrapyrrole biosynthetic pathway that eventually produces chlorophyll and heme [284]. GUN4 and GUN5 are part of the Mg chelatase that couples Mg to tetrapyrroles on the chlorophyll branch of the pathway [285],[286],[287],[288]. GUN2, GUN3 and GUN6 belong to the pathway that couples protoporphyrin IX to iron, eventually producing heme and phytochromobilin [284].

Studies with the chloroplast-resident RNA helicase *ISE2* have served as an entry point to further probing the chloroplast-PD relationship. *ISE2* is a chloroplast DEAH-type RNA helicase critical for chloroplast RNA processing and translation, and it is conserved among green photosynthetic organisms [141],[289]. Plants with reduced *ISE2* expression have decreased photosynthetic capacity and defects in chloroplast development [142]. In addition, Arabidopsis *ISE2* mutant embryos and *N. benthamiana* leaves in which *ISE2* was silenced by

VIGS had defects in intercellular trafficking and PD formation [144],[143]. Deficiency in *ISE2* expression also led to changes in the expression of target genes of CRS pathways as well as changes in the expression of several genes implicated in PD function, e.g. callose metabolism genes like *AtBG-PPAP*, and numerous genes with roles in cell wall biosynthesis or modification [17]. Based on these gene expression analyses, a relationship between chloroplasts and PD was proposed and articulated in the organelle-nucleus-plasmodesmata signaling (ONPS) hypothesis [142],[242]. One predicted consequence of ONPS is that it would be a mechanism by which chloroplasts could regulate carbon partitioning.

The signals that connect chloroplasts with PD function and biogenesis remain to be elucidated and this is the question investigated in this study. One challenge with examining this question is the embryonic or seedling lethality of mutants with defects in chloroplast and/or PD function [290],[291]. Therefore, we adopted *Nicotiana benthamiana* and virus-induced gene silencing (VIGS) as a model system for assessing the acute effects of chloroplast dysfunction on PD-mediated intercellular trafficking. Expression of several genes with known roles in regulating chloroplast gene expression was knocked down and intercellular trafficking was then measured in the silenced leaves. CRS was then assessed in plants with altered intercellular trafficking. Finally, we measured the effects of CRS resulting from the silencing of the target genes on PD formation. Here we present data suggesting that intercellular trafficking is correlated with numbers of

plasmodesmal pores. We interpret these results to mean that CRS exerts influence on intercellular trafficking by controlling the formation of PD.

## Results

### *Silencing genes for chloroplast gene expression produces varying degrees of chlorosis*

Reduced expression of the genes encoding the RNA helicase *ISE2* or the plastid ribosomal protein uL15c led to increased intercellular trafficking via PD [143],[292]. *ISE2* also interacted with numerous proteins involved in chloroplast gene expression [292]. In order to test whether chloroplast gene expression was broadly involved in ONPS and regulating PD, we silenced six genes encoding proteins found to interact with *ISE2* or be important for expression of the plastid genome and then monitored intercellular trafficking via PD in silenced tissues. For this, we used VIGS with vectors derived from the tobacco rattle virus (TRV) in *N. benthamiana* [155],[293]. The silenced genes were those encoding RNA helicases *RH22* [294], *RH39* [295] or *RH3* [296], a gene encoding a pentratricopeptide repeat (PPR) protein reported to be important for translation in maize plastids and found to interact with *ISE2* (here called *IPI1*) [292],[297], the RNA surveillance factor RNase J [298], and the RNA maturation and degradation factor PNPase [299]. In all experiments, wild type plants infected with TRV but with no silencing were used as the negative control, and VIGS of *PHYTOENE DESATURASE* (*PDS*) was used as a positive control for silencing. The inclusion

of *ISE2* in the silencing experiments also served as in internal control since the behaviour of *ISE2*-silenced plants has been well characterized.

Silencing of the target genes was confirmed by quantitativeRT-PCR and genes expression in all cases was reduced by at least 87%. Knockdown of *RH22* expression produced plants that were almost indistinguishable from the non-silenced WT+TRV control plants in both appearance and photosynthetic pigment content (figure 12a-b,k-m). Silencing *RH39* caused mild chlorosis in newly emerged leaves (figure 12c,k-m) while silencing a single or both *PNPase* homologs led to more severe yellowing, similar to that observed with silencing *ISE2* (figure 12d-f, k-m). *P*lants with reduced expression of *RNaseJ, IPI1* or *RH3* yielded severe chlorotic phenotypes and reduction in photosynthetic pigment contents that were similar to those observed in plants where *PDS* was silenced (figure 12g-m). Despite chlorosis, the silenced plants continued to grow and they eventually matured and set seed.

***Intercellular trafficking changes in plants with defective chloroplast RNA processing***

Intercellular trafficking via PD was measured in silenced leaves. *F*or this we used movement of a GFP probe from a single cell into adjacent, contiguous layers of epidermal cells to report on PD function [143],[27],[146]. In this assay, GFP travels variable distances, generating foci of GFP of different sizes (figure 13a). Because of the inherent variation in the sizes of foci in any sample,

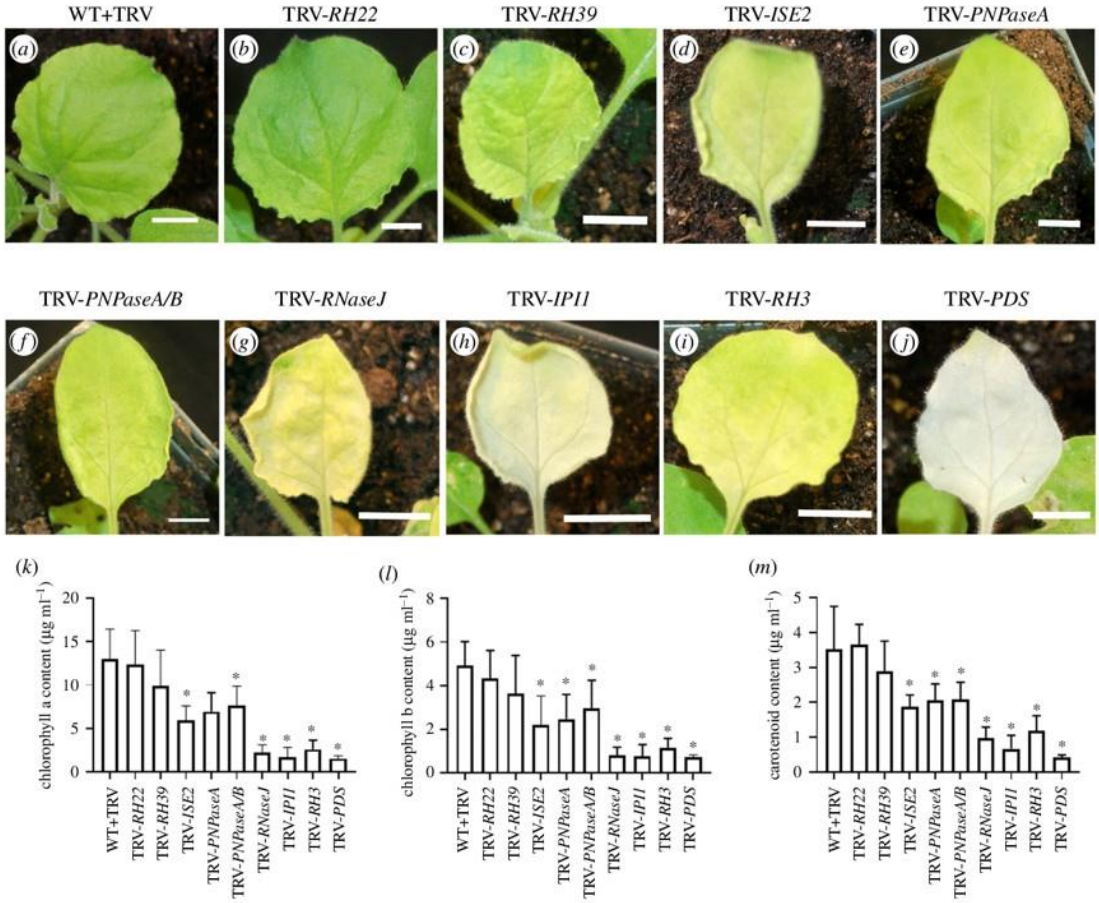


**Figure 12 Phenotypes of silenced plants and their photosynthetic pigment content.**

(a-j) Representative leaves from silenced plants. Silenced gene is shown above figure. WT *N. benthamiana* infected with TRV virus only (a). Plants with silenced *RH22* (b), *RH39* (c), *ISE2* (d ), *PNPaseA* (e), *PNPaseA/B* ( f ), *RNaseJ* (g), *IPI1* (h), *RH3* (i), and *PDS* ( j ). Silencing of *PDS* results in severely chlorotic tissue. Chlorophyll a and b content of silenced plants (k,l), and total carotenoid content of silenced plants (m). Asterisk denotes statistical significance, Students t-test $p < 0.05$.

**Figure 13 Measurement of PD-mediated intercellular trafficking in silenced plants.**

PD-mediated trafficking was measured by counting the layers of epidermal cells to which GFP spread. At least 10 foci were scored for each of three biological replicates. (a) Representative images depicting GFP trafficking between contiguous layers of epidermal cells. The presence of GFP in cell nuclei was used to determine the presence of GFP in a cell. The cell labelled 0 showed expression of GFP in the primary transformed cell but no GFP was seen in surrounding epidermal layers. In the image labelled 1, GFP expression was observed in the primary transformed cell and in the nuclei of cells immediately adjacent to the transformed cell only. For subsequent images, the number below the image corresponds to the number of layers away from the primary transformed cell that showed GFP accumulation in the nucleus. Scale bar = 100 m. (b) Quantitative representation of GFP trafficking data showing the distribution of foci sizes observed for each silenced plant. (c) Layers were assigned values (0 layers = 0, 1 layer = 1, 2 layers = 2, 3 layers = 3, greater than 3 layers = 4) and the median value is shown. Statistical significance was determined by the Mann Whitney U-test. *$p < 0.05$.

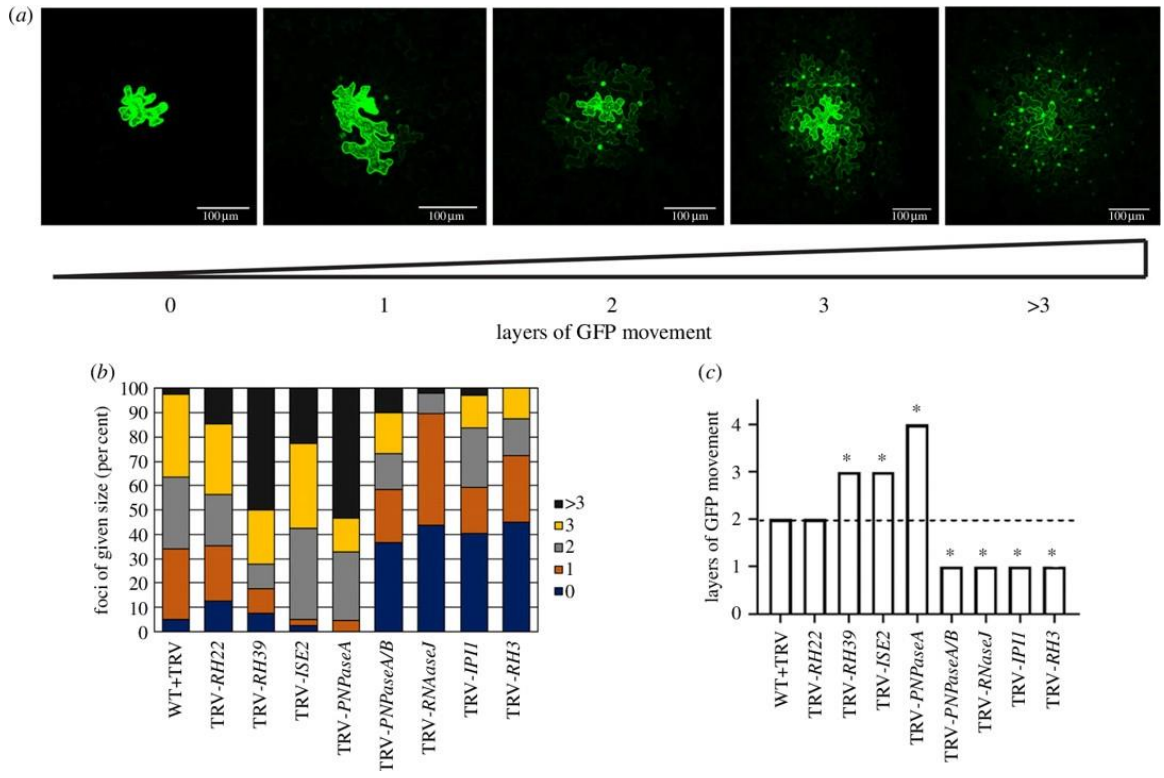
(a)
100 µm
0
1
2
3
>3
layers of GFP movement
(b)
foci of given size (per cent)
>3
3
2
1
0
WT+TRV
TRV-RH22
TRV-RH39
TRV-JSE2
TRV-PNPaseA
TRV-PNPaseA/B
TRV-RNAaseJ
TRV-IP11
TRV-RH3
(c)
layers of GFP movement
WT+TRV
TRV-RH22
TRV-RH39
TRV-JSE2
TRV-PNPaseA
TRV-PNPaseA/B
TRV-RNaseJ
TRV-IP11
TRV-RH3

movement data are presented in two ways. Figure 13b presents the complete distribution of foci sizes observed for a sample while figure 13c presents a quantification of the average (median) size of foci for a given sample. In *RH22*-silenced leaves, there was no difference in the average size of foci compared to those observed in the non-silenced WT+TRV control leaves (figure 13c). In leaves where *RH39*, *ISE2* or *PNPaseA* were silenced and chlorosis was more severe, there was an increase in the size of GFP foci and hence, intercellular trafficking (figure 13b-c). Strikingly, when *RNaseJ*, *IPI1* or *RH3* was silenced and leaves exhibited severe chlorosis (figure 12), there were large decreases in the size of GFP foci reflected in the increase in the proportion of foci that were restricted to one cell layer, indicating reduced intercellular trafficking (figure 13). Leaves in which both PNPase genes were silenced (TRV-*PNPaseA/B*) also showed a large decrease in GFP foci sizes, in striking contrast to the results from silencing only *PNPaseA*. *I*t should be noted that there were no differences in the chlorosis or the photosynthetic pigment content between the *PNPaseA* or *PNPaseA/B* plants (figure 12). These data support previous observations that chloroplast function modulates intercellular trafficking. However, they also reveal a more complex relationship in which the degree of chloroplast (dys)function does not exclusively determine changes to intercellular trafficking.

***PD density is altered in plants with defective chloroplast gene expression***

The silencing of genes important for chloroplast gene expression resulted in defects in intercellular trafficking (figure 13). In *ISE2*-silenced plants, defects in

intercellular trafficking were associated with changes in PD [143]. We therefore tested whether changes in PD were also involved in the changes to intercellular trafficking observed in the silenced plants. For this, Arabidopsis PLASMODESMATA-LOCATED PROTEIN1 (PDLP1-GFP), a general marker for PD [300], was expressed in leaves equivalent to those used in the trafficking assays. Using confocal fluorescence microscopy, we monitored the appearance of GFP punctae in cell walls. *P*D are nanopores with an average diameter of 30 nm, so for our analysis we assumed that the fluorescent foci we observed were due to clusters of PD in the cell wall, called pitfields [16]. Direct observation by microscopy revealed striking changes in the patterns of pitfields compared to those in non-silenced TRV-infected controls. *I*n some silenced plants there were more, larger punctae that had greater fluorescence intensity (measured under the same imaging settings) than in control plants, exemplified by TRV-*PNPaseA* (figure 14a-b). *I*n other plants, as shown for TRV-*IPI1*, the GFP punctae were much less abundant and had weaker fluorescence intensity compared to the control plants (figure 14c). Images of cells were collected as z-stacks and then the maximum intensity projections were used to measure the number, size and fluorescence intensity of GFP punctae in a field of view (figure 14d). Based on these parameters, a 'PD density score' was developed to quantitatively describe these observations (See Materials and Methods). In *RH22*-, *RH39*-, *ISE2*- and *PNPaseA*-silenced plants, the average PD density was higher than that of non-silenced control plants and in all cases this difference was statistically significant

**Figure 14 Quantification of PD density in silenced plants. PD in pitfields were labelled with the general PD marker PDLP1-GFP.**

Representative maximum projections of fields of view showing PDLP1-GFP-labelled pitfields in (a) WT+TRV, (b) TRV-*PNPaseA* (increased number of pitfields), and (c) TRV-*IPI1* (decreased numbers of pitfields) plants. (d ) Individual images (confocal planes 314 of a confocal stack) from z-stacks used to generate maximum projections (MP) showing the distribution of pitfields in the z-axis. Images correspond to the region outlined in white in (a). Scale bar = 10 um. (e) PD density scores were calculated for each image from three biological replicates (rep. 1 (blue squares), rep. 2 (yellow circles) and rep. 3 (red diamonds). See Material and methods for more details. Statistical significance was determined by MannWhitney U-test. *p < 0.0001. ( f ) Linear regression curve showing the positive correlation of PD density score with layers of GFP movement. The average PD density score and the median layers of movement across the three biological replicates were used to generate the graph.

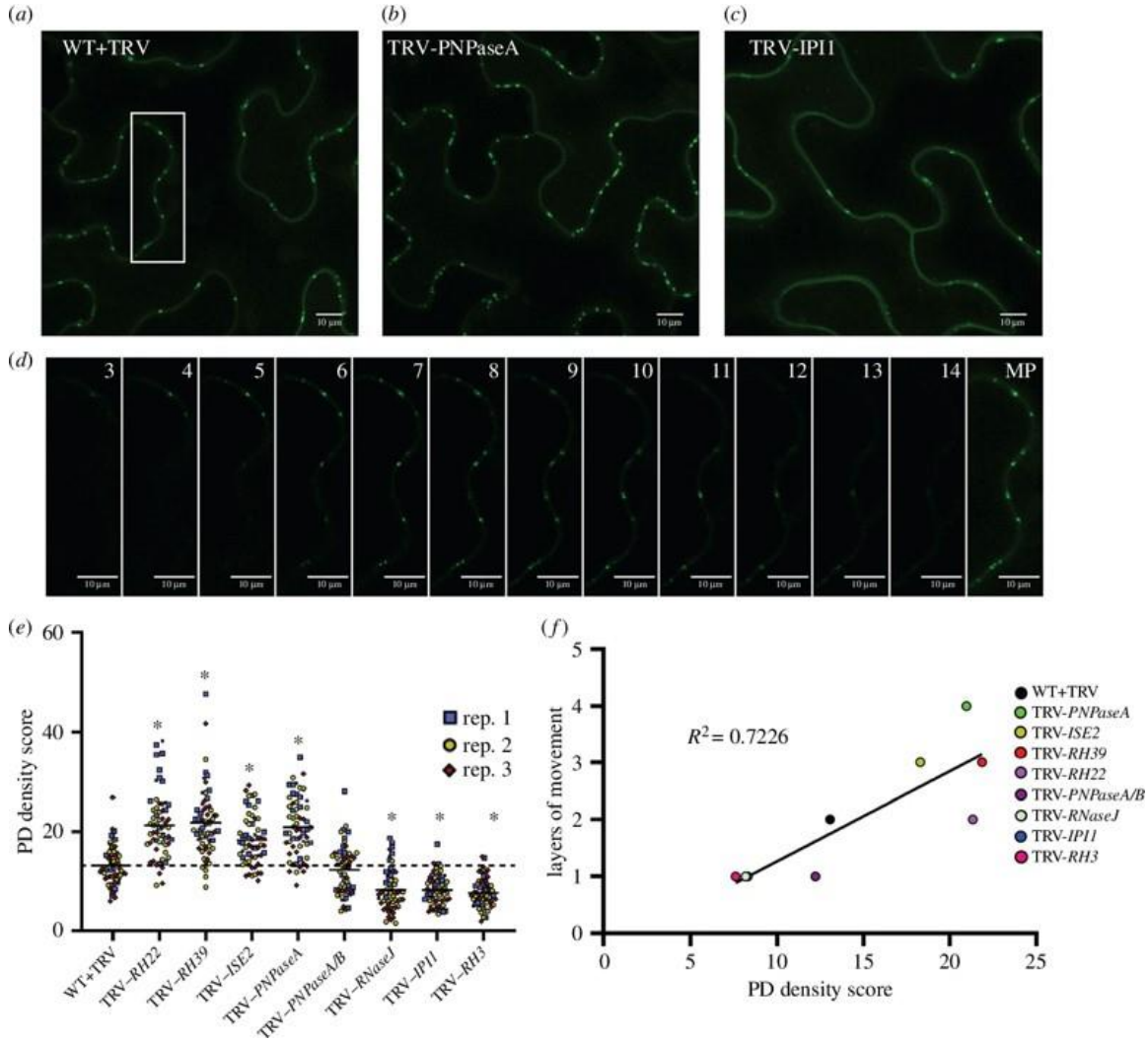
(a)
WT+TRV
(b)
TRV-PNPaseA
(c)
TRV-IPI1
(d)
3
4
5
6
7
8
9
10
11
12
13
14
MP
(e)
PD density score
rep. 1
rep. 2
rep. 3
WT+TRV
TRV–RH22
TRV–RH39
TRV–ISE2
TRV–PNPaseA
TRV–PNPaseA/B
TRV–RNaseJ
TRV–IPI1
TRV–RH3
(f)
layers of movement
PD density score
$R^2$ = 0.7226
WT+TRV
TRV-PNPaseA
TRV-ISE2
TRV-RH39
TRV-RH22
TRV-PNPaseA/B
TRV-RNaseJ
TRV-IPI1
TRV-RH3

(figure 14e). Note that, except for *RH22*, silencing these genes led to increased intercellular trafficking of GFP (figure 13). In contrast, in epidermal cells in leaves where *RNaseJ*, *IPI1* or *RH3* were silenced, there were drastic, statistically significant decreases in PD density (figure 14e). Silencing of those genes had led to decreased intercellular trafficking (figure 13). Relative to the non-silenced control, silencing both PNPase homologs with the TRV-*PNPaseA/B* construct did not affect the PD density (figure 14e), although it led to decreased intercellular trafficking (figure 13). Comparing intercellular trafficking to PD density revealed a positive correlation between PD density and intercellular trafficking (figure 14f). *H*owever, the data for TRV-*RH22* and TRV-*PNPaseA/B* do not fit the curve suggesting that other factors beyond PD density may contribute to the changes observed in intercellular trafficking.

## Discussion

In this study we took a reverse genetics approach to investigating the relationship between chloroplasts and PD in coordinating intercellular trafficking, called ONPS. Expression of genes encoding factors needed for chloroplast gene expression was knocked down by VIGS, resulting in varying degrees of chlorosis in the silenced plants. Movement assays in epidermal cells of silenced leaves revealed that in 7 of the 8 samples examined, perturbing chloroplast gene expression disrupted intercellular trafficking (figure 13). The use of reverse genetics allowed us to sidestep one of the main challenges that encumbers investigations of PD. Mutants with defects in PD are scarce, likely due to their

embryonic and seedling lethality [291],[301]. Similarly, Arabidopsis *RH22*, rh3, *RH39*, pnpase, *IPI1* and rnase j mutants all display embryonic or seedling lethality [294],[295],[296],[302],[303],[304]. It would therefore be difficult to examine the roles of these genes in other aspects of plant development. The use of VIGS in *N. benthamiana p*lants provides a relatively straightforward system to reduce gene expression and measure effects on PD function. Another advantage of *N. benthamiana* and VIGS is that it allows the acute effects of perturbation of gene expression to be assessed. Plants are wild type until initiation of VIGS, and have presumably induced relatively few responses to cope with the loss of gene function as they would in a true genetic mutant. Thus, *N. benthamiana* and VIGS represent a powerful new system for probing CRS and ONPS.

Exogenous application of oxidising or reducing agents to plant samples was shown to influence PD-mediated intercellular trafficking [305]. Interestingly, low concentrations of hydrogen peroxide increased PD-mediated trafficking in Arabidopsis roots, while at higher concentrations trafficking was inhibited. Thus, it seems that mild stress induces one PD response while more, or a different stress, can induce a distinct PD response. The results from the silencing of the PNPase homologs support the notion that there is complex regulation of PD responses to signals. The PNPase genes are highly similar, encoding proteins with 97% identity (electronic supplemental figure S3). When only *PNPaseA* was silenced, the plants displayed chlorosis and there was greatly increased PD-mediated intercellular trafficking (figure 13). When both genes were silenced, the

plants displayed the same degree of chlorosis - as when only *PNPaseA* was silenced - but there was a striking change in PD function. Silencing both homologs of PNPase drastically decreased intercellular trafficking (figure 13). While the results from the other silenced plants suggest that degree of chlorosis is predictive for PD, the results from PNPase clearly argue against this. Indeed, when *ISE1*, a gene encoding a mitochondrial DEAD-box RNA helicase, was silenced in parallel to *ISE2*, the *ISE1*-silenced plants had milder chlorosis than *ISE2*-silenced plants but had a larger increase in intercellular trafficking between epidermal cells than did *ISE2*-silenced plants [143].

Interestingly, *PNPaseA*-silenced leaves contained increased PD density while *PNPaseA/B*-silenced leaves showed no difference in PD density relative to the non-silenced controls (figure 14). The increased PD density and intercellular trafficking observed in *PNPaseA*-silenced plants agree with the general trend observed for the other silenced lines (figure 14e) and support a simple model in which the increased cell-to-cell diffusion of free GFP is facilitated by having more PD pores. The results from *PNPaseA/B* confound this simple model, and suggest that it is not only the availability of PD pores that accounts for intercellular trafficking. Similarly, *RH22*-silenced leaves had no change in intercellular trafficking relative to the controls but showed a marked increase in PD density (figure 14e). Previous analysis of *ISE2*-silenced plants and *ISE2* mutant embryos revealed increased occurrence of twinned and branched PD along with increased

intercellular trafficking, suggesting that the formation of secondary (complex) PD facilitate increased cell-to-cell trafficking [143].

Often overlooked in discussions of PD is their variety and apparent subfunctionalization. Primary PD form during cytokinesis when strands of the endoplasmic reticulum (ER) are trapped in the nascent cell wall while secondary PD form de novo across existing cell walls in the absence of cytokinesis [17]. In mature tissues PD are more elaborate with branching channels that may contain large central cavities compared to the simpler linear pores that are often observed in developing tissues. This change in structure may be associated with changes in their trafficking capacities. Simple PD in sink leaves were reported to allow trafficking of larger molecules than do the branched PD of source leaves [26]. The PD marker used in this study, PDLP1-GFP, localizes to all PD and does not distinguish between simplex and more complex PD in the manner of other markers, e.g. MP17-GFP derived from the potato leafroll virus [53,65]. Thus, the possibility that silencing different chloroplast-related genes resulted in the formation of different classes of PD (primary versus secondary, and simple versus branched) with distinct trafficking properties cannot be ruled out. Taken together, our results can be integrated into a model where during leaf development CRS regulates expression of PD associated nuclear genes (PDANGs) to control the formation of secondary PD that would complement the existing primary PD generated during cell division, allowing the flux of carbon into or out of cells to match the developmental state of chloroplasts. When chloroplast

development and CRS are disrupted, the regulation of PDANGs expression is disturbed and, depending on the strength and identity of the signaling molecules regulating gene expression, the number of secondary PD formed exceeds or falls short of normal levels, resulting in altered intercellular trafficking. *F*urther examination of PD ultrastructure in our system to delineate the contributions of simple or complex and PD of primary or secondary origins to intercellular trafficking is therefore warranted. Such studies would address longstanding questions regarding the function of different classes of PD. However, studies on ONPS are constrained by our limited understanding of the genetic underpinnings of PD formation and function. Further elucidation of ONPS will depend on the identification of PDANGs whose expression in response to CRS can be validated and used as reliable markers for chloroplast-nuclear communication for PD regulation.

## Conclusions

Our findings support the role of chloroplasts in regulating intercellular trafficking via PD formation. The tetrapyrrole biosynthetic pathway has been identified in this study as one potential source of CRS that mediate changes in PD-mediated intercellular trafficking (data not shown see [260]). However, other CRS may also be involved in communicating the physiological state of the chloroplasts to the nucleus to then modulate expression of genes important for PD function. A positive correlation between PD density and intercellular trafficking was measured, suggesting that the presence of more pores can allow

increased diffusion of molecules from one cell to another. However, the results also suggest that other factors in addition to simple numbers of PD are important for determining intercellular flux and these will be the subjects of future investigation. The system used in these studies, consisting of VIGS in *N. benthamiana* , is amenable to the study of chloroplast- and/or PD-related genes whose loss results in lethality, and this system should prove useful for further studies of ONPS and PD formation and function.

## Materials and Methods

### *Plant material and growth conditions*

*N. benthamiana* plants were grown in light carts with 16 h light (approximately 120 µmol m-2 s-1) and 8 h dark. Silencing was done on 3-week-old plants (around the time of 2 – 4 true leaves were present). After infiltration with silencing constructs, plants were grown on the light cart for an additional 2 weeks until silencing of PHYTOENE DESATURASE (*PDS*), the positive control, could be observed and other analyses were performed. Photographs of plants were taken with a Nikon D60 camera (Nikon, Inc.).

### *RNA extraction and cDNA synthesis*

Wild type or silenced *N. benthamiana* tissue was collected and snap frozen in liquid nitrogen. RNA from three independent samples was isolated using the Trizol method (Thermo Fisher Scientific, Waltham, MA) according to manufacturer's instructions. RNA was DNAse treated using the DNA-free DNA

removal kit (Invitrogen, Carlsbad, CA). cDNA was synthesized using oligo-dT primers with M-MLV reverse transcriptase (Promega, Madison, WI) according to manufacturer's instructions. cDNA was used for gene cloning or quantitative-PCR.

### *Gene cloning and generation of recombinant VIGS vectors*

*N. benthamiana* gene sequences were obtained from the Sol Genomics Network Database (https://solgenomics.net) or the University of Sydney's *Nicotiana benthamiana* genome page (http://benthgenome.qut.edu.au/). Gene fragments were cloned by PCR and inserted into the multiple cloning site of pYL156 (pTRV-RNA2) vector [306] by restriction digestion-ligation to generate silencing constructs. The primers for cloning VIGS fragments are listed in electronic supplementary material Table S1. The resulting plasmids were transformed into chemically competent Agrobacterium tumefaciens strain GV3101. Infiltrations for VIGS were done according to published protocols [307].

### *Carotenoid and chlorophyll determination*

Total carotenoids x + c (xanthophylls and carotenes), chlorophyll a and b were extracted with 100% acetone. The extracts were centrifuged at room temperature for 5 minutes at 500 x g and supernatants were used to measure the absorption at 661.6 nm, 644.8 nm and 470 nm. The level of total carotenoids x + c, chlorophyll a and b were determined following the equation by [308].

### *Measuring intercellular trafficking by movement assay*

Movement assays to measure intercellular trafficking were performed as described previously [254]. Briefly, silenced leaves were infiltrated with Agrobacterium carrying a binary construct for expression of GFP (p35S:GFP) at OD600=0.0001, and then imaged approximately 48 hours later. z-stacks of foci of GFP were collected on a Leica SP8 confocal microscope with White Light Laser (Leica Microsystems, Buffalo Groove, IL) with a 10X lens and z-stacks were reconstructed and analyzed in Image J [309],[251]. For analysis of movement, the number of layers of cells in the epidermis surrounding the original cell expressing GFP was scored and the highest number was recorded. Movement assays were performed for at least three biological replicates and each replicate included at least 10 foci. Statistical significance was measured with the Mann-Whitney U test ($p<0.05$) compared to non-silenced WT+TRV samples.

### *Measuring PD density*

#### *PDLP1 expression for measuring pitfield distribution*

Arabidopsis PDLP1 fused to GFP (p35S:PDLP1-GFP) was transiently expressed in leaves of silenced and non-silenced control *N. benthamiana* plants via Agrobacterium infiltration at OD600=0.001. Images were collected 72 hours post infiltration with a Leica SP8 confocal microscope with White Light Laser (Leica Microsystems, Buffalo Groove, IL) using a 25X water emersion objective with 4.00X optical zoom. All images were collected with the same laser power and gain settings. 15 µm z-stacks were collected of epidermal cells expressing

PDLP1-GFP at a step-size of 1µm. A total of 60 stacks were collected across three biological replicates for the control and each of the silenced plants.

***Image analysis for measuring pitfield distribution***

All image analysis was performed using ImageJ. Maximum intensity projections were generated for each the z-stacks collected. Cell wall lengths were measured by tracing the cell wall in the field of view. For quantification of the total number of GFP punctae in the image, images were converted to 8-bit images and inverted. The brightness and contrast were adjusted in order to ensure that all pitfields were clearly defined. Binary images were generated by adjusting the threshold of intensity. The Particle Analyzer function in ImageJ was used to count the total number of punctae in the image. For measuring pitfield area and fluorescence intensity, a copy of the inverted 8-bit maximum projection was generated to use as a reference image for measurements. A binary image was generated from the original maximum projection by setting the threshold using the auto-threshold function. The particle analyzer was used to measure the area and the Integrated Density (IntDen, i.e., the average intensity of all the pixels X the area) of each GFP punctum in the un-edited reference image for the regions defined in the binary image.

***Quantifying the PD Density Score***

To assess the total number of PD within each field of view, the following calculation was performed:

PD Density Score=Pitfield density × Average Integrated Density

This measure generates a single value that accounts for differences in number of PDLP1-GFP punctae, their size, and their fluorescence intensity. Statistical significance was measured using the Mann-Whitney U test ($p<0.0001$) compared to non-silenced WT+TRV controls.

# CHAPTER 4
# VIRUSES INDUCE SECONDARY PLASMODESMATA FORMATION

## Abstract

Plasmodesmata (PD) are responsible for the direct exchange of nutrients and information between neighboring plant cells. They also provide pathogens, including viruses, a direct route for cell-to-cell spread, bypassing the defense mechanisms of the apoplast. Increased intercellular trafficking through PD during virus infection has long been observed, but the mechanism viruses use to facilitate this increase in trafficking has remained elusive. Here, we demonstrate that infection by a diverse set of viruses triggers an increase in the total number of PD in infected leaves. This increase is triggered by the expression of viral movement proteins and can be replicated by expressing movement proteins in the absence of virus infection. Further, type I Remorins, known inhibitors of virus infection, are negative regulators of plasmodesmata formation. Our results lead to the hypothesis that gating of plasmodesmata during virus infection is a direct result of increased secondary plasmodesmata formation and open new avenues for investigating PD structure-function relationships.

## Introduction

With the evolution of multicellularity, intercellular communication became critical to support growth and development. In plants, the cell wall constitutes a physical barrier that separates neighboring cells and places an extra constraint on intercellular communication. Plants have evolved complex cell-wall-spanning organelles called plasmodesmata (PD). PD are membrane-lined pores that form

direct cytoplasmic connections between neighboring cells, allowing the exchange of nutrients and signaling molecules between neighboring cells and, as such, they are essential for plant growth, development, and defense.

While PD are essential for plant viability, they serve as conduits for the cell-to-cell spread of pathogens and pathogen-derived molecules including effectors [310],[311],[312],[313]. Unlike animal viruses, plant viruses do not spread from cell to cell by budding from the surface of infected cells but instead move between cells via PD [73, 74, 313]. The cell wall is freely permeable to very small molecules with stokes radii less than 3.3 nm that are transported through the apoplast and viruses exceed the size limit of molecules that can diffuse through the extracellular matrix [8]. Therefore, plant viruses co-evolved with their hosts to ensure their ability to establish an infection and systemic spread via PD. Most viruses encode specialized proteins called movement proteins (MPs) that are responsible for trafficking the viral genome to and through the PD [313, 314]. The MPs are also responsible for increasing intercellular trafficking through PD during infection. The process of increasing intercellular trafficking through PD during virus infection is referred to as gating. While gating has been demonstrated to be a hallmark of infection for almost all plant viruses, it was first characterized for the TMV 30K movement protein [49],[44],[193]. Early experiments with GFP-tagged TMV MP and microinjected fluorescent dextrans demonstrated that gating of PD occurs at the leading edge of infection and trafficking reverts back to normal levels in cells at the center of the infection focus

[193]. This suggests that the effects of gating on PD are not permanent and trafficking can return to normal levels once the virus has been cleared from the cell.

There are several models for how viruses gate PD during infection. Callose homeostasis at PD is considered to be the primary regulator of intercellular trafficking through PD [91],[315]. Accumulation of callose at the PD has been correlated with decreased trafficking and depleted callose levels at the PD have been correlated with increased trafficking through PD. The leading model of gating centers on the role of callose degradation at PD to dilate the pore allowing increased intercellular flux [55]. In diverse plants, multiple callose degrading enzymes called β-1,3-glucanases are upregulated during virus infection. During infection with turnip vein clearing virus (TVCV), expression of *AtBG2* and *AtBG3* was induced, suggesting that the encoded proteins were important for facilitating host susceptibility to the virus [97]. Surprisingly, Arabidopsis *AtBG2* and *AtBG3* mutants showed no difference in course or outcomes of virus infection compared to wild-type plants, indicating that they are not important for gating PD during infection. Rather, a constitutively expressed PD-associated β-1,3-glucanase (*AtBG_ppap*) was found to mediate virus-induced callose degradation at PD during infection [38]. Additionally, incorporation of a class I β-1,3-glucanase (*GLU1*) from tobacco (Nicotiana tabacum) into the genome of Tobacco mosaic virus (TMV) resulted in increased rates of viral spread concomitant with decreased levels of PD-associated callose [316]. Further complicating the

current models for gating of PD is the contradictory evidence from high-resolution imaging by electron microscopy that fails to reveal changes in PD ultrastructure, i.e. dilated pores, during virus infections. Striking recent work based on electron tomography has unexpectedly revealed that PD with narrow cytoplasmic sleeves exhibited increased trafficking capacities compared to PD with larger cytoplasmic sleeves [188]. Consistent with this, PD in transgenic Arabidopsis plants expressing the TMV MP, MP30, were indistinguishable from PD from control plants [317]. MP30 is known to be sufficient to gate PD [49]. Collectively, these findings suggest that gating may not depend on PD dilation.

One alternative mechanism for regulating intercellular trafficking is through the formation of new PD [143, 260]. Plasmodesmata can be formed via two distinct mechanisms [183],[142]. PD can be formed during cell division as the developing cell plate is formed. This type of PD formation is called Primary PD formation [318]. In addition to primary PD formation, pores can also be inserted into existing cell walls in the absence of cell division. This process is referred to as secondary PD formation [16, 17]. Secondary PD are often structurally more complex than primary PD and frequently adopt branched morphologies [319]. While tissues with high trafficking capacities typically contain more PD than do other tissues, PD formation as a mechanism to regulate trafficking is rarely considered. This model of how intercellular trafficking can be modified has gained less traction than the callose degradation model, possibly because of the challenging experiments needed to test its predictions. One of the first examples

showing a direct link between secondary PD formation and increased levels of intercellular trafficking came from studies on the chloroplast RNA helicase, *ISE2*. Silencing of *ISE2* resulted in increased intercellular trafficking and this increase was correlated with an increase in secondary PD formation [143]. Ganusova et al. further demonstrated a link between PD number and trafficking capacity by demonstrating a linear correlation between the number of plasmodesmata and the amount of intercellular trafficking of GFP [260]. Notably, viral movement proteins have been shown to associate preferentially with secondary, or branched, PD [77, 320]. Immuno-gold labeling has been used to demonstrate that TMV MP30 and the movement protein of the phloem limited Potato leaf roll virus (PLRV MP17) accumulate in branched PD but not simple plasmodesmata indicating a preference for secondary PD [320]. Interestingly, expression of these movement proteins in tissues with few secondary PD has been used to demonstrate that MP30, but not MP17, can localize to primary PD [17]. This observation suggests that MP30 can interact with both primary and secondary PD.

Many PD-associated host proteins have been identified as being important regulators of virus infection. The remorin family of proteins has emerged as a major regulator of plant defense. Remorins are plant-specific proteins that associate with the inner leaflet of the plasma membrane and accumulate in PD and lipid rafts [117, 321], [322].

Type I Remorins are negative regulators of virus infection [94, 117, 323]. Potato remorin (StREM1) mutants exhibited increased susceptibility to Potato virus X as evidenced by increased local and systemic spread of the virus [117]. Conversely, overexpression of StREM1.3 in *Solanum lycopersicum* has been shown to restrict the cell-to-cell movement and gating PD by multiple viruses, including PVX, TMV, and Turnip mosaic virus (TuMV) [117, 119, 323]. It is unclear how remorins regulate virus movement, but several viral proteins, including the movement proteins of Tomato mosaic virus and PVX, have been shown to interact with Group 1 remorins [94, 125, 323]. Additionally, Rice stripe virus has been shown to target *Nicotiana benthamiana* REM1 for degradation via the proteosome and autophagy, indicating that viruses have evolved mechanisms to circumvent the negative regulatory effects of group 1 remorins on virus infection [94].

We were interested in better understanding the cellular mechanism of virus-induced gating of PD. Here, we demonstrate that during infection with diverse viruses, there is an increase in the total number of PD in infected leaves. PD formation was induced during the early stages of infection in the primary infected leaf and during invasion of systemically infected leaves and that viral MPs alone were able to induce pore formation in the absence of infection. Using virus-induced gene silencing, we discovered that *NbREM1* is a negative regulator of PD formation. Overexpression of *NbREM1* blocked MPs effects on intercellular trafficking and PD formation, thereby decreasing intercellular spread of the virus.

These findings lead to a new model of PD gating during virus infection where gating is achieved through the de novo formation of PD.

## Results

### *Tobacco mosaic virus infection results in increased numbers of pitfields*

In order to determine if virus infection increases the number plasmodesmata, *Nicotiana benthamiana* plants were infected with TMV-GFP via agroinfiltration. Empty vector Agrobacterium was used as a control. An agrobacterium strain encoding AtPDCB1-mCherry, a known PD marker, was co-infiltrated with the TMV infectious clone or the control to label the PD pitfields. Inoculated leaves were imaged 96 hours post infiltration with confocal microscopy. TMV-GFP infection resulted in a substantially increased numbers of PDCB1-mCherry labeled pitfields indicating that virus infection triggers an increase in the number of plasmodesmata compared to uninfected leaves (Figure 15a and b).

In order to determine if systemically infected leaves also show increases in the number of plasmodesmata during infection, upper leaves from infected plants were agroinfiltrated with PDCB1-mCherry 7 days post infection and imaged with confocal microscopy at 10 days post infection (72 hours post second infiltration). Systemically infected leaves showed an increase in the number of pitfields compared to uninfected control plants, indicating that TMV also increases PD formation during systemic infection (Figure 15 c and d).

**Figure 15 Tobacco mosaic virus induces secondary plasmodesmata formation.**

PD pitfields in uninfected and TMV-30BGFP infected plants were quantified using AtPDCB1-mCherry as a marker for PD pitfields. Images were collected from the inoculated leaf 96 hours post infection (a) and from systemically infected leaves 10 days post infection (c). Representative images of *N. benthamiana* epidermal cells expressing PDCB1-mCherry. TMV-30BGFP encodes a monomeric GFP marker (a and c, lower left panel). Pitfield densities were quantified for at least 20 fields of view for 2 biological replicates (b and d, red and blue circles). (e) Representative TEM images of cell wall and PD from uninfected (left) and TMV infected (right) *N. benthamiana leaves.* PD frequency, the number of PD per $\mu m^2$ of cell wall was calculated by TEM. Statistical significance was determined by student's t-test ($p < 0.005$). Scale bar = 10μm.

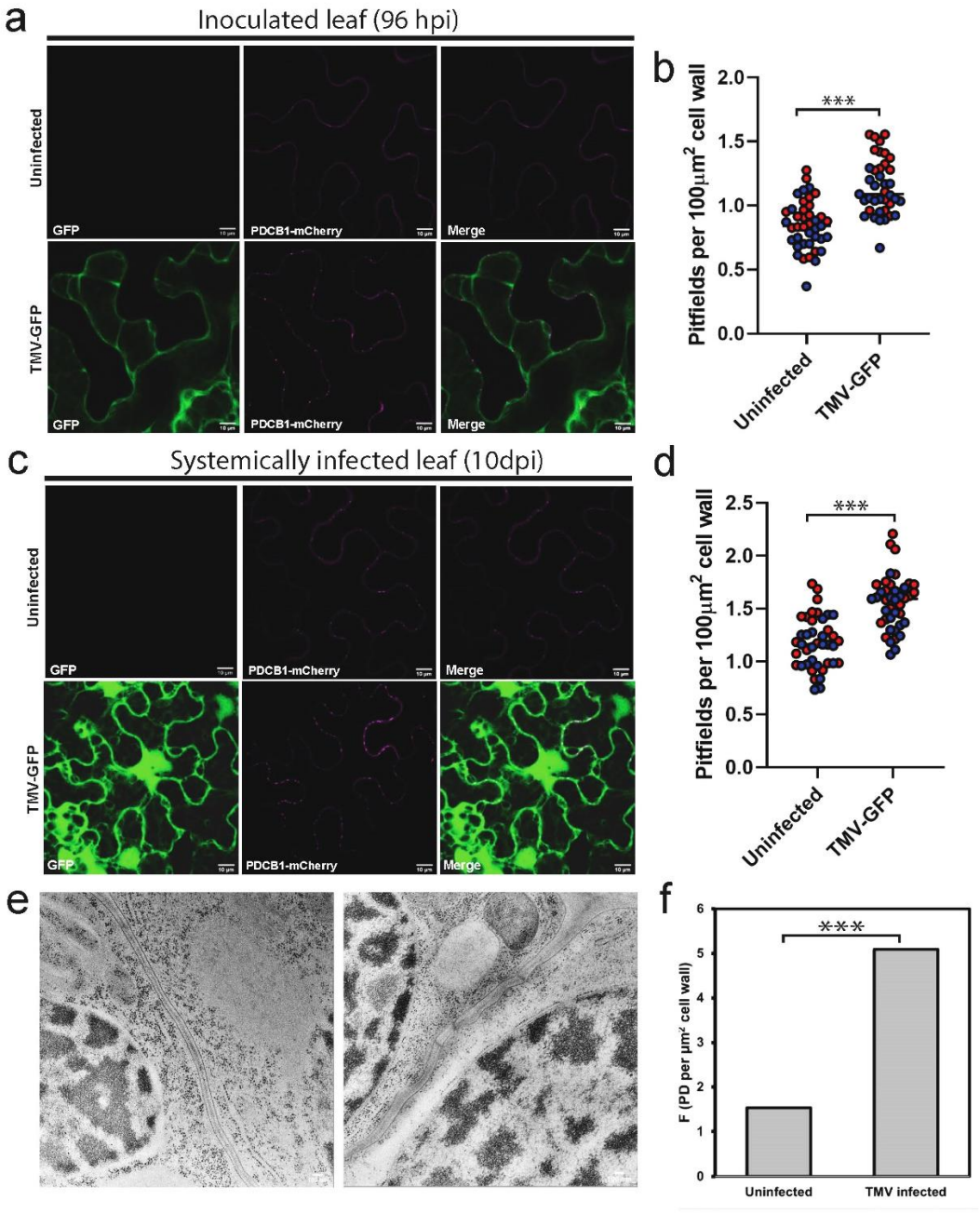
a
Inoculated leaf (96 hpi)
Uninfected
TMV-GFP
GFP
PDCB1-mCherry
Merge
b
Pitfields per 100μm² cell wall
***
Uninfected
TMV-GFP
c
Systemically infected leaf (10dpi)
d
e
f
F (PD per μm² cell wall)
Uninfected
TMV infected

This increase in PD density was confirmed by TEM (Figure 15e). Consistent with the increased pitfield densities observed in infected leaves, TMV-infection resulted in an increase in the number of PD connecting neighboring epidermal cells in systemically infected leaves of *N. benthamiana*.

In order to determine if the increase in PD formation in upper leaves is triggered by a mobile signaling molecule ahead of virus movement, PDCB1-mCherry was expressed in upper leaves of uninfected and TMV-GFP infected plants and imaged 84 hours post infection (Figure 16a and b). At this stage of infection, TMV-GFP has begun replication and local cell-to-cell spread in the inoculated leaf, but it has not moved into the systemic leaves. Quantification of PDCB1-mCherry labeled pitfields revealed that there was no change in the number of pitfields in the upper leaves of TMV-infected leaves prior to viral invasion of the uninfected tissue (Figure 16a and b). This indicates that the virus must be present in the tissue to induce PD formation.

***The TMV movement protein induces PD formation***

Viral movement proteins are responsible for gating PD during infection. In order to determine if the increase in pitfield densities observed in TMV-GFP infected leaves was initiated by the movement protein, the TMV movement protein, MP30-GFP, was co-expressed with the pitfield marker, PDCB1-mCherry, in uninfected *N. benthamiana* leaves. Analysis of the number of pitfields labeled by PDCB1-mCherry in the presence or absence of MP30-GFP revealed that the pitfield density is increased in plants expressing MP30-GFP compared to when

**Figure 16 The movement protein of TMV induces PD formation.**

In order to determine if the virus must be present in the tissue to induce PD formation, images were collected from young leaves of uninfected and TMV-GFP infected *N. benthamiana* leaves 84 hours post infection, before infection had reached the young leaves (a). Pitfield densities were quantified for at least 20 fields of view for 2 biological replicates (b, red and blue circles). In order to determine if the presence of the viral movement protein in the cell induces PD formation, PDCB1-mCherry was expressed either alone or with TMV MP30-GFP. Representative images of epidermal cells expression either PDCB1-mCherry alone (c, top row) or with MP30-GFP (c, bottom row) are shown. Pitfield densities were quantified for both PDCB1-mChery and MP30-GFP for at least 20 fields of view for 3 biological replicates (d, red, blue, and yellow circles). Statistical significance was determined by student's t-test ($p < 0.001$). Scale bar = 10μm.

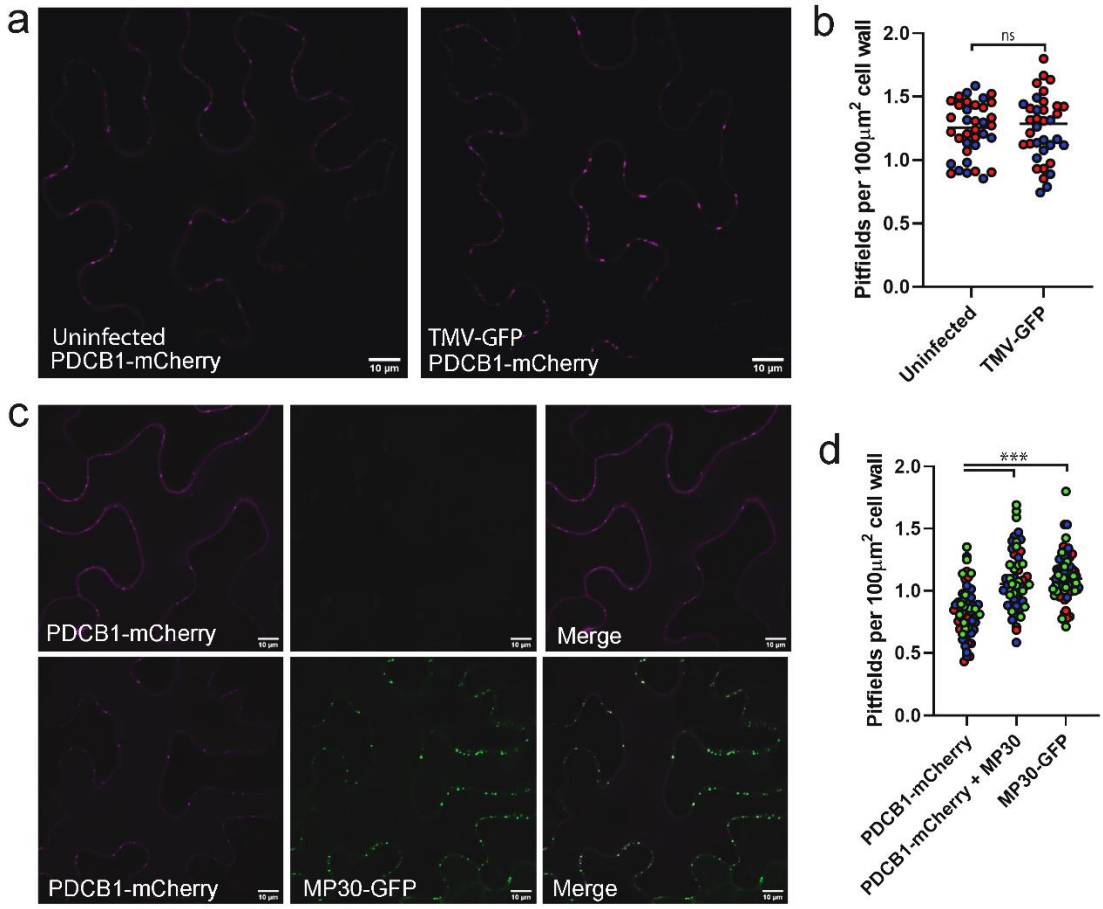
a
Uninfected
PDCB1-mCherry
TMV-GFP
PDCB1-mCherry
b
Pitfields per 100μm² cell wall
2.0
1.5
1.0
0.5
0.0
ns
Uninfected
TMV-GFP
c
PDCB1-mCherry
Merge
PDCB1-mCherry
MP30-GFP
Merge
d
Pitfields per 100μm² cell wall
2.0
1.5
1.0
0.5
0.0
***
PDCB1-mCherry
PDCB1-mCherry + MP30
MP30-GFP

PDCB1-mCherry is expressed alone (Figure 16c and d). This indicates that expression of viral movement proteins in the absence of the full virus is sufficient to induce PD formation. Strikingly, the increase in pitfield density induced by expression of MP30-GFP is equal to the increase observed during TMV infection (Figure 16d).

In order to determine if PD localization of MP30 is required to trigger the increase in pitfield density, a mutation previously shown to block PD localization of MP30 was introduced into the coding sequence of MP30 (MP30(V4A)) [130]. Expression of MP30(V4A)-GFP in *N. benthamiana* leaf epidermal cells revealed that the protein accumulates in the nucleus, ER, cytoplasm, along microtubules, and in association with chloroplasts (Figure 17b). Co-expression with PDCB1-mCherry revealed that the mutant MP30 does not localize to PD. Expression of MP30(V4A)-GFP failed to increase intercellular trafficking of free mScarlet indicating that the mutant MP is unable to gate PD (Figure 17 c and d). Quantification of pitfield densities in cells co-expressing MP30(V4A)-GFP and PDCB1-mCherry revealed that proper localization of the movement protein to the PD is also required to increase the number of PDCB1-mCherry labeled pitfields (Figure 17e). This indicates that proper localization of MP30 to PD is required to induce plasmodesmata formation.

***Diverse families of viruses induce secondary PD formation during infection***

To determine if induction of PD formation is a conserved feature of virus infection, *N. benthamiana* plants were infected with Turnip mosaic virus carrying

**Figure 17 PD localization of MP30 is required to increase trafficking and induce PD formation.**

A point mutation was introduced into the N-terminal PD localization signal of MP30 to generate MP30(V4A)-GFP. Representative images of *N. benthamiana* leaf epidermal cells expressing WT MP30-GFP (a) and MP30(V4A)-GFP (b) are shown. PD localization of MP30(V4A) is severely disrupted and the protein associates with the ER, chloroplasts, and what appear to be microtubules (b). Intercellular trafficking was measured by counting the number of layers of intercellular movement of free mScarlet in plants expressing WT MP30-GFP, MP30(V4A), or control plants. Data for two biological replicates are shown (c and d). For each replicate, 20 foci were collected. A quantitative representation of the data is depicted in panel c to show the distribution of data for each condition. The Mean layer of movement plus the standard deviation is shown in panel d. Statistical significance was determined using the Mann-Whitney U-test ($p < 0.001$). Pitfield densities were calculated by expressing PDCB1-mCherry alone or with either MP30-GFP or MP30(V4A)-GFP. PDCB1-mCherry labeled pitfields were quantified (e). Data for 1 biological replicate (n = 20 fields of view) is shown. Significance was determined with a student's t-test ($p < 0.01$).

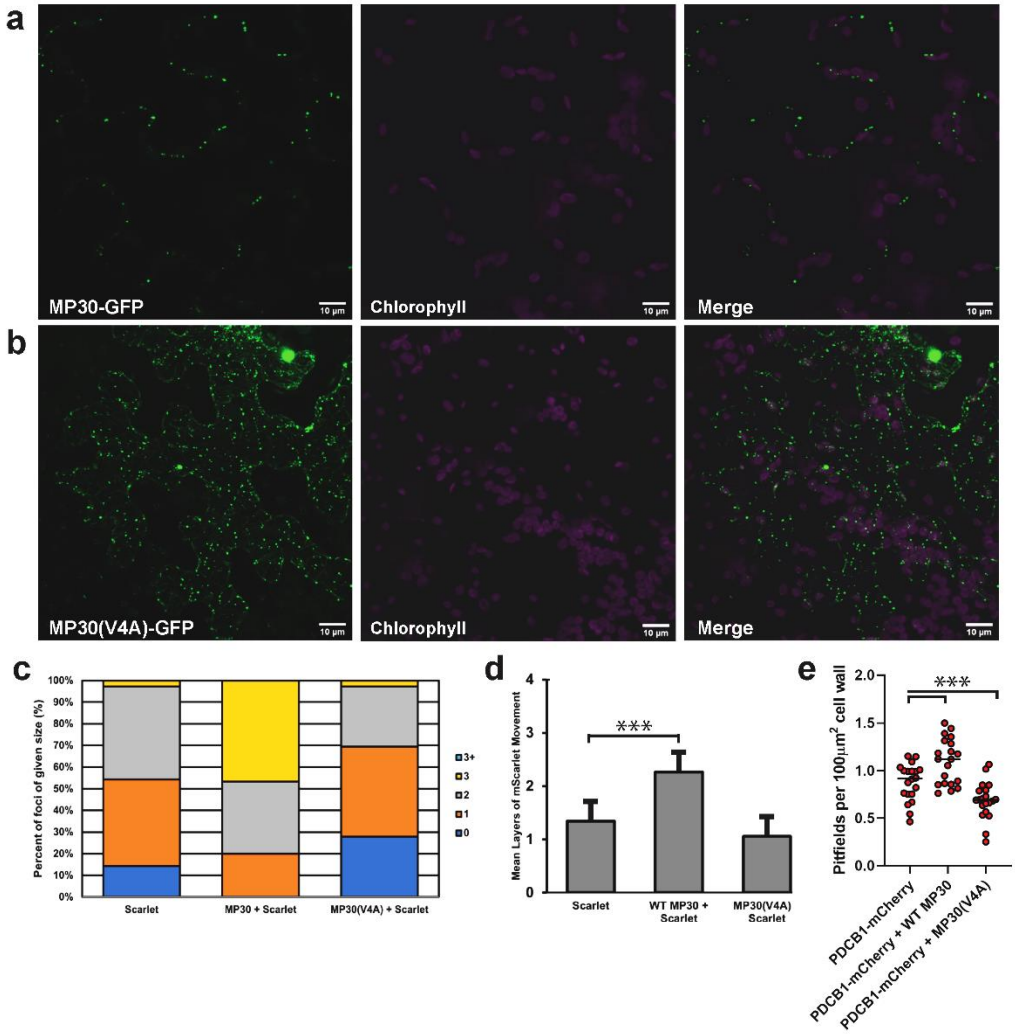
a
MP30-GFP
Chlorophyll
Merge
b
MP30(V4A)-GFP
Chlorophyll
Merge
10 µm
c
Percent of foci of given size (%)
100%
90%
80%
70%
60%
50%
40%
30%
20%
10%
0%
Scarlet
MP30 + Scarlet
MP30(V4A) + Scarlet
3+
3
2
1
0
d
Mean Layers of mScarlet Movement
***
Scarlet
WT MP30 + Scarlet
MP30(V4A) Scarlet
e
Pitfields per 100µm² cell wall
***
PDCB1-mCherry
PDCB1-mCherry + WT MP30
PDCB1-mCherry + MP30(V4A)

a GFP tag (TuMV-GFP,potyviridae), Tobacco rattle virus (TRV, Tobraviridae), African cassava mosaic virus (ACMV) and East African cassava mosaic Cameroon virus (geminiviridae). PD distributions in GFP-tagged viruses were quantified using PDCB1-mCherry and in plants infected with non-tagged viruses, PD densities were quantified using the strong PD marker PDLP1-GFP. Consistent with TMV-GFP, leaves systemically infected with every virus tested showed elevated numbers of PD pitfields compared to uninfected controls indicating that diverse families of viruses induce secondary PD formation as a step of their infection (Figure 18a and b).

Expression of MP30-GFP in systemically infected leaves resulted in no significant change in PD density compared to uninfected controls (Figure 18c). This indicates that the induction of PD formation elicited by MP30 alone is not enhanced by the presence of virus infection

***NbREM1 is a negative regulator of PD formation***

Type I remorins have previously been described as negative regulators of virus-induced gating of PD [117] [94, 323] . In order to investigate the role of *NbREM1* in inhibiting gating, a silencing construct that targets both *N. benthamiana* homologs, *NbREM1*.1 and *NbREM1*.2, was designed for virus induced gene silencing.

Consistent with previous work with Remorin-mutant plants, *REM1*-silenced plants, exhibit increased levels of intercellular trafficking of free GFP compared to non-silencing TRV control plants (Figure 19a-c). Expression of

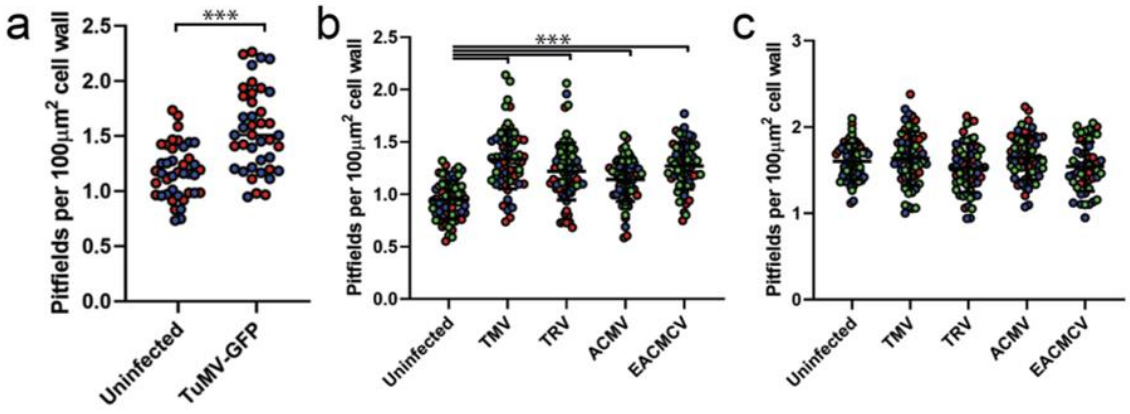


**Figure 18 Diverse viruses induce PD formation as part of their infection**

Pitfield densities were quantified in plants systemically infected with TuMV-GFP (a), TMV, TRV, ACMV, and EACMCV 10 days post infection (b). Pitfields in TuMV-GFP infected plants were labeled with PDCB1-mCherry (a). Pitfield densities for 2 biological replicates are shown (a, red and blue circles). Pitfields in non-tagged viruses (TMV, TRV, ACMV, and EACMCV) were labeled with the strong PD marker, PDLP1-GFP. Pitfield densities for 20 foci for each of 3 biological replicates are shown (b, red, blue, and yellow circles). Statistical significance was determined using a student's t-test ($p < 0.0001$). Expression of MP30-GFP in systemically infected leaves does not enhance the effects of PD formation in virus infected leaves (c). 20 foci for each of 3 biological replicates are shown (c, red, blue, and yellow circles). No statistical difference was observed ($p > 0.05$).

**Figure 19 *NbREM1* is a negative regulator of PD formation.**

. (a-c) Intercellular trafficking was measured by counting the number of layers of GFP spread in *N. benthamiana* leaf epidermal cells. Representative images of foci from non-silencing controls (a, left) and *NbREM1*-silenced plants are shown. Scale bar = 50 μm. Data for three biological replicates are shown. 20 foci were collected for each biological replicate. Data is depicted as a Quantitativeplot of the percentage of foci of each size (b) and the Mean layers of movement and standard deviation (c). Statistical significance was determined using the Mann-Whitney U-test ($p < 0.001$). (d- g) Pitfield distribution assays were performed using PDLP1-GFP (d and e) and MP30-GFP (f and g). Representative images for cells expressing PDLP1-GFP (d) and MP30-GFP (f) are shown. Pitfield densities for 20 fields of view for each of 3 biological replicates (e and g, red, blue, and yellow circles) are shown for PDLP1-GFP (e) and MP30-GFP (g). Statistical significance was determined using a student's t-test ($p < 0.001$). Scale bar = 10 μm.

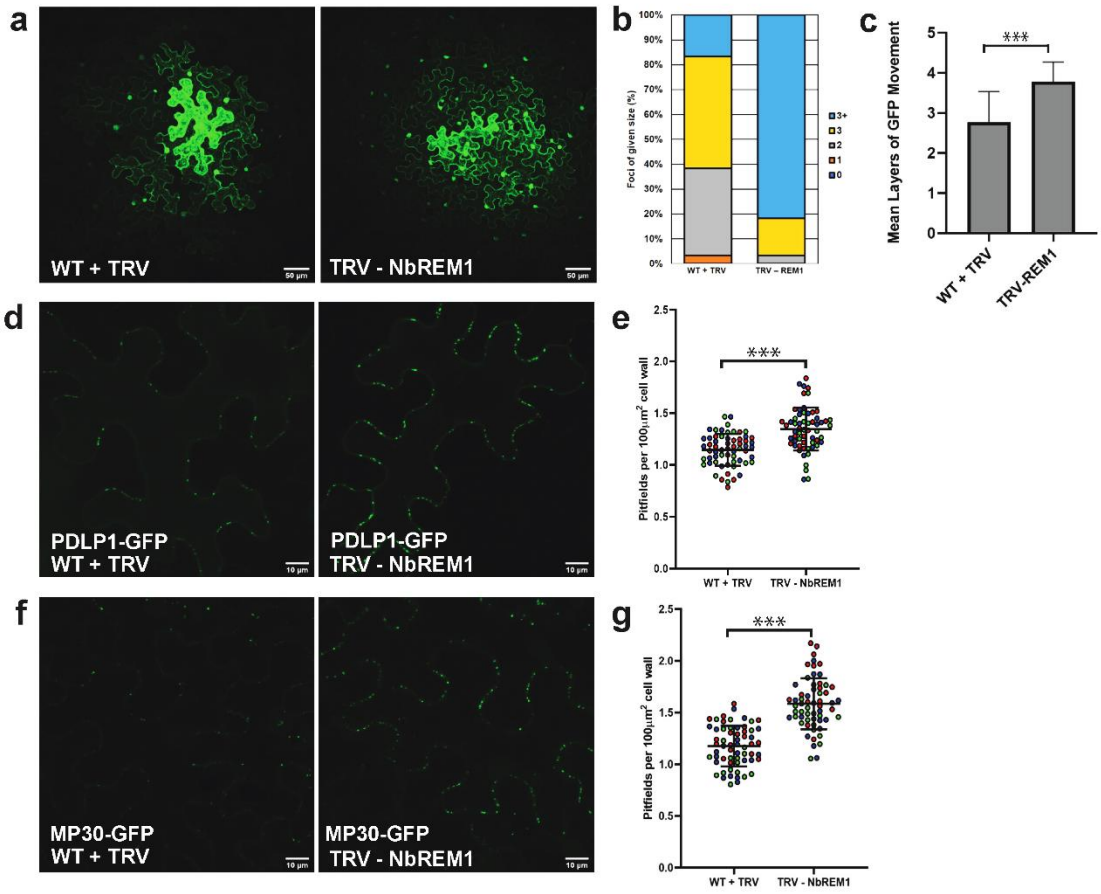
a
WT + TRV
TRV - NbREM1
b
Foci of given size (%)
100%
90%
80%
70%
60%
50%
40%
30%
20%
10%
0%
3+
3
2
1
0
WT + TRV
TRV – REM1
c
Mean Layers of GFP Movement
***
WT + TRV
TRV-REM1
d
PDLP1-GFP
WT + TRV
PDLP1-GFP
TRV - NbREM1
e
Pitfields per 100μm² cell wall
***
WT + TRV
TRV - NbREM1
f
MP30-GFP
WT + TRV
MP30-GFP
TRV - NbREM1
g
Pitfields per 100μm² cell wall
***
WT + TRV
TRV - NbREM1

PDLP1-GFP in REM1-silenced plants revealed that *REM*-silenced plants have elevated numbers of pitfields compared to non-silencing controls (Figure 19d and e). This suggests that *NbREM1* is a negative regulator of secondary PD formation.

In order to determine if virus induced PD formation is affected in *REM*-silenced plants, MP30-GFP was expressed in REM1-silenced leaves. Quantification of the number of MP30-labeled pitfields revealed an increase in the number of pitfields in *REM*-silenced plants compared to non-silenced control plants (Figure 19 f and g). This suggests that *NbREM1* restricts the effects of movement protein-induced PD formation.

When transiently expressed in *N. benthamiana* leaves, REM1-GFP labels the plasma membrane as previously reported (Figure 20 a and b). In contrast to *REM*-silenced plants, overexpression of *35S:REM1-HA* or *35S:REM1-GFP* (data not shown) results in decreased intercellular trafficking (Figure 20 c and d). Overexpression of REM1-HA also results in decreased numbers of PDLP1-GFP labeled pitfields indicating that overexpression restricts PD formation (Figure 20 e and f).

***Overexpression of NbREM1.1 blocks virus induced PD formation***

To determine if overexpression of REM1-HA can block MP30-GFP induced PD formation, MP30-GFP distribution assays were performed in plants over-expressing REM1-HA. Overexpression of REM1-HA resulted in decreased pitfield densities in plants expressing MP30-GFP, indicating that overexpression

**Figure 20 Overexpression of *NbREM1* decreases trafficking, PD**

PD. Intercellular movement was quantified for plants overexpressing either *NbREM1*-GFP or *NbREM1*-GFP. Representative images of foci from WT controls (a) and plants overexpressing *NbREM1*-GFP are shown (b). For consistency with PD distribution data (e-h), intercellular movement data from Nb*REM*-HA overexpressing plant are shown (c and d). Data is depicted as a Quantitativeplot of the percentage of foci of each size (c) and the Mean layers of movement and standard deviation (d). Statistical significance was determined using the Mann-Whitney U-test ($p < 0.001$). PD distribution assays with PDLP1-GFP (e and f) were performed in WT plants and plants overexpressing *NbREM1*-HA. Pitfield densities for 20 foci for each sample for each of three biological replicates are shown (f, red, blue, and yellow circles). Statistical significance was determined with a student's t-test ($p < 0.001$).

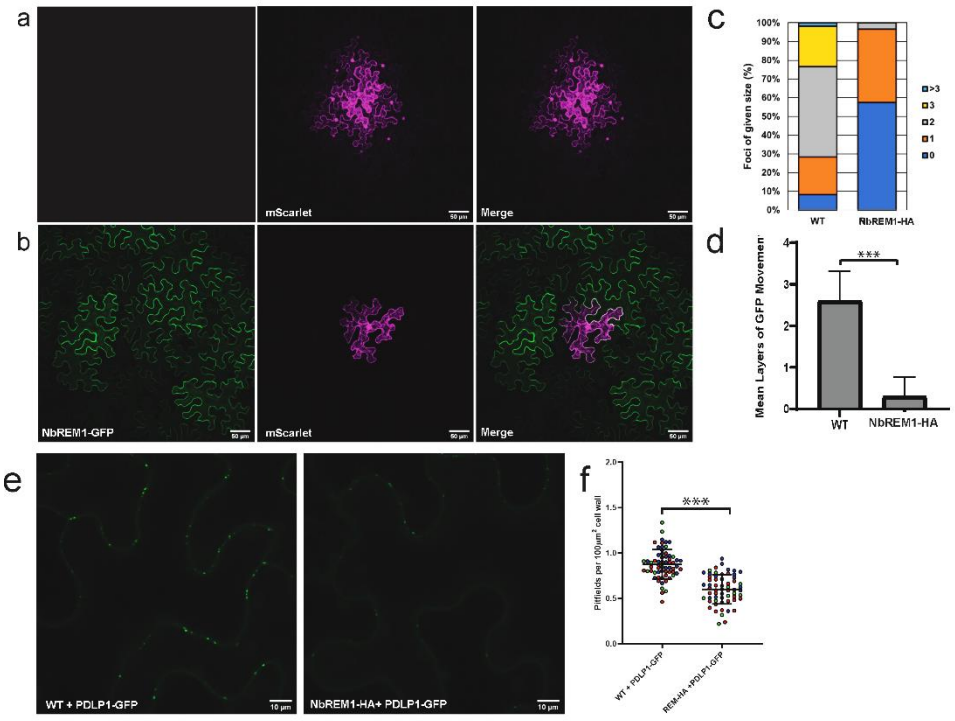
a
mScarlet
Merge
b
NbREM1-GFP
mScarlet
Merge
c
Foci of given size (%)
100%
90%
80%
70%
60%
50%
40%
30%
20%
10%
0%
>3
3
2
1
0
WT
NbREM1-HA
d
Mean Layers of GFP Movemen
***
WT
NbREM1-HA
e
WT + PDLP1-GFP
NbREM1-HA+ PDLP1-GFP
f
Pitfields per 100μm² cell wall
***
WT + PDLP1-GFP
REM-HA +PDLP1-GFP

of *NbREM1* inhibits MP induced secondary PD formation (Figure 21 a and b). To determine if blocking PD formation corresponds to decreased trafficking, movement assays were performed in plants co-expressing *REM*-HA, MP30-GFP, and mScarlet (Figure 21c). Expression of MP30 was unable to increase trafficking of mScarlet in plants overexpressing REM1-HA compared to control plants indicated that MP30 induced PD formation is responsible for the increased trafficking capacity associated with virus infection (Figure 21c).

## Discussion

Despite the long-studied relationship between viruses and plasmodesmata, little is known about how the viruses alter PD function. It has been clear that one of the key features of virus infection is to increase intercellular trafficking through the PD, but the mechanism behind this increase has remained elusive. Our data indicate that the increase in trafficking observed during infection is the result of increased numbers of plasmodesmata in the infected leaves. This model is consistent with the growing evidence supporting a positive correlation between the number of PD in tissue with the trafficking capacity of the tissue [143, 260]. This correlation was first proposed by Burch-Smith et al. when they showed that *ISE2*-silenced plants had increased intercellular trafficking and increased numbers of plasmodesmata [143]. Further investigation into the role of chloroplast RNA processing on PD regulation provided further support for this model of PD regulation [260]. Here, we have shown that the induction of PD formation is a conserved feature of infection by diverse families of plant viruses.

**Figure 21 Overexpression of *NbREM1* block MP30-induced gating of PD**

PD distribution assays with MP30-GFP were performed in WT plants and plant overexpressing *NbREM1*-HA. Pitfield densities for 20 foci for each sample for each of three biological replicates are shown (b, red, blue, and yellow circles). Statistical significance was determined with a student's t-test ($p < 0.001$). (c) Intercellular movement assays were performed in WT, *REM*-HA OE, or MP30-GFP expressing plants and plants co-expressing *REM*-HA and MP30-GFP. Data is depicted as a Quantitativeplot of the percentage of foci of each size (c) and the Mean layers of movement and standard deviation (d). Statistical significance was determined using the Mann-Whitney U-test ($p < 0.001$).

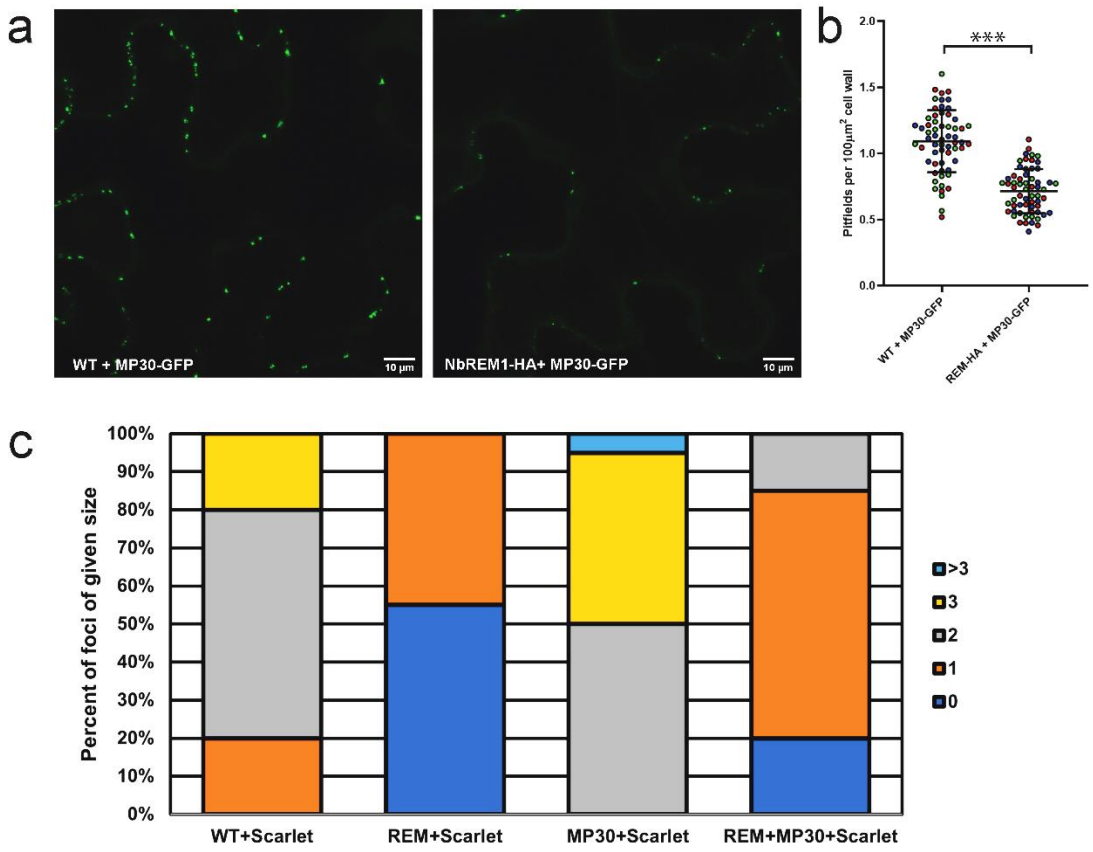
a
WT + MP30-GFP
10 µm
NbREM1-HA+ MP30-GFP
10 µm
b
***
Pitfields per 100µm² cell wall
2.0
1.5
1.0
0.5
0.0
WT + MP30-GFP
REM-HA + MP30-GFP
c
Percent of foci of given size
100%
90%
80%
70%
60%
50%
40%
30%
20%
10%
0%
WT+Scarlet
REM+Scarlet
MP30+Scarlet
REM+MP30+Scarlet
>3
3
2
1
0

in all viruses tested, infection resulted in a significant increase in the number of PD in inoculated and systemically infected leaves. While this does not mean that all plant viruses induce pore formation, it does strongly suggest that it is a common mechanism used by viruses to increase trafficking through PD and to promote their cell-to-cell spread.

Chloroplasts are known targets of virus infection [324],[82],[133],[313]. Many examples of viruses disrupting chloroplast function have been previously reported. It has become clear that chloroplasts are key regulators in PD function and formation. By targeting the chloroplast during infection, viruses can therefore disrupt not only plant defense, but also the plasmodesmata. Notably, silencing and overexpression of the chloroplast localized RNA helicase INCREASED SIZE EXCLUSION LIMIT2 (*ISE2*) disrupts intercellular trafficking in opposite directions. Plants silencing *ISE2* exhibit increased intercellular trafficking and plants overexpressing *ISE2* have decreased trafficking. Surprisingly, *ISE2*-silenced and *ISE2*-overexpressing plants both have increased susceptibility to virus infection [146]. This finding has been difficult to explain, but our data showing that viruses induce PD formation may provide an explanation for how viruses are able to overcome the decreased trafficking observed in *ISE2*-overexpressing plants.

The movement proteins of viruses have long been shown to be responsible for gating PD during infection, but how the movement proteins, which are typically associated with the endoplasmic reticulum and desmotubule of PD, alter the plasmodesmata is unclear. Additionally, while viral movement proteins

share many similarities in their functions, they are also diverse and have evolved to have distinct functions. Our data demonstrate that expression of the TMV movement protein, MP30, is sufficient to induce secondary PD formation. Expression of the GFP-fused MP resulted in a similar increase in the number of pitfields as was seen in plants infected with TMV. Introduction of a point mutation into the plasmodesmata localization signal (PLS) of MP30 (MP30(V4A)), which was previously shown to have disrupted localization, also fails to induce PD formation. This suggests that proper localization of the MP to the PD is required for the induction of PD formation. This is consistent with the idea that new PD are formed in proximity of existing PD proposed by the multiple twinning model of secondary PD formation [16]. In this model, new pores are formed near existing PD suggesting that the machinery required for regulating PD formation reside at the PD and that the local environment of the cell wall at PD is ideal for pore insertion. How MP30-GFP induces PD formation is not clear, but our data provide the first solid evidence that pathogens can modulate PD density in order to promote cell to cell spread.

TMV MP30 is one of the most well characterized viral movement proteins. It is the type member for the 30K movement proteins and is likely to have vastly different functions than the movement proteins of other viral families, such as the Triple gene block movement proteins. Additionally, unlike most viruses, potyviruses do not encode distinct movement proteins. Here, we show that even in the absence of a true movement protein, the potyvirus, TuMV, is able to induce

secondary PD formation. This clearly demonstrates that the mechanisms utilized by the different viruses to induce PD formation are likely different, but the induction of PD formation remains an important step in the spread of virus infection.

The Remorin family of plant specific proteins has emerged as mediators of plasmodesmata function and virus infection. Remorins are plasma membrane associated proteins and associate with PM-nanodomains and plasmodesmata [117, 321], [322]. The Remorin family is separated into 4 sub-families and members of these subfamilies have been shown to have differing roles in regulating PD function. Group 1 remorins have typically been shown to be negative regulators of virus infection [117]. Group 4 remorins have been shown to have a positive role in geminivirus infection [126].

Our data indicates that *N. benthamiana* REM1a restricts virus infection by restricting secondary PD formation. This finding suggests that one of REM1's underlying functions in the plant is to regulate plasmodesmata formation. This raises many interesting questions about the process of pore formation. Remorins have been shown to localize to and be responsible for regulating the organization of plasma membrane nanodomains. In the context of our findings, this suggests that specialized organization of the plasma membrane is critical in determining the position of de novo plasmodesmata formation. Increasing evidence suggests that the specialized lipid composition of PD membranes is critical for their function [37],[188],[325],[326]. The plasma membrane of PD are enriched in

sterols and long chain sphingolipids consistent with lipid rafts [37]. Mutants with defects in sphingolipid biosynthesis were shown to have increased intercellular trafficking and altered PD development [188]. Lipid composition has also been shown to be important for localization of PD proteins such as the GPI-anchored PD-callose binding proteins [326]. Lipid rafts, like PD PMs, have specialized lipid compositions that help to sequester specific groups of membrane-associated proteins. REM1 may act to regulate PD formation by sequestering the machinery needed to insert a new pore into these specialized domains. While the identity of these proteins remains unknown, it is known that specific types of proteins associate with both lipid rafts and PD membranes [327],[37, 328]. One family of proteins that are known to accumulate in both lipid rafts and PD plasma membranes are the GPI-anchored proteins [36, 37]. Addition of a GPI-anchor targets proteins to PD and is one of the few known signals for targeting proteins to the PD [39]. Many known PD-regulatory proteins have been shown or are predicted to be associated with the outer layer of the PM through a GPI-anchor. Notably, several proteins involved in callose metabolism have been shown to be GPI-anchored. The PD callose binding proteins (PDCBs) and several β-glucanases, including *AtBG_ppap* and *AtBG2*, are tethered to the PM by GPI-anchors. Attention on these families has primary been directed towards their role in regulation of intercellular trafficking through PD by degrading callose in order to dilate the PD [55],[91],[315]. The role of these proteins in PD formation have

not been investigated to date, but could serve as a link between PD regulation, callose metabolism, and viruses.

REM1 has also been shown to be involved in different hormone signaling pathways. One example of this is in Salicylic acid signaling. REM1 was shown to rearrange the PM in response to salicylic acid [329]. These changes in membrane organization in response to salicylic acid were correlated with PD closure. Additionally, Salicylic acid-driven Remorin-dependent membrane remodeling was shown to be important for regulating the positioning of the auxin transporter, PIN2 [330]. This connection between hormone signaling and the PM would provide the plant with a mechanism to finely tune PD formation throughout plant development and in response to pathogens. It also could serve as a direct signal from the chloroplast, where salicylic acid is produced, to the PD. SA is one of the key hormones involved in defense against pathogens. While its role in regulating the PD-specific response to bacterial pathogens has be well studied, the role of SA signaling in defense against viruses is less clear. SA signaling is involved in restricting virus replication and cell-to-cell movement by mediating callose deposition at the PD, but it has become clear that some viruses may also benefit from SA signaling pathways to modulate their infection. Salicylic acid induces the accumulation of callose at PD through Plasmodesmata located protein 5 (PDLP5) and Callose Synthase 1 (CalS1) [102, 104]. By targeting REM1 during infection, viruses would be able to disrupt the SA signaling response on the plasma membrane.

Notably, *NbREM1* was also shown to be targeted for degradation by Tomato mosaic virus, indicating that pathogens have evolved mechanisms to circumvent the plants regulatory networks for regulating PD densities. In this example, the movement protein, which is part of the 30K movement protein family, like TMV MP30, is responsible for sequestering *NbREM1* in the ER and targeting it for degradation. It will be interesting to see how removal of Remorin from the plasma membrane affects the cell's ability to compartmentalize the PM into nano-domains and how this loss of organization affects PD structure, function, and formation.

## Materials and Methods

### *Plant growth*

*Nicotiana benthamiana* plants were grown on light carts under long day conditions (16hrs light and 8 hours of dark, 80-120 µmol/m/s). Seedlings were germinated and transferred to individual pots 10-12 days post germination. All plants used for experiments were at least 4-weeks old. Fertilizer was applied once, 5 days after transplanting.

### *RNA extraction and cDNA synthesis*

Leaves from 4-week-old *N. benthamiana* plants were collected and frozen in liquid nitrogen. RNA was extracted with the Trizol method (Thermo Fisher Scientific, Waltham, MA). RNA was DNase treated with DNA-free DNA removal

kit (Invitrogen, Carlsbad, CA). cDNA was synthesized with M-MLV reverse transcriptase (Promega, Madison, WI) using oligo-dT primers.

### *Cloning of NbREM1 fragment for VIGS*

*N. benthamiana* homologs for StREM1.3 were identified using the Solgenomics BLAST tool (https://solgenomics.net/tools/blast). Two highly similar homologs were identified with BLAST (NB IDs for REM1a and REM1b). A silencing construct targeting both homologs was designed using the Solgenomics VIGS Tool (https://vigs.solgenomics.net/). Primers were designed to amplify the VIGS fragment and add EcoRI and XbaI restriction enzyme sites to the ends of the fragment for cloning into the multiple cloning site of the pYL156 (pTRV-RNA2) plasmid for VIGS.

### *Cloning of NbREM1.1*

*NbREM1*.1 and *NbREM1*.2 were previously shown to have redundant functions and therefore *NbREM1*.1 was selected for overexpression experiments [94]. The full-length coding sequence for *NbREM1*.1 was identified from the Solgenomics database (https://solgenomics.net). Primers were designed to amplify the CDS of *NbREM1*.1 with attB sites for Gateway cloning. The amplified fragment was cloned using standard Gateway cloning procedures. The sequence integrity of the entry clone was verified by Sanger sequencing. The *NbREM1*.1 CDS was cloned into Gateway destination vectors (pGWB405 (C-terminal GFP fusion) and

pGWB4XX (C-terminal HA tag) with the LR reaction kit. Expression clones were verified with Sanger sequencing.

### *Cloning TMV MP30-GFP and MP30-V4A-GFP*

Gateway compatible primers were designed to amplify WT MP30 and MP30(V4A) with attB sites for Gateway cloning. In order to generate the V4A mutation, a single nucleotide substitution (T to C) was introduced with the forward primer. The amplified fragments were cloned into the pDONR-Zeo entry vector using the BP reaction kit. Sequence integrity and the introduction of the point mutation were verified by Sanger sequencing. The CDS for WT and MP30(V4A) were cloned into the Gateway destination vector pGWB405 to generate WT and MP30(V4A)-GFP following standard cloning methods. Expression clones were verified with Sanger sequencing.

### *Viruses and virus infection*

4 or 5-week-old plants were infected with the different viruses. For viruses with infectious clones (TMV, TRV, TuMV-GFP, ACMV, and EACMCV), two leaves from 4-week-old plants were agroinfiltrated with the corresponding infectious clone. Infiltrations were done at an OD of 0.1 to ensure that the majority of cells within the infiltrated leaf were infected with virus. Agroinfiltration of several of the viruses (TRV, ACMV, and EACMV) resulted in severe cell death in the primary infected leaves. All experiments with systemically infected leaves were

completed 10 days post infection. Infection with the virus was confirmed via RT-PCR with primers for the coat protein for each virus.

### *Intercellular Movement Assays*

Movement assays were performed as described in [254];[260]. Briefly, fully expanded leaves of 4- or 5-week-old *N. benthamiana* plants were agroinfiltrated with strains encoding either free GFP or free mScarlet at very low optical density ($OD_{600}$= 0.0001) to insure sporadic transformation of epidermal cells. 48 hours post infiltration, z-stacks were collected with a Leica SP8 confocal microscope with the white light laser at 488nm excitation of GFP and 569nm for excitation of mScarlet and emission between 609-618nm. Intercellular movement was quantified by counting the number of layers of movement. For *REM*-HA, MP30-GFP, and PDLP1-GFP overexpression experiments, leaves were co-infiltrated with agrobacterium strains encoding the corresponding fluorescently labeled protein at OD=0.1 with strains encoding free fluorescent proteins at OD=0.0001. Images were collected 48 hours post infiltration (hpi).

### *Pitfield distribution assays and confocal microscopy*

Pitfield distribution assays were completed as previously described [260]. Images were collected with a Leica SP8 confocal microscope Leica with the WLL with filters for 488nm excitation of GFP and 587nm for excitation of mCherry and emission at 601-618nm.

***Primary Infected Leaf Experiments***

For experiments in the inoculated leaf, 4-week-old *N. benthamiana* plants were co-agroinfiltrated with an agrobacterium strain carrying a fluorescently labeled PD marker (PDCB1-mCherry) for experiments with GFP-tagged viruses and PDLP1-GFP, MP17-GFP, or MP30-GFP for experiments with non-tagged viruses and either empty agrobacterium or an infectious clone of the virus.

***PD distribution in upper leaves before systemic virus movement***

For experiments with systemic leaves before infection, young leaves of the infected plants were agroinfiltrated with PDCB1-mCherry or PDLP1-GFP and imaged 84 hpi.

***PD distributions in systemically infected leaves***

For systemically infected leaves, upper leaves of the infected plants were agroinfiltrated with the corresponding PD markers 7 dpi and images were collected 10 dpi with the Leica SP8 confocal microscope.

PD distributions in Remorin and movement protein overexpressing leaves

Expanded leaves of 4 or 5-week old *N. benthamiana* plants were coinfiltrated with *REM*-HA, *REM*-GFP, MP30-GFP, or PDLP1-GFP and PDCB1-mCherry. Images were collected 72 hpi.

***Image acquisition for PD distribution assays***

Images of epidermal cells of the abaxial surface of the leaf were collected 72 hpi as previously described [260]. Leaf sections were vacuum infiltrated with water and mounted on slides for imaging. 15 µm z-stacks were collected with a step

size of 1μm. A minimum of 15 stacks were collected for each sample for three biological replicates. For quantification of pitfield distributions, Maximum projections were generated for each stack and the cell wall was manually traced using ImageJ [251]. Cell wall area was approximated by multiplying the total length of cell wall measured by the thickness of the z-stack (15 μm). Images were converted to 8-bit images and inverted. A binary image was generated for each image using the thresholding tool in ImageJ. The particle analyzer tool in ImageJ was used to quantify the number of the pitfields in each image. Pitfield density was calculated by dividing the number of pitfields by the cell wall area.

***Sample fixation and Transmission electron microscopy***

Samples were prepared for TEM via High Pressure freezing and quick freeze substitution as described previously [231]. Leaf punches were collected from newly emerged leaves of systemically infected and uninfected plants. The leaf punches were coated with yeast paste for cryoprotection and were frozen with a Wohlwend Compact 02 High Pressure Freezer (Techno Trade International). Freeze substitution was completed as previously described [231]. A FS solution composed of 2% Osmium Tetroxide and 0.1% Uranyl Acetate in pure acetone was used for fixation of all samples. The yeast paste was carefully removed and samples were embedded in epoxy resin (EMBed812, Epon). Embedding was conducted over 8 days according to the following protocol: 5%, 10%, 15%, 25%, 50%, 75%, 100%, 100% under vacuum, (v/v) resin/acetone for 24hrs. Samples were transferred into molds and baked for 48 hours at 60°C. Blocks were

sectioned using a Leica ultramicrotome EM UC7. 70-100 nm sections were collected and mounted on carbon coated copper slot grids. Grids were post stained with Reynolds Lead Citrate and imaged with a JEOL 1400 Flash TEM (JEOL USA).

***Quantification of plasmodesmata frequency by TEM***

Images were collected of cell walls between adjacent epidermal cells. Cell wall lengths were measured in ImageJ [251] More than 100 microns of cell wall were collected for each sample. The total number of PD per cell wall were counted. PD frequency per 100 square microns was quantified by dividing the total number of PD by the area of cell wall (cell wall length times the section thickness).

# CHAPTER 5

# THE MECHANISM OF SECONDARY PLASMODESMATA FORMATION

## Abstract

Secondary plasmodesmata formation has emerged as a mechanism cells use to regulate intercellular trafficking. While it is becoming increasingly clear that secondary PD formation is critical for proper regulation of trafficking, the mechanism behind de novo PD formation remains poorly understood. Traditional models for PD formation focus on 3 primary steps in pore formation: Cell wall modification and thinning, ER insertion, and membrane remodeling and fusion during desmotubule formation. To date, no mechanistic model for secondary PD formation has ever been proposed. Here, we target the three separate steps in pore formation using a combination of reverse genetics and drug treatments targeting different cellular components. Our data implicates callose metabolism in the de novo formation of PD. Silencing of genes involved in callose deposition (callose synthases) or callose degradation (β-glucanases) results in decreased numbers of plasmodesmata. Additionally, we demonstrate that ER-PM contacts are important for PD formation. Finally, we demonstrate that endocytosis is important for secondary PD formation. Our results provide the first mechanistic model of secondary PD formation.

## Introduction

With the evolution of multicellularity, organisms had to develop mechanisms to relay information between cells in order to coordinate growth and development. Plants have had to evolve specialized pores that pass through the cell wall and form cytoplasmic connections between neighboring cells [3]. These

structures are called plasmodesmata and are essential for proper plant growth, development, and defense.

The plasma membranes of neighboring cells are continuous through the plasmodesmata. Plasmodesmata also contain a tightly furled tubule of endoplasmic reticulum called the desmotubule that forms a direct connection between the ER networks of neighboring cells. A thin strip of cytoplasm, known as the cytoplasmic sleeve, separates these two continuous membrane elements and serves as the site for the bulk of diffusive trafficking.

Plasmodesmata can be classified into two separate categories based on their origin. The first class of plasmodesmata are referred to as primary plasmodesmata. These pores are formed during cell division as the developing cell wall is deposited [183, 318]. During formation of the cell plate, strands of cortical ER become trapped in the forming cell plate and prevent complete closure of the wall. These instances of incomplete cell division give rise to the primary plasmodesmata. Several ER remodeling factors have been identified as having roles in primary PD formation [318]. The most well characterized players in primary PD formation are the Reticulon-like B proteins AtRTNLB3 and AtRTNLB6. Reticulons are specialized membrane associated proteins that induce membrane curvature [331],[318]. These reticulon like proteins localize to the PD and are believed to have a role in formation and stabilization of the tightly appressed desmotubule. Several other PD-associated proteins, including

Remorin1.3 and Synaptotagmin A, were shown to interact with RTNLB3 and RTNLB6 indicating that they may also have roles in PD formation [318].

The second class of pores are referred to as secondary plasmodesmata. This class of PD refers to any pore that forms in the absence of a cell division event [142]. Secondary PD include pores that form between neighboring cells of separate cellular lineages, such as leaf epidermal cells and mesophyll cells, and PD that are added to division walls after completion of cell division [183]. Pores that have been structurally modified through the addition of branches are also classified as secondary PD [319],[17].

The mechanisms behind secondary PD formation remain poorly understood. Several models of secondary PD formation have been proposed, but these models have not been well characterized and host factors involved in pore insertion have not been identified [16, 183]. Most of the proposed models of secondary PD formation suggest that pore formation is ER-dependent [332]. In these models, pieces of ER are randomly inserted into the cell wall until two ‘half’ PD meet and form a connection between neighboring cells [183],[333]. Transmission electron microscopy images of half PD have been used to support these models, but it is impossible to eliminate the possibility that these half PD are actually full PD that are only partially captured in the thin sections used for TEM. The multiple twinning model of secondary PD formation suggests that new PD form in close proximity to existing PD giving rise to clusters of PD called piftields [16]. From these models, it has been suggested that the machinery

required for PD formation may be present at the PD and that the cell wall environment at existing pores is primed for formation of new PD. This model proposes that twinned PD, or PD that are found within 100nm of each other, are sites of de novo secondary PD formation [16].

In order for secondary PD formation to occur, multiple conditions must be met. The first event that must take place is remodeling of the cell wall. Current models suggest that modification of the cell wall results in the gradual thinning and expansion of the wall until finally the wall is split and the plasma membranes of neighboring cells fuse and the cytoplasms form a bridge between neighboring cells [183]. Cellulase has been implicated in secondary PD formation in pollen mother cells, but this observation made by visualization of cellulase reaction products at PD, which present as electron dense regions of cell wall by TEM, has not been thoroughly investigated [334]. Other cell wall remodeling factors involved in the thinning process have not been identified. In order for the cell to regulate PD formation, cell wall thinning must be tightly regulated in order to ensure that the integrity of the bulk cell wall is maintained [333].

The second key component of the PD that must be incorporated into the forming pore is the desmotubule. While it is possible that not all new PD contain a desmotubule, electron micrographs of branched PD with clearly defined desmotubules have been reported as have micrographs of PD with desmotubules between host cells and parasitic plants [335]. How the ER is inserted into the newly formed pore is unknown. As described above, current

models of PD formation suggest that the ER is randomly inserted into the wall until it fuses with the ER of the neighboring cell. In these models, the ER is the primary driving force for secondary PD formation and desmotubule insertion [183]. One alternative explanation involves endoplasmic reticulum-plasma membrane contact sites (EPCS) being used to tether the ER to the PM and to pull the ER into the forming pore during cell wall thinning. PD are known examples of EPCS and these contacts have been shown to be critical for regulating PD function [13, 129, 196, 336]. Multiple ER-PM tethering proteins have been identified as being associated with PD. Two key examples of this are the Multiple C2 domain containing proteins (MCTP) and the synaptotagmins [337],[129],[338].

We have previously shown that the group I Remorin, *NbREM1*, is a negative regulator of PD formation (see chapter 4). *NbREM1* is a PM associated protein that has been shown to act as a regulator of PM organization [329]. How REM1 regulates PD formation remains unclear. Its role in membrane organization and its importance for PD function suggests that it may regulate PD formation by sequestering specialized proteins into membrane nanodomains, or lipid rafts, as was described for the hyperclustering of PIN2 [330].

One class of proteins that accumulate in lipid rafts are the GPI-anchored proteins. Addition of a GPI-anchor targets proteins to the outer leaflet of the plasma membrane. Once in the PM, GPI-anchored proteins accumulate in the PD PM and in lipid rafts [339]. GPI-anchors are one of the most well

characterized PD targeting signals identified to date [39]. Many PD regulatory proteins, including proteins involved in callose metabolism, are predicted or have been shown to be GPI-anchored proteins [36, 38, 326]. The Plasmodesmata callose binding protein family (PDCBs) are known to be GPI-anchored [36]. PDCBs have been shown to bind callose in vitro and overexpression of these proteins has been shown to result in decreased intercellular trafficking and increased accumulation of PD-associated callose. In addition to the PDCBs, multiple β-glucanases are also GPI-anchored [38],[340],[92]. Members of the glycoside hydrolase 17 family of β-glucanases are primarily responsible for the degradation of callose at PD [340]. As a primary component of the cell wall around PD, callose metabolism would be an ideal candidate for targeted remodeling of the cell wall for insertion of new PD. Recent work with synthetic biopolymers have also indicated that incorporation of callose increases the elasticity of the cell wall which would assist in the thinning of the wall required for pore formation [93].

We were interested in uncovering the mechanism of secondary PD formation. Here, we present the first mechanistic model of secondary PD formation. TEM tomography revealed intermediates in secondary PD formation and demonstrated that pore formation is initiated by individual cells. Additionally, we have used reverse genetics to identify proteins involved secondary PD formation. For the first time, our results directly implicate callose metabolism, lipid

rafts, and ER-PM contacts in the de novo formation of secondary PD. Additionally, we show that endocytosis is essential for regulating PD formation.

## Results

### *Secondary PD formation is initiated by single cells*

Traditional models of secondary PD formation suggest that new PD are formed through a synchronized event where neighboring cells both initiate pore formation. Intermediates in the formation of secondary PD were captured by TEM tomography (Figure 22). These image stacks and 3D reconstructions of the forming PD show that pore formation is initiated by individual cells. In the representative tomogram depicted in Figure 22, two partially formed PD can be seen flanking a fully formed pore (Figure 22a, arrow and asterisk and b). One of the intermediates was captured at the late stage of formation just before the PD plasma membrane fused with the PM of the neighboring cell (Figure 22a, middle panel, denoted by an asterisk and c right panel). The other partially formed pore was captured at the beginning of pore formation (Figure 22a, middle panel, denoted by an arrow and c, left panel). This pore forms a slight indentation in the wall that has a diameter of approximately 20nm, which is consistent with the diameter of fully formed PD. A closer look at the cell wall revealed a differential staining pattern of the wall extending from the forming pore to the other side of the wall (Figure 22a middle panel, red rectangle). The light staining of the cell wall at this position suggests that the local composition of the cell wall is distinct from the bulk cell wall. This pattern was observed in all three instances of

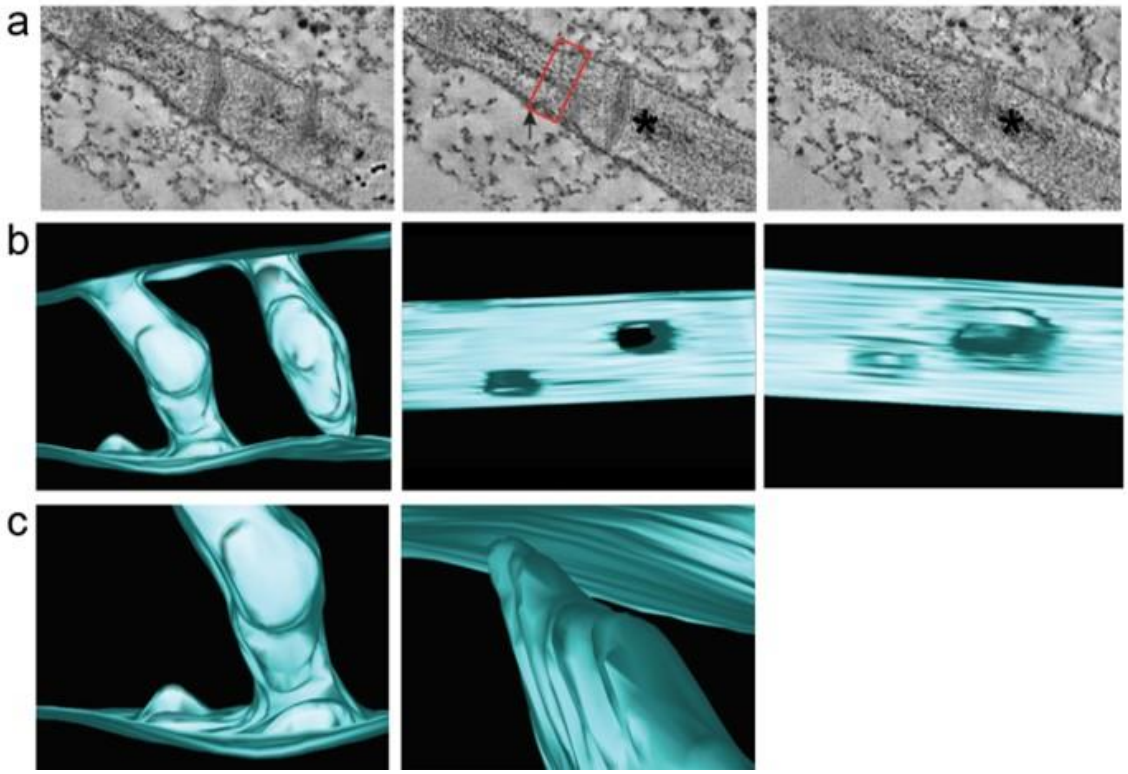


**Figure 22 Intermediates in secondary PD formation captured by dual axis TEM tomography.**

Representative images from the tomogram of a pitfield of PD are shown (a). Two intermediates in PD formation (early stage (arrow) and late stage (asterisk) are shown (a). Differential staining of the cell wall extending out from the early stage intermediate is shown (red box). Scale bar = 10 nm. Representative images of the 3D reconstruction of the tomogram are shown (b and c). Views from the top and either face of the PM are shown (b). Close up images of the two intermediates (early, left) and late (right) are shown.

partially formed PD captured by TEM tomography. This suggests that PD formation occurs at specific sites in the cell wall that are compositionally distinct from the bulk wall.

### *GPI-anchored proteins are required for secondary PD formation*

In order to investigate the role of REM1, a raft associated protein on the inner leaflet of the plasma membrane, in the cell wall modification required during plasmodesmata formation, we next targeted Glycosylphosphatidylinositol-anchored (GPI-anchored) proteins. GPI-anchored proteins are known to accumulate in the outer leaflet of PM lipid rafts and have been previously shown to serve as a post-translational modification that targets proteins to PD [39].

*AtGPI8* is a transamidase that is involved in the addition of the GPI-anchor [341]. A *GPI8* mutant was previously shown to exhibit severe growth defects and decreased intercellular trafficking in Arabidopsis [341]. In order to determine if GPI-anchored proteins are involved in the formation of PD, the *N. benthamiana* homolog of *AtGPI8* was silenced by VIGS. *NbGPI8*-silenced plants exhibit chlorosis, curled leaves, and slightly stunted growth, consistent with Arabidopsis mutants [341]. Consistent with the Arabidopsis mutant, *GPI8*-silenced plants exhibited a substantial decrease in intercellular trafficking of GFP (Figure 23a-c). *GPI8*-silenced plants also have fewer PDLP1-GFP labeled pitfields compared to the TRV non-silencing control plants indicating that loss of all GPI-anchored proteins results in decreased numbers of PD (Figure 23d and e). In order to determine if this defect is a result in decreased secondary PD formation,

**Figure 23 GPI-anchored proteins are important for PD formation.**

(a) Intercellular movement assays were performed by measuring the layers of movement of GFP in *N. benthamiana* leaf epidermal cells. Representative images of non-silencing (left) and *NbGPI8*-silenced plants (right). Scale bar = 50 μm. Data for three biological replicates are shown. 20 foci were collected for each biological replicate. Data is depicted as a Quantitativeplot of the percentage of foci of each size (b) and the Mean layers of movement and standard deviation (c). Statistical significance was determined using the Mann-Whitney U-test ($p < 0.001$). (d- g) Pitfield distribution assays were performed using PDLP1-GFP (d and e) and MP30-GFP (f and g). Representative images for cells expressing PDLP1-GFP (d) and MP30-GFP (f) are shown. Pitfield densities for 20 fields of view for each of 3 biological replicates (e and g, red, blue, and yellow circles) are shown for PDLP1-GFP (e) and MP30-GFP (g). Statistical significance was determined using a student's t-test ($p < 0.001$). Scale bar = 10 μm.

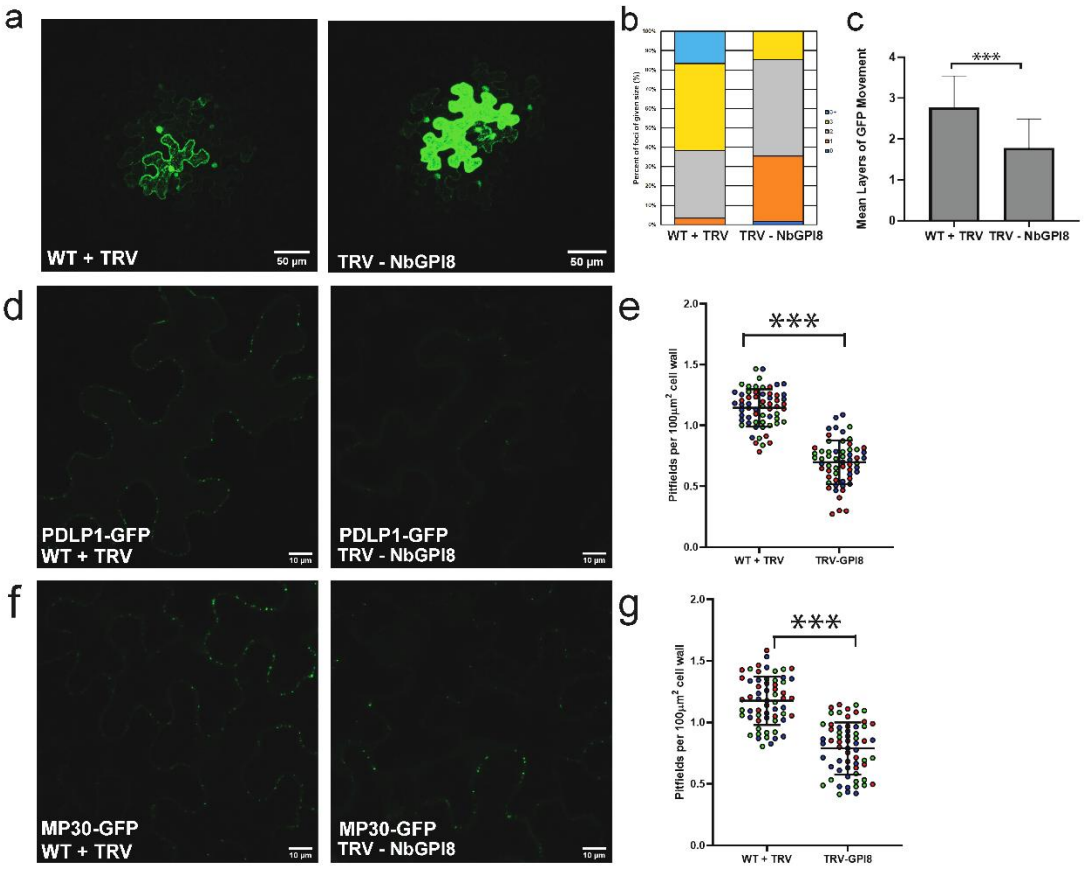
a
WT + TRV
50 µm
TRV - NbGPI8
50 µm
b
WT + TRV
TRV - NbGPI8
c
Mean Layers of GFP Movement
***
WT + TRV
TRV - NbGPI8
d
PDLP1-GFP
WT + TRV
10 µm
PDLP1-GFP
TRV - NbGPI8
10 µm
e
Pitfields per 100µm² cell wall
***
WT + TRV
TRV-GPI8
f
MP30-GFP
WT + TRV
10 µm
MP30-GFP
TRV - NbGPI8
10 µm
g
Pitfields per 100µm² cell wall
***
WT + TRV
TRV-GPI8

TMV MP30-GFP was expressed in silenced leaves (Figure 23 f). Expression of MP30-GFP failed to trigger an increase in secondary PD formation indicating that GPI-anchored proteins are required for secondary PD formation (Figure 23 f and g). .

***GPI-anchored β-glucanases are involved in secondary PD formation***

Two well characterized families of GPI-anchored proteins with known roles in regulating PD function are the Plasmodesmata callose binding proteins (PDCBs) and several β-glucanases.

In order to target β-glucanases, silencing constructs were developed to target *N. benthamiana* genes in the glycosyl hydrolase family 17 that are similar to *AtBG2* and *AtBG_ppap* (*NbBG11*, *NbBG14*(targets *NbBG14a* and *Nb14b*), *NbBG_ppap*, *NbBG17_1*, and *NbBG17_6* (targets *NbBG17_1* plus five addition glycoside hydrolase family 17 genes). Additionally, a silencing construct was designed to target the *N. benthamiana* homolog of the class I β-glucanase, *GLU1*, that was previously incorporated into the TMV genome and resulted in increased virus movement [316]. 4 out of 11 of the β-glucanases targeted were predicted to contain a GPI-anchor cleavage site (*NbBG11, NbBG14, NbBG17_1*, and *NbBG_ppap*) (GPI-SOM, http://gpi.unibe.ch/). Consistent with previous findings with β-glucanase mutants, silencing of individual β-glucanases (*BG11, BG14, BG17_1*) resulted in a modest decrease in intercellular trafficking compared to non-silencing TRV control plants (Figure 24 a-c). Silencing of all targets in a single plant resulted in the strongest decrease in trafficking of GFP.

**Figure 24 Intercellular trafficking is decreased in specific β-glucanase-silenced plants**

Intercellular movement assays were performed in plants silencing a various β-glucanases by measuring the layers of movement of GFP in *N. benthamiana* leaf epidermal cells. Representative images of non-silencing and the targeted β-glucanase-silenced plants are shown. Scale bar = 50 μm. Data for two biological replicates are shown. 20 foci were collected for each biological replicate. Data is depicted as a Quantitativeplot of the percentage of foci of each size (b) and the Mean layers of movement and standard deviation (c). Statistical significance was determined using the Mann-Whitney U-test ($p < 0.001$).

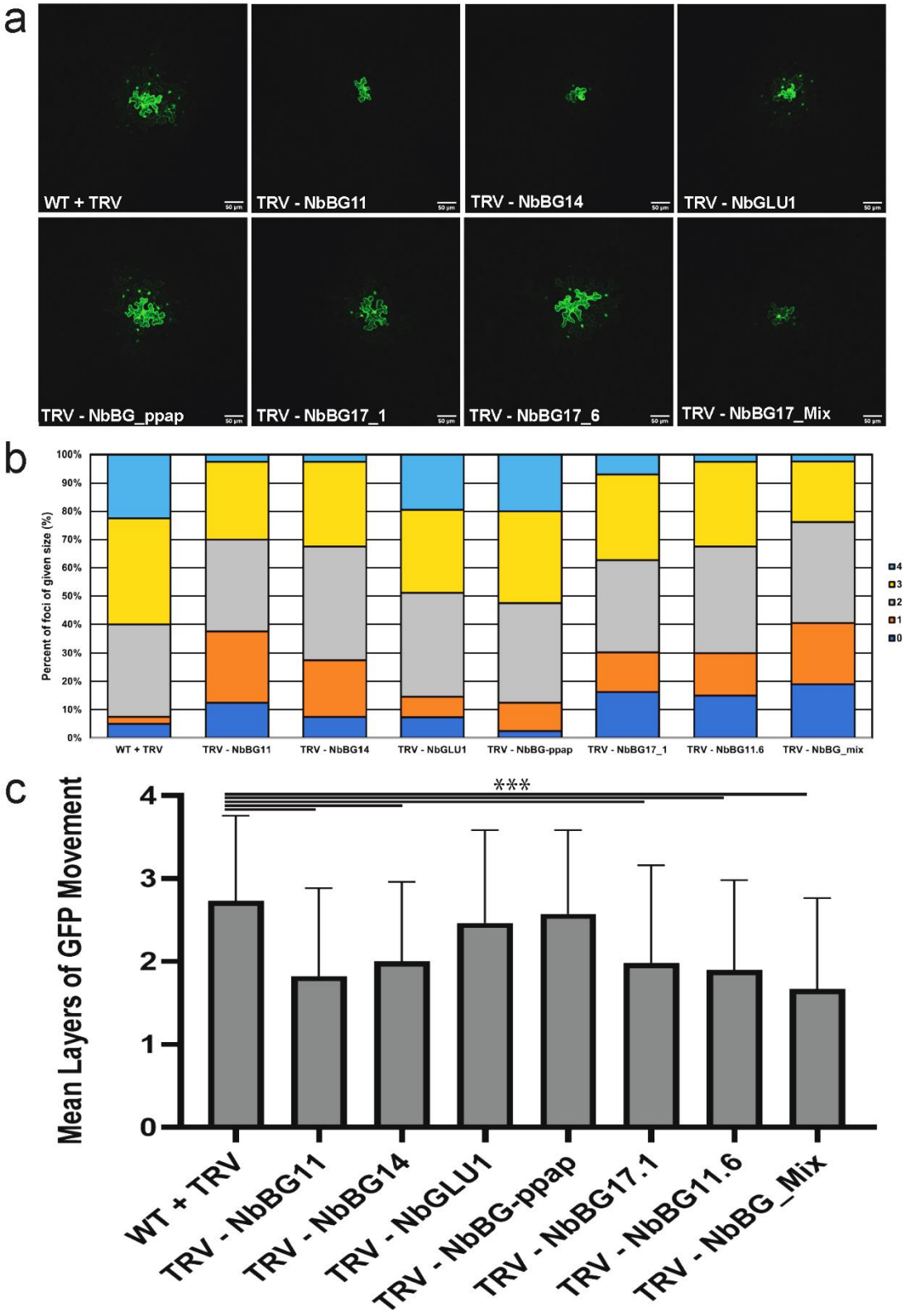
a
WT + TRV
TRV - NbBG11
TRV - NbBG14
TRV - NbGLU1
TRV - NbBG_ppap
TRV - NbBG17_1
TRV - NbBG17_6
TRV - NbBG17_Mix
b
Percent of foci of given size (%)
100%
90%
80%
70%
60%
50%
40%
30%
20%
10%
0%
WT + TRV
TRV - NbBG11
TRV - NbBG14
TRV - NbGLU1
TRV - NbBG-ppap
TRV - NbBG17_1
TRV - NbBG11.6
TRV - NbBG_mix
4
3
2
1
0
c
Mean Layers of GFP Movement
***
4
3
2
1
0
WT + TRV
TRV - NbBG11
TRV - NbBG14
TRV - NbGLU1
TRV - NbBG-ppap
TRV - NbBG17.1
TRV - NbBG11.6
TRV - NbBG_Mix

Interestingly, *BG17_6* had the same effect as *BG17_1* indicating that the other five targets do not play a major role in regulating trafficking through PD. Strikingly of the six targets of *BG17_6, BG17_1* is the only protein predicted to be GPI-anchored.

Silencing *NbBG11, NbBG14, NbBG17_1*, or *Nb17_6* resulted in decreased numbers of PDLP1-GFP labeled pitfields (Figure 25 a and b). *NbBG11, NbBG14, NbBG17_1*, and *NbBG17_6*-silenced plants also exhibited decreased numbers of MP30-GFP labeled foci indicating that secondary PD formation is disrupted in the absence of these β-glucanases (Figure 26). Notably, silencing of *NbBG17a*, which was previously shown to be induced during infection with Tobacco curly shoot virus, resulted in the most substantial decrease in secondary PD formation indicating that induction of *NbBG17_1* may play an important role in virus-induced PD formation (Figure 26b).

***Callose deposition is required for secondary plasmodesmata formation***

In order to further test the role of callose metabolism in secondary PD formation, silencing constructs were designed to target homologs of the three PD-specific callose synthases (CalS1, CalS8, and CalS10). *NbCalS1*-silenced plants exhibit a chlorotic phenotype and exhibited mild to severe necrosis on silenced leaves. NbCalS8 and *NbCalS1*0-silenced plants are phenotypically indistinguishable from non-silencing control plants.

Previous work with callose synthase mutants found that trafficking through the PD was increased compared to WT plants [102]. Surprisingly, silencing of

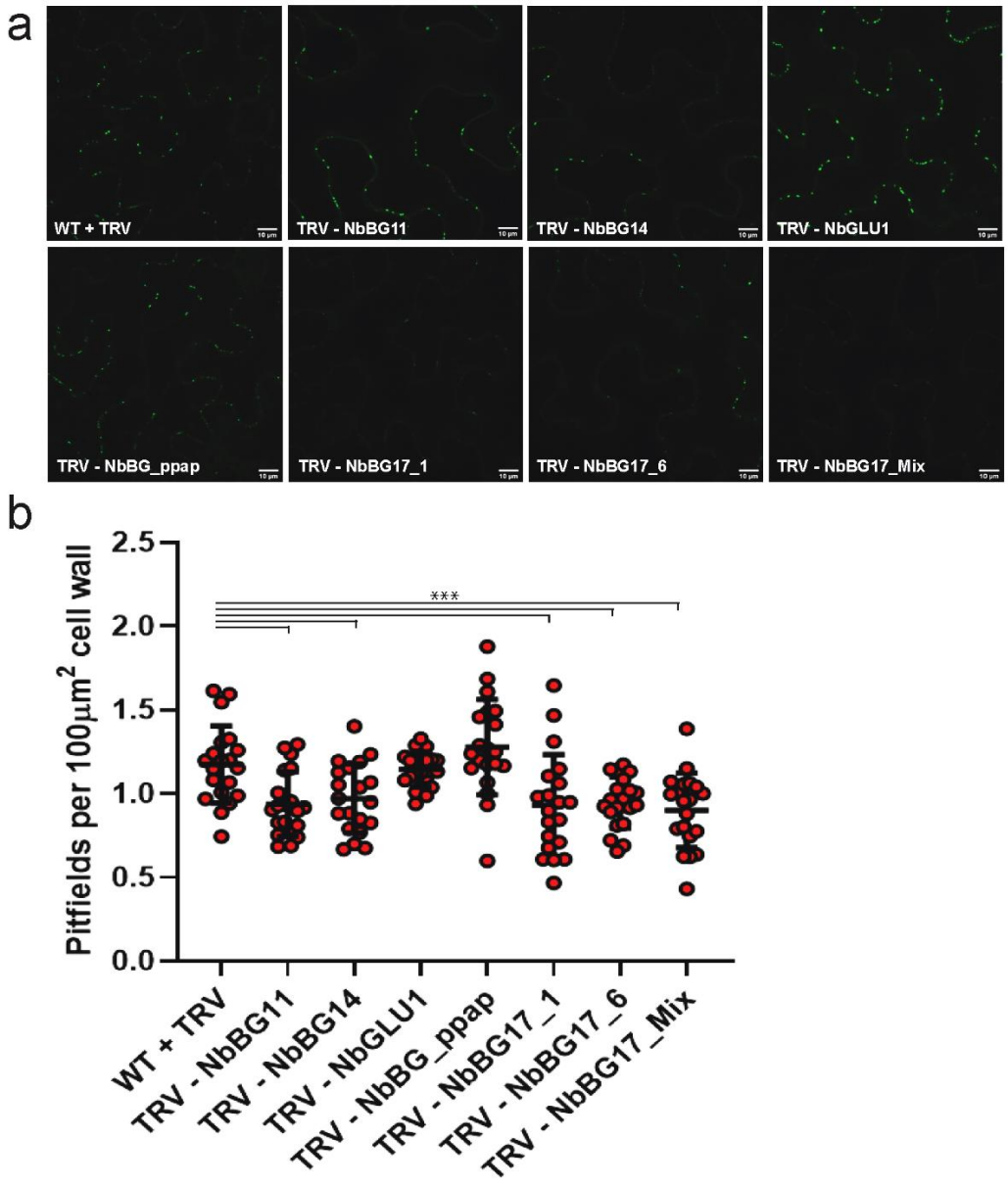


**Figure 25 GPI-anchored β-glucanases are involved in secondary PD formation.**

Pitfield distribution assays were performed using PDLP1-GFP. Representative images for cells expressing PDLP1-GFP (a) are shown. Pitfield densities for 20 fields of view for 1 biological replicate is shown. Statistical significance was determined using a student's t-test ($p < 0.001$). Scale bar = 10 µm.

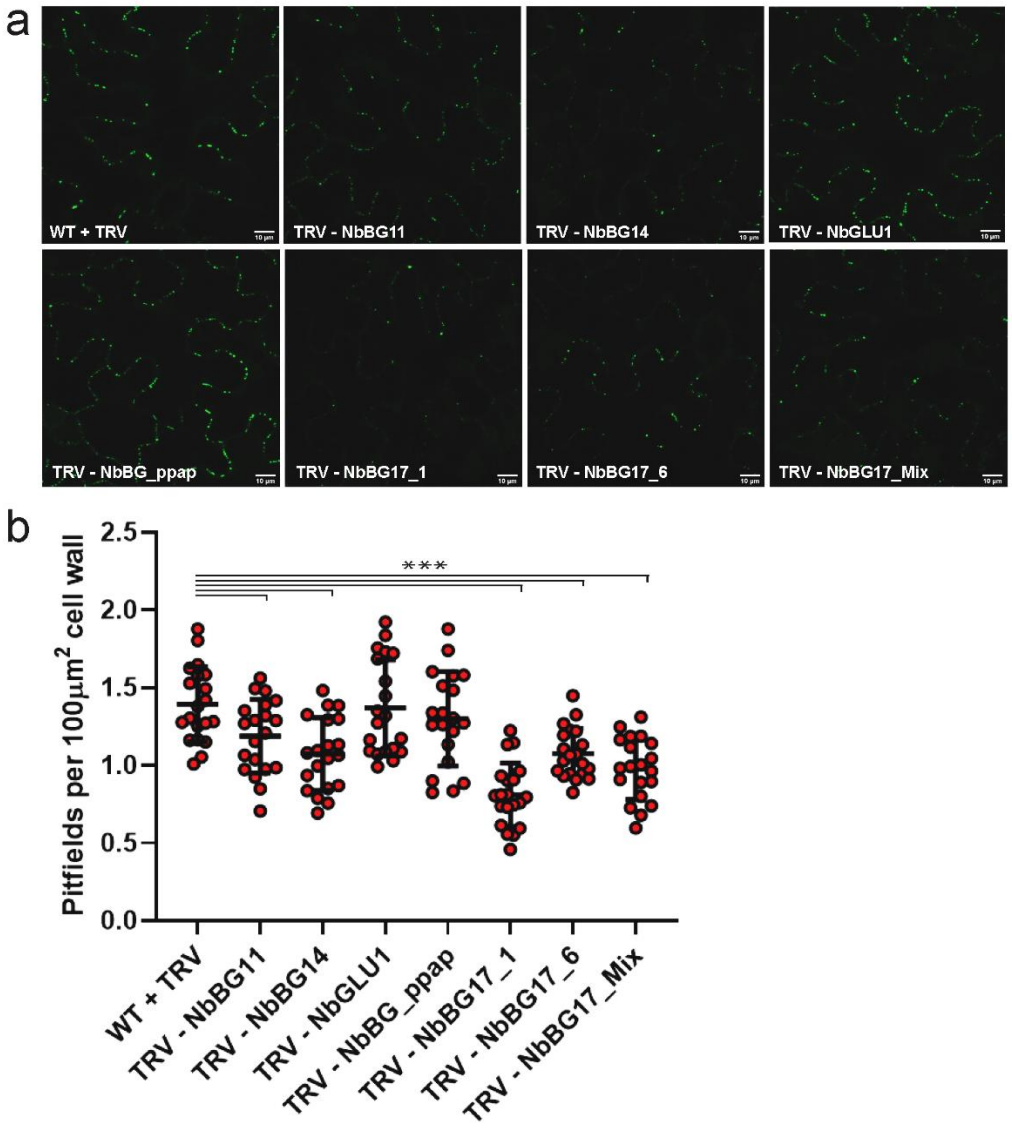


**Figure 26 GPI-anchored β-glucanases are involved in virus induced secondary PD formation.**

Pitfield distribution assays were performed using MP30-GFP. Representative images for cells from non-silenced and silenced plants expressing MP30-GFP are shown (a). Pitfield densities for 20 fields of view for 1 biological replicate are shown. Statistical significance was determined using a student's t-test ($p < 0.001$). Scale bar = 10 µm.

either *NbCalS1* or *NbCalS1*0 resulted in a marked decrease in intercellular trafficking of GFP while silencing *NbCalS8* showed a slight but not statistically significant increase in intercellular trafficking of GFP (Figure 27).

Consistent with the decreased trafficking capacity of *NbCalS1* and *NbCalS1*0-silenced plants, these plants also have fewer PDLP1-GFP labeled pitfields compared to non-silencing controls (Figure 28). Additionally, expression of MP30-GFP failed to increase the number of pitfields in *NbCalS1* and *NbCalS1*0 silenced plants further indicating that callose deposition is important for secondary PD formation (Figure 29). *NbCalS1*-silenced plants exhibited more severe defects in trafficking and PD formation than *NbCalS1*0-silenced plants indicating that *NbCalS1* may play a more important role in PD formation.

***Loss of Remorin results in decreased accumulation of PDCB1-mCherry in PD pitfields***

Remorins are known regulators of plasma membrane organization [329]. Both Remorins and GPI-anchored proteins associate with highly ordered membrane nanodomains. In order to determine if silencing *NbREM1* disrupts PD-association of GPI-anchored proteins, AtPDCB1-mCherry was expressed in *REM*-silenced and nonsilencing control leaves. PD-enrichment of AtPDCB1-mCherry was quantified as previously described in [342]. Loss of *NbREM1* resulted in decreased the association of PDCB1-mCherry with PD pitfields indicating that loss of *NbREM1* results in changes in GPI-anchored protein accumulation in PD (Figure 30). This suggests that REM1-silenced plants have decreased membrane order.

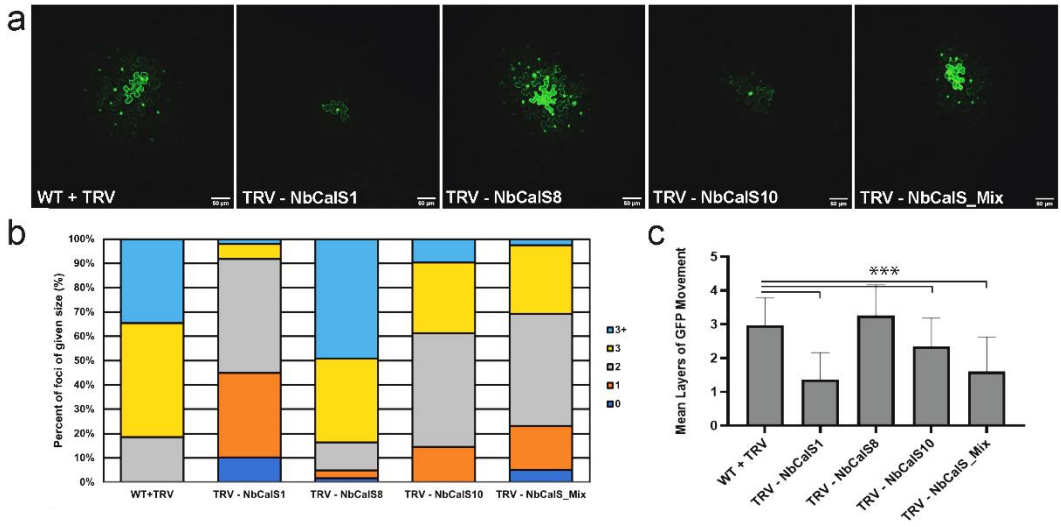


**Figure 27 Silencing of specific callose synthases in results in decreased intercellular trafficking.**

Intercellular movement assays were performed in plants silencing a 3 PD specific Callose synthases (*NbCalS1*, NbCalS8, *NbCalS1*0) and plants silencing all three CalS genes by measuring the layers of movement of GFP in *N. benthamiana* leaf epidermal cells. Representative images of non-silencing and the targeted CalS-silenced plants are shown. Scale bar = 50 μm. Data for three biological replicates is shown. 20 foci were collected for each biological replicate. Data is depicted as a Quantitativeplot of the percentage of foci of each size (b) and the Mean layers of movement and standard deviation (c). Statistical significance was determined using the Mann-Whitney U-test ($p < 0.001$).

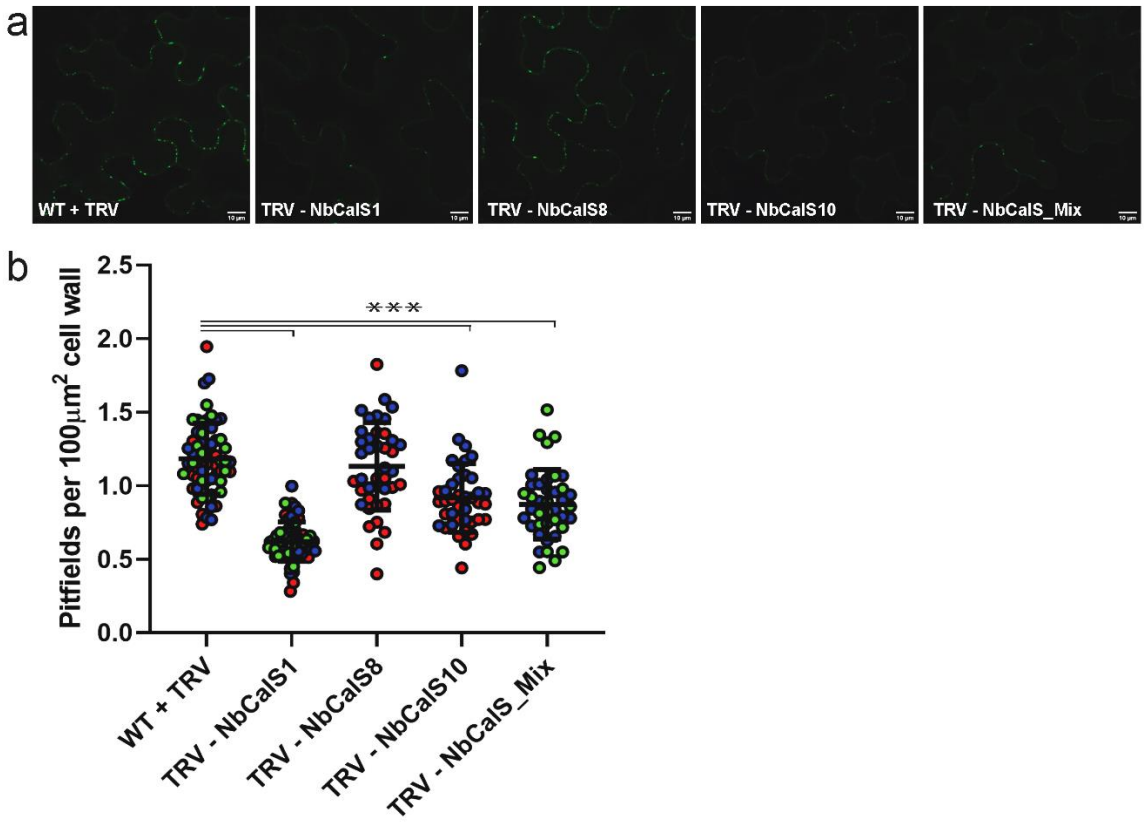


**Figure 28 Callose deposition is important for plasmodesmata formation**

Pitfield distribution assays were performed using PDLP1-GFP. Representative images of cells from silenced and non-silenced control plants expressing PDLP1-GFP are shown (a). Pitfield densities for 20 fields of view for 2 or 3 biological replicates (b, red, blue, and yellow circles) are shown. Statistical significance was determined using a student's t-test ($p < 0.001$). Scale bar = 10 μm.

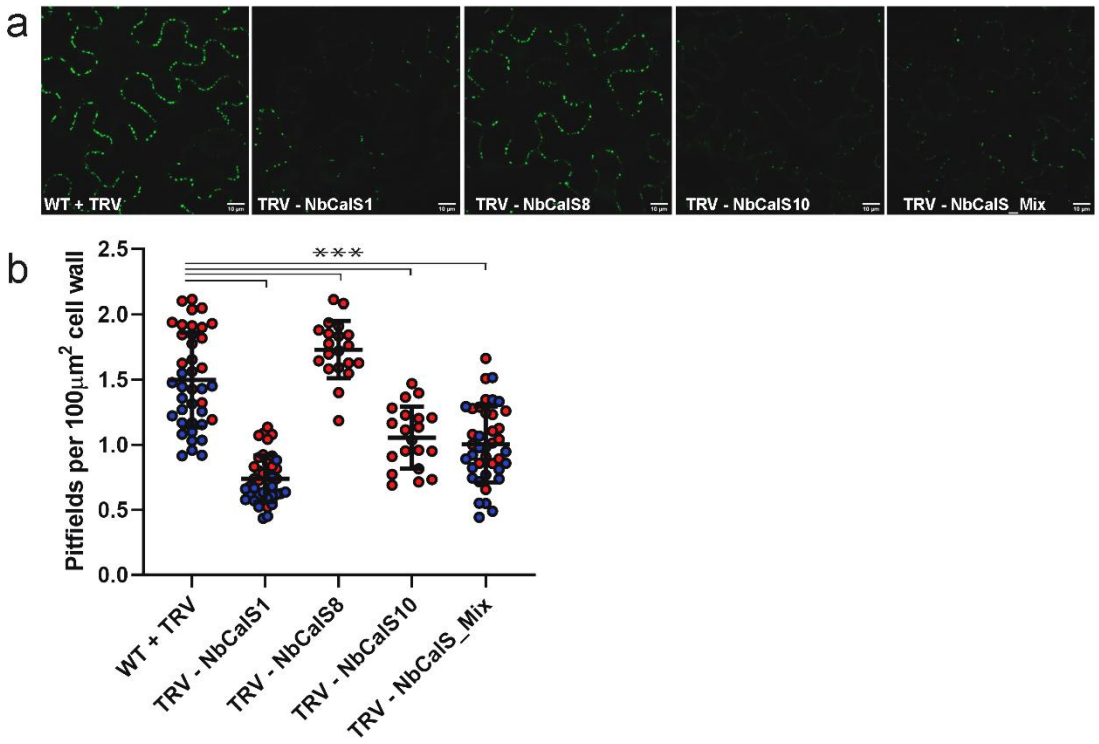


**Figure 29 Callose deposition is required for MP30-induced secondary PD formation.**

Pitfield distribution assays were performed using MP30-GFP. Representative images for cells from non-silenced and silenced plants expressing MP30-GFP are shown (a). Pitfield densities for 20 fields of view for 1 or 2 biological replicates are shown. Statistical significance was determined using a student's t-test ($p < 0.001$). Scale bar = 10 μm.

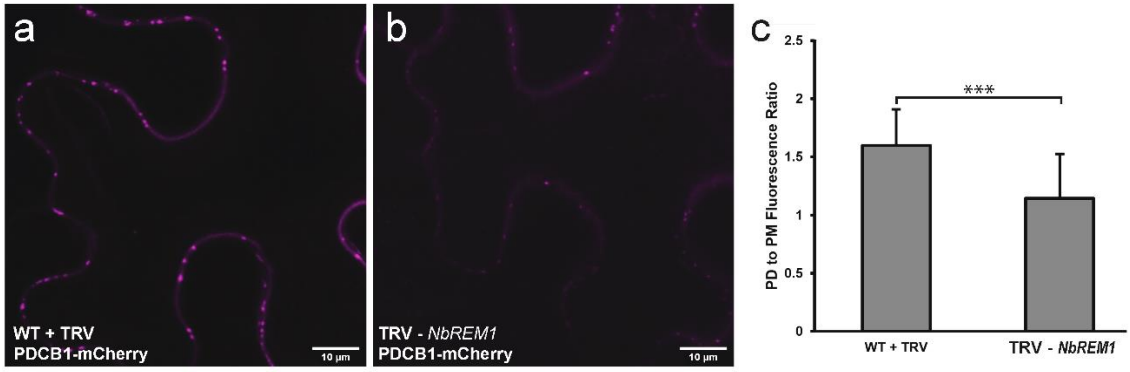


**Figure 30 Silencing *NbREM1* decreases GPI-anchored protein accumulation at PD.**

Representative images non-silencing and *NbREM1*-silenced plants expressing AtPDCB1-mCherry are shown. The average ratio of the fluorescence intensities of PD pitfields vs randomly sampled regions of the PM are shown (c). Data presented represents the average of more than 500 pitfields for each sample across 10 fields of view for 1 biological replicate. Scale bar = 10 µm. Statistical significance was determined using a student's t-test ($p < 0.05$).

### *ER-Plasma membrane contact sites are important for secondary PD formation*

Aside from the cell wall modification needed to form a new PD, the desmotubule must also be inserted into the forming pore. This insertion could be achieved through specialized ER-PM contact sites (EPCS) that pull the ER through the forming pore as the cell wall is remodeled.

Several proteins have been identified as ER-PM tethers at the PD. The Multiple C2 domain containing proteins (MCTPs) have emerged as candidates for being the spoke like structures that were identified in early electron microscopy images of PD ultrastructure [337]. Additionally, the synaptotagmins have been identified as factors involved in tethering the ER to the PM and having a role in PD regulation during virus infection [129, 338]. *SYTA* is a regulator of endocytosis and was previously shown to be recruited to PD during virus infection through an interaction with the TMV movement protein indicating that these tethers may have roles in virus-induced PD formation [127, 129].

Homologs of AtMCTP2 were identified by performing a BLAST search against the *N. benthamiana* genome (Solegenomics.net). This search revealed multiple candidates with similar degrees of similarity to AtMCTP2. A single silencing construct was designed to knock down the top 5 genes. *NbMCTP*-silenced plants exhibited decreased levels of intercellular trafficking of free GFP (Figure 31 a-c). Additionally, loss of MCTPs resulted in a decrease in the number of PDLP1-GFP foci indicating that the silenced plants have decreased numbers of PD (Figure 32). Expression of MP30-GFP also failed to induce PD formation in

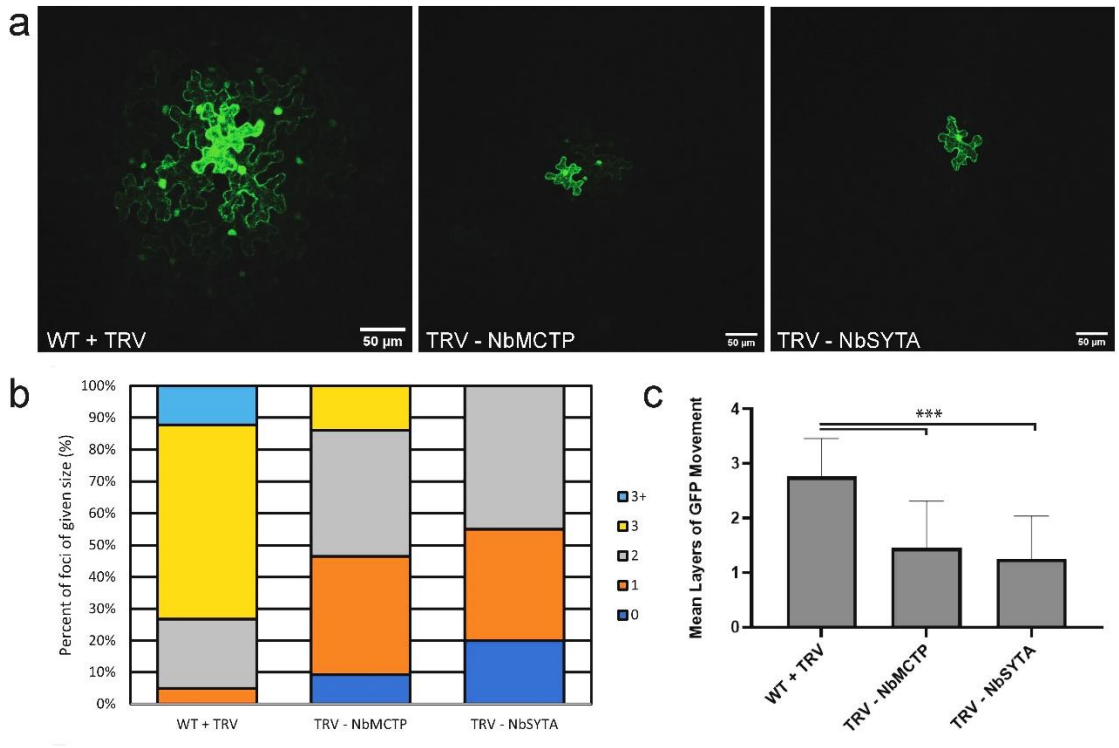


**Figure 31 Disruption of ER-PM contact sites results in decreased intercellular trafficking.**

Intercellular movement assays were performed in plants silencing two ER-PM tethering proteins (*NbMCTP* and *NbSYTA*) by measuring the layers of movement of GFP in *N. benthamiana* leaf epidermal cells. Representative images of non-silencing and silenced plants are shown. Scale bar = 50 µm. Data for 1 (*NbSYTA*) or 2 (*NbMCTP*) biological replicates is shown. 20 foci were collected for each biological replicate. Data is depicted as a Quantitativeplot of the percentage of foci of each size (b) and the Mean layers of movement and standard deviation (c). Statistical significance was determined using the Mann-Whitney U-test ($p < 0.001$).

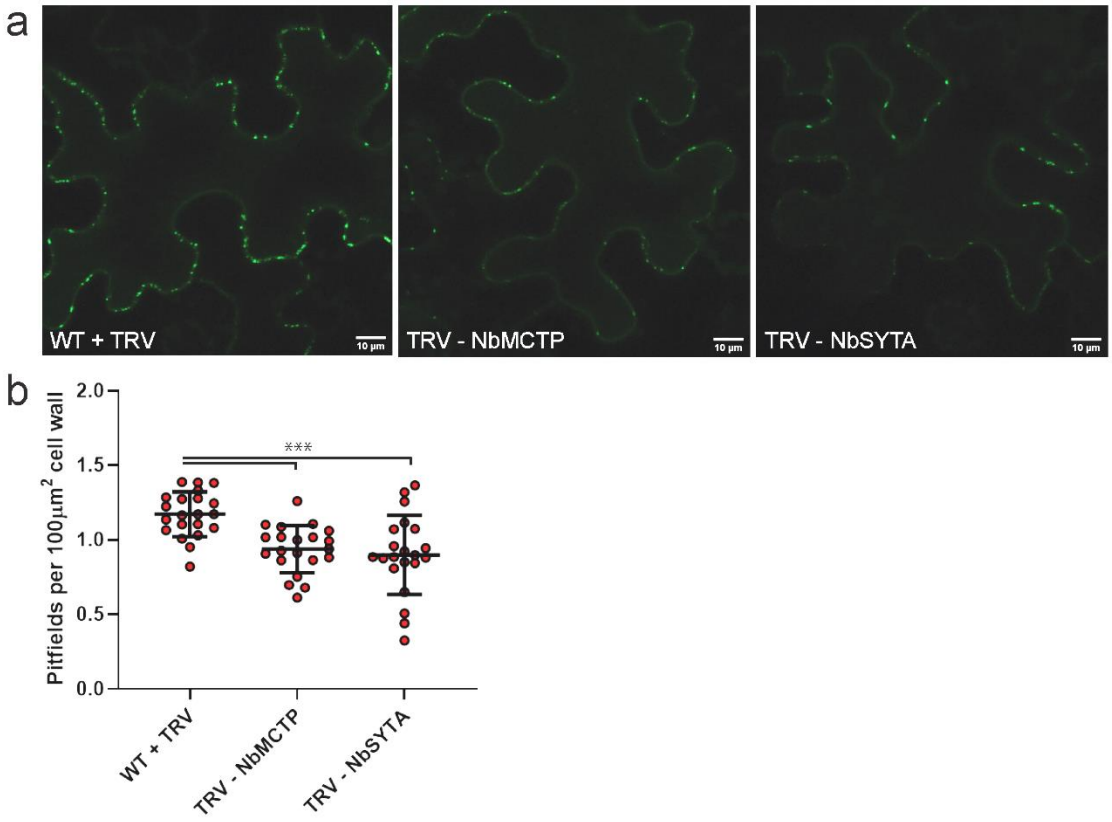


**Figure 32 Membrane contacts are important for plasmodesmata formation.** Pitfield distribution assays were performed using PDLP1-GFP. Representative images of cells from silenced and non-silenced control plants expressing PDLP1-GFP are shown (a). Pitfield densities for 20 fields of view for 1 biological replicate is shown. Statistical significance was determined using a student's t-test ($p < 0.001$). Scale bar = 10 µm.

the absence of *NbMCTP* indicating that ER-PM tethers are involved in secondary PD formation (Figure 33).

A BLAST search using the At*SYTA* amino acid sequence identified multiple homologs in the *N. benthamiana* genome. A single silencing construct to target more than two homologs could not be designed. Therefore, three 400 bp silencing constructs that each target two homologs were designed and combined into one 1200bp silencing construct that was then incorporated in the TRV2 VIGS plasmid (pYL156). Similar to MCTP-silenced plants, silencing At*SYTA* resulted in decreased intercellular trafficking of GFP (Figure 31). Additionally, loss of *SYTA* resulted in decreased numbers of PDLP1-GFP labeled pitfields (Figure 32) and blocked MP30-induced PD formation indicating that *SYTA* is also important for PD formation (Figure 33).

***Loss of two Reticulon-like proteins does not affect PD formation***

Previous work in Arabidopsis identified to Reticulon-like B proteins (RTNLB3 and RTNLB6) that localize to PD and are involved in primary PD formation [318]. Silencing constructs were designed to target these homologs in *N. benthamiana*. Silencing of either RTNLB3 or both genes in the same plant resulted in increased intercellular trafficking of GFP while silencing RTNLB6 resulted in a slight, but not statistically significant decrease in trafficking (Figure 34). Surprisingly, silencing of either homolog alone had no effect on PD formation (Figure 35). This suggests that these reticulons may have other roles in regulation of intercellular trafficking. Notably, silencing of both RTNLB3 and

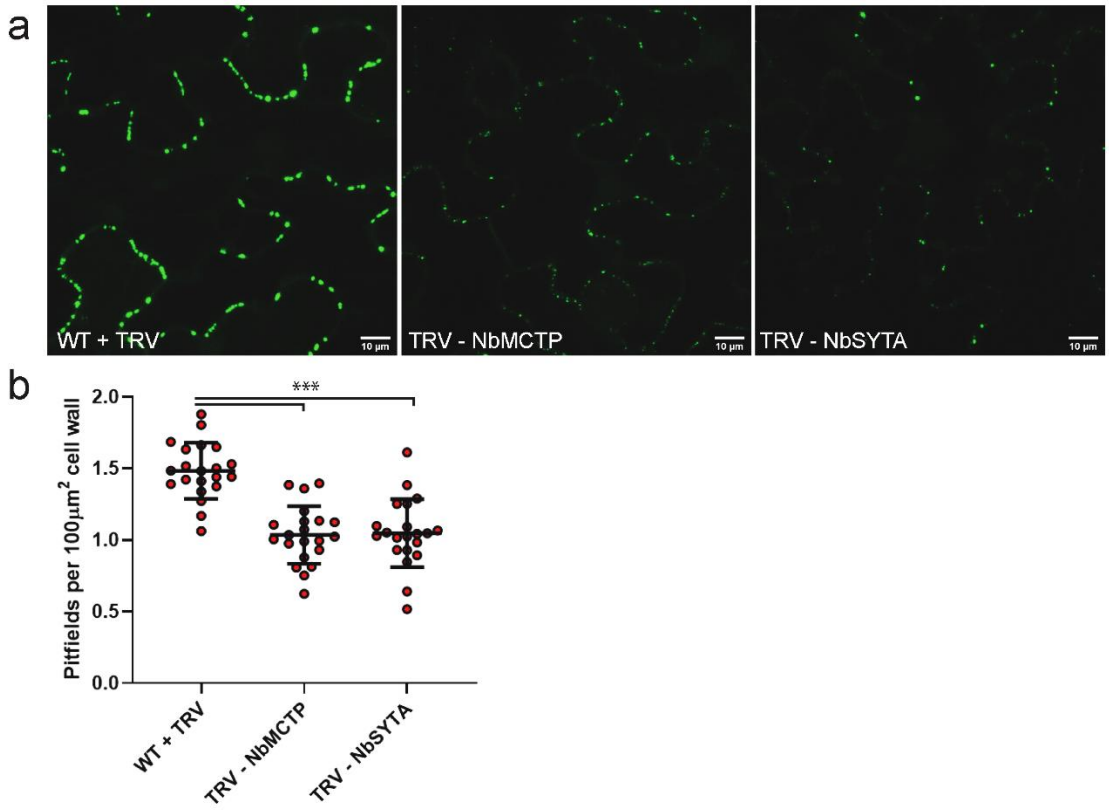


**Figure 33 ER-PM tethers are required for MP30-induced secondary PD formation.**

Pitfield distribution assays were performed using MP30-GFP. Representative images for cells from non-silenced and silenced plants expressing MP30-GFP are shown (a). Pitfield densities for 20 fields of view for 1 replicate are shown. Statistical significance was determined using a student's t-test ($p < 0.001$). Scale bar = 10 µm.

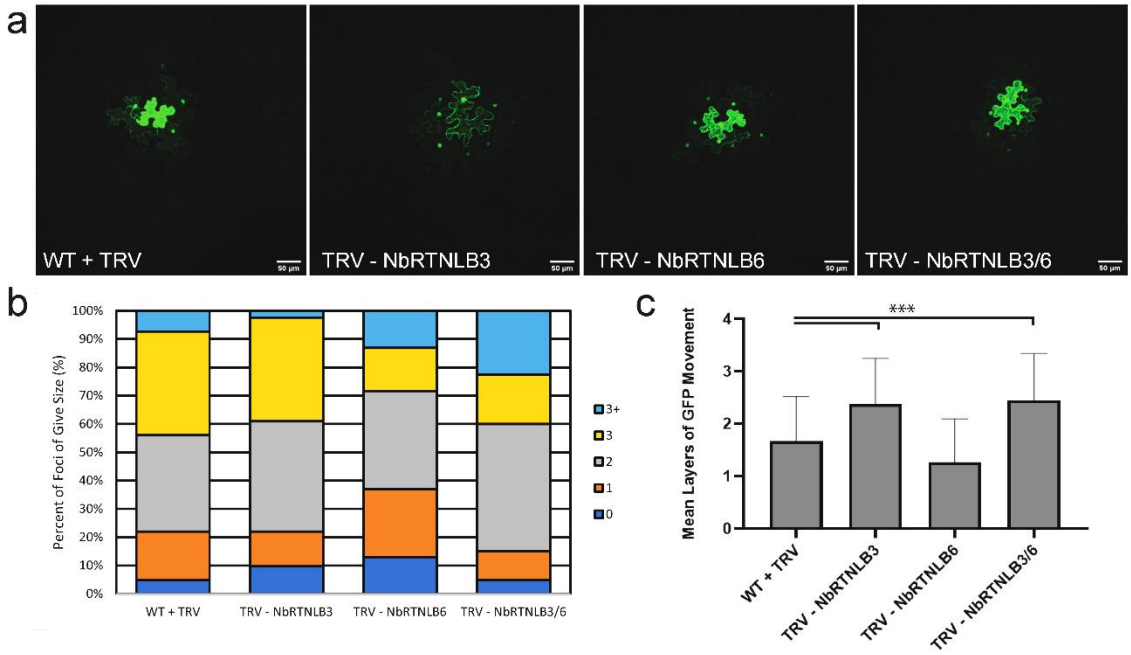


**Figure 34 Reticulon-like proteins are important for regulating intercellular trafficking.**

Intercellular movement assays were performed in plants silencing two Reticulon-like B genes (*NbRTNLB3* and *NbRTNLB6*) and plants silencing both genes by measuring the layers of movement of GFP in *N. benthamiana* leaf epidermal cells. Representative images of non-silencing and silenced plants are shown. Scale bar = 50 μm. Data for 2 biological replicates is shown. 20 foci were collected for each biological replicate. Data is depicted as a Quantitativeplot of the percentage of foci of each size (b) and the Mean layers of movement and standard deviation (c). Statistical significance was determined using the Mann-Whitney U-test ($p < 0.001$).

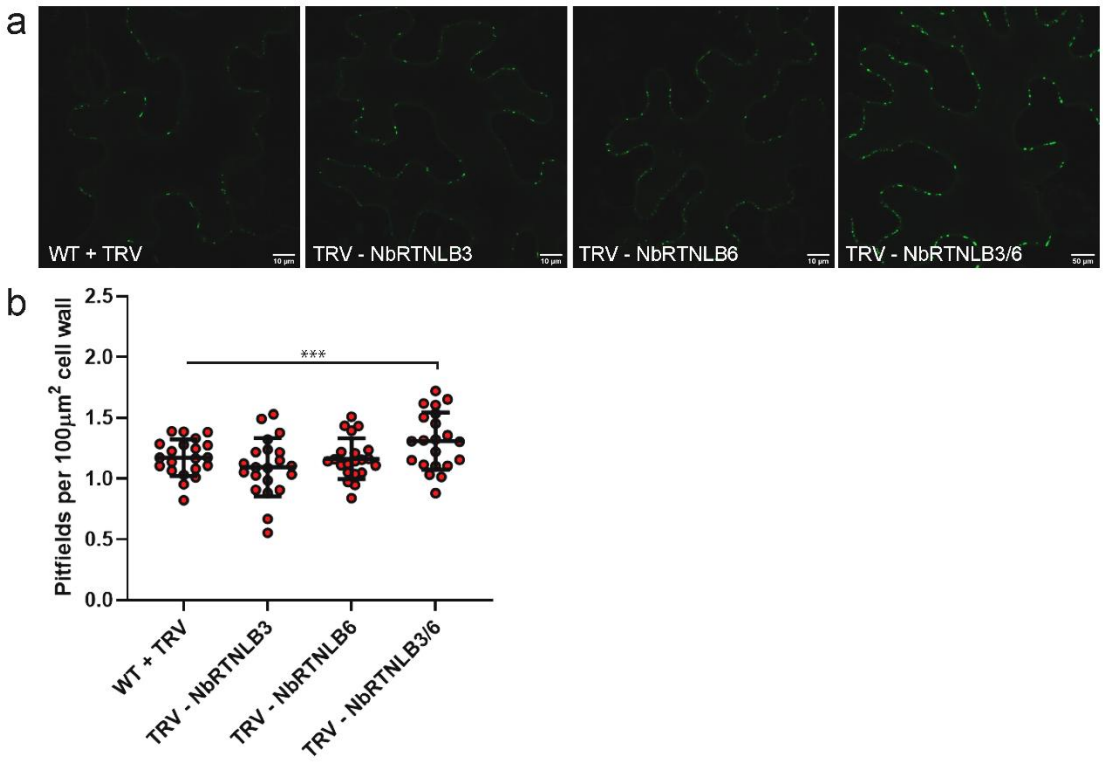


**Figure 35 Reticulon-like B proteins may restrict PD formation**

Pitfield distribution assays were performed in plants silencing two Reticulon-like B genes (*NbRTNLB3* and *NbRTNLB6*) and plants silencing both genes using PDLP1-GFP. Representative images of cells from silenced and non-silenced control plants expressing PDLP1-GFP are shown (a). Pitfield densities for 20 fields of view for 1 biological replicate is shown. Statistical significance was determined using a student's t-test ($p < 0.001$). Scale bar = 10 µm.

RTNLB6 in the same plant resulted in increased numbers of pitfields indicating that these proteins may have redundant functions in restricting PD formation (Figure 35).

In order to determine if loss of either RTNLB had an effect on virus-induced secondary PD formation, PD distribution assays were performed in silenced and non-silenced plants. Silencing individual RTNLB genes individually or together had no effect on MP30-GFP induced secondary PD formation indicating that these specific reticulon like proteins are not involved in forming the desmotubule during virus induced PD formation (Figure 36)..

***Identification of cellular machinery involved in PD formation***

The role of the cytoskeleton and membrane trafficking pathways on the regulation of intercellular trafficking has been elusive. In order to identify cytoskeletal elements and membrane trafficking pathways involved in PD formation, we performed an inhibitor screen with drugs that target specific components of the cytoskeleton and membrane trafficking systems.

***Endocytosis and not exocytosis is important for PD formation***

Because *SYTA* has been shown to regulate endocytosis, we next decided to see if disruption of endocytosis also had an effect on secondary PD formation. 12 and 4 hour treatment of *N. benthamiana* leaves with 30 µM Tyrphostin A23, an inhibitor of clathrin-mediated endocytosis, resulted in decreased intercellular trafficking of GFP (Figure 37 a-c). 4 hour treatment with 40 µM Endosidin2, an

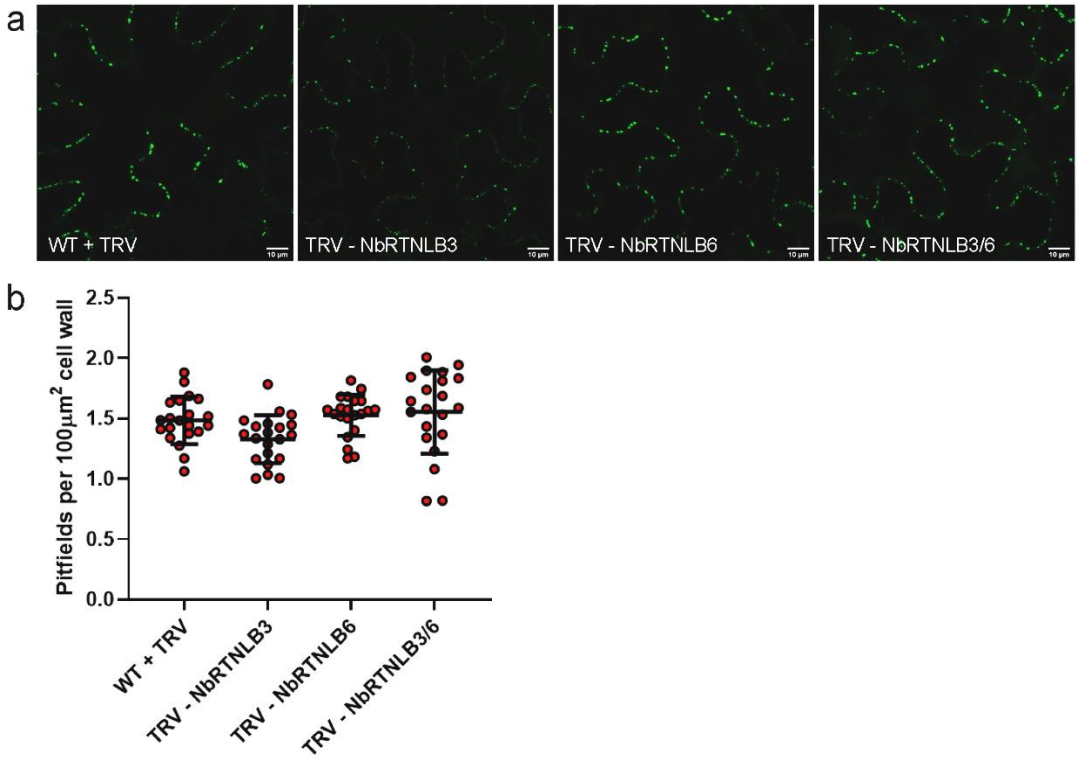


**Figure 36 Reticulon-like B proteins are not required for MP30-induced PD formation.**

Pitfield distribution assays were performed in plants silencing two Reticulon-like B genes (*NbRTNLB3* and *NbRTNLB6*) and plants silencing both genes using MP30-GFP. Representative images of cells from silenced and non-silenced control plants expressing MP30-GFP are shown (a). Pitfield densities for 20 fields of view for 1 biological replicate is shown. No statistical difference was observed between silencing and nonsilencing plants. Scale bar = 10 µm.

**Figure 37 Endocytosis is important for PD formation and virus induced PD formation**

(a-c) Intercellular trafficking was measured by counting the number of layers of GFP spread in *N. benthamiana* leaf epidermal cells treated with either Endosidin2 or Tyrphostin A23 and DMSO control plants. Plants were treated either 4 (left) or 12 (right) hours before image acquisition. Data for 2 biological replicates are shown. 20 foci were collected for each biological replicate. Data is depicted as a Quantitativeplot of the percentage of foci of each size (a) and the Mean layers of movement and standard deviation (b (4 hours) and c (12 hours)). Statistical significance was determined using the Mann-Whitney U-test ($p < 0.001$). (d- g) Pitfield distribution assays were performed using PDLP1-GFP (d and e) and MP30-GFP (f and g) in plants treated with Tyrphostin A23 24 hours before image acquisition. Representative images for control (left) and tyrphostinA23 treated cells expressing PDLP1-GFP (d) and MP30-GFP (f) are shown. Pitfield densities for 20 fields of view for 1 (MP30-GFP) or 2 (PDLP1-GFP) biological replicates (e and g, red and blue circles) are shown for PDLP1-GFP (e) and MP30-GFP (g). Statistical significance was determined using a student's t-test ($p < 0.001$). Scale bar = 10 μm.

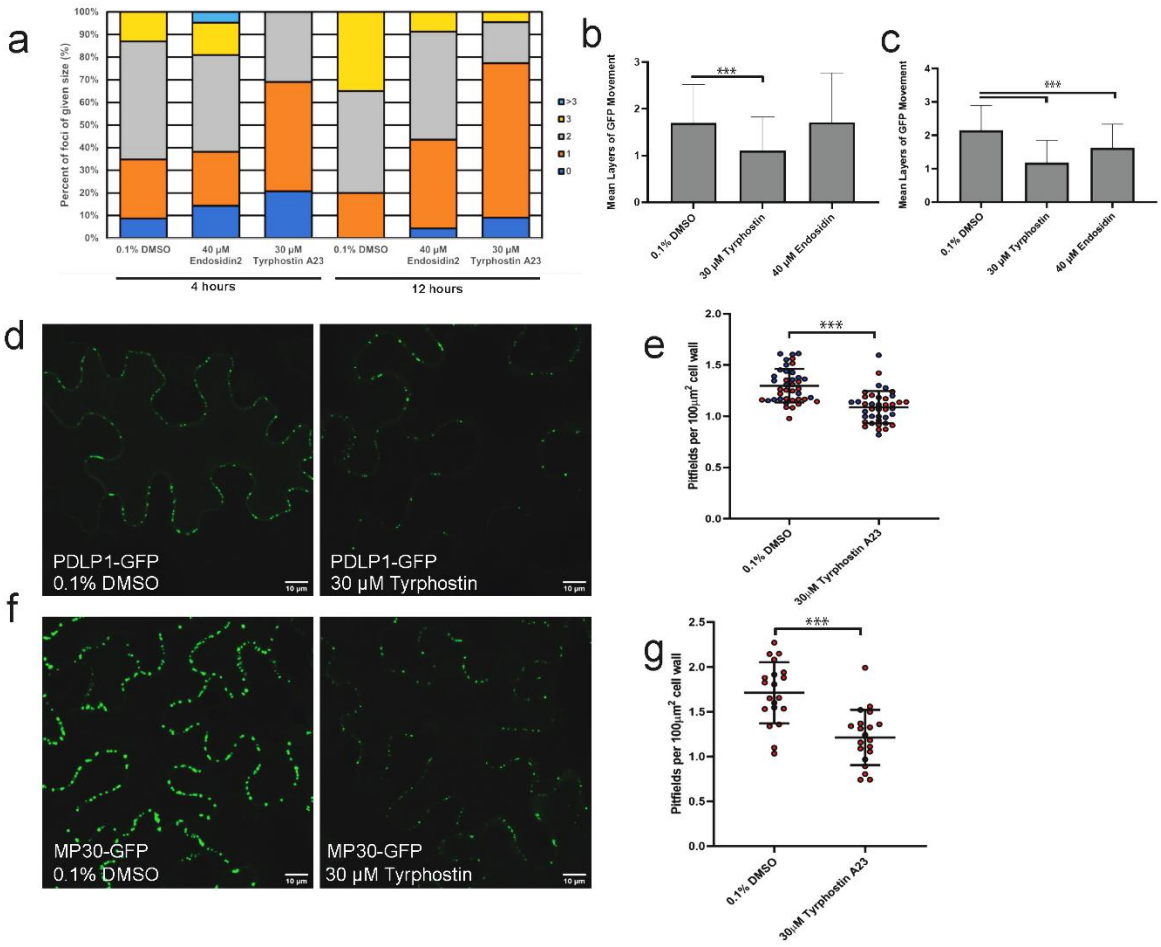
a
Percent of foci of given size (%)
100%
90%
80%
70%
60%
50%
40%
30%
20%
10%
0%
>3
3
2
1
0
0.1% DMSO
40 µM Endosidin2
30 µM Tyrphostin A23
0.1% DMSO
40 µM Endosidin2
30 µM Tyrphostin A23
4 hours
12 hours
b
Mean Layers of GFP Movement
***
0.1% DMSO
30 µM Tyrphostin
40 µM Endosidin
c
Mean Layers of GFP Movement
***
0.1% DMSO
30 µM Tyrphostin
40 µM Endosidin
d
PDLP1-GFP
0.1% DMSO
PDLP1-GFP
30 µM Tyrphostin
e
Pitfields per 100µm² cell wall
***
0.1% DMSO
30µM Tyrphostin A23
f
MP30-GFP
0.1% DMSO
MP30-GFP
30 µM Tyrphostin
g
Pitfields per 100µm² cell wall
***
0.1% DMSO
30µM Tyrphostin A23

inhibitor of exocytosis, had no effect on intercellular trafficking of GFP. Interestingly Long term treatment with Endosidin2 resulted in a modest decrease in intercellular trafficking..

In order to determine if the decrease in intercellular trafficking observed in Tyrphostin A23 treated leaves is a result of defects in PD formation, PDLP1-GFP was expressed in *N. benthamiana* leaves and leaves were treated with 30 µM Tyrphostin A23 36 hours post infiltration (24 hours before image acquisition). Treatment with Tyrphostin A23 resulted in decreased numbers of PDLP1-GFP labeled pitfields compared to leaves treated with 0.1% DMSO (Figure 37). This strongly suggests that endocytosis is required for PD formation. Treatment with Tyrphostin A23 also blocked MP30-induced secondary PD formation (Figure 37 f and d) indicating that endocytosis is also required for gating of plasmodesmata during virus infection.

***Disruption of the actin cytoskeleton alters intercellular trafficking***

Previous studies have demonstrated that the actin cytoskeleton is involved in PD regulation [182, 184]. Immunogold labeling was previously used to show that actin spans the PD pore and disruption of actin filaments was previously shown to increase intercellular trafficking [160].

Fully expanded leaves of *N. benthamiana* plants were agroinfiltrated for GFP movement assays and treated with 10 µM Latrunculin B to destabilize actin filaments 36 and 44 hours post agroinfiltration. Consistent with previous findings,

**Figure 38 Disruption of the cytoskeleton and membrane trafficking pathways alters intercellular trafficking.**

Intercellular movement assays were performed in plants treated with drugs targeting the actin cytoskeleton (Jasplankinolide and Latrunculin B), microtubules (Taxol and oryzalin) and ER-Golgi trafficking (Brefeldin A) for 4 (left) or 12 (right) hours before image acquisition. Intercellular trafficking was quantified by measuring the layers of movement of GFP in *N. benthamiana* leaf epidermal cells. Scale bar = 50 μm. Data for 2 biological replicates is shown. 20 foci were collected for each biological replicate. Data is depicted as a Quantitativeplot of the percentage of foci of each size (b) and the Mean layers of movement and standard deviation (c). Statistical significance was determined using the Mann-Whitney U-test ($p < 0.001$).

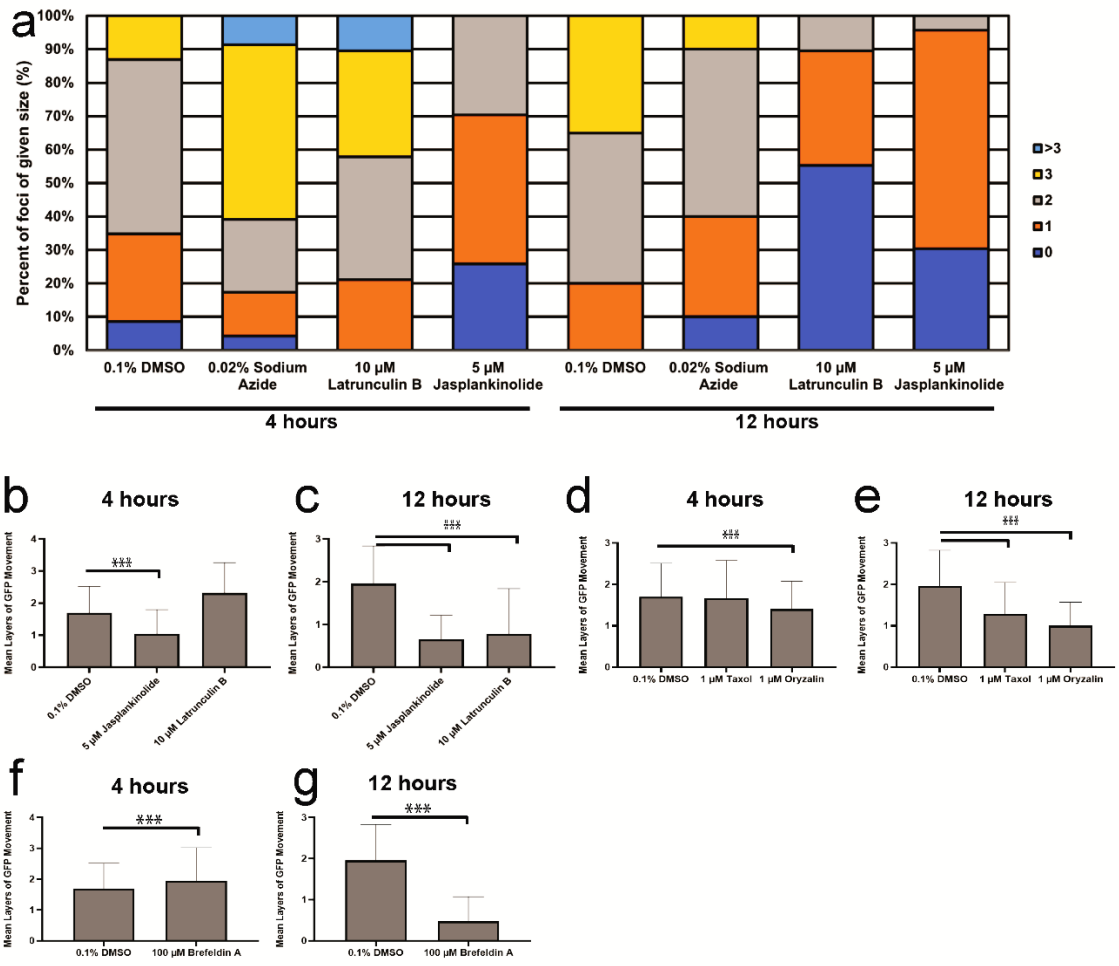
a
Percent of foci of given size (%)
100%
90%
80%
70%
60%
50%
40%
30%
20%
10%
0%
>3
3
2
1
0
0.1% DMSO
0.02% Sodium Azide
10 µM Latrunculin B
5 µM Jasplankinolide
0.1% DMSO
0.02% Sodium Azide
10 µM Latrunculin B
5 µM Jasplankinolide
4 hours
12 hours
b
4 hours
Mean Layers of GFP Movement
***
0.1% DMSO
5 µM Jasplankinolide
10 µM Latrunculin B
c
12 hours
***
Mean Layers of GFP Movement
0.1% DMSO
5 µM Jasplankinolide
10 µM Latrunculin B
d
4 hours
***
Mean Layers of GFP Movement
0.1% DMSO
1 µM Taxol
1 µM Oryzalin
e
12 hours
***
Mean Layers of GFP Movement
0.1% DMSO
1 µM Taxol
1 µM Oryzalin
f
4 hours
***
Mean Layers of GFP Movement
0.1% DMSO
100 µM Brefeldin A
g
12 hours
***
Mean Layers of GFP Movement
0.1% DMSO
100 µM Brefeldin A

short term treatment (4 hours) with LatB resulted in increased intercellular trafficking of GFP (Figure 38a-c). Interestingly, long term treatment with LatB (12 hours) resulted in a substantial decrease in intercellular trafficking (Figure 38a and c). Stabilizing actin filaments with 5 µM Jasplankinolide resulted in decreased intercellular trafficking regardless of duration of treatment indicating that actin dynamics are important for regulating PD.

### *Disruption of microtubule dynamics results in altered intercellular trafficking*

The role of microtubules in PD regulation are poorly understood. In order to determine if microtubules have a role in PD regulation, movement assays were performed on plants that treated with 1 µM Oryzalin to destabilize or 1 µM Taxol to stabilize the microtubules. Plants were treated 36 (12 hour) and 44 (4 hours) hours post agroinfiltration. Short term treatment with taxol had no effect on the intercellular movement of GFP (Figure 38a and d). In contrast, long term treatment resulted in a substantial decrease in intercellular trafficking (Figure 38 a and e). Both long and short term treatment with oryzalin resulted in decreased intercellular trafficking of GFP (Figure 38a, d, and e). The decrease in trafficking was more pronounced after long term treatment (Figure 38). This suggests a role for microtubules in regulating PD, potentially through PD formation. But more experiments and are needed to better understand this relationship.

### *Disruption of ER to Golgi trafficking results in decreased intercellular trafficking*

In order to determine if disruption of protein transport through the ER-Golgi pathway results in changes in PD trafficking, movement assays were performed in plants treated with 100 µM Brefeldin A or 0.1% DMSO. Short term treatment with BFA had no effect on trafficking of GFP through PD (Figure 38 a,f, and g)). Long term treatment with BFA had a significant effect on diffusive trafficking of GFP through PD indicating that a properly functioning ER-Golgi trafficking pathway is important for regulation of PD.

## Discussion

It is becoming increasingly clear that plants use multiple mechanisms to regulate intercellular trafficking through PD. One of the emerging pathways for regulating trafficking is through the *de novo* formation of plasmodesmata.

Burch-Smith et al. first demonstrated that increased trafficking could be correlated with increased levels of secondary PD formation through their work with the chloroplast RNA helicase *ISE2* [143]. This relationship was further demonstrated by Ganusova et al. where they demonstrated that disruption of specific of steps in chloroplast RNA processing results in changes in the number of PD in the leaves and that these changes are proportional to the change in intercellular trafficking that was observed for silenced plants [260].

While secondary PD formation has been reported in the literature for many years and multiple models for PD formation have been proposed, the details of

the mechanism of pore formation have not been elucidated. Our results for the first time demonstrate the complex cell biology involved in the formation of secondary PD.

Callose metabolism has long been considered a critical regulator of PD. Traditional views of its roles focused on its role in modifying the aperture diameter of the PD through the localized deposition or degradation of the glucan polymer at PD [91],[315]. From this perspective, elevated levels of callose at PD was correlated with decreased intercellular trafficking and suggested decreased PD aperture diameters. Conversely, depleted callose levels at PD has been correlated with increased trafficking, and therefore increased PD apertures.

Models for callose-mediated regulation of PD have historically ignored its potential role in secondary PD formation. While it was proposed that the cell wall at existing PD are likely primed for new pore insertion due to their specific composition, callose metabolism as a means for pore formation has never been discussed. Our results clearly demonstrate that deposition of callose is required for PD formation. Loss of either CalS1 or CalS10 results in decreased intercellular trafficking compared to non-silencing controls. This observation is in direct contrast to previously reported results with CalS mutants in Arabidopsis were loss of PD associated callose synthases resulted in increased intercellular trafficking [102]. Strikingly, silencing of CalS8 resulted in a slight increase in intercellular trafficking consistent with previous reports, but there was not an

increase in the number of PD. This suggests that different callose synthases have different roles in the regulation of intercellular trafficking.

Consistent with previous findings, silencing of various β-glucanases results in decreased intercellular trafficking. While this has historically been associated with the inability to dilate PD through the degradation of callose, our results indicate that these β-glucanases are important for PD formation as well. *NbBG11*, *NbBG14*, and *NbBG17_1*-silenced plants all exhibited decreased intercellular trafficking and decreased numbers of PD. Notably, each of these proteins are predicted to be GPI-anchored. *NbBG11* and *NbBG14* are closely related to the known PD associated β-glucanase *AtBG_ppap* [38]. *NbBG17_1* was selected as a candidate β-glucanase because it was shown to be induced during Tobacco curly shoot virus infection [343]. Interestingly, loss of *NbBG17_1* had the strongest effect on MP30-induced PD formation. This suggests that *NbBG17_1* is likely responsible for much of the PD formation induced during virus infection. The class I β-glucanase, *GLU1*, which was previously incorporated into the genome of TMV and accelerated virus movement had no effect on intercellular trafficking or PD formation suggesting that not all β-glucanases are involved in PD formation. Why incorporation of this enzyme into the viral genome was able to aid in virus intercellular movement remains unclear.

Probably the most surprising result from this work was that endocytosis is required for secondary PD formation. While treatment with tyrphostin A23 results in decreased numbers of PDLP1-labeled pitfields, the strong effect of treatment

on movement regardless of the duration of treatment suggests that endocytosis may play multiple roles in regulating PD. Strikingly, MP30 requires endocytosis to induce PD formation. This finally provides an explanation for MP30 physically interacting with *SYTA* and recruiting it to PD during virus infection. *SYTA* is a regulator of endocytosis and it was previously unclear how *SYTA* was functioning in virus infection. Collectively, this suggests that some yet to be identified component of the plasma membrane is endocytosed in order to facilitate PD formation. One promising candidate for the target of endocytosis during PD formation is Remorin. As a negative regulator of PD formation, removal of REM1 from the PM could allow for pore formation to occur. REM1.3 and *SYTA* were both identified as interacting with RTNLB3 and RTNLB6, the PD specific reticulon-like proteins involved in primary PD formation [318]. Additionally, REM1 silenced plants exhibited decreased sensitivity to tyrphostin treatment (data not shown). REM1 is also targeted by viruses and removal from the PM is required for virus-mediated gating of PD. Collectively, this suggests that REM1 is likely one of the PM components endocytosed in order to form new PD.

Endocytosis of a negative regulator of PD formation rather than exocytosis of PD formation machinery is consistent with the proposed models that suggest the components for PD formation reside at existing PD. Careful removal of the negative regulator by endocytosis would allow the plant to tightly regulate pore formation.

Notably, long term treatment with most of the cytoskeleton and membrane trafficking inhibitors screened resulted in a substantial decrease in intercellular trafficking of GFP (Figures 37 and 38). This could suggest that each of the targeted systems are involved in PD regulation, potentially through regulating PD formation, but it could also suggest that the long term treatments elicit a stress response in the cell that results in the shutting down of PD through the deposition of callose. Callose deposition in response to stress is a well characterized aspect the response to both biotic and abiotic stresses [344],[102]. PD distribution assays were not able to be performed for drugs that target the cytoskeleton and membrane trafficking pathways because our PD markers utilize these pathways for delivery to the PD. Intensive examination of treated cells with TEM or alternative methods for labeling PD will be required to investigate the effects of these disruptions of PD formation.

## Materials and Methods

### *Plant growth*

*Nicotiana benthamiana* plants were grown on light carts under standard long day conditions (16hrs light and 8 hours of dark, 80-120µmol/m/s). Seedlings were germinated and transferred to individual pots 10-12 days post germination. All plants used for experiments were at least 4-weeks old. Fertilizer was applied one time 5 days after transplanting.

### *Cloning and transient expression*

### *RNA extraction and cDNA synthesis*

Leaves from 4 week old *N. benthamiana* plants were collected and frozen in liquid nitrogen. RNA was extracted with the Trizol method (Thermo Fisher Scientific, Waltham, MA). RNA was DNase treated with DNA-free DNA removal kit (Invitrogen, Carlsbad, CA). cDNA was synthesized with M-MLV reverse transcriptase (Promega, Madison, WI) using oligo-dT primers.

### *Dual axis TEM Tomography*

Leaf samples were prepared for TEM via high pressure freezing. 200 nm thick sections were cut and mounted on formvar coated slot grids. Dual axis tomograms were collected between +/- 70 degrees using SerialEM.

### *Cloning fragments for VIGS*

*N. benthamiana* homologs for candidate genes were identified using the Solgenomics BLAST tool (https://solgenomics.net/tools/blast). 6 highly similar homologs were identified with BLAST. Primers were designed to amplify the VIGS fragment and add EcoRI and XbaI restriction enzyme sites to the ends of the fragment for cloning into the multiple cloning site of the pYL156 (pTRV-RNA2) plasmid for VIGS.

For the large *SYTA* VIGS fragment, 3 separate 400 bp fragments were designed using the VIGS tool (Solgenomics.net). The sequences for these three fragments were combined into a single fragment and synthesized by ThermoFisher. The synthesized produce was used as a template to amplify the full length fragment by PCR and add EcoRI and XbaI sites to the ends of the

fragment. The full length fragment was cloned into the TRV2 vector (pYL156) by following standard protocols.

***Virus induced gene silencing***

Three week old N. benthamina plants were agroinfiltrated for virus induced gene silencing (VIGS) as described previously. Agrobacterium strains carrying either TRV1 (pYL192) or TRV2 (pYL156 + the custom VIGS fragment) were diluted to OD600=0.1 and mixed 1:1. Two leaves per plant were infiltrated with the combined agrobacterium culture. For plants silencing multiple target genes, multiple constructs were infiltrated into the same leaf (two leaves per construct). Silencing was confirmed by qPCR.

***Pitfield distribution assays and confocal microscopy***

Pitfield distribution assays were completed with a Leica SP8 confocal microscope with the White Light Laser and 488, 570, and 586 nm laser lines as previously described [260]. Images of epidermal cells on the abaxial side of the infiltrated leaf. Images were collected 72 hours post infiltration. 15 micron z-stacks were collected with a step size of 1 micron. At least 20 fields of view were collected for each sample across all biological replicates.

***Intercellular Movement Assays***

Movement assays were performed as described in [254]. Briefly, silenced and non-silenced control *N. benthamiana* plants were agroinfiltrated with Agrobacterium encoding monomeric GFP at low optical density ($OD_{600}$= 0.0001)

to insure low rates transformation of epidermal cells. 48 hours post infiltration, z-stacks were collected with a Leica SP8 confocal microscope with the White Light Laser. Intercellular movement was quantified by counting the number of layers of GFP movement.

***Quantification of PDCB1-mCherry enrichment at PD***

A modified protocol from [342] was used to quantify PD enrichment of PDCB1-mCherry in REM1-silenced plants. Briefly, PDCB1-mCherry was agroinfiltrated into expanded *N. benthamiana* leaves. Images of epidermal cells on the abaxial side of the leave were collected 72 hours post infiltration with the Leica SP8 Laser Scanning Confocal microscope using the WLL and 488, 570, and 586 nm laser lines. Fluorescence intensities of PD pitfields were measured using the particle analyzer tool in ImageJ. Fluorescence intensities of the bulk plasma membrane were measured by random sampling of the PM with at least 50 regions of interest along the length of the PM using the circle tool in ImageJ [251]. PD enrichment was quantified by calculating the ratio of PD intensity to PM intensity.

***Drug treatments***

Fully expanded leaves of 4-6 week old *N. benthamiana* plants were agroinfiltrated for movement assays or PD distribution assays as described above. Leaves were then infiltrated with each drug (0.1% DMSO control, 0.02% Sodium Azide, 100 µM Brefeldin A, 10 µM Latrunculin B, 5 µM Jasplankinolide, 1 µM Taxol, 1 µM Oryzalin, 30 µM Tyrphostin A23, 40 µM Endosidin2) 36

(Movement and PD distribution) and 44 (movement) hours post agroinfiltration. Images of *N. benthamiana* leaf epidermal cells were collected with the Leica SP8 Scanning confocal microscope 48 hours (movement) or 72 hours (PD distribution) post agroinfiltration. A minimum of 20 foci were analyzed for each drug treatment for each of 3 biological replicates.

# Appendix

**Table 1 Primers used for cloning**

| Primer Name | Target | Primer Sequence |
|---|---|---|
| BCR1177 | attB1-PAGFP | ggggACAAGTTTGTACAAAAAAGCAGGCTATGGTGAGCAAGGGCGAGGAG |
| BCR1178 | attB2- | ggggACCACTTTGTACAAGAAAGCTGGGTTTACTTGTACAGCTCGTCCAT |
| BCR1179 | attB1-Dendra2 | ggggACAAGTTTGTACAAAAAAGCAGGCTatgaacaccccgggaattaacct |
| BCR1180 | attB2-Dendra2 | ggggACCACTTTGTACAAGAAAGCTGGGTttaccacacctggctgggcag |
| BCR1293 | FWD Primer for atPDLP1 | GGGGACAAGTTTGTACAAAAAAGCAGGCTTCATGAAACTCACCTATCAATTCTT |
| BCR1294 | RVSE Primer for atPDLP1 | GGGGACCACTTTGTACAAGAAAGCTGGGTAATAAGCATCATATTTATTACTCT |
| BCR1303 | PDLP1 (FWD) | ATGAAACTCACCTATCAATTC |
| BCR1304 | PDLP1 (RVSE) | ATAAGCATCATATTTATTACTCTTC |
| BCR1394 | PDLP-mRFP RVSE | GATCTAGTAACATAGATGACACCG |
| BCR1856 | XTH01 qPCR | CCACCAATGGGGGCAAATAC |
| BCR1857 | XTH01 qPCR | CATGAAGGGCAAAGTCGGAA |
| BCR1858 | XTH02 qPCR | CGACGCTCTTCCGATCTC |
| BCR1859 | XTH02 qPCR | GGCACCAAAAGCCAAGAACT |
| BCR1860 | XTH03 qPCR | TGGTCGACAACACACCGATA |
| BCR1861 | XTH03 qPCR | TCCTCTTGTTGCCCAGTCAT |
| BCR1862 | XTH04 qPCR | GTTCTTGGGAAACAGGTCGG |
| BCR1863 | XTH04 qPCR | TGTACACTCTAATGGGTACTTGGT |

**Table 2 Primers used for cloning cont.**

| Primer Name | Target | Primer Sequence |
|---|---|---|
| BCR1864 | XTH05 qPCR | AAGGCAGGAGGATCCAAACA |
| BCR1865 | XTH05 qPCR | CCCACTTGCAATAGCAAAACC |
| BCR1998 | NbEXP15 FWD + attB | GGGGACAAGTTTGTACAAAAAAGCAGGCTTCATGTCGATACTGTGGTCCTCC |
| BCR1999 | NbEXP15 RVSE + attB | GGGGACCACTTTGTACAAGAAAGCTGGGTAAGTGAACTGGGCGCCGGT |
| BCR2000 | NbEXPA1 FWD + attB | GGGGACAAGTTTGTACAAAAAAGCAGGCTTCATGGCTAAATTTGTGATTTTTCT |
| BCR2001 | NbEXPA1 RVSE + attB | GGGGACCACTTTGTACAAGAAAGCTGGGTAAGTGAATTGACCACCAGTAT |
| BCR2002 | NbEXPA4 FWD + attB | GGGGACAAGTTTGTACAAAAAAGCAGGCTTCATGGAGATAATGAACTTCTC |
| BCR2003 | NbEXPA4 RVSE + attB | GGGGACCACTTTGTACAAGAAAGCTGGGTAGACTCTAAAGTTCTTTCCAACAA |
| BCR2004 | NbEXPA8 FWD + attB | GGGGACAAGTTTGTACAAAAAAGCAGGCTTCATGGGGGGTGCTTGTGGT |
| BCR2005 | NbEXPA8 RVSE + attB | GGGGACCACTTTGTACAAGAAAGCTGGGTAAAATTGAGCCCCTTCAAAAGTTT |
| BCR2006 | *NbREM1* FWD + attB | GGGGACAAGTTTGTACAAAAAAGCAGGCTTCATGGCAGAAGTAGAAGCTACGAA |
| BCR2007 | *NbREM1* RVSE + attB | GGGGACCACTTTGTACAAGAAAGCTGGGTAAAAACATCCAAGGAGTTTCTTG |
| BCR2008 | NbXTH5 FWD + attB | GGGGACAAGTTTGTACAAAAAAGCAGGCTTCATGGGGATGAATATGTTGTTGTT |
| BCR2009 | NbXTH5 RVSE + attB | GGGGACCACTTTGTACAAGAAAGCTGGGTAAGGAGACTTTTTTGATGATT |
| BCR2010 | NbXTH9 FWD + attB | GGGGACAAGTTTGTACAAAAAAGCAGGCTTCATGGTTTCTTTTTCTATGG |
| BCR2011 | NbXTH9 RVSE + attB | GGGGACCACTTTGTACAAGAAAGCTGGGTAGTTGCGAGTCTTGTGCTTGTGC |

**Table 2 Primers used for cloning cont.**

| Primer Name | Target | Primer Sequence |
|---|---|---|
| BCR2012 | NbXTH23 FWD + attB | GGGGACAAGTTTGTACAAAAAAGCAGGCTTCATGAAGAAATCTTTCTTGTTTGT |
| BCR2013 | NbXTH23 RVSE + attB | GGGGACCACTTTGTACAAGAAAGCTGGGTAATTGAGAGAGCATTCAGG |
| BCR2014 | NbXTH30 FWD + attB | GGGGACAAGTTTGTACAAAAAAGCAGGCTTCATGGATTTCATCAGAAAGAAGAA |
| BCR2015 | NbXTH30 RVSE + attB | GGGGACCACTTTGTACAAGAAAGCTGGGTACTCTTCATCTTGATTTCCATG |
| BCR2016 | REM1 VIGS FWD EcoRI | AAAGAATTCCCATGGCAGAAGTAGAAGC |
| BCR2017 | REM1 VIGS RVSE XbaI | TTTTCTAGATCTCTGTTGCAACTCGAGCAAGC |
| BCR2018 | XTH5 VIGS FWD EcoRI | AAAGAATTCGGCATGTGCATATCTCCGTTA |
| BCR2019 | XTH5 VIGS RVSE XbaI | TTTTCTAGACACCCATGGTGAAAGTTCTAAAG |
| BCR2020 | XTH9 VIGS FWD EcoRI | AAAGAATTCAGCGACTACACCCACTGTGCT |
| BCR2021 | XTH9 VIGS RVSE XbaI | TTTTCTAGAGAAAAAGAAACCATTTTTCACAA |
| BCR2022 | *GPI8* VIGS FWD EcoRI | AAAGAATTCATTCAAGGAGCTGCTAATAATGG |
| BCR2023 | *GPI8* VIGS RVSE XbaI | TTTTCTAGAAGCTGACGAGGGTATAGATC |
| BCR2024 | XTH23 VIGS FWD EcoRI | AAAGAATTCGATATTACATGGGGTGAT |
| BCR2025 | XTH23 VIGS RVSE XbaI | TTTTCTAGACTGCTCTCTATTTCCTTTCCCTT |
| BCR2026 | XTH30 VIGS FWD EcoRI | AAAGAATTCCGATTCTTTGAGATATTCAGTGC |
| BCR2027 | XTH30 VIGS RVSE XbaI | GGGGTCTAGAGTAATATTTAGTATACATAATT |

**Table 2 Primers used for cloning cont.**

| Primer Name | Target | Primer Sequence |
|---|---|---|
| BCR2028 | EXPA15 VIGS FWD EcoRI | AAAGAATTCTTAATCAATTTAACTATTAAAAA |
| BCR2029 | EXPA15 VIGS RVSE XbaI | TTTTCTAGACCGAAAGAAGAATTAGAAAAGAA |
| BCR2030 | EXPA1 VIGS FWD EcoRI | AAAGAATTCAAAAACTTTGGCTGCTCA |
| BCR2031 | EXPA1 VIGS RVSE XbaI | TTTTCTAGAAAAGAGCGGCCTCAAGAAT |
| BCR2032 | EXPA4 VIGS FWD EcoRI | AAAGAATTCGCATAATTAAGGAGAGGATA |
| BCR2033 | EXPA4 VIGS RVSE XbaI | TTTTCTAGATAGTTCCGGAAGCATCAC |
| BCR2034 | EXPA8 VIGS FWD EcoRI | AAAGAATTCGCAATTCCTATCTCAATACTCAG |
| BCR2035 | EXPA8 VIGS RVSE XbaI | TTTTCTAGAAAAGACTCAAAATGCAGCA |
| BCR2045 | BG11 for VIGS ECORI | AAAGAATTCGTCCAATTTTGCTGGATAT |
| BCR2046 | BG11 for VIGS XbaI | TTTTCTAGAGATCAATGGCAAGTCTAAAAC |
| BCR2047 | BG14 for VIGS EcoRI | AAAGAATTCAGATCTATCAATGTTACGAGAGT |
| BCR2048 | BG14 for VIGS XbaI | TTTTCTAGATGTATTCAGCAAGATCTTGTCGA |
| BCR2053 | REM1 FWD | ATGGCAGAAGTAGAAGCTACGAA |
| BCR2054 | REM1 RVSE | AAACATCCAAGGAGTTTCTTG |

**Table 2 Primers used for cloning cont.**

| Primer Name | Target | Primer Sequence |
|---|---|---|
| BCR2055 | *GPI8* FWD full length | ATGAAATCCACATTTCTGTTGTGT |
| BCR2056 | *GPI8* RVSE Full length | AAATGAGAGCCAAGAGGAAAATG |
| BCR2057 | *GPI8* attB FWD | GGGGACAAGTTTGTACAAAAAAGCAGGCTTCATGAAATCCACATTTCTGTTGT |
| BCR2058 | *GPI8* attB RVSE | GGGGACCACTTTGTACAAGAAAGCTGGGTAAAATGAGAGCCAAGAGGAAAATG |
| BCR2067 | NbPDCB3.1 FWD VIGS EcoRI | AAAGAATTCCTTATTGGCATTAGTGTTTTATC |
| BCR2068 | NbPDCB3.1 RVSE VIGS XbaI | TTTTCTAGACTTCCACTAACAGGATAAGCACA |
| BCR2069 | NbPDCB3.2 FWD VIGS EcoRI | AAAGAATTCCGCCACCCCTACAACTCCAG |
| BCR2070 | NbPDCB3.2 RVSE VIGS XbaI | TTTTCTAGATACAGAGGGGAAGGTAAAAACAA |
| BCR2071 | *NbBG_ppap* FWD VIGS EcoRI | AAAGAATTCGTTGAAACTGAATGCGTTTAG |
| BCR2072 | *NbBG_ppap* RVSE VIGS XbaI | TTTTCTAGAGAAAACCAGGCATGCAAGAAG |
| BCR2073 | NbPDCB3.3 FWD VIGS EcoRI | AAAGAATTCTACTGACCCCAGCACAGCT |
| BCR2074 | NbPDCB3.3 RVSE VIGS XbaI | TTTTCTAGAAAGGCAGTCCTAACATAGCAACT |

**Table 2 Primers used for cloning cont.**

| Primer Name | Target | Primer Sequence |
|---|---|---|
| BCR2075 | 1 (BG_ppap_ SS + RFP) FWD | ATGGAACCCTTCACACATAGACATTGCTCTTTTACCACATTGCTTCTTGCATGCCTGGTTTTCAGCCCA ATAATGGTGGCTTCTATGAGCGAGCTGATTA |
| BCR2076 | 1 (BG_ppap_ SS + RFP) RVSE | CGATTTGGCCGTAGTTGATACCTAGGCCGCCGCCGCCCTTGTGCCCCAGT |
| BCR2077 | 2 (RFP overlap + BG_ppap) FWD | ACTGGGGCACAAGGGCGGCGGCGGCCTAGGTATCAACTACGGCCAAA |
| BCR2078 | 2 (RFP overlap + BG_ppap) RVSE | TCAAAGGTGGAGAGCCAGTGAAATAAAACCCA |
| BCR2079 | Full TagRFP_BG _ppap FWD (Short) | ATGGAACCCTTCACACATAGAC |
| BCR2080 | NbBGppap internal FWD (minus signal uence) | CTAGGTATCAACTACGGCCAAA |
| BCR2081 | NbBGppap attB1 FWD | GGGGACAAGTTTGTACAAAAAAGCAGGCTTCATGGAACCCTTCACACATAGACA |
| BCR2082 | NbBGppap attB2 RVSE | GGGGACCACTTTGTACAAGAAAGCTGGGTATCAAAGGTGGAGAGCCAGTGAAA |
| BCR2083 | Full Length mTurq2_PD CB3 FWD | ATGGCTGGTTTTCTCTTTGC |

**Table 2 Primers used for cloning cont.**

| Primer Name | Target | Primer Sequence |
|---|---|---|
| BCR2084 | Full Length mTurq2_PD CB3 RVSE | TCAAAGAAATGCAAGTGCAGAAA |
| BCR2085 | 1 mTurq2_PD CB3 (Sig uence + Mturq2) FWD | ATGGCTGGTTTTCTCTTTGCACTCCTCTTTTTAGCCATGGTTGGCCACTCTAGTGGTGTGAGCAAGGG CGAGGAGCTG |
| BCR2086 | 1 mTurq2_PD CB3 (Sig uence + Mturq2) RVSE | TCCTTTGCAAGCACACCATGCGCCGCCGCCGCCCTTGTACAGCTCGTCCA |
| BCR2087 | ement 2 mTurq2_PD CB3 FWD | ATGGACGAGCTGTACAAGGGCGGCGGCGGCGCATGGTGTGCTTGCAAAGGATTGAG |
| BCR2088 | NbPDCB attB1 FWD | GGGGACCACTTTGTACAAGAAAGCTGGGTATCAAAGGTGGAGAGCCAGTGAAA |
| BCR2089 | NbPDCB attB1 RVSE | GGGGACCACTTTGTACAAGAAAGCTGGGTATCAAAGGTGGAGAGCCAGTGAAA |
| BCR2090 | *NbCalS1* homologs VIGS FWD EcoRI | AAAGAATTCGAGAGCTGAGCATGGTTTTC |
| BCR2091 | *NbCalS1* homologs VIGS RVSE XbaI | CCCTCTAGACACAATTTTGTAGTGTGATCTCTC |
| BCR2092 | NbCalS8 homologs | AAAGAATTCTGATTCAACTTCCTTTTTTGATTTC |

**Table 2 Primers used for cloning cont.**

| Primer Name | Target | Primer Sequence |
|---|---|---|
| | VIGS FWD EcoRI | |
| BCR2093 | NbCalS8 homologs VIGS RVSE XbaI | TTTTCTAGACACTGGCAATTTCTCACTGTCA |
| BCR2094 | *NbCalS1*0 homologs VIGS FWD EcoRI | AAAGAATTCAGGAGTGCTATTACAGTATTGAAAAGA |
| BCR2095 | *NbCalS1*0 homologs VIGS RVSE XbaI | TTTTCTAGAAAATGCAGCCTTTTCACCTGC |
| SP2144 | RDH3 Vigs FWD EcoRI | AAAGAATTCGATAATAAGGATGGGTGTTGTTC |
| SP2145 | RDH3 Vigs RVSE XbaI | TTTTCTAGACCTTCATGAAGTTATCAACTCCG |
| SP2146 | RTNLB3 Vigs FWD EcoRI | AAAGAATTCCTCAGGTTCGAAATCACGC |
| SP2147 | RTNLB3 Vigs RVSE XbaI | TTTTCTAGAATTGCAGTGGCAAACCCAA |
| SP2148 | RTNLB6 Vigs FWD EcoRI | AAAGAATTCGTCAAGGCTAAGATCTATCGTC |
| SP2149 | RTNLB6 Vigs RVSE XbaI | TTTTCTAGACAATAACAGCAAGGAATTTCTTCA |
| SP2150 | *SYTA* Vigs FWD EcoRI | AAAGAATTCTTTGGGCACTATTCGCTTAAC |

**Table 2 Primers used for cloning cont.**

| Primer Name | Target | Primer Sequence |
|---|---|---|
| SP2151 | *SYTA* Vigs RVSE XbaI | TTTTCTAGATCCTTAACATCACAAGGCTGG |
| SP2152 | MCTP3 Vigs FWD EcoRI | AAAGAATTCAAGCCACAAACAGAAACACA |
| SP2153 | MCTP3 Vigs RVSE XbaI | TTTTCTAGAGCCAAAACCATTCAAAGCC |
| SP2154 | MCTP4 Vigs FWD EcoRI | AAAGAATTCAAGCCACAAACAGAAACACA |
| SP2155 | MCTP4 Vigs RVSE XbaI | TTTTCTAGAGCCAAAACCATTCAAAGCC |
| BCR2156 | MCTP MultiTarget Vigs FWD EcoRI | AAAGAATTCCACTCGCCTTTCTTGTGCT |
| BCR2157 | MCTP MultiTarget Vigs RVSE XbaI | TTTTCTAGAACATAAAATCCAGTCAAGAGTGCC |
| BCR2158 | RHD3_Multi_target MultiTarget Vigs FWD EcoRI | AAAGAATTCGAAGGGGTTAGATCCTCAAAG |
| BCR2159 | RHD3_Multi Target MultiTarget Vigs RVSE XbaI | TTTTCTAGATTCAGCAATATGAGCATCTACATCA |
| BCR2160 | TGB1 Gateway FWD attB | GGGGACAAGTTTGTACAAAAAAGCAGGCTTCATGGATATTCTCATCAGTAGTT |

**Table 2 Primers used for cloning cont.**

| Primer Name | Target | Primer Sequence |
|---|---|---|
| BCR2161 | TGB1 Gateway RVSE attB | GGGGACCACTTTGTACAAGAAAGCTGGGTACTATGTCCCTGCGCGGACAT |
| BCR2162 | TGB2 Gateway FWD attB | GGGGACAAGTTTGTACAAAAAAGCAGGCTTCATGTCCGCGCAGGGACATAG |
| BCR2163 | TGB2 Gateway RVSE attB | GGGGACCACTTTGTACAAGAAAGCTGGGTACTAATGACTGCTATGATTGTTAC |
| BCR2164 | TGB3 Gateway FWD attB | GGGGACAAGTTTGTACAAAAAAGCAGGCTTCATGGAAGCAAATACATATCTCAA |
| BCR2165 | TGB3 Gateway RVSE attB | GGGGACCACTTTGTACAAGAAAGCTGGGTATCAATGGAAACTTAACCGTTCAA |
| BCR2166 | ACMV/EACMV FWD primer for CP | ATGTCGAAGCGACCAGGAGAT |
| BCR2167 | ACMV RVSE primer for CP | TGTTTATTAATTGCCAATACT |
| BCR2168 | EACMV RVSE Primer for CP | CCTTTATTAATTTGTCACTGC |
| BCR2169 | TRV CP FWD | ATGGGAGATATGTACGATGAATCATTT |
| BCR2170 | TRV CP RVSE | CTAGGGATTAGGACGTATCGGACC |
| BCR2171 | PVX CP FWD | ATGTCAGCACCAGCTAGCACAAC |

**Table 2 Primers used for cloning cont.**

| Primer Name | Target | Primer Sequence |
|---|---|---|
| BCR2172 | PVX CP RVSE | TTATGGTGGTGGTAGAGTGACAACAG |
| BCR2173 | TMV CP FWD | ATGTCTTACAGTATCACTACTCCATCTCAGTTCG |
| BCR2174 | TMV CP RVSE | TGGGCCCCTACCGGGGGTAA |
| BCR2175 | PVY CP FWD | GCAAATGACACAATCGATGCAG |
| BCR2176 | PVY CP RVSE | CATGTTCTTAACTCCAAGTAGAGTATGC |
| BCR2177 | PVX GPF ATG to cgt mutation FWD for Q5 SDM kit | TGGAGGGACCcgtGTGAGCAAGGGCG |
| BCR2178 | PVX GPF ATG to cgt mutation RVSE for Q5 SDM kit | CCTCCACCGTCGACGTAT |
| BCR2191 | PVX Delete GFP (CP + SalI and SpeI) FWD | AAGGTCGACATGTCAGCACCAGCTAG |
| BCR2192 | PVX Delete GFP (CP + SalI and SpeI) RVSE | CCCACTAGTTTTTTTTTTTTTTTTTTTTTTTT |
| BCR2199 | BG17s_6 FWD EcoRI | AAAGAATTCAAGAGTTTCATTAATCCT |
| BCR2200 | BG17s_6RV SE Xba1 | AAATCTAGAGTTTCTATAGTCTTTCCAGG |

**Table 2 Primers used for cloning cont.**

| Primer Name | Target | Primer Sequence |
|---|---|---|
| BCR2201 | BG17_1 FWD EcoRI | AAAGAATTCCTATTTGTTTGCCAT |
| BCR2202 | BG17_1 RVSE Xba1 | CCCTCTAGAAATAACATGTCGTATTAAT |
| BCR2203 | PDCB_multi FWD EcoRI | AAAGAATTCCAAGCTCTGTTATCCT |
| BCR2204 | PDCB_Multi RVSE Xba1 | TTTTCTAGAGCAGTAACAGTGGCAG |
| BCR2205 | BG_ppap2 FWD EcoRI | AAAGAATTCGCTATCTTGCCATTA |
| BCR2206 | BG_ppap2 RVSE XbaI | CCCTCTAGATACAAACTCATTAAACTGA |
| BCR2207 | PVX FWD Colony PCR | GTTTGGGCTGCAACTAGATGCAGAAAC |
| BCR2208 | PVX RVSE colony PCR | AAATCCCCATCCCGGGATAGTGAACA |
| BCR2209 | REM_mCherry gateway FWD | GGGGACAAGTTTGTACAAAAAAGCAGGCTTCATGGCAGAAGTAGAAGCTACGAA |
| BCR2210 | REM_mCherry gateway RVSE | GGGGACCACTTTGTACAAGAAAGCTGGGTATTACTTGTACAGCTCGTCCAT |
| BCR2211 | mCherry FWD | GGTGGTGGTATGGTGAGCAAGGGCGA |
| BCR2212 | mCherry RVSE | TTACTTGTACAGCTCGTCCATGCCGCC |
| BCR2213 | REM_mCherry merge FWD | CTCCCAAGAAACTCCTTGGATGTTTTGGTGGTGGTATGGTGAGCAAG |
| BCR2214 | REM_mCherry merge RVSE | ATCCTCCTCGCCCTTGCTCACCATACCACCACCAAAACATCCAAG |

**Table 2 Primers used for cloning cont.**

| Primer Name | Target | Primer Sequence |
|---|---|---|
| BCR2242 | MP30-GFP plasmid uence extension FWD | CGCGATCACATGGTCCTGCTGGA |
| BCR2243 | MP30-GFP plasmid uence extension RVSE | ATTAATTCCCCGGATCATGAGCGG |
| BCR2244 | *SYTA* Large VIGS FWD XbaI | AAAtctagaATTTCTTGAGCTCATGTG |
| BCR2245 | *SYTA* Large VIGS RVSE BamHI | TTTGGATCCACACGTGGTGCG |
| BCR2246 | *NbREM1a* qPCR FWD | CCAACGGCTCTGTCATGATT |
| BCR2247 | *NbREM1a* qPCR RVSE | CTTGCAATGGTGAGCTGTCA |
| BCR2248 | *NbREM1b* qPCR FWD | TCCTGCACAGAAAGCCTCTT |
| BCR2249 | *NbREM1b* qPCR RVSE | CCATCTCGCTAAGGGGATGTA |
| BCR2250 | MP30 V4A FWD attB | GGGGACAAGTTTGTACAAAAAAGCAGGCTTCATGGCTCTAGCTGTTAAAGGAAA |
| BCR2251 | MP30 V4A RVSE attB | GGGGACCACTTTGTACAAGAAAGCTGGGTAAAACGAATCCGATTCGG |
| BCR2252 | WT MP30 FWD attB | GGGGACAAGTTTGTACAAAAAAGCAGGCTTCATGGCTCTAGTTGTTAAAGGAAA |

**Table 2 Primers used for cloning cont.**

| Primer Name | Target | Primer Sequence |
|---|---|---|
| BCR2295 | Full length *SYTA* +attb Forward | GGGGACAAGTTTGTACAAAAAAGCAGGCTTCATGGGCTTTTTCAGTACGATA |
| BCR2296 | Full length *SYTA* +attb Reverse | GGGGACCACTTTGTACAAGAAAGCTGGGTAAGAGGCAGTTCGCCACTCG |
| BCR2297 | Full length *SYTA* Forward | ATGGGCTTTTTCAGTACGATACTAGGATTT |
| BCR2298 | Full length *SYTA* Reverse (no stop) | AGAGGCAGTTCGCCACTCGAGC |
| BCR2299 | Sequence *SYTA* full length 5' end | TCCTCAATGATCGGTTTTGCTA |
| BCR2300 | Sequence *SYTA* full length 3' end | GAGAGAAAAACAAAGCACGTGA |

# CHAPTER 6

# A NEW MODEL FOR PLASMODESMATA FORMATION AND VIRUS-INDUCED GATING

Ever since Edward Tangl first described plasmodesmata in the late 1800s, the complexity of these tiny pores has enamored plant biologist from all disciplines. Throughout the years, many different mechanisms for regulating intercellular trafficking through PD have emerged. From callose deposition to organelle-chloroplast-plasmodesmata signaling (ONPS), PD regulation has been thoroughly investigated and discussed for many years and from many different perspectives [142],[91],[315],[4]. The work presented in this dissertation introduces a novel mechanism utilized by viruses to increase trafficking through PD via the induction of the *de novo* formation of PD and provides the first mechanistic model for secondary PD formation (Figure 40 and Figure 41).

***PD density is correlated with intercellular trafficking***

While the concept of PD densities being proportional to trafficking capacity is not novel, the idea that changes in intercellular trafficking are often related to changes in PD density has been historically overlooked [264, 345-348]. Figure 39 shows a modified version of the plot presented in Chapter 3 Figure 14 where the mean value of intercellular trafficking is plotted against the PD density for all conditions tested in this dissertation. From the graph, it is clear that trafficking capacity and PD density are linked but there are exceptions. The PD distribution assay that I developed in Chapter 3 allows for a fairly rapid assessment of PD densities in living tissues. Traditionally, this type of analysis would require rigorous quantification of PD numbers by electron microscopy. Even with the

advances in 3D-SEM techniques such as FIB-SEM (Chapter 2) or serial block face-SEM (SBF-SEM) for studying PD distributions, large scale screens with electron microscopy are not feasible [29, 189, 270]. Because of the simplicity of this assay and its amenability to different biological conditions, we have been able to address two long standing questions regarding PD regulation and pore formation.

The relationship between PD and viruses has been heavily scrutinized [349],[350],[313]. Because viruses are dependent on PD for their cell-to-cell spread, the virus-PD relationship has emerged as a key informant regarding PD function and regulation. Many early studies on intercellular trafficking of macromolecules focused on viruses and viral proteins [26, 44, 193, 252, 253, 320, 351]. The foundation of much of our knowledge on PD regulation comes from studies with viruses. Through these investigations, it became clear that viruses not only used PD for their spread, but they also disrupt the regulation of PD [49],[44],[193]. While this has been known for many decades, how the viruses manage to gate the PD has remained unclear due to absence of electron microscopic evidence for dilation of the PD. The work presented in this dissertation introduces a new model for gating where viruses gate the PD by inducing secondary PD formation to increase the number of PD available for their intercellular spread. While this mechanism for virus-induced gating of PD has never been fully discussed in the literature, it is consistent with many of the early

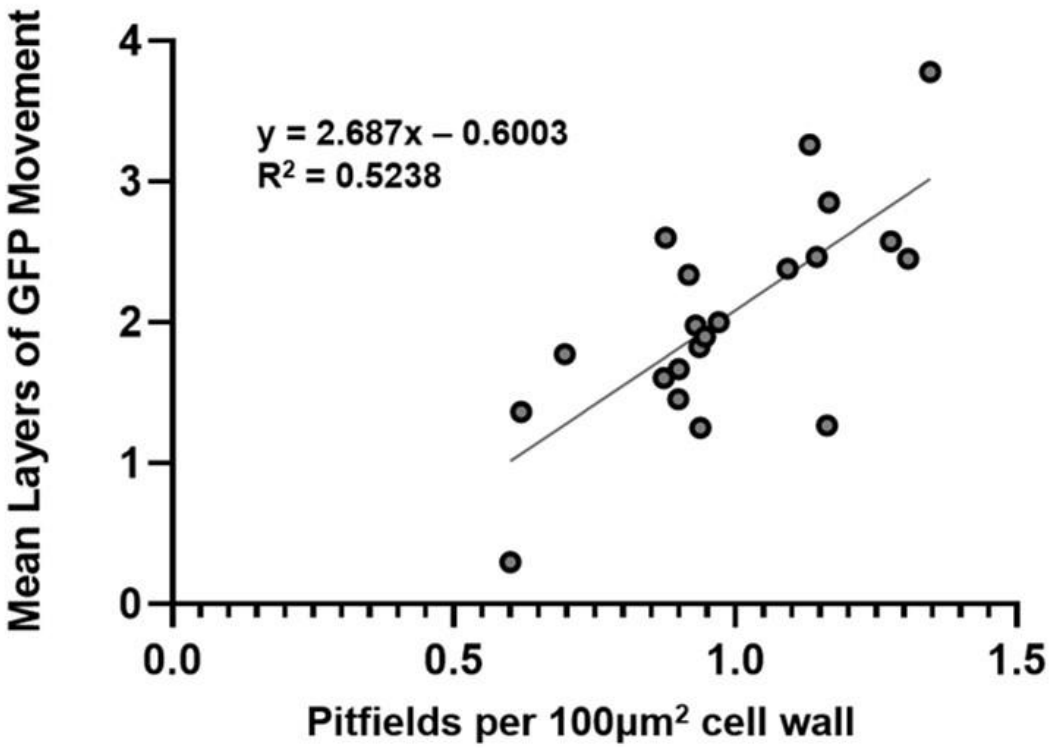


**Figure 39 Intercellular trafficking and pitfield density are positively correlated.**

The mean layers of GFP movement from movement assays was plotted against the average number of pitfields per 100 µm2 cell wall for all conditions presented in this dissertation where both PDLP1-GFP pitfield density and intercellular trafficking were measured.

**Figure 40 A mechanistic model of secondary PD formation.**

The data presented in this dissertation indicate that chloroplast retrograde signaling and signaling directly between the chloroplast and the PD and PM regulate secondary PD formation. In this model of PD formation, Remorin acts as a negative regulator of PD formation by maintaining PM organization and responding to signals from the chloroplast. *REM*-dependent organization of the PM allows for the cell to regulate positioning of *de novo* formation of PD. Under normal conditions, new PD are inserted in close proximity to existing PD. Specific GPI-anchored β-glucanases accumulate in these REM1-dependent nanodomains and coordinate pore formation through the targeted degradation of callose in the cell wall. Other PD formation machinery, such as callose synthases may also accumulate in the *REM*-dependent nanodomains. These nanodomains are also sites of specific ER-PM contacts that allow for the ER to be inserted into the forming pore. The data presented here also suggests that endocytosis is important for basal levels of secondary PD formation. Careful coordination of endocytosis of negative regulators, such as remorin, would allow the chloroplast (and cell) to tightly regulate when and where new PD are inserted into the cell wall.

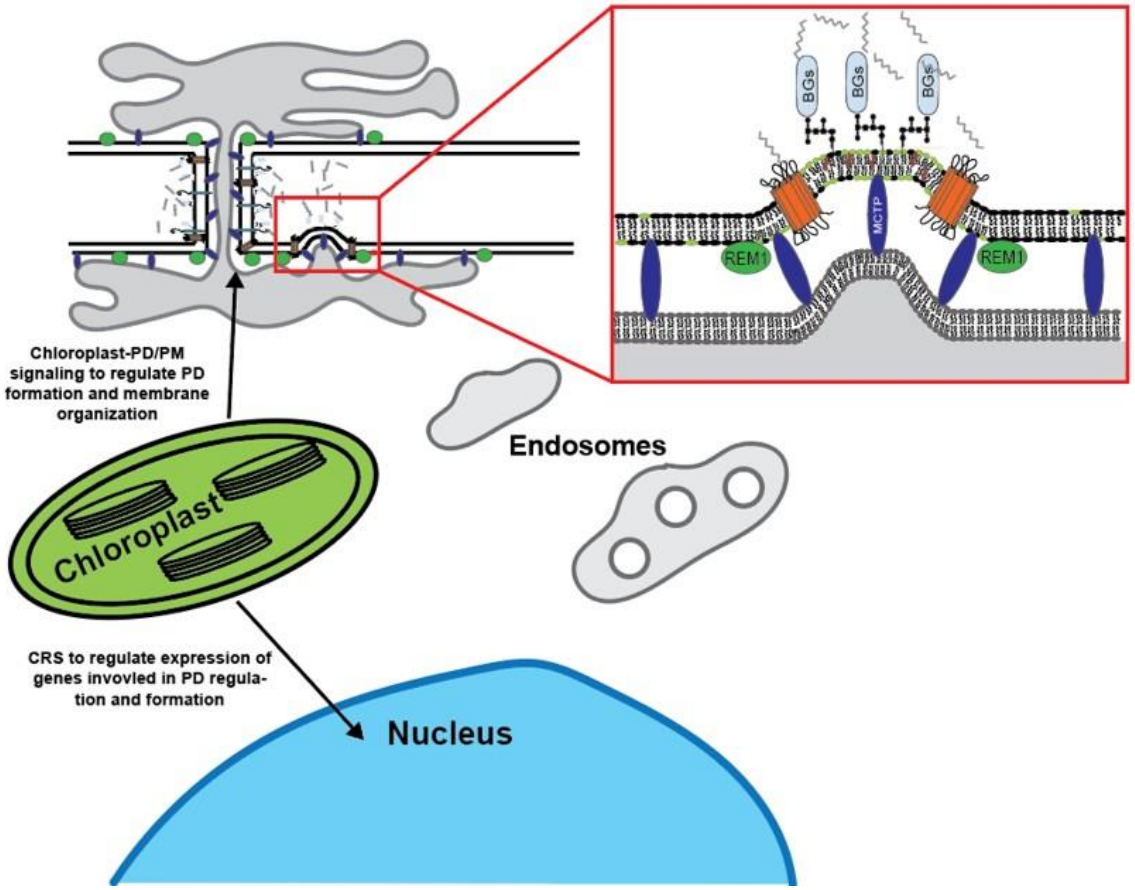
BGs
BGs
BGs
MCTP
REM1
REM1
Chloroplast-PD/PM signaling to regulate PD formation and membrane organization
Endosomes
Chloroplast
CRS to regulate expression of genes invovled in PD regulation and formation
Nucleus

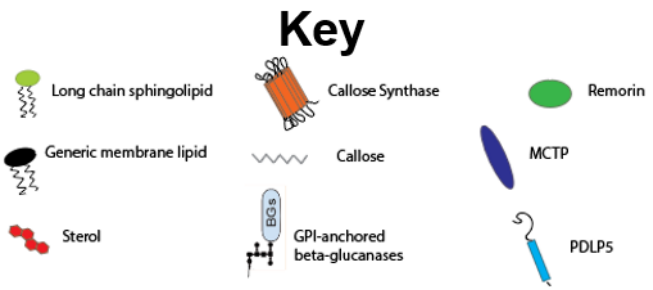
Key
Long chain sphingolipid
Callose Synthase
Remorin
Generic membrane lipid
Callose
MCTP
Sterol
BGs
GPI-anchored beta-glucanases
PDLPs

**Figure 41  A new model for virus induced gating of PD through PD formation.**

The data presented in this dissertation indicate that viruses induce PD formation by disrupted PM nanodomain organization and by using the plants defense pathways to its advantage. Once detected by the cell, the plant elicits a defense response. The chloroplast signals to the PD and PM (likely via SA signaling) to increase PM order and close off PD through the deposition of callose. This signaling stops basal secondary PD formation from occuring. SA signals also disrupt clathrin-mediated endocytosis which further restricts PD formation. The movement protein localizes to the PD and recruits *SYTA* to the PD to facilate the targeted endocytosis of remorin. By removing remorin from the PM, the virus blocks the chloroplast-to-PD/PM signaling that were initiated to stop the spread of the virus. The PM organization is lost and PD formation machinery dissociate from the lipid rafts and PD PMs. Once released from the nanodomains, the PD formation machinery can begin pore insertion wherever the callose is present. Removal of the callose that was deposited to restrict virus spread results in the proliferation of PD in the wall giving rise to the increased intercellular trafficking associated with virus infection.

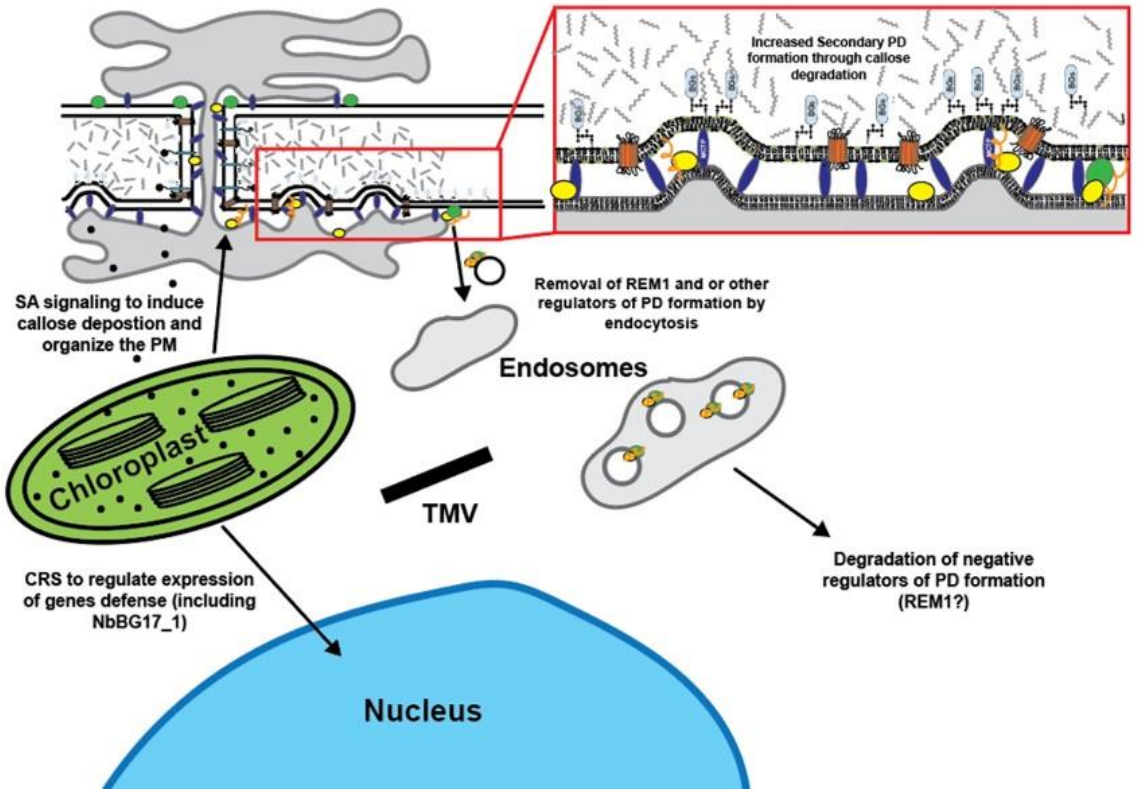
Increased Secondary PD formation through callose degradation
SA signaling to induce callose depostion and organize the PM
Removal of REM1 and or other regulators of PD formation by endocytosis
Endosomes
Chloroplast
TMV
Degradation of negative regulators of PD formation (REM1?)
CRS to regulate expression of genes defense (including NbBG17_1)
Nucleus

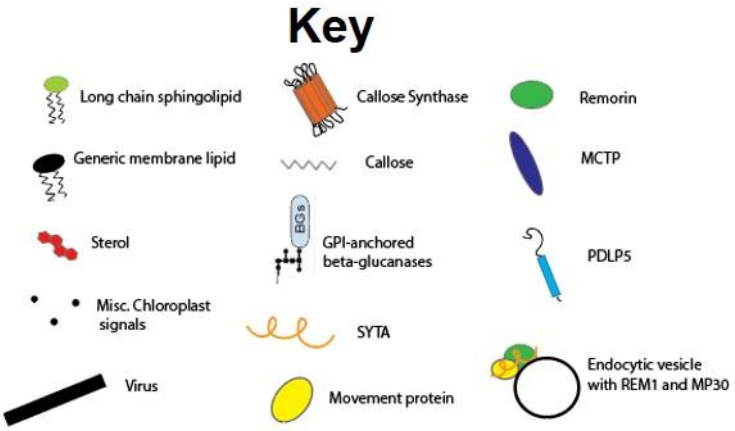
Key
Long chain sphingolipid
Generic membrane lipid
Sterol
Misc. Chloroplast signals
Virus
Callose Synthase
Callose
BGs
GPI-anchored beta-glucanases
SYTA
Movement protein
Remorin
MCTP
PDLP5
Endocytic vesicle with REM1 and MP30

studies on viruses and PD that found that viruses interacted preferentially with secondary, or branched PD [44, 77, 320]. The movement protein of TMV was originally shown to accumulate specifically in secondary PD, however when MP30-GFP was expressed in cells in Arabidopsis roots where secondary PD are not typically abundant, MP30-GFP was able to localize to PD suggesting that MP30, unlike MP17 from the phloem limited Potato leafroll virus, could also localize to primary PD [17]. Because our data demonstrate that MP30-GFP alone is sufficient to induce secondary PD formation, it is possible that the PD labeled in the Arabidopsis root were actually secondary PD that were formed in response to MP30 expression.

***Are these new PD different than regular PD?***

This discovery raises an intriguing question; are the PD formed during virus infection functionally, structurally, or compositionally distinct from PD formed in the absence of infection? One of the issues that has long obstructed the study of PD is the inability to probe individual pore function. Every assay currently available for studying PD function and composition are founded on bulk measurements of the PD in the tissue.

Thorough investigation of PD structure by electron microscopy, especially with recent advances in 3D EM, can provide insights into differences in PD structure on a pore-by-pore basis, but these images only represent snapshots of PD structure [143];[25];[188]. Do the PD formed during virus infection contain desmotubules? It is not clear how important the desmotubule is for virus

movement. It has been suggested that mobile RNPs move cell-to-cell along the outer leaflet of the desmotubule [55]. This would suggest that if the PD formed during infection are indeed used by the virus for spread, then the desmotubule would be an essential component of the pore. How viruses manage to facilitate the insertion of the ER into the forming pore remains to be determined. Viruses have been shown to make substantial changes to the ER structure during infection [352];[82];[353]. It has also become clear that viruses recruit ER-PM contacts to PD during the formation of their ER-derived replication structures [58];[129];[354]. It is likely that these recruited contacts serve as sights for the formation of new PD, but the details of this relationship will require further investigation.

While informative on differences in pore structure, these images do not provide information on the composition of PD. Proteomic analysis of PD-enriched cell walls has been used to identify PD-associated proteins, however there is currently no way to isolate specific groups or types of PD [33]; [355];[34]. Because of this, proteins that localize specifically to specific types of PD have not been identified. Viral movement proteins were believed to label specifically secondary PD, however the data presented in this dissertation demonstrate that MPs alter the population by inducing the production of new PD and therefore do not serve as accurate labels for branched or secondary PD. The only currently available technique to identify PD-type specific proteins is immune-gold labeling because this provides individual pore-level resolution of protein localization. This

approach, while informative is severely limited by the availability of antibodies against PD proteins. This technique also requires extensive time and expertise and is not conducive for screening for candidates. More directed approaches and novel techniques will be required to identify true markers for distinct classes of PD and to determine if these new PD formed during infection are compositionally distinct from PD in uninfected plants.

### *Learning from viruses: details of PD formation uncovered by studying viruses*

As with many other fundamental discoveries regarding PD regulation, many of the proteins identified in this dissertation as having roles in secondary PD formation were chosen as candidates due to their importance for both PD regulation and virus infection. REM1, SYTA, AtBG_ppap, and NbBG17_1 were all previously identified as having roles during virus infection [38],[117],[127],[128],[129],[94],[343]. Strikingly, silencing these genes had major effects on PD formation. Remorin was the only negative regulator of PD formation identified in this reverse genetics screen. As described throughout this dissertation, many viruses, including RSV, TMV, ToMV, TuMV, and PVX have all been shown to target Group 1 remorins as part of their infection [94, 117, 125, 323]. The movement protein of ToMV, a tobamovirus closely related to TMV, was shown to interact with REM1 and sequester REM1 in the ER and target it for degradation [125]. RSV has been shown to target remorin for autophagic degradation [94]. Removal of REM1 from the PM could serve as an entry point

for viruses to induce PD formation. Recruitment of the endocytosis regulator, *SYTA*, to PD by TMV could serve as a mechanism to facilitate the targeted removal of REM1 from the plasma membrane. This removal would then result in the loss of *REM*-dependent nanodomain organization at the PD. Consistent with endocytosis being involved in secondary PD formation, treatment of leaves with the clathrin-mediated endocytosis inhibitor, Tyrphostin A23, resulted in decreased intercellular trafficking, decreased numbers of PDLP1-GFP labeled pitfields, and blocked MP30-induced PD formation. Collectively, this suggests that TMV, and potentially other viruses, recruit *SYTA* to the PD to remove specific negative regulators from the PM at PD in order to induce pore formation. While the target of this endocytosis was not fully characterized in the work presented here, *NbREM1* is a promising candidate for future investigation.
The data presented here also indicate that GPI-anchored β-glucanases are involved in secondary PD formation. As previously discussed, GPI-anchored proteins accumulate in lipid rafts and the PD PM. Silencing *NbREM1* results in decreased enrichment of GPI-anchored proteins at PD compared to the bulk plasma membrane. This finding further supports the idea that REM1-mediated membrane organization sequesters PD formation machinery at the PD in order to regulate PD formation which is consistent with current models that propose the PD formation machinery reside at existing PD.

The membrane composition of the PD plasma membrane is critical for proper PD function and maturation [37]. The PM of PD are enriched in sterols

and long chain sphingolipids. Disruption of the PD membrane composition has been shown to result in mislocalization of GPI-anchored proteins [37]. One of the only mutants ever described as having decreased secondary PD formation is deficient in choline import [190]. Plants with a mutation in the CHOLINE TRANSPORTER-LIKE 1 gene (*cher1*) exhibit strong defects in PD formation [190]. While major changes in the lipid profiles of these plant were not detected, the authors argue that due two their low contributions to the bulk lipid profile in Arabidopsis, minor changes in PD lipid compositions may not be detected. Proteomic analysis of the *cher1* mutants revealed decreased abundance of predicted PD proteins [190]. Among the proteins identified in these mutants, the GPI-anchored β-glucanase, *AtBG_ppap*, stands out with regards to the results presented in this dissertation.

***A new role for callose metabolism at PD***

Several of the β-glucanases identified as having roles in PD formation are also predicted to be GPI-anchored (*NbBG11*, *NbBG14*, and *NbBG17*). *NbBG11* and *NbBG14* were both selected as candidates for silencing because of their high degree of similarity to *AtBG_ppap*. *NbBG17* was identified as being strongly upregulated during Tobacco curly shoot virus infection [90]. Loss of these GPI-anchored β-glucanases resulted in both decreased intercellular trafficking and decreased numbers of PD. Loss of each of the β-glucanases alone had a modest effect on PD formation indicating that multiple proteins are involved in PD formation. Silencing of *NbGPI8*, which results in the loss of all GPI-anchored

proteins had a more pronounced effect on PD formation than loss of these β-glucanases alone or in combination with each other indicating that there are likely other GPI-anchored proteins involved in PD formation. Future work will further characterize the players involved in PD formation.

The results presented in this dissertation clearly demonstrate that callose metabolism is important for PD formation. Both synthesis and degradation of callose are important for pore formation. These findings challenge the pre-existing notation the callose degradation at PD allows for the dilation of the pore to increase transport through existing PD. While it is possible that callose deposition and degradation at existing PD are used to regulate flux through the pore, our results show that the relationship between callose and PD is more complex than previously thought.

The identification of ‘ghost’ PD via electron tomography raises many interesting questions. First, what are the differences in the composition of these microdomains in the cell wall that result in their altered staining patterns? Our model and data indicate that they may be local deposits of callose in the wall that are degraded during pore insertion, however, other cell wall modifications may contribute to their characteristic appearance. Future work with immuno-gold labeling will be required to uncover the composition of these regions of cell wall.

The dynamics of callose metabolism at PD during and in the absence of infection are also likely to be different and therefore have different effects on PD regulation. Under normal conditions, callose is not highly abundant in the cell wall

of most plants. Under these conditions, callose primarily accumulates at or around PD, which is one of the reasons why callose staining has traditionally been used to label PD for light microscopy [356]. One of the first steps in any defense response to pathogens is the deposition of callose in the cell wall [357];[358];[359];[360];[361];[362];[363]. This deposition is triggered, in part, by SA-stimulated callose synthase activity (Specifically CalS1 in *Arabidopsis*) [364];[102]. However, during virus infection, this increased deposition of callose is followed by acute degradation of callose to increase the trafficking through PD. This observation served as the basis for the entire phenomenon of PD gating during virus infection. As described earlier, gating was shown to be reversible and to occur specifically at the leading edge of infection foci [193]. Because our results demonstrate that infection triggers the formation of new PD (which are likely permanent or lasting changes to PD composition), the reversibility of gating indicates that the cell is able to regain control of the PD once the virus infection has been cleared from the cell or synthesis of the movement protein ends and production of virions begins. Future work will be needed to uncover the mechanisms utilized by the cell to regain control and to return trafficking levels to uninfected levels despite having increased PD densities. This return to normal may be the result of the traditional PD callose balancing mechanisms thought to regulate trafficking, but it cannot be ruled out that mechanisms may be in place to remove, or close off, PD in order to regulate trafficking levels in the post-infection

cells. Evidence for the removal of PD from the wall is limited, but has been described for specific cell types [365];[366].

***ER-PM contact sites allow for the formation of the desmotubule***

The challenge of targeted insertion of the ER into forming plasmodesmata has also been a long standing question about secondary PD formation. *SYTA* was not the only membrane tether identified to have a role in PD formation. The Multiple C2 domain containing proteins have emerged as tethers that connect the ER to the PM at PD [337],[367]. Our data demonstrate that silencing *NbMCTP* family members results in decreased intercellular trafficking and decreased numbers of PD. This suggests that these ER-PM contacts may serve as sites for secondary PD formation. MTCPs were also identified in the *cher1* mutants [368]. Specialized ER-PM contact sites have previously been implicated in endocytosis [369]. The ER membrane-associated VAMP-associated-proteins, VAP27-1 and VAP27-3, were shown to interact with clathrin and to be required for maintenance of endocytosis. Notably, VAP27-1 was also previously identified as potentially having a role in primary PD formation. VAP27-1 was found to interact with AtRTNLB3 and AtRTNLB6, two reticulon like proteins that localize to PD in Arabidopsis and are involved in primary PD formation [370]. Interestingly, this screen also identified *SYTA* and REM1.3 as interacting with these reticulon like proteins. Collectively, this strongly suggests that ER-PM contacts are sites for targeted endocytosis required for secondary PD formation.

Surprisingly, silencing of *N. benthamiana* homologs the Arabidopsis Reticulon like B (RTNLB) proteins had little to no effect on PD distributions. *AtRTNLB3* and *AtRTNLB6* were previously implicated in primary PD formation. Silencing of either reticulon individually had no effect on PD distributions indicating that they may not be involved in PD formation or that, as with many plant proteins, other proteins have redundant functions in PD formation. Curiously, silencing both homologs in the same plant resulted in a slight increase in the number of PD present indicating that they may have redundant roles in restricting PD formation. This observation warrants further investigation into the roles of reticulons in formation of the desmotubule and secondary PD.

***Salicylic acid as a regulator of PD formation***

While not directly tested here, the results presented in this dissertation strongly implicate salicylic acid signaling in the regulation of PD formation. SA is primarily viewed through the context of defense, but it also has fundamental roles in regulating cellular processes. From the PD perspective, SA is known to induce callose deposition at the PD in order to restrict intercellular trafficking [102, 147, 371]. This occurs through a signaling pathway involving PDLP5 and CalS1 [102]. Our data demonstrate that *NbCalS1* is involved in pore formation indicating that SA dependent callose deposition is important for PD formation. SA signaling has also been shown to regulate PM organization in a remorin-dependent manner [329],[330]. SA has also been shown to regulate endocytosis in plants via a pathway unrelated to the well characterized transcriptional changes associated

with SA signaling [372]. From the PD formation perspective, SA signaling may act to restrict PD formation by inhibiting the endocytosis of remorin. Accumulation of remorin in the PM results in increased membrane order and sequestration of GPI-anchored β-glucanases invovled in PD formation. Additionally, SA-dependent callose deposition restricts trafficking through existing PD in order to coordinate the defense response and to restrict cell-to-cell spread of viruses and other pathogen effectors. This model also serves as a direct link to the chloroplast in support for the ONPS hypothesis of PD regulation [142, 260]. Salicylic acid is produced in the chloroplast and its controlled release would allow the chloroplast to tightly regulate secondary PD formation. Previous work on *ISE2* and other chloroplast localized proteins with effects on PD function have found that disruption of chloroplast processes such as RNA processing may elicit a stress response in the chloroplast as indicated by changes in the redox state of the chloroplast [88, 373-375]. It is possible that this stress response results in changes in SA signaling that differentially affects PD formation. Future work should investigate this role of SA signaling in PD formation.

Our model for PD formation also explains why SA is less effective as a defense hormone at limiting the spread of virus infection. This could also explain the surprising observation that *ISE2*-silenced and overexpressing plants that have opposite effects on trafficking through PD, increased and (presumably) decreased numbers of PD respectively, both exhibit increased susceptibility to virus infection [146]. By targeting remorin, the virus cuts off the signaling pathway

between the chloroplast and the PM. The virus also recruits *SYTA* to the PD to facilitate endocytosis of REM1 at the PD. Removal of remorin from the plasma membrane decreases membrane order and releases the sequestered β-glucanases which are then able to break down the callose that was synthesized by CalS1 in response to SA resulting in the formation of new PD. In this way, viruses have evolved mechanisms to circumvent the plants defense pathways to facilitate their intercellular spread through the induction of secondary PD.

One limitation to studies on the roles of specific hormones on intercellular trafficking and cellular processes in general is that they are typically performed in a targeted and minimalistic manner. Traditionally, these studies involve the application of a specific hormone, for example salicylic acid, to a plant and then the change in cellular behavior is assessed using various experiments. While informative, like most minimalistic approaches to explaining biological processes, these experiments are not typically representative of the full picture. SA is typically considered to be the primary hormone involved in defense, but in reality, defense responses involve the coordination of many hormone signaling pathways including jasmonic acid, ethylene, and auxin [376];[377];[378];[379]. Non-hormone signaling pathways, such as calcium waves and ROS-mediate responses are also typically triggered during defense [380];[381];[382];[383];[384]. In order to study cellular processes in their real context, it will be important to move away from the minimalistic approaches commonly utilized and move towards more complex, but accurate, systems.

### *Concluding Statements*

Recent years have brought about many exciting discoveries regarding PD structure, function, and regulation. The results presented here push our understanding of to distinct, but connected, aspects of PD regulation forward and provide novel insights into the complex mechanisms of virus-induced gating of PD and secondary PD formation. These results will serve as a starting point for the future characterization of host factors involved in PD formation. They will also force a revisitation of our interpretations of callose metabolism and PD regulation. Keeping with tradition, viruses have again proven to be powerful tools for studying basic cell biological processes.

# REFERENCES


1. Dunny GM, Winans SC: **Cell-cell signaling in bacteria**, vol. 520: ASM press Washington, DC; 1999.

2. Bloemendal S, Kück UJN: **Cell-to-cell communication in plants, animals, and fungi: a comparative review**. 2013, **100**(1):3-19.

3. Brunkard JO, Zambryski PCJCOiPB: **Plasmodesmata enable multicellularity: new insights into their evolution, biogenesis, and functions in development and immunity**. 2017, **35**:76-83.

4. Azim MF, Burch-Smith TMJCOiPB: **Organelles-nucleus-plasmodesmata signaling (ONPS): an update on its roles in plant physiology, metabolism and stress responses**. 2020, **58**:48-59.

5. Van Norman JM, Breakfield NW, Benfey PN: **Intercellular communication during plant development**. *Plant Cell* 2011, **23**(3):855-864.

6. Bonnemain J-L, Chollet J-F, Rocher F: **Transport of salicylic acid and related compounds**. In: *Salicylic acid.* Springer; 2013: 43-59.

7. Kachroo P, Liu H, Kachroo AJCOiV: **Salicylic acid: transport and long-distance immune signaling**. 2020, **42**:53-57.

8. Baron-Epel O, Gharyal PK, Schindler MJP: **Pectins as mediators of wall porosity in soybean cells**. 1988, **175**(3):389-395.

9. Van Roy F, Berx GJC, sciences ml: **The cell-cell adhesion molecule E-cadherin**. 2008, **65**(23):3756-3788.

10. Chen T, Yuan D, Wei B, Jiang J, Kang J, Ling K, Gu Y, Li J, Xiao L, Pei GJSc: **E-Cadherin-Mediated Cell–Cell Contact Is Critical for Induced Pluripotent Stem Cell Generation**. 2010, **28**(8):1315-1325.

11. Ding B, Turgeon R, Parthasarathy MV: **Substructure of freeze-substituted plasmodesmata**. *Protoplasma* 1992, **169**(1-2):28-41.

12. Overall RL, Blackman LM: **A model of the marcomolecular structure of plasmodesmata**. *Trends in Plant Science* 1996, **1**(9):307-311.

13. Tilsner J, Amari K, Torrance L: **Plasmodesmata viewed as specialised membrane adhesion sites**. *Protoplasma* 2011, **248**(1):39-60.

14. Grabski S, De Feijter AW, Schindler M: **Endoplasmic Reticulum Forms a Dynamic Continuum for Lipid Diffusion between Contiguous Soybean Root Cells**. *Plant Cell* 1993, **5**(1):25-38.

15. Guenoune-Gelbart D, Elbaum M, Sagi G, Levy A, Epel BL: **Tobacco mosaic virus (TMV) replicase and movement protein function synergistically in facilitating TMV spread by lateral diffusion in the plasmodesmal desmotubule of Nicotiana benthamiana**. *Mol Plant Microbe Interact* 2008, **21**(3):335-345.

16. Faulkner C, Akman OE, Bell K, Jeffree C, Oparka K: **Peeking into pit fields: a multiple twinning model of secondary plasmodesmata formation in tobacco**. *Plant Cell* 2008, **20**(6):1504-1518.

17. Burch-Smith TM, Stonebloom S, Xu M, Zambryski PC: **Plasmodesmata during development: re-examination of the importance of primary, secondary, and branched plasmodesmata structure versus function**. *Protoplasma* 2011, **248**(1):61-74.

18. Faulkner CR, Blackman LM, Collings DA, Cordwell SJ, Overall RL: **Anti-tropomyosin antibodies co-localise with actin microfilaments and label plasmodesmata**. *Eur J Cell Biol* 2009, **88**(6):357-369.

19. Bell K, Oparka K: **Imaging plasmodesmata**. *Protoplasma* 2011, **248**(1):9-25.

20. Fitzgibbon J, Bell K, King E, Oparka K: **Super-resolution imaging of plasmodesmata using 3D-structured illumiination microscopy (3D-SIM).** *Plant Physiol* 2010.

21. Tilney LG, Cooke, T.J., Connelly, P.S. and Tilney, M.S.: **The structure of plasmodesmata as revealed by plasmolysis, detergent extraction, and protease digestion**. *The Journal of Cell Biology* 1991, **112**(4):739-747.

22. Hofius D, Herbers K, Melzer M, Omid A, Tacke, E., Wolf S, Sonnewald U: **Evidence for expression level-dependent modulation of carbohydrate status and viral resistance by the potato leafroll virus movement protein in transgenic tobacco plants**. *The Plant Journal* 2001, **28**(5):529-543.

23. Hull R: **Matthew's Plant Virology**, 4th edn. San Diego: Academic Press; 2002.

24. Harrison B, Barker H, Derrick P: **Intercellular spread of potato leafroll luteovirus: effects of co-infection and plant resistance**. In: *Recognition and response in plant-virus interactions.* Springer; 1990: 405-414.

25. Nicolas WJ, Grison MS, Trépout S, Gaston A, Fouché M, Cordelières FP, Oparka K, Tilsner J, Brocard L, Bayer EMJNp: **Architecture and permeability of post-cytokinesis plasmodesmata lacking cytoplasmic sleeves**. 2017, **3**(7):17082.

26. Oparka KJ, Roberts AG, Boevink P, Santa Cruz S, Roberts I, Pradel KS, Imlau A, Kotlizky G, Sauer N, Epel B: **Simple, but not branched, plasmodesmata allow the nonspecific trafficking of proteins in developing tobacco leaves**. *Cell* 1999, **97**(6):743-754.

27. Brunkard JO, Runkel AM, Zambryski PC: **The cytosol must flow: intercellular transport through plasmodesmata**. *Current opinion in cell biology* 2015, **35**:13-20.

28. Kim J-Y: **Symplasmic intercellular communication through plasmodesmata**. In.: Multidisciplinary Digital Publishing Institute; 2018.

29. Reagan BC, Ganusova EE, Fernandez JC, McCray TN, Burch-Smith TMJPS: **RNA on the move: The plasmodesmata perspective**. 2018, **275**:1-10.

30. Sager RE, Lee J-YJJocs: **Plasmodesmata at a glance**. 2018, **131**(11):jcs209346.

31. White RG, Barton DA: **The cytoskeleton in plasmodesmata: a role in intercellular transport?** *J Exp Bot* 2011, **62**(15):5249-5266.

32. Epel B, van Lent JWM, Cohen L, Kotlizky G, Katz A, Yahalom A: **A 41 kDa protein isolated from maize mesocotyl cell walls immunolocalizes to plasmodesmata**. *Protoplasma* 1996, **191**:70-78.

33. Fernandez-Calvino L, Faulkner C, Walshaw J, Saalbach G, Bayer E, Benitez-Alfonso Y, Maule A: **Arabidopsis plasmodesmal proteome**. *PLoS One* 2011, **6**(4):e18880.

34. Leijon F, Melzer M, Zhou Q, Srivastava V, Bulone VJFips: **Proteomic analysis of plasmodesmata from populus cell suspension cultures in relation with callose biosynthesis**. 2018, **9**:1681.

35. Park SH, Li F, Renaud J, Shen W, Li Y, Guo L, Cui H, Sumarah M, Wang AJTPJ: **NbEXPA1, an α-expansin, is plasmodesmata-specific and a novel host factor for potyviral infection**. 2017, **92**(5):846-861.

36. Simpson C, Thomas C, Findlay K, Bayer E, Maule AJ: **An Arabidopsis GPI-anchor plasmodesmal neck protein with callose binding activity**

**and potential to regulate cell-to-cell trafficking**. *Plant Cell* 2009, **21**(2):581-594.

37. Grison MS, Brocard L, Fouillen L, Nicolas W, Wewer V, Dormann P, Nacir H, Benitez-Alfonso Y, Claverol S, Germain V *et al*: **Specific membrane lipid composition is important for plasmodesmata function in Arabidopsis**. *Plant Cell* 2015, **27**(4):1228-1250.

38. Levy A, Erlanger M, Rosenthal M, Epel BL: **A plasmodesmata-associated beta-1,3-glucanase in Arabidopsis**. *Plant J* 2007, **49**(4):669-682.

39. Zavaliev R, Dong X, Epel BLJPp: **Glycosylphosphatidylinositol (GPI) modification serves as a primary plasmodesmal sorting signal**. 2016, **172**(2):1061-1073.

40. Martín-Hernández AM, Baulcombe DCJJov: **Tobacco rattle virus 16-kilodalton protein encodes a suppressor of RNA silencing that allows transient viral entry in meristems**. 2008, **82**(8):4064-4071.

41. Schwach F, Vaistij FE, Jones L, Baulcombe DCJPp: **An RNA-dependent RNA polymerase prevents meristem invasion by potato virus X and is required for the activity but not the production of a systemic silencing signal**. 2005, **138**(4):1842-1852.

42. Liang D, White RG, Waterhouse PMJP: **Mobile gene silencing in Arabidopsis is regulated by hydrogen peroxide**. 2014, **2**:e701.

43. Heinlein M: **Plasmodesmata: channels for viruses on the move**. *Methods Mol Biol* 2015, **1217**:25-52.

44. Atkins D, Hull R, Wells B, Roberts K, Moore P, Beachy RJJoGV: **The tobacco mosaic virus 30K movement protein in transgenic tobacco plants is localized to plasmodesmata**. 1991, **72**(1):209-211.

45. Citovsky V, Knorr D, Schuster G, Zambryski P: **The P30 movement protein of tobacco mosaic virus is a single-strand nucleic acid binding protein**. *Cell* 1990, **60**(4):637-647.

46. Ban T, Ke J, Chen R, Gu X, Tan MH, Zhou XE, Kang Y, Melcher K, Zhu JK, Xu HE: **Structure of a PLS-class pentatricopeptide repeat protein provides insights into mechanism of RNA recognition**. *J Biol Chem* 2013, **288**(44):31540-31548.

47. Sambade A, Brandner K, Hofmann C, Seemanpillai M, Mutterer J, Heinlein M: **Transport of TMV movement protein particles associated with the targeting of RNA to plasmodesmata**. *Traffic* 2008, **9**(12):2073-2088.

48. Deom CM, Schubert KR, Wolf S, Holt CA, Lucas WJ, Beachy RN: **Molecular characterization and biological function of the movement protein of tobacco mosaic virus in transgenic plants**. *Proc Natl Acad Sci U S A* 1990, **87**(9):3284-3288.

49. Wolf S, Deom CM, Beachy RN, Lucas WJ: **Movement protein of tobacco mosaic virus modifies plasmodesmatal size exclusion limit**. *Science* 1989, **246**(4928):377-379.

50. Boyko V, van der Laak J, Ferralli J, Suslova E, Kwon M-O, Heinlein MJJoV: **Cellular targets of functional and dysfunctional mutants of tobacco mosaic virus movement protein fused to green fluorescent protein**. 2000, **74**(23):11339-11346.

51. Mas P, Beachy RN: **Replication of tobacco mosaic virus on endoplasmic reticulum and role of the cytoskeleton and virus movement protein in intracellular distribution of viral RNA**. *J Cell Biol* 1999, **147**(5):945-958.

52. Beachy RN, Heinlein M: **Role of P30 in replication and spread of TMV**. *Traffic* 2000, **1**(7):540-544.

53. Brill LM, Nunn RS, Kahn TW, Yeager M, Beachy RNJPotNAoS: **Recombinant tobacco mosaic virus movement protein is an RNA-binding, α-helical membrane protein**. 2000, **97**(13):7112-7117.

54. Peiró A, Martínez-Gil L, Tamborero S, Pallás V, Sánchez-Navarro JA, Mingarro IJJov: **The Tobacco mosaic virus movement protein associates with but does not integrate into biological membranes**. 2014, **88**(5):3016-3026.

55. Epel BL: **Plant viruses spread by diffusion on ER-associated movement-protein-rafts through plasmodesmata gated by viral induced host beta-1,3-glucanases**. *Semin Cell Dev Biol* 2009, **20**(9):1074-1081.

56. Hirashima K, Watanabe YJJov: **Tobamovirus replicase coding region is involved in cell-to-cell movement**. 2001, **75**(18):8831-8836.

57. Yuan C, Lazarowitz SG, Citovsky VJM: **The plasmodesmal localization signal of TMV MP is recognized by plant synaptotagmin SYTA**. 2018, **9**(4).

58. Tilsner J, Linnik O, Louveaux M, Roberts IM, Chapman SN, Oparka KJ: **Replication and trafficking of a plant virus are coupled at the entrances of plasmodesmata**. *J Cell Biol* 2013, **201**(7):981-995.

59. Oparka K, Roberts A, Roberts I, Prior D, Santa Cruz SJTPJ: **Viral coat protein is targeted to, but does not gate, plasmodesmata during cell-to-cell movement of potato virus X**. 1996, **10**(5):805-813.

60. Dolja VV, Haldeman-Cahill R, Montgomery AE, Vandenbosch KA, Carrington JCJV: **Capsid protein determinants involved in cell-to-cell**

**and long distance movement of tobacco etch potyvirus**. 1995, **206**(2):1007-1016.

61. Kasschau KD, Carrington JCJV: **Long-distance movement and replication maintenance functions correlate with silencing suppression activity of potyviral HC-Pro**. 2001, **285**(1):71-81.

62. Roberts I, Wang D, Findlay K, Maule AJV: **Ultrastructural and temporal observations of the potyvirus cylindrical inclusions (CIs) show that the CI protein acts transiently in aiding virus movement**. 1998, **245**(1):173-181.

63. Schaad MC, Lellis AD, Carrington JCJJov: **VPg of tobacco etch potyvirus is a host genotype-specific determinant for long-distance movement**. 1997, **71**(11):8624-8631.

64. Wei T, Huang TS, McNeil J, Laliberte JF, Hong J, Nelson RS, Wang A: **Sequential recruitment of the endoplasmic reticulum and chloroplasts for plant potyvirus replication**. *J Virol* 2010, **84**(2):799-809.

65. Grangeon R, Jiang J, Wan J, Agbeci M, Zheng H, Laliberte JF: **6K2-induced vesicles can move cell to cell during turnip mosaic virus infection**. *Frontiers in microbiology* 2013, **4**:351.

66. Carrington JC, Jensen PE, Schaad MCJTPJ: **Genetic evidence for an essential role for potyvirus CI protein in cell-to-cell movement**. 1998, **14**(4):393-400.

67. Vijayapalani P, Maeshima M, Nagasaki-Takekuchi N, Miller WAJPP: **Interaction of the trans-frame potyvirus protein P3N-PIPO with host protein PCaP1 facilitates potyvirus movement**. 2012, **8**(4):e1002639.

68. Lazarowitz SG, Beachy RNJTPC: **Viral movement proteins as probes for intracellular and intercellular trafficking in plants**. 1999, **11**(4):535-548.

69. Kasteel D, Wellink J, Verver J, Van Lent J, Goldbach R, Van Kammen AJJoGV: **The involvement of cowpea mosaic virus M RNA-encoded proteins in tubule formation**. 1993, **74**(8):1721-1724.

70. Liu Y, Jia D, Chen H, Chen Q, Xie L, Wu Z, Wei TJAov: **The P7-1 protein of southern rice black-streaked dwarf virus, a fijivirus, induces the formation of tubular structures in insect cells**. 2011, **156**(10):1729-1736.

71. van Lent J, Storms M, van der Meer F, Wellink J, Goldbach RJJoGV: **Tubular structures involved in movement of cowpea mosaic virus are also formed in infected cowpea protoplasts**. 1991, **72**(11):2615-2623.

72. Xie L, Shang W, Liu C, Zhang Q, Sunter G, Hong J, Zhou XJSr: **Mutual association of Broad bean wilt virus 2 VP37-derived tubules and plasmodesmata obtained from cytological observation**. 2016, **6**(1):1-11.

73. Bird SW, Kirkegaard KJV: **Escape of non-enveloped virus from intact cells**. 2015, **479**:444-449.

74. Lv Y, Zhou S, Gao S, Deng HJP, cell: **Remodeling of host membranes during herpesvirus assembly and egress**. 2019, **10**(5):315-326.

75. Cotton S, Grangeon R, Thivierge K, Mathieu I, Ide C, Wei T, Wang A, Laliberte JF: **Turnip mosaic virus RNA replication complex vesicles are mobile, align with microfilaments, and are each derived from a single viral genome**. *J Virol* 2009, **83**(20):10460-10471.

76. Schmitz J, Stussi-Garaud C, Tacke E, Prüfer D, Rohde W, Rohfritsch OJV: **In SituLocalization of the putative movement protein (pr17) from**

**potato Leafroll Luteovirus (PLRV) in infected and transgenic potato plants**. 1997, **235**(2):311-322.

77. Vogel F, Hofius D, Sonnewald UJT: **Intracellular trafficking of potato leafroll virusmovement protein in transgenic arabidopsis**. 2007, **8**(9):1205-1214.

78. Barker HJJoGV: **Invasion of non-phloem tissue in Nicotiana clevelandii by potato leafroll luteovirus is enhanced in plants also infected with potato Y potyvirus**. 1987, **68**(4):1223-1227.

79. Herbers K, Tacke E, Hazirezaei M, Krause KP, Melzer M, Rohde W, Sonnewald U: **Expression of a luteoviral movement protein in transgenic plants leads to carbohydrate accumulation and reduced photosynthetic capacity in source leaves**. *Plant J* 1997, **12**(5):1045-1056.

80. Sun YD, Folimonova SYJNP: **The p33 protein of Citrus tristeza virus affects viral pathogenicity by modulating a host immune response**. 2019, **221**(4):2039-2053.

81. de Castro IF, Tenorio R, Risco CJCOiV: **Virus assembly factories in a lipid world**. 2016, **18**:20-26.

82. Jin X, Cao X, Wang X, Jiang J, Wan J, Laliberté J-F, Zhang YJFips: **Three-dimensional architecture and biogenesis of membrane structures associated with plant virus replication**. 2018, **9**:57.

83. Nagy PD, Strating JR, van Kuppeveld FJJPp: **Building viral replication organelles: close encounters of the membrane types**. 2016, **12**(10):e1005912.

84. Cosgrove DJJF: **Catalysts of plant cell wall loosening**. 2016, **5**.

85. Welner DH, Shin D, Tomaleri GP, DeGiovanni AM, Tsai AY-L, Tran HM, Hansen SF, Green DT, Scheller HV, Adams PDJPo: **Plant cell wall glycosyltransferases: High-throughput recombinant expression screening and general requirements for these challenging enzymes**. 2017, **12**(6):e0177591.

86. Sagi G, Katz A, Guenoune-Gelbart D, Epel BL: **Class 1 reversibly glycosylated polypeptides are plasmodesmal-associated proteins delivered to plasmodesmata via the golgi apparatus**. *Plant Cell* 2005, **17**(6):1788-1800.

87. Zavaliev R, Sagi G, Gera A, Epel BL: **The constitutive expression of Arabidopsis plasmodesmal-associated class 1 reversibly glycosylated polypeptide impairs plant development and virus spread**. *J Exp Bot* 2010, **61**(1):131-142.

88. Burch-Smith TM, Cui Y, Zambryski PC: **Reduced levels of class 1 reversibly glycosylated polypeptide increase intercellular transport via plasmodesmata**. *Plant Signal Behav* 2012, **7**(1):62-67.

89. Kong D, Karve R, Willet A, Chen MK, Oden J, Shpak ED: **Regulation of plasmodesmatal permeability and stomatal patterning by the glycosyltransferase-like protein KOBITO1**. *Plant Physiol* 2012, **159**(1):156-168.

90. Amsbury S, Kirk P, Benitez-Alfonso YJJoeb: **Emerging models on the regulation of intercellular transport by plasmodesmata-associated callose**. 2018, **69**(1):105-115.

91. De Storme N, Geelen D: **Callose homeostasis at plasmodesmata: molecular regulators and developmental relevance**. *Frontiers in plant science* 2014, **5**:138.

92. Zavaliev R, Ueki S, Citovsky V, Epel BL: **Biology of callose (beta-1,3-glucan) turnover at plasmodesmata**. *Protoplasma* 2011, **248**(1):117-130.

93. Abou-Saleh RH, Hernandez-Gomez MC, Amsbury S, Paniagua C, Bourdon M, Miyashima S, Helariutta Y, Fuller M, Budtova T, Connell SDJNc: **Interactions between callose and cellulose revealed through the analysis of biopolymer mixtures**. 2018, **9**(1):1-13.

94. Fu S, Xu Y, Li C, Li Y, Wu J, Zhou XJMp: **Rice stripe virus interferes with S-acylation of remorin and induces its autophagic degradation to facilitate virus infection**. 2018, **11**(2):269-287.

95. Beffa RS, Hofer RM, Thomas M, Meins F, Jr.: **Decreased Susceptibility to Viral Disease of [beta]-1,3-Glucanase-Deficient Plants Generated by Antisense Transformation**. *Plant Cell* 1996, **8**(6):1001-1011.

96. Iglesias VA, Meins F, Jr.: **Movement of plant viruses is delayed in a beta-1,3-glucanase-deficient mutant showing a reduced plasmodesmatal size exclusion limit and enhanced callose deposition**. *Plant J* 2000, **21**(2):157-166.

97. Zavaliev R, Levy A, Gera A, Epel BL: **Subcellular dynamics and role of Arabidopsis beta-1,3-glucanases in cell-to-cell movement of tobamoviruses**. *Mol Plant Microbe Interact* 2013, **26**(9):1016-1030.

98. Tamai A, Meshi TJMp-mi: **Cell-to-cell movement of Potato virus X: the role of p12 and p8 encoded by the second and third open reading frames of the triple gene block**. 2001, **14**(10):1158-1167.

99. Fridborg I, Grainger J, Page A, Coleman M, Findlay K, Angell S: **TIP, a novel host factor linking callose degradation with the cell-to-cell movement of Potato virus X**. *Mol Plant Microbe Interact* 2003, **16**(2):132-140.

100. Ueki S, Spektor R, Natale DM, Citovsky V: **ANK, a host cytoplasmic receptor for the Tobacco mosaic virus cell-to-cell movement protein, facilitates intercellular transport through plasmodesmata**. *PLoS pathogens* 2010, **6**(11):e1001201.

101. Amari K, Boutant E, Hofmann C, Schmitt-Keichinger C, Fernandez-Calvino L, Didier P, Lerich A, Mutterer J, Thomas CL, Heinlein M *et al*: **A family of plasmodesmal proteins with receptor-like properties for plant viral movement proteins**. *PLoS pathogens* 2010, **6**(9):e1001119.

102. Cui W, Lee J-YJNp: **Arabidopsis callose synthases CalS1/8 regulate plasmodesmal permeability during stress**. 2016, **2**(5):1-9.

103. Lee MW, Jelenska J, Greenberg JTJTPJ: **Arabidopsis proteins important for modulating defense responses to Pseudomonas syringae that secrete HopW1-1**. 2008, **54**(3):452-465.

104. Lee JY, Wang X, Cui W, Sager R, Modla S, Czymmek K, Zybaliov B, van Wijk K, Zhang C, Lu H *et al*: **A plasmodesmata-localized protein mediates crosstalk between cell-to-cell communication and innate immunity in Arabidopsis**. *Plant Cell* 2011, **23**(9):3353-3373.

105. Carella P, Wilson DC, Cameron RKJPs, behavior: **Mind the gap: Signal movement through plasmodesmata is critical for the manifestation of SAR**. 2015, **10**(10):e1075683.

106. Lim GH, Shine MB, de Lorenzo L, Yu K, Cui W, Navarre D, Hunt AG, Lee JY, Kachroo A, Kachroo P: **Plasmodesmata Localizing Proteins Regulate Transport and Signaling during Systemic Acquired Immunity in Plants**. *Cell Host Microbe* 2016, **19**(4):541-549.

107. Lee JY, Taoka K, Yoo BC, Ben-Nissan G, Kim DJ, Lucas WJ: **Plasmodesmal-associated protein kinase in tobacco and Arabidopsis**

**recognizes a subset of non-cell-autonomous proteins**. *Plant Cell* 2005, **17**(10):2817-2831.

108. Citovsky V, McLean BG, Zupan JR, Zambryski P: **Phosphorylation of tobacco mosaic virus cell-to-cell movement protein by a developmentally regulated plant cell wall-associated protein kinase**. *Genes Dev* 1993, **7**(5):904-910.

109. Waigmann E, Chen MH, Bachmaier R, Ghoshroy S, Citovsky V: **Regulation of plasmodesmal transport by phosphorylation of tobacco mosaic virus cell-to-cell movement protein**. *EMBO J* 2000, **19**(18):4875-4884.

110. Trutnyeva K, Bachmaier R, Waigmann EJV: **Mimicking carboxyterminal phosphorylation differentially effects subcellular distribution and cell-to-cell movement of Tobacco mosaic virus movement protein**. 2005, **332**(2):563-577.

111. Baluska F, Samaj J, Napier R, Volkmann D: **Maize calreticulin localizes preferentially to plasmodesmata in root apex**. *Plant J* 1999, **19**(4):481-488.

112. Demchenko KN, Voitsekhovskaja OV, Pawlowski KJFips: **Plasmodesmata without callose and calreticulin in higher plants–open channels for fast symplastic transport?** 2014, **5**:74.

113. Chen M-H, Tian G-W, Gafni Y, Citovsky VJPp: **Effects of calreticulin on viral cell-to-cell movement**. 2005, **138**(4):1866-1876.

114. Chen MH, Sheng J, Hind G, Handa AK, Citovsky V: **Interaction between the tobacco mosaic virus movement protein and host cell pectin methylesterases is required for viral cell-to-cell movement**. *EMBO J* 2000, **19**(5):913-920.

115. Dorokhov YL, Makinen K, Frolova OY, Merits A, Saarinen J, Kalkkinen N, Atabekov JG, Saarma M: **A novel function for a ubiquitous plant enzyme pectin methylesterase: the host-cell receptor for the tobacco mosaic virus movement protein**. *FEBS Lett* 1999, **461**(3):223-228.

116. Chen MH, Citovsky VJTPJ: **Systemic movement of a tobamovirus requires host cell pectin methylesterase**. 2003, **35**(3):386-392.

117. Raffaele S, Bayer E, Lafarge D, Cluzet S, German Retana S, Boubekeur T, Leborgne-Castel N, Carde JP, Lherminier J, Noirot E *et al*: **Remorin, a solanaceae protein resident in membrane rafts and plasmodesmata, impairs potato virus X movement**. *Plant Cell* 2009, **21**(5):1541-1555.

118. Raffaele S, Mongrand S, Gamas P, Niebel A, Ott TJPp: **Genome-wide annotation of remorins, a plant-specific protein family: evolutionary and functional perspectives**. 2007, **145**(3):593-600.

119. Perraki A, Binaghi M, Mecchia MA, Gronnier J, German-Retana S, Mongrand S, Bayer E, Zelada AM, Germain VJFl: **StRemorin1. 3 hampers Potato virus X TGBp1 ability to increase plasmodesmata permeability, but does not interfere with its silencing suppressor activity**. 2014, **588**(9):1699-1705.

120. Reymond P, Kunz B, Paul-Pletzer K, Grimm R, Eckerskorn C, Farmer EEJTPC: **Cloning of a cDNA encoding a plasma membrane-associated, uronide binding phosphoprotein with physical properties similar to viral movement proteins**. 1996, **8**(12):2265-2276.

121. Perraki A, Gronnier J, Gouguet P, Boudsocq M, Deroubaix A-F, Simon V, German-Retana S, Zipfel C, Bayer E, Mongrand SJPp: **REM1. 3's phospho-status defines its plasma membrane nanodomain organization and activity in restricting PVX cell-to-cell movement**. 2018, **14**(11):e1007378.

122. Konrad SS, Popp C, Stratil TF, Jarsch IK, Thallmair V, Folgmann J, Marín M, Ott TJNP: **S-acylation anchors remorin proteins to the plasma membrane but does not primarily determine their localization in membrane microdomains**. 2014, **203**(3):758-769.

123. Gui J, Zheng S, Shen J, Li L: **Grain setting defect1 (GSD1) function in rice depends on S-acylation and interacts with actin 1 (OsACT1) at its C-terminal**. *Frontiers in plant science* 2015, **6**:804.

124. Hemsley PA, Weimar T, Lilley K, Dupree P, Grierson CJPs, behavior: **Palmitoylation in plants: new insights through proteomics**. 2013, **8**(8):e25209.

125. Sasaki N, Takashima E, Nyunoya HJFips: **Altered subcellular localization of a tobacco membrane raft-associated remorin protein by tobamovirus infection and transient expression of viral replication and movement proteins**. 2018, **9**:619.

126. Son S, Oh CJ, An CSJTppj: **Arabidopsis thaliana remorins interact with SnRK1 and play a role in susceptibility to beet curly top virus and beet severe curly top virus**. 2014, **30**(3):269.

127. Lewis JD, Lazarowitz SG: **Arabidopsis synaptotagmin SYTA regulates endocytosis and virus movement protein cell-to-cell transport**. *Proc Natl Acad Sci U S A* 2010, **107**(6):2491-2496.

128. Uchiyama A, Shimada-Beltran H, Levy A, Zheng JY, Javia PA, Lazarowitz SGJFips: **The Arabidopsis synaptotagmin SYTA regulates the cell-to-cell movement of diverse plant viruses**. 2014, **5**:584.

129. Levy A, Zheng JY, Lazarowitz SG: **Synaptotagmin SYTA forms ER-plasma membrane junctions that are recruited to plasmodesmata for plant virus movement**. *Curr Biol* 2015, **25**(15):2018-2025.

130. Yuan C, Lazarowitz SG, Citovsky VJM: **Identification of a functional plasmodesmal localization signal in a plant viral cell-to-cell-movement protein**. 2016, **7**(1).

131. Fernandez JC, Burch-Smith TMJCoipb: **Chloroplasts as mediators of plant biotic interactions over short and long distances**. 2019, **50**:148-155.

132. Lu Y, Yao JJIjoms: **Chloroplasts at the crossroad of photosynthesis, pathogen infection and plant defense**. 2018, **19**(12):3900.

133. Zhao J, Zhang X, Hong Y, Liu YJFiM: **Chloroplast in plant-virus interaction**. 2016, **7**:1565.

134. Bhattacharyya D, Chakraborty SJMPP: **Chloroplast: the Trojan horse in plant–virus interaction**. 2018, **19**(2):504-518.

135. Ni F, Wu L, Wang Q, Hong J, Qi Y, Zhou XJMp: **Turnip yellow mosaic virus P69 interacts with and suppresses glk transcription factors to cause pale-green symptoms in Arabidopsis**. 2017, **10**(5):764-766.

136. Bhat S, Folimonova SY, Cole AB, Ballard KD, Lei Z, Watson BS, Sumner LW, Nelson RS: **Influence of host chloroplast proteins on Tobacco mosaic virus accumulation and intercellular movement**. *Plant Physiol* 2013, **161**(1):134-147.

137. Hanson MR, Hines KMJPp: **Stromules: probing formation and function**. 2018, **176**(1):128-137.

138. Krenz B, Windeisen V, Wege C, Jeske H, Kleinow T: **A plastid-targeted heat shock cognate 70kDa protein interacts with the Abutilon mosaic virus movement protein**. *Virology* 2010, **401**(1):6-17.

139. Krenz B, Jeske H, Kleinow T: **The induction of stromule formation by a plant DNA-virus in epidermal leaf tissues suggests a novel intra- and**

**intercellular macromolecular trafficking route**. *Frontiers in plant science* 2012, **3**:291.

140. Ding X, Jimenez-Gongora T, Krenz B, Lozano-Duran RJMpp: **Chloroplast clustering around the nucleus is a general response to pathogen perception in Nicotiana benthamiana**. 2019, **20**(9):1298-1306.

141. Bobik K, McCray TN, Ernest B, Fernandez JC, Howell KA, Lane T, Staton M, Burch-Smith TMJTPJ: **The chloroplast RNA helicase ISE 2 is required for multiple chloroplast RNA processing steps in Arabidopsis thaliana**. 2017, **91**(1):114-131.

142. Burch-Smith TM, Brunkard JO, Choi YG, Zambryski PC: **Organelle-nucleus cross-talk regulates plant intercellular communication via plasmodesmata**. *Proc Natl Acad Sci U S A* 2011, **108**(51):E1451-1460.

143. Burch-Smith TM, Zambryski PC: **Loss of INCREASED SIZE EXCLUSION LIMIT (ISE)1 or ISE2 increases the formation of secondary plasmodesmata**. *Curr Biol* 2010, **20**(11):989-993.

144. Kobayashi K, Otegui MS, Krishnakumar S, Mindrinos M, Zambryski P: **INCREASED SIZE EXCLUSION LIMIT 2 encodes a putative DEVH box RNA helicase involved in plasmodesmata function during Arabidopsis embryogenesis**. *Plant Cell* 2007, **19**(6):1885-1897.

145. Xu M, Cho E, Burch-Smith TM, Zambryski PC: **Plasmodesmata formation and cell-to-cell transport are reduced in decreased size exclusion limit 1 during embryogenesis in Arabidopsis**. *Proc Natl Acad Sci U S A* 2012, **109**(13):5098-5103.

146. Ganusova EE, Rice JH, Carlew TS, Patel A, Perrodin-Njoku E, Hewezi T, Burch-Smith TMJMP-MI: **Altered expression of a chloroplast protein affects the outcome of virus and nematode infection**. 2017, **30**(6):478-488.

147. Wang X, Sager R, Cui W, Zhang C, Lu H, Lee JY: **Salicylic acid regulates Plasmodesmata closure during innate immune responses in Arabidopsis**. *Plant Cell* 2013, **25**(6):2315-2329.

148. Verchot JJFips: **Cellular chaperones and folding enzymes are vital contributors to membrane bound replication and movement complexes during plant RNA virus infection**. 2012, **3**:275.

149. Avisar D, Prokhnevsky AI, Dolja VVJJov: **Class VIII myosins are required for plasmodesmatal localization of a closterovirus Hsp70 homolog**. 2008, **82**(6):2836-2843.

150. Prokhnevsky AI, Peremyslov VV, Dolja VVJJov: **Actin cytoskeleton is involved in targeting of a viral Hsp70 homolog to the cell periphery**. 2005, **79**(22):14421-14428.

151. Aoki K, Kragler F, Xoconostle-Cázares B, Lucas WJJPotNAoS: **A subclass of plant heat shock cognate 70 chaperones carries a motif that facilitates trafficking through plasmodesmata**. 2002, **99**(25):16342-16347.

152. Meldau S, Baldwin IT, Wu JJNP: **SGT1 regulates wounding-and herbivory-induced jasmonic acid accumulation and Nicotiana attenuata's resistance to the specialist lepidopteran herbivore Manduca sexta**. 2011, **189**(4):1143-1156.

153. Qian X, Xiang Q, Yang T, Ma H, Ding XS, Tao XJV: **Molecular Co-Chaperone SGT1 Is Critical for Cell-to-Cell Movement and Systemic Infection of Tomato Spotted Wilt Virus in Nicotiana benthamiana**. 2018, **10**(11):647.

154. Das PP, Macharia MW, Lin Q, Wong S-MJJop: **In planta proximity-dependent biotin identification (BioID) identifies a TMV replication**

**co-chaperone NbSGT1 in the vicinity of 126 kDa replicase**. 2019, **204**:103402.

155. Liu Y, Schiff M, Dinesh-Kumar SP: **Virus-induced gene silencing in tomato**. *Plant J* 2002, **31**(6):777-786.

156. Xu XM, Wang J, Xuan Z, Goldshmidt A, Borrill PG, Hariharan N, Kim JY, Jackson DJS: **Chaperonins facilitate KNOTTED1 cell-to-cell trafficking and stem cell function**. 2011, **333**(6046):1141-1144.

157. Fichtenbauer D, Xu XM, Jackson D, Kragler FJPs, behavior: **The chaperonin CCT8 facilitates spread of tobamovirus infection**. 2012, **7**(3):318-321.

158. Harries PA, Schoelz JE, Nelson RSJMp-mi: **Intracellular transport of viruses and their components: utilizing the cytoskeleton and membrane highways**. 2010, **23**(11):1381-1393.

159. Heinlein M: **Viral transport and interaction with the host cytoskeleton**. In: *Plant-Virus Interactions.* Springer; 2016: 39-66.

160. Blackman LM, Overall RL: **Immunolocalisation of the cytoskeleton to plasmodesmata of Chara corallina**. *Plant J* 1998, **14**(6):733-741.

161. Boyko V, Hu Q, Seemanpillai M, Ashby J, Heinlein MJTPJ: **Validation of microtubule-associated Tobacco mosaic virus RNA movement and involvement of microtubule-aligned particle trafficking**. 2007, **51**(4):589-603.

162. Seemanpillai M, Elamawi R, Ritzenthaler C, Heinlein MJJov: **Challenging the role of microtubules in Tobacco mosaic virus movement by drug treatments is disputable**. 2006, **80**(13):6712-6715.

163. Wright KM, Wood NT, Roberts AG, Chapman S, Boevink P, MacKenzie KM, Oparka KJJT: **Targeting of TMV movement protein to**

**plasmodesmata requires the actin/ER network; evidence from FRAP**. 2007, **8**(1):21-31.

164. Harries PA, Park J-W, Sasaki N, Ballard KD, Maule AJ, Nelson RSJPotNAoS: **Differing requirements for actin and myosin by plant viruses for sustained intercellular movement**. 2009, **106**(41):17594-17599.

165. Gillespie T, Boevink P, Haupt S, Roberts AG, Toth R, Valentine T, Chapman S, Oparka KJJTPC: **Functional analysis of a DNA-shuffled movement protein reveals that microtubules are dispensable for the cell-to-cell movement of Tobacco mosaic virus**. 2002, **14**(6):1207-1222.

166. Ashby J, Boutant E, Seemanpillai M, Sambade A, Ritzenthaler C, Heinlein MJJov: **Tobacco mosaic virus movement protein functions as a structural microtubule-associated protein**. 2006, **80**(17):8329-8344.

167. Ouko MO, Sambade A, Brandner K, Niehl A, Peña E, Ahad A, Heinlein M, Nick PJTPJ: **Tobacco mutants with reduced microtubule dynamics are less susceptible to TMV**. 2010, **62**(5):829-839.

168. Agbeci M, Grangeon R, Nelson RS, Zheng H, Laliberté J-FJPP: **Contribution of host intracellular transport machineries to intercellular movement of turnip mosaic virus**. 2013, **9**(10):e1003683.

169. Mitra R, Krishnamurthy K, Blancaflor E, Payton M, Nelson RS, Verchot-Lubicz JJV: **The Potato virus X TGBp2 protein association with the endoplasmic reticulum plays a role in but is not sufficient for viral cell-to-cell movement**. 2003, **312**(1):35-48.

170. Tilsner J, Linnik O, Wright KM, Bell K, Roberts AG, Lacomme C, Santa Cruz S, Oparka KJJPp: **The TGB1 movement protein of Potato virus X**

**reorganizes actin and endomembranes into the X-body, a viral replication factory**. 2012, **158**(3):1359-1370.

171. Pouwels J, van der Velden T, Willemse J, Borst J, van Lent J, Bisseling T, Wellink JJJogv: **Studies on the origin and structure of tubules made by the movement protein of Cowpea mosaic virus**. 2004, **85**(12):3787-3796.

172. Bertens P, Wellink J, Goldbach R, van Kammen AJV: **Mutational analysis of the cowpea mosaic virus movement protein**. 2000, **267**(2):199-208.

173. Bertens P, Heijne W, Van der Wel N, Wellink J, Van Kammen AJAov: **Studies on the C-terminus of the Cowpea mosaic virus movement protein**. 2003, **148**(2):265-279.

174. Laporte C, Vetter G, Loudes A-M, Robinson DG, Hillmer S, Stussi-Garaud C, Ritzenthaler CJTPC: **Involvement of the secretory pathway and the cytoskeleton in intracellular targeting and tubule assembly of Grapevine fanleaf virus movement protein in tobacco BY-2 cells**. 2003, **15**(9):2058-2075.

175. Gallagher KL, Benfey PNJTPJ: **Both the conserved GRAS domain and nuclear localization are required for SHORT-ROOT movement**. 2009, **57**(5):785-797.

176. Koizumi K, Gallagher KL: **Identification of SHRUBBY, a SHORT-ROOT and SCARECROW interacting protein that controls root growth and radial patterning**. *Development* 2013, **140**(6):1292-1300.

177. Spiegelman Z, Wu S, Gallagher KLJP: **A role for the endoplasmic reticulum in the cell-to-cell movement of SHORT-ROOT**. 2019, **256**(5):1455-1459.

178. Wu S, Gallagher KL: **Intact microtubules are required for the intercellular movement of the SHORT-ROOT transcription factor**. *Plant J* 2013, **74**(1):148-159.

179. Wu S, Gallagher KLJTPJ: **The movement of the non-cell-autonomous transcription factor, SHORT-ROOT relies on the endomembrane system**. 2014, **80**(3):396-409.

180. Aaziz R, Dinant S, Epel BL: **Plasmodesmata and plant cytoskeleton**. *Trends Plant Sci* 2001, **6**(7):326-330.

181. Roberts AG, Oparka KJ: **Plasmodesmata and the control of symplastic transport**. *Plant Cell Environ* 2003, **26**(1):103-124.

182. White RG, Badelt K, Overall RL, Vesk M: **Actin associated with plasmodesmata**. *Protoplasma* 1994, **180**(3-4):169-184.

183. Ehlers K, Kollmann R: **Primary and secondary plasmodesmata: structure, origin, and functioning**. *Protoplasma* 2001, **216**(1-2):1-30.

184. Ding B, Kwon MO, Warnberg L: **Evidence that actin filaments are involved in controlling the permeability of plasmodesmata in tobacco mesophyll.** *Plant J* 1996, **10**:157-164.

185. Radford JE, White RGJP: **Inhibitors of myosin, but not actin, alter transport through Tradescantia plasmodesmata**. 2011, **248**(1):205-216.

186. Albrecht V, Simkova K, Carrie C, Delannoy E, Giraud E, Whelan J, Small ID, Apel K, Badger MR, Pogson BJ: **The cytoskeleton and the peroxisomal-targeted snowy cotyledon3 protein are required for chloroplast development in Arabidopsis**. *Plant Cell* 2010, **22**(10):3423-3438.

187. Kronberg K, Vogel F, Rutten T, Hajirezaei M-R, Sonnewald U, Hofius DJPp: **The silver lining of a viral agent: increasing seed yield and harvest index in Arabidopsis by ectopic expression of the potato leaf roll virus movement protein**. 2007, **145**(3):905-918.

188. Yan D, Yadav SR, Paterlini A, Nicolas WJ, Petit JD, Brocard L, Belevich I, Grison MS, Vaten A, Karami LJNp: **Sphingolipid biosynthesis modulates plasmodesmal ultrastructure and phloem unloading**. 2019, **5**(6):604-615.

189. Ross-Elliott TJ, Jensen KH, Haaning KS, Wager BM, Knoblauch J, Howell AH, Mullendore DL, Monteith AG, Paultre D, Yan DJE: **Phloem unloading in Arabidopsis roots is convective and regulated by the phloem-pole pericycle**. 2017, **6**:e24125.

190. Kraner ME, Link K, Melzer M, Ekici AB, Uebe S, Tarazona P, Feussner I, Hofmann J, Sonnewald UJTpj: **Choline transporter-like1 (CHER 1) is crucial for plasmodesmata maturation in Arabidopsis thaliana**. 2017, **89**(2):394-406.

191. Deom CM, Oliver MJ, Beachy RNJS: **The 30-kilodalton gene product of tobacco mosaic virus potentiates virus movement**. 1987, **237**(4813):389-394.

192. Fujiwara T, Giesman-Cookmeyer D, Ding B, Lommel SA, Lucas WJ: **Cell-to-Cell Trafficking of Macromolecules through Plasmodesmata Potentiated by the Red Clover Necrotic Mosaic Virus Movement Protein**. *Plant Cell* 1993, **5**(12):1783-1794.

193. Oparka KJ, Prior DA, Santa Cruz S, Padgett HS, Beachy RN: **Gating of epidermal plasmodesmata is restricted to the leading edge of expanding infection sites of tobacco mosaic virus (TMV)**. *Plant J* 1997, **12**(4):781-789.

194. Adkar-Purushothama CR, Brosseau C, Giguère T, Sano T, Moffett P, Perreault J-PJTPC: **Small RNA derived from the virulence modulating region of the potato spindle tuber viroid silences callose synthase genes of tomato plants**. 2015, **27**(8):2178-2194.

195. Bayer EM, Mongrand S, Tilsner JJFips: **Specialized membrane domains of plasmodesmata, plant intercellular nanopores**. 2014, **5**:507.

196. Tilsner J, Nicolas W, Rosado A, Bayer EMJAropb: **Staying tight: plasmodesmal membrane contact sites and the control of cell-to-cell connectivity in plants**. 2016, **67**.

197. Kasteel D, Van der Wel N, Jansen K, Goldbach R, Van Lent JJJoGV: **Tubule-forming capacity of the movement proteins of alfalfa mosaic virus and brome mosaic virus**. 1997, **78**(8):2089-2093.

198. Lewandowski DJ, Adkins SJV: **The tubule-forming NSm protein from Tomato spotted wilt virus complements cell-to-cell and long-distance movement of Tobacco mosaic virus hybrids**. 2005, **342**(1):26-37.

199. STORMS MM, KORMELINK R, PETERS D, Van Lent JW, GOLDBACH RWJV: **The nonstructural NSm protein of tomato spotted wilt virus induces tubular structures in plant and insect cells**. 1995, **214**(2):485-493.

200. Poirson A, Turner AP, Giovane C, Berna A, Roberts K, Godefroy-Colburn T: **Effect of the alfalfa mosaic virus movement protein expressed in transgenic plants on the permeability of plasmodesmata**. *J Gen Virol* 1993, **74 ( Pt 11)**:2459-2461.

201. Murant A, Roberts I, Goold RJJoGV: **Cytopathological changes and extractable infectivity in Nicotiana clevelandii leaves infected with carrot mottle virus**. 1973, **21**(2):269-283.

202. Derrick PM, Barker H, Oparka KJ: **Effect of virus infection on symplastic transport of fluorescent tracers in Nicotiana clevelandii leaf epidermis**. *Planta* 1990, **181**(4):555-559.

203. Otegui MS, Mastronarde DN, Kang BH, Bednarek SY, Staehelin LA: **Three-dimensional analysis of syncytial-type cell plates during endosperm cellularization visualized by high resolution electron tomography**. *Plant Cell* 2001, **13**(9):2033-2051.

204. Staehelin LA, Kang BH: **Nanoscale architecture of endoplasmic reticulum export sites and of Golgi membranes as determined by electron tomography**. *Plant Physiol* 2008, **147**(4):1454-1468.

205. Terauchi M, Nagasato C, Kajimura N, Mineyuki Y, Okuda K, Katsaros C, Motomura T: **Ultrastructural study of plasmodesmata in the brown alga Dictyota dichotoma (Dictyotales, Phaeophyceae)**. *Planta* 2012, **236**(4):1013-1026.

206. Sousa AA, Azari AA, Zhang G, Leapman RD: **Dual-axis electron tomography of biological specimens: Extending the limits of specimen thickness with bright-field STEM imaging**. *Journal of structural biology* 2011, **174**(1):107-114.

207. Okamoto N, Keeling PJ: **The 3D structure of the apical complex and association with the flagellar apparatus revealed by serial TEM tomography in Psammosa pacifica, a distant relative of the Apicomplexa**. *PLoS One* 2014, **9**(1):e84653.

208. Bammes BE, Rochat RH, Jakana J, Chen DH, Chiu W: **Direct electron detection yields cryo-EM reconstructions at resolutions beyond 3/4 Nyquist frequency**. *Journal of structural biology* 2012, **177**(3):589-601.

209. Iacovache I, De Carlo S, Cirauqui N, Dal Peraro M, van der Goot FG, Zuber B: **Cryo-EM structure of aerolysin variants reveals a novel**

**protein fold and the pore-formation process**. *Nature communications* 2016, **7**:12062.

210. Kremer A, Lippens S, Bartunkova S, Asselbergh B, Blanpain C, Fendrych M, Goossens A, Holt M, Janssens S, Krols M *et al*: **Developing 3D SEM in a broad biological context**. *J Microsc* 2015, **259**(2):80-96.

211. Kittelmann M, Hawes C, Hughes L: **Serial block face scanning electron microscopy and the reconstruction of plant cell membrane systems**. *J Microsc* 2016, **263**(2):200-211.

212. Young RJ, Dingle T, Robinson K, Pugh PJA: **An application of scanned focused ion beam milling to studies on the internal morphology of small arthropods.** *J Microsc-Oxford* 1993, **172**(1):81-88.

213. Drobne D, Milani M, Zrimec A, Zrimec MB, Tatti F, Draslar K: **Focused ion beam/scanning electron microscopy studies of Porcellio scaber (Isopoda, Crustacea) digestive gland epithelium cells**. *Scanning* 2005, **27**(1):30-34.

214. Kopek BG, Shtengel G, Xu CS, Clayton DA, Hess HF: **Correlative 3D superresolution fluorescence and electron microscopy reveal the relationship of mitochondrial nucleoids to membranes**. *Proc Natl Acad Sci U S A* 2012, **109**(16):6136-6141.

215. Cretoiu D, Gherghiceanu M, Hummel E, Zimmermann H, Simionescu O, Popescu LM: **FIB-SEM tomography of human skin telocytes and their extracellular vesicles**. *Journal of cellular and molecular medicine* 2015, **19**(4):714-722.

216. Schmidt F, Kuhbacher M, Gross U, Kyriakopoulos A, Schubert H, Zehbe R: **From 2D slices to 3D volumes: image based reconstruction and morphological characterization of hippocampal cells on charged and**

**uncharged surfaces using FIB/SEM serial sectioning**. *Ultramicroscopy* 2011, **111**(4):259-266.

217. Park SJ, Schertel A, Lee KE, Han SS: **Ultra-structural analysis of the brain in a Drosophila model of Alzheimer's disease using FIB/SEM microscopy**. *Microscopy* 2014, **63**(1):3-13.

218. Wanner G, Schafer T, Lutz-Meindl U: **3-D analysis of dictyosomes and multivesicular bodies in the green alga Micrasterias denticulata by FIB/SEM tomography**. *Journal of structural biology* 2013, **184**(2):203-211.

219. Lutz-Meindl U, Luckner M, Andosch A, Wanner G: **Structural stress responses and degradation of dictyosomes in algae analysed by TEM and FIB-SEM tomography**. *J Microsc* 2016, **263**(2):129-141.

220. Crumpton-Taylor M, Grandison S, Png KM, Bushby AJ, Smith AM: **Control of starch granule numbers in Arabidopsis chloroplasts**. *Plant Physiol* 2012, **158**(2):905-916.

221. House A, Balkwill K: **FIB-SEM: an additional technique for investigating internal structure of pollen walls**. *Microscopy and microanalysis : the official journal of Microscopy Society of America, Microbeam Analysis Society, Microscopical Society of Canada* 2013, **19**(6):1535-1541.

222. House A, Balkwill K: **Labyrinths, columns and cavities: new internal features of pollen grain walls in the Acanthaceae detected by FIB-SEM**. *Journal of plant research* 2016, **129**(2):225-240.

223. Bhawana, Miller JL, Cahoon AB: **3D Plant cell architecture of Arabidopsis thaliana (Brassicaceae) using focused ion beam-scanning electron microscopy**. *Applications in plant sciences* 2014, **2**(6).

224. Mersey B, Mccully ME: **Monitoring the course od fixation of plant cells.** *J Microsc-Oxford* 1978, **114**(1):49-76.

225. Dahl R, Staehelin LA: **High-pressure freezing for the preservation of biological structure: theory and practice**. *Journal of electron microscopy technique* 1989, **13**(3):165-174.

226. McDonald K: **High-pressure freezing for preservation of high resolution fine structure and antigenicity for immunolabeling**. *Methods Mol Biol* 1999, **117**:77-97.

227. Wei D, Jacobs S, Modla S, Zhang S, Young CL, Cirino R, Caplan J, Czymmek K: **High-resolution three-dimensional reconstruction of a whole yeast cell using focused-ion beam scanning electron microscopy**. *BioTechniques* 2012, **53**(1):41-48.

228. Villinger C, Gregorius H, Kranz C, Hohn K, Munzberg C, von Wichert G, Mizaikoff B, Wanner G, Walther P: **FIB/SEM tomography with TEM-like resolution for 3D imaging of high-pressure frozen cells**. *Histochemistry and cell biology* 2012, **138**(4):549-556.

229. Schertel A, Snaidero N, Han HM, Ruhwedel T, Laue M, Grabenbauer M, Mobius W: **Cryo FIB-SEM: volume imaging of cellular ultrastructure in native frozen specimens**. *Journal of structural biology* 2013, **184**(2):355-360.

230. McDonald KL, Webb RI: **Freeze substitution in 3 hours or less**. *J Microsc-Oxford* 2011, **243**(3):227-233.

231. Bobik K, Dunlap JR, Burch-Smith TM: **Tandem high-pressure freezing and quick freeze substitution of plant tissues for transmission electron microscopy**. *J Vis Exp* 2014(92):e51844.

232. Overall R, Wolfe J, Gunning BJP: **Intercellular communication inAzolla roots: I. Ultrastructure of plasmodesmata**. 1982, **111**(2):134-150.

233. Hayles M, Stokes D, Phifer D, Findlay KJJom: **A technique for improved focused ion beam milling of cryo-prepared life science specimens**. 2007, **226**(3):263-269.

234. Cran DG, Dyer AF: **Membrane continuity ans associations in the fern, Dryopteris borreri.** *Protoplasma* 1973, **76**:103-108.

235. Crotty WJ, Ledbetter MC: **Membrane continuities involving chloroplasts and other organelles in plant cells**. *Science* 1973, **182**(4114):839-841.

236. Melo RC, Morgan E, Monahan-Earley R, Dvorak AM, Weller PF: **Pre-embedding immunogold labeling to optimize protein localization at subcellular compartments and membrane microdomains of leukocytes**. *Nat Protoc* 2014, **9**(10):2382-2394.

237. Vaughn KC, Campbell WHJPp: **Immunogold localization of nitrate reductase in maize leaves**. 1988, **88**(4):1354-1357.

238. Milne R, Ramasso E, Lenzi R, Masenga V, Sarindu N, Clark MJEJoPP: **Pre-and post-embedding immunogold labeling and electron microscopy in plant host tissues of three antigenically unrelated MLOs: primula yellows, tomato big bud and bermudagrass white leaf**. 1995, **101**(1):57-67.

239. McLean B, Whatley JM, Juniper BE: **Continuity of chloroplast and endoplasmic reticulum membranes in *Chara* and *Equisetum.*** 1988, **New Phytologist**(109):59-65.

240. Mehrshahi P, Johnny C, DellaPenna D: **Redefining the metabolic continuity of chloroplasts and ER**. *Trends Plant Sci* 2014, **19**(8):501-507.

241. Mehrshahi P, Stefano G, Andaloro JM, Brandizzi F, Froehlich JE, DellaPenna D: **Transorganellar complementation redefines the**

**biochemical continuity of endoplasmic reticulum and chloroplasts**. *Proc Natl Acad Sci U S A* 2013, **110**(29):12126-12131.

242. Burch-Smith TM, Zambryski PC: **Plasmodesmata paradigm shift: regulation from without versus within**. *Annu Rev Plant Biol* 2012, **63**:239-260.

243. Bapaume L, Reinhardt D: **How membranes shape plant symbioses: signaling and transport in nodulation and arbuscular mycorrhiza**. *Frontiers in plant science* 2012, **3**:223.

244. Studer D, Hennecke H, Muller M: **High-pressure freezing of soybean nodules leads to an improved preservation of ultrastructure**. *Planta* 1992, **188**(2):155-163.

245. Vance CP: **Rhizobium infection and nodulation: a beneficial plant disease?** *Annu Rev Microbiol* 1983, **37**:399-424.

246. Udvardi MK, Day DA: **Metabolite Transport across Symbiotic Membranes of Legume Nodules**. *Annu Rev Plant Physiol Plant Mol Biol* 1997, **48**:493-523.

247. Bergersen FJ: **Regulation of nitrogen fixation in infected cells of leguminous root nodules in relation to O2 supply.** *Plant and Soil* 1997, **191**(2):189-203.

248. Selker JM, Newcomb EH: **Spatial relationships between uninfected and infected cells in root nodules of soybean**. *Planta* 1985, **165**(4):446-454.

249. Newcomb EH, Tandon SR: **Uninfected cells of soybean root nodules: ultrastructure suggests key role in ureide production**. *Science* 1981, **212**(4501):1394-1396.

250. Hanks JF, Schubert K, Tolbert NE: **Isolation and characterization of infected and uninfected cells from soybean nodules : role of uninfected cells in ureide synthesis**. *Plant Physiol* 1983, **71**(4):869-873.

251. Schneider CA, Rasband WS, Eliceiri KW: **NIH Image to ImageJ: 25 years of image analysis**. *Nature methods* 2012, **9**(7):671-675.

252. Crawford KM, Zambryski PC: **Non-targeted and targeted protein movement through plasmodesmata in leaves in different developmental and physiological states**. *Plant Physiol* 2001, **125**(4):1802-1812.

253. Schönknecht G, Brown J, Verchot-Lubicz JJP: **Plasmodesmata transport of GFP alone or fused to potato virus X TGBp1 is diffusion driven**. 2008, **232**(3-4):143.

254. Brunkard JO, Burch-Smith TM, Runkel AM, Zambryski P: **Investigating plasmodesmata genetics with virus-induced gene silencing and an agrobacterium-mediated GFP movement assay**. In: *Plasmodesmata.* Springer; 2015: 185-198.

255. Roberts IM, Boevink P, Roberts AG, Sauer N, Reichel C, Oparka KJ: **Dynamic changes in the frequency and architecture of plasmodesmata during the sink-source transition in tobacco leaves**. *Protoplasma* 2001, **218**(1-2):31-44.

256. Seagull RWJP: **Differences in the frequency and disposition of plasmodesmata resulting from root cell elongation**. 1983, **159**(6):497-504.

257. Danila FR, Quick WP, White RG, Furbank RT, von Caemmerer SJTPC: **The metabolite pathway between bundle sheath and mesophyll: quantification of plasmodesmata in leaves of C3 and C4 monocots**. 2016, **28**(6):1461-1471.

258. Baron C, Zambryski PC: **The plant response in pathogenesis, symbiosis, and wounding: variations on a common theme?** *Annu Rev Genet* 1995, **29**:107-129.

259. Dmitrieva VA, Ivanova AN, Tyutereva EV, Evkaikina AI, Klimova EA, Voitsekhovskaja OVJPs, behavior: **Chlorophyllide-a-Oxygenase (CAO) deficiency affects the levels of singlet oxygen and formation of plasmodesmata in leaves and shoot apical meristems of barley**. 2017, **12**(4):e1300732.

260. Ganusova E, Reagan, BC, Fernandez, JC, Azim, M, Sankoh, A, Freeman, K, McCray, T, Patterson, K, Kim, C, Burch-Smith, TM.: **Chloroplast-to-nucleus retrograde signalling controls intercellular trafficking via plasmodesmata formation**. *Philosophical Transactions of the Royal Society B: Biological Sciences* 2020.

261. Livingston LJAJoB: **The nature and distribution of plasmodesmata in the tobacco plant**. 1935:75-87.

262. Juniper BE, Barlow PWJP: **The distribution of plasmodesmata in the root tip of maize**. 1969, **89**(4):352-360.

263. Evert R, Eschrich W, Heyser WJP: **Distribution and structure of the plasmodesmata in mesophyll and bundle-sheath cells of Zea mays L**. 1977, **136**(1):77-89.

264. Tilney LG, Cooke TJ, Connelly PS, Tilney MSJD: **The distribution of plasmodesmata and its relationship to morphogenesis in fern gametophytes**. 1990, **110**(4):1209-1221.

265. Fitzgibbon J: **Structure and development of complex plasmodesmata**. 2012.

266. Reagan BC, Kim PJ-Y, Perry PD, Dunlap JR, Burch-Smith TMJFPB: **Spatial distribution of organelles in leaf cells and soybean root**

**nodules revealed by focused ion beam-scanning electron microscopy**. 2018, **45**(2):180-191.

267. Denk W, Horstmann HJPB: **Serial block-face scanning electron microscopy to reconstruct three-dimensional tissue nanostructure**. 2004, **2**(11):e329.

268. Deerinck T, Bushong E, Lev-Ram V, Shu X, Tsien R, Ellisman MJM, Microanalysis: **Enhancing serial block-face scanning electron microscopy to enable high resolution 3-D nanohistology of cells and tissues**. 2010, **16**(S2):1138-1139.

269. Hughes L, Hawes C, Monteith S, Vaughan SJP: **Serial block face scanning electron microscopy—the future of cell ultrastructure imaging**. 2014, **251**(2):395-401.

270. Paterlini A, Belevich I, Jokitalo E, Helariutta YJPP: **Computational tools for serial block electron microscopy reveal plasmodesmata distributions and wall environments**. 2020, **184**(1):53-64.

271. Milani M, Drobne D, Tatti FJMR, Microscopy ETi: **How to study biological samples by FIB/SEM**. 2007:787-794.

272. Drobne D: **3D imaging of cells and tissues by focused ion beam/scanning electron microscopy (FIB/SEM)**. In: *Nanoimaging.* Springer; 2013: 275-292.

273. McDonald KL: **Out with the old and in with the new: rapid specimen preparation procedures for electron microscopy of sectioned biological material**. *Protoplasma* 2014, **251**(2):429-448.

274. Lucas WJ, Lee JY: **Plasmodesmata as a supracellular control network in plants**. *Nat Rev Mol Cell Biol* 2004, **5**(9):712-726.

275. Patrick JW: **Does Don Fisher's high-pressure manifold model account for phloem transport and resource partitioning?** *Frontiers in plant science* 2013, **4**:184.

276. Pogson BJ, Woo NS, Forster B, Small ID: **Plastid signalling to the nucleus and beyond**. *Trends Plant Sci* 2008, **13**(11):602-609.

277. Chan KX, Phua SY, Crisp P, McQuinn R, Pogson BJJAropb: **Learning the languages of the chloroplast: retrograde signaling and beyond**. 2016, **67**:25-53.

278. Bobik K, Burch-Smith TM: **Chloroplast signaling within, between and beyond cells**. *Frontiers in plant science* 2015, **6**:781.

279. Gollan PJ, Tikkanen M, Aro E-MJCoipb: **Photosynthetic light reactions: integral to chloroplast retrograde signalling**. 2015, **27**:180-191.

280. Kleine T, Leister DJBEBA-B: **Retrograde signaling: organelles go networking**. 2016, **1857**(8):1313-1325.

281. Brunkard JO, Burch-Smith TMJEib: **Ties that bind: the integration of plastid signalling pathways in plant cell metabolism**. 2018, **62**(1):95.

282. Glasser C, Haberer G, Finkemeier I, Pfannschmidt T, Kleine T, Leister D, Dietz KJ, Hausler RE, Grimm B, Mayer KF: **Meta-analysis of retrograde signaling in Arabidopsis thaliana reveals a core module of genes embedded in complex cellular signaling networks**. *Mol Plant* 2014, **7**(7):1167-1190.

283. Surpin M, Larkin RM, Chory J: **Signal transduction between the chloroplast and the nucleus**. *Plant Cell* 2002, **14 Suppl**:S327-338.

284. Larkin RMJFips: **Tetrapyrrole signaling in plants**. 2016, **7**:1586.

285. Larkin RM, Alonso JM, Ecker JR, Chory J: **GUN4, a regulator of chlorophyll synthesis and intracellular signaling**. *Science* 2003, **299**(5608):902-906.

286. Adhikari ND, Froehlich JE, Strand DD, Buck SM, Kramer DM, Larkin RMJTPC: **GUN4-porphyrin complexes bind the ChlH/GUN5 subunit of Mg-Chelatase and promote chlorophyll biosynthesis in Arabidopsis**. 2011, **23**(4):1449-1467.

287. Voigt C, Oster U, Börnke F, Jahns P, Dietz KJ, Leister D, Kleine TJPP: **In-depth analysis of the distinctive effects of norflurazon implies that tetrapyrrole biosynthesis, organellar gene expression and ABA cooperate in the GUN-type of plastid signalling**. 2010, **138**(4):503-519.

288. Kobayashi K, Masuda TJFips: **Transcriptional regulation of tetrapyrrole biosynthesis in Arabidopsis thaliana**. 2016, **7**:1811.

289. Carlotto N, Wirth S, Furman N, Ferreyra Solari N, Ariel F, Crespi M, Kobayashi KJP, cell, environment: **The chloroplastic DEVH-box RNA helicase INCREASED SIZE EXCLUSION LIMIT 2 involved in plasmodesmata regulation is required for group II intron splicing**. 2016, **39**(1):165-173.

290. Bryant N, Lloyd J, Sweeney C, Myouga F, Meinke D: **Identification of nuclear genes encoding chloroplast-localized proteins required for embryo development in Arabidopsis**. *Plant Physiol* 2011, **155**(4):1678-1689.

291. Kim I, Hempel FD, Sha K, Pfluger J, Zambryski PC: **Identification of a developmental transition in plasmodesmatal function during embryogenesis in Arabidopsis thaliana**. *Development* 2002, **129**(5):1261-1272.

292. Bobik K, Fernandez JC, Hardin SR, Ernest B, Ganusova EE, Staton ME, Burch-Smith TMJNP: **The essential chloroplast ribosomal protein uL 15c interacts with the chloroplast RNA helicase ISE 2 and affects intercellular trafficking through plasmodesmata**. 2019, **221**(2):850-865.

293. Burch-Smith TM, Anderson JC, Martin GB, Dinesh-Kumar SP: **Applications and advantages of virus-induced gene silencing for gene function studies in plants**. *Plant J* 2004, **39**(5):734-746.

294. Chi W, He B, Mao J, Li Q, Ma J, Ji D, Zou M, Zhang L: **The function of RH22, a DEAD RNA helicase, in the biogenesis of the 50S ribosomal subunits of Arabidopsis chloroplasts**. *Plant Physiol* 2012, **158**(2):693-707.

295. Nishimura K, Ashida H, Ogawa T, Yokota A: **A DEAD box protein is required for formation of a hidden break in Arabidopsis chloroplast 23S rRNA**. *Plant J* 2010, **63**(5):766-777.

296. Asakura Y, Galarneau E, Watkins KP, Barkan A, van Wijk KJ: **Chloroplast RH3 DEAD Box RNA Helicases in Maize and Arabidopsis Function in Splicing of Specific Group II Introns and Affect Chloroplast Ribosome Biogenesis**. *Plant Physiol* 2012, **159**(3):961-974.

297. Hammani K, Takenaka M, Miranda R, Barkan A: **A PPR protein in the PLS subfamily stabilizes the 5'-end of processed rpl16 mRNAs in maize chloroplasts**. *Nucleic acids research* 2016, **44**(9):4278-4288.

298. Sharwood RE, Halpert M, Luro S, Schuster G, Stern DBJR: **Chloroplast RNase J compensates for inefficient transcription termination by removal of antisense RNA**. 2011, **17**(12):2165-2176.

299. Germain A, Herlich S, Larom S, Kim SH, Schuster G, Stern DBJTPJ: **Mutational analysis of Arabidopsis chloroplast polynucleotide**

**phosphorylase reveals roles for both RNase PH core domains in polyadenylation, RNA 3′-end maturation and intron degradation**. 2011, **67**(3):381-394.

300. Fitzgibbon J, Beck M, Zhou J, Faulkner C, Robatzek S, Oparka K: **A developmental framework for complex plasmodesmata formation revealed by large-scale imaging of the Arabidopsis leaf epidermis**. *Plant Cell* 2013, **25**(1):57-70.

301. Benitez-Alfonso Y, Cilia M, San Roman A, Thomas C, Maule A, Hearn S, Jackson D: **Control of Arabidopsis meristem development by thioredoxin-dependent regulation of intercellular transport**. *Proc Natl Acad Sci U S A* 2009, **106**(9):3615-3620.

302. Walter M, Kilian J, Kudla JJTEj: **PNPase activity determines the efficiency of mRNA 3′-end processing, the degradation of tRNA and the extent of polyadenylation in chloroplasts**. 2002, **21**(24):6905-6914.

303. Cushing DA, Forsthoefel NR, Gestaut DR, Vernon DM: **Arabidopsis emb175 and other ppr knockout mutants reveal essential roles for pentatricopeptide repeat (PPR) proteins in plant embryogenesis**. *Planta* 2005, **221**(3):424-436.

304. Chen H, Zou W, Zhao JJJoeb: **Ribonuclease J is required for chloroplast and embryo development in Arabidopsis**. 2015, **66**(7):2079-2091.

305. Rutschow HL, Baskin TI, Kramer EM: **Regulation of solute flux through plasmodesmata in the root meristem**. *Plant Physiol* 2011

**155**(4):1817-1826.

306. Liu Y, Schiff M, Dinesh-Kumar SJTPJ: **Virus-induced gene silencing in tomato**. 2002, **31**(6):777-786.

307. Liu Y, Nakayama N, Schiff M, Litt A, Irish VF, Dinesh-Kumar SP: **Virus induced gene silencing of a DEFICIENS ortholog in Nicotiana benthamiana**. *Plant Mol Biol* 2004, **54**(5):701-711.

308. Lichtenthaler HKJMie: **[34] Chlorophylls and carotenoids: pigments of photosynthetic biomembranes**. 1987, **148**:350-382.

309. Schindelin J, Arganda-Carreras I, Frise E, Kaynig V, Longair M, Pietzsch T, Preibisch S, Rueden C, Saalfeld S, Schmid BJNm: **Fiji: an open-source platform for biological-image analysis**. 2012, **9**(7):676-682.

310. Lee JY, Lu H: **Plasmodesmata: the battleground against intruders**. *Trends Plant Sci* 2011, **16**(4):201-210.

311. Cao L, Blekemolen MC, Tintor N, Cornelissen BJ, Takken FLJMp: **The Fusarium oxysporum Avr2-Six5 effector pair alters plasmodesmatal exclusion selectivity to facilitate cell-to-cell movement of Avr2**. 2018, **11**(5):691-705.

312. Aung K, Kim P, Li Z, Joe A, Kvitko B, Alfano JR, He SYJTPC: **Pathogenic bacteria target plant plasmodesmata to colonize and invade surrounding tissues**. 2020, **32**(3):595-611.

313. Reagan BC, Burch-Smith TMJMP-MI: **Viruses Reveal the Secrets of Plasmodesmal Cell Biology**. 2020, **33**(1):26-39.

314. Lucas WJ: **Plant viral movement proteins: agents for cell-to-cell trafficking of viral genomes**. *Virology* 2006, **344**(1):169-184.

315. Wu S-W, Kumar R, Iswanto ABB, Kim J-YJJoEB: **Callose balancing at plasmodesmata**. 2018, **69**(22):5325-5339.

316. Bucher GL, Tarina C, Heinlein M, Di Serio F, Meins F, Jr., Iglesias VA: **Local expression of enzymatically active class I beta-1, 3-glucanase**

**enhances symptoms of TMV infection in tobacco**. *Plant J* 2001, **28**(3):361-369.

317. Moore PJ, Fenczik CA, Deom C, Beachy RJP: **Developmental changes in plasmodesmata in transgenic tobacco expressing the movement protein of tobacco mosaic virus**. 1992, **170**(3):115-127.

318. Knox K, Wang P, Kriechbaumer V, Tilsner J, Frigerio L, Sparkes I, Hawes C, Oparka K: **Putting the Squeeze on Plasmodesmata: A Role for Reticulons in Primary Plasmodesmata Formation**. *Plant Physiol* 2015, **168**(4):1563-1572.

319. Volk GM, Turgeon R, Beebe DU: **Secondary plasmodesmata formation in the minor-vein phloem of *Cucumis pepo L.*** *Planta* 1996, **199**(3):425-432.

320. Ding B, Haudenshield JS, Hull RJ, Wolf S, Beachy RN, Lucas WJ: **Secondary plasmodesmata are specific sites of localization of the tobacco mosaic virus movement protein in transgenic tobacco plants**. *Plant Cell* 1992, **4**(8):915-928.

321. Jarsch IK, Ott T: **Perspectives on remorin proteins, membrane rafts, and their role during plant-microbe interactions**. *Mol Plant Microbe Interact* 2011, **24**(1):7-12.

322. Gouguet P, Gronnier J, Legrand A, Perraki A, Jolivet M-D, Deroubaix A-F, German-Retana S, Boudsocq M, Habenstein B, Mongrand SJPP: **Connecting the dots: from nanodomains to physiological functions of REMORINs**. 2020.

323. Cheng G, Yang Z, Zhang H, Zhang J, Xu JJNP: **Remorin interacting with PCaP1 impairs Turnip mosaic virus intercellular movement but is antagonised by VPg**. 2020, **225**(5):2122-2139.

324. Magyarosy AC, Buchanan BB, Schürmann PJV: **Effect of a systemic virus infection on chloroplast function and structure**. 1973, **55**(2):426-438.

325. Iswanto ABB, Kim J-YJP: **Lipid raft, regulator of plasmodesmal callose homeostasis**. 2017, **6**(2):15.

326. Iswanto ABB, Shon JC, Liu KH, Vu MH, Kumar R, Kim J-YJPP: **Sphingolipids Modulate Secretion of Glycosylphosphatidylinositol-Anchored Plasmodesmata Proteins and Callose Deposition**. 2020, **184**(1):407-420.

327. Sangiorgio V, Pitto M, Palestini P, Masserini MJTIjob: **GPI-anchored proteins and lipid rafts**. 2004, **53**(2):98-111.

328. Lingwood D, Simons KJs: **Lipid rafts as a membrane-organizing principle**. 2010, **327**(5961):46-50.

329. Huang D, Sun Y, Ma Z, Ke M, Cui Y, Chen Z, Chen C, Ji C, Tran TM, Yang LJPotNAoS: **Salicylic acid-mediated plasmodesmal closure via Remorin-dependent lipid organization**. 2019, **116**(42):21274-21284.

330. Ke M, Ma Z, Wang D, Sun Y, Wen C, Huang D, Chen Z, Yang L, Tan S, Li RJNP: **Salicylic acid regulates PIN2 auxin transporter hyperclustering and root gravitropic growth via Remorin-dependent lipid nanodomain organisation in Arabidopsis thaliana**. 2021, **229**(2):963-978.

331. Tolley N, Sparkes I, Craddock CP, Eastmond PJ, Runions J, Hawes C, Frigerio LJTPJ: **Transmembrane domain length is responsible for the ability of a plant reticulon to shape endoplasmic reticulum tubules in vivo**. 2010, **64**(3):411-418.

332. Hepler PJP: **Endoplasmic reticulum in the formation of the cell plate and plasmodesmata**. 1982, **111**(2):121-133.

333. Jones M: **The origin and development of plasmodesmata**. In: *Intercellular communication in plants: Studies on plasmodesmata.* Springer; 1976: 81-105.

334. Wang X-Y, Guo G-Q, Nie X-W, Zheng G-CJP: **Cytochemical localization of cellulase activity in pollen mother cells of David lily during meiotic prophase I and its relation to secondary formation of plasmodesmata**. 1998, **204**(3):128-138.

335. Dörr I, Kollmann RJBA: **Symplasmic sieve element continuity between Orobanche and its host**. 1995, **108**(1):47-55.

336. Pankratenko A, Atabekova A, Morozov S, Solovyev AJB: **Membrane contacts in plasmodesmata: structural components and their functions**. 2020, **85**:531-544.

337. Brault ML, Petit JD, Immel F, Nicolas WJ, Glavier M, Brocard L, Gaston A, Fouché M, Hawkins TJ, Crowet JMJEr: **Multiple C2 domains and transmembrane region proteins (MCTP s) tether membranes at plasmodesmata**. 2019, **20**(8):e47182.

338. Ishikawa K, Tamura K, Fukao Y, Shimada TJNP: **Structural and functional relationships between plasmodesmata and plant endoplasmic reticulum–plasma membrane contact sites consisting of three synaptotagmins**. 2020, **226**(3):798-808.

339. Kierszniowska S, Seiwert B, Schulze WXJM, Proteomics C: **Definition of Arabidopsis sterol-rich membrane microdomains by differential treatment with methyl-β-cyclodextrin and quantitative proteomics**. 2009, **8**(4):612-623.

340. Maule AJ, Benitez-Alfonso Y, Faulkner CJCoipb: **Plasmodesmata–membrane tunnels with attitude**. 2011, **14**(6):683-690.

341. Bundy MG, Kosentka PZ, Willet AH, Zhang L, Miller E, Shpak EDJPp: **A mutation in the catalytic subunit of the glycosylphosphatidylinositol transamidase disrupts growth, fertility, and stomata formation**. 2016, **171**(2):974-985.

342. Grison MS, Petit JD, Glavier M, Bayer EMJB-p: **Quantification of Protein Enrichment at Plasmodesmata**. 2020, **10**(5).

343. Li K, Wu G, Li M, Ma M, Du J, Sun M, Sun X, Qing LJVj: **Transcriptome analysis of Nicotiana benthamiana infected by Tobacco curly shoot virus**. 2018, **15**(1):1-15.

344. Voigt CA, Somerville SC: **Callose in biotic stress (pathogenesis): biology, biochemistry and molecular biology of callose in plant defence: callose deposition and turnover in plant–pathogen interactions**. In: *Chemistry, Biochemistry, and Biology of 1-3 Beta Glucans and Related Polysaccharides.* Elsevier; 2009: 525-562.

345. Sowinski P, Rudzinska-Langwald A, Kobus P: **Changes in plasmodesmata frequency in vascular bundles of maize seedling leaf induced by growth at sub-optimal temperatures in relation to photosynthesis and assimilate export**. *Environ Exp Bot* 2003, **50**(2):183-193.

346. Liesche J, Gao C, Binczycki P, Andersen SR, Rademaker H, Schulz A, Martens HJJPp: **Direct comparison of leaf plasmodesma structure and function in relation to Phloem-Loading type**. 2019, **179**(4):1768-1778.

347. Sowinski P, Bilska A, Baranska K, Fronk J, Kobus P: **Plasmodesmata density in vascular bundles in leaves of C4 grasses grown at different light conditions in respect to photosynthesis and photosynthate export efficiency.** *Environ Exp Bot* 2007, **61**:74-84.

348. Danila FR, Quick WP, White RG, Kelly S, von Caemmerer S, Furbank RTJJoeb: **Multiple mechanisms for enhanced plasmodesmata density in disparate subtypes of C4 grasses**. 2018, **69**(5):1135-1145.

349. Gibbs A: **Viruses and plasmodesmata**. In: *Intercellular communication in plants: studies on plasmodesmata.* Springer; 1976: 149-164.

350. Lucas WJ, Gilbertson RLJArop: **Plasmodesmata in relation to viral movement within leaf tissues**. 1994, **32**(1):387-415.

351. Waigmann E, Zambryski P: **Tobacco mosaic virus movement protein-mediated protein transport between trichome cells**. *Plant Cell* 1995, **7**(12):2069-2079.

352. Laliberté J-F, Sanfaçon HJArop: **Cellular remodeling during plant virus infection**. 2010, **48**:69-91.

353. Xie L, Song X-j, Liao Z-f, Wu B, Yang J, Zhang H, Hong JJM: **Endoplasmic reticulum remodeling induced by Wheat yellow mosaic virus infection studied by transmission electron microscopy**. 2019, **120**:80-90.

354. Levy A, Tilsner JJFiPS: **Creating contacts between replication and movement at plasmodesmata–a role for membrane contact sites in plant virus infections?** 2020, **11**.

355. Bayer EMF, Salmon MSJFips: **Dissecting plasmodesmata molecular composition by mass spectrometry-based proteomics**. 2013, **3**:307.

356. Zavaliev R, Epel BL: **Imaging callose at plasmodesmata using aniline blue: quantitative confocal microscopy**. In: *Plasmodesmata.* Springer; 2015: 105-119.

357. Flors V, Ton J, Jakab G, Mauch-Mani BJJoP: **Abscisic acid and callose: team players in defence against pathogens?** 2005, **153**(7-8):377-383.

358. Luna E, Pastor V, Robert J, Flors V, Mauch-Mani B, Ton JJMP-MI: **Callose deposition: a multifaceted plant defense response**. 2011, **24**(2):183-193.

359. Ellinger D, Voigt CAJAob: **Callose biosynthesis in Arabidopsis with a focus on pathogen response: what we have learned within the last decade**. 2014, **114**(6):1349-1358.

360. Li W, Zhao Y, Liu C, Yao G, Wu S, Hou C, Zhang M, Wang DJPcr: **Callose deposition at plasmodesmata is a critical factor in restricting the cell-to-cell movement of Soybean mosaic virus**. 2012, **31**(5):905-916.

361. Faulkner C, Petutschnig E, Benitez-Alfonso Y, Beck M, Robatzek S, Lipka V, Maule AJ: **LYM2-dependent chitin perception limits molecular flux via plasmodesmata**. *Proc Natl Acad Sci U S A* 2013, **110**(22):9166-9170.

362. Voigt CAJFiPS: **Callose-mediated resistance to pathogenic intruders in plant defense-related papillae**. 2014, **5**:168.

363. Wang Y, Li X, Fan B, Zhu C, Chen ZJIJoMS: **Regulation and Function of Defense-Related Callose Deposition in Plants**. 2021, **22**(5):2393.

364. Yi SY, Shirasu K, Moon JS, Lee S-G, Kwon S-YJPo: **The activated SA and JA signaling pathways have an influence on flg22-triggered oxidative burst and callose deposition**. 2014, **9**(2):e88951.

365. Esau K, Thorsch JJAjob: **Sieve plate pores and plasmodesmata, the communication channels of the symplast: ultrastructural aspects and developmental relations**. 1985, **72**(10):1641-1653.

366. Kragler F, Lucas WJ, Monzer J: **Plasmodesmata: Dynamics, Domains and Patterning**. *Annals of Botany* 1998, **81**:1-10.

367. Petit JD, Li ZP, Nicolas WJ, Grison MS, Bayer EMJCoipb: **Dare to change, the dynamics behind plasmodesmata-mediated cell-to-cell communication**. 2020, **53**:80-89.

368. Kraner ME, Müller C, Sonnewald UJTPJ: **Comparative proteomic profiling of the choline transporter-like1 (CHER 1) mutant provides insights into plasmodesmata composition of fully developed Arabidopsis thaliana leaves**. 2017, **92**(4):696-709.

369. Stefano G, Renna L, Wormsbaecher C, Gamble J, Zienkiewicz K, Brandizzi FJCr: **Plant endocytosis requires the ER membrane-anchored proteins VAP27-1 and VAP27-3**. 2018, **23**(8):2299-2307.

370. Kriechbaumer V, Botchway SW, Slade SE, Knox K, Frigerio L, Oparka K, Hawes C: **Reticulomics: Protein-Protein Interaction Studies with Two Plasmodesmata-Localized Reticulon Family Proteins Identify Binding Partners Enriched at Plasmodesmata, Endoplasmic Reticulum, and the Plasma Membrane**. *Plant Physiol* 2015, **169**(3):1933-1945.

371. Nishimura MT, Stein M, Hou BH, Vogel JP, Edwards H, Somerville SC: **Loss of a callose synthase results in salicylic acid-dependent disease resistance**. *Science* 2003, **301**(5635):969-972.

372. Du Y, Tejos R, Beck M, Himschoot E, Li H, Robatzek S, Vanneste S, Friml JJPotNAoS: **Salicylic acid interferes with clathrin-mediated endocytic protein trafficking**. 2013, **110**(19):7946-7951.

373. Benitez-Alfonso Y, Jackson D: **Redox homeostasis regulates plasmodesmal communication in Arabidopsis meristems**. *Plant Signal Behav* 2009, **4**(7):655-659.

374. Stonebloom S, Brunkard JO, Cheung AC, Jiang K, Feldman L, Zambryski P: **Redox states of plastids and mitochondria differentially regulate**

**intercellular transport via plasmodesmata**. *Plant Physiol* 2012, **158**(1):190-199.

375. Sager R, Lee JY: **Plasmodesmata in integrated cell signalling: insights from development and environmental signals and stresses**. *J Exp Bot* 2014, **65**(22):6337-6358.

376. Bari R, Jones JD: **Role of plant hormones in plant defence responses**. *Plant Mol Biol* 2009, **69**(4):473-488.

377. Pieterse CM, Leon-Reyes A, Van der Ent S, Van Wees SC: **Networking by small-molecule hormones in plant immunity**. *Nature chemical biology* 2009, **5**(5):308-316.

378. Davies PJ: **The plant hormones: their nature, occurrence, and functions**. In: *Plant hormones.* Springer; 2010: 1-15.

379. Islam W, Naveed H, Zaynab M, Huang Z, Chen HYJPs, behavior: **Plant defense against virus diseases; growth hormones in highlights**. 2019, **14**(6):1596719.

380. Kawano TJPcr: **Roles of the reactive oxygen species-generating peroxidase reactions in plant defense and growth induction**. 2003, **21**(9):829-837.

381. War AR, Paulraj MG, Ahmad T, Buhroo AA, Hussain B, Ignacimuthu S, Sharma HCJPs, behavior: **Mechanisms of plant defense against insect herbivores**. 2012, **7**(10):1306-1320.

382. Gilroy S, Białasek M, Suzuki N, Górecka M, Devireddy AR, Karpiński S, Mittler RJPp: **ROS, calcium, and electric signals: key mediators of rapid systemic signaling in plants**. 2016, **171**(3):1606-1615.

383. Noctor G, Reichheld J-P, Foyer CH: **ROS-related redox regulation and signaling in plants**. In: *Seminars in Cell & Developmental Biology: 2018*. Elsevier: 3-12.

384. Toyota M, Spencer D, Sawai-Toyota S, Jiaqi W, Zhang T, Koo AJ, Howe GA, Gilroy SJS: **Glutamate triggers long-distance, calcium-based plant defense signaling**. 2018, **361**(6407):1112-1115.

# VITA

Brandon Chase Reagan was born is Riverdale, Georgia on September 2nd 1992 and grew up in Fayetteville Georgia. He attended Whitewater High School where he graduated with honors and was a member of the multiple Honor Societies as part of the class of 2011. He completed his Bachelors of Science degree in Biology with a concentration in Biochemistry and Molecular Biology at Mercer University in Macon, Georgia. As an undergraduate. he conducted research in the lab of Dr. Amy Wiles at Mercer University where he studied the effects of competition on bacterial growth and developed an immersive teaching laboratory experiment for a mathematical modeling course. He also participated in a National Science Foundation-funded Research Experience for Undergraduates in the lab of Dr. Joshua Bembenek at the University of Tennessee studying the regulation of exocytosis and cell division in *C. elegans*. During his REU in the Bembenek lab, Brandon developed a love for microscopy and cell biology. He returned to the University of Tennessee-Knoxville to complete his PhD in Biochemistry & Cellular and Molecular Biology in the lab of Dr. Tessa Burch-Smith studying intercellular communication in plants and virus-host interactions. He will defend his thesis on March 29th and complete his doctoral degree in May of 2021. He will then move to East Lansing, Michigan to begin his Postdoctoral Research Associate position in the lab of Dr. Federica Brandizzi at The Department of Energy-Plant Research Lab at Michigan State University studying the relationship between ER structure maintenance and ER stress.